A STATE SPACE APPROACH TO CHEMICAL PLANT FAULT DETECTION

by

CHRISTOPHER RICHARD BELL, B.Sc

July 1983

A thesis submitted for the
degree of Doctor of Philosophy
of the University of London
and for the Diploma of
Membership of the Imperial
College

Department of Electrical Engineering
Imperial College
London, S.W.7

TO MARCIA

ABSTRACT

Any plant under automatic control is heavily dependent on instrumentation for safe, reliable operation. A sudden fault on a measuring instrument, particularly if used in a control loop, can lead to inefficient, unstable or even dangerous operation.

This project takes as its starting point part of an existing pilot scale gas separation plant and assumes that a fault can occur on any one instrument at any time. The plant is to remain under computer implemented 3-term control with occasional small changes in setpoint, the problem being to detect and isolate any such fault that should occur.

The part of the plant selected for study comprises a heat exchanger and cooler, with measurement of seven liquid temperatures and two regulated flow rates. Plant data is used in the development of a discrete-time state space model from which a Kalman filter can be constructed.

Under no-fault conditions, a Kalman filter utilizing 'r' measurements generates an r-dimensional innovation vector with zero mean. A subsequent measurement fault causes the expected value of this vector to align itself in a fixed direction in r-space that is characteristic of the fault. This leads to an algorithm employing a log-likelihood ratio test to detect statistically significant departures from zero mean and achieving fault isolation by comparing the innovation vector direction with a set of reference directions.

An estimate of fault magnitude can be obtained from the post-fault innovations and expressions are derived for the estimation error statistics. It is shown that a suboptimal filter can in certain cases provide improved isolation and estimation.

Several algorithms are tested with real data, fault examples being obtained either by setpoint change or by superimposition of faults on to data records. A possible extension to include a level control loop is also discussed.

ACKNOWLEDGMENTS

Firstly I should like to thank my supervisor, Professor J H Westcott of the Control Section, Imperial College, for all his help and encouragement throughout the project. I also acknowledge the joint financial support, through an 'Industrial Sponsorship', of my employers, George Wimpey M E & C Limited, together with the Science and Engineering Research Council. I am very grateful not only to the company for giving me the opportunity to work full-time towards a PhD, but especially to Mr G W Spall, Director, for his support during my three-year absence.

I am indebted to the staff of the Department of Chemical Engineering at Imperial College for their co-operation, particularly to Dr L S Kershenbaum for fruitful discussions on plant modelling and to Mr J M Whitfield for his invaluable assistance during practical work on the pilot plant itself.

While thanking my fellow research students for their company and for many useful discussions I must also include my Wimpey colleagues for helpful suggestions during the writing-up period, and in particular Steve Harris who produced some of the diagrams using the Wimpey 'GW2D' CAD facility.

A special 'thank you' goes to Joyce Marsh for transforming my handwriting into flowing typescript and last, but not least, I thank my wife, Marcia, for her patience and understanding.

CONTENTS

CHAPTER 2 PLANT MODELLING IN THE STEADY STATE

CHAPTER 3 MODELLING OF SYSTEM TRANSIENTS

CHAPTER 4 FILTER DESIGN AND SIMPLE FAULT DETECTION

CHAPTER 7 CONCLUSION

APPENDICES

LIST OF FIGURES

LIST OF TABLES

LIST OF SYMBOLS

$\hat{a}$	Estimate of scalar 'a'
$\|A\|$	Determinant of matrix 'A'
A^*	Generalized inverse of matrix 'A'
$\hat{A}$	Estimate of matrix 'A'
A_c	System matrix for t.i., d.t. state space system
$\underline{b}$	Bias vector
B_c	Input matrix for t.i., d.t. state space system
$B_u(\gamma;\theta+j)$	Innovation bias matrix at time $\theta+j$ due to input fault at θ
$B_y(\hat{x};\theta+j)$	State estimate bias matrix at $\theta+j$ due to output fault at θ
$B_u(\gamma)$	Steady state innovation bias matrix due to input fault
$B_y(\hat{x})$	Steady state state estimate bias matrix due to output fault
c_1, c_2	Matrix exponential coefficients
c.t.	Continuous time
c/w	Cooling water
C_c	Observation matrix for t.i., d.t. state space system
C_j	Autocorrelation function with lag 'j'
C_p	Specific heat at constant pressure
CGLR	Constrained generalized likelihood ratio (algorithm)
CV	Control valve
d.t.	Discrete time
d_i	Steady state reference vector for unit step fault in direction 'i'
D_n	Kolmogorov-Smirnov statistic
$E[\ ]$	Expected value
f_i	Transient reference vector whose s/s value is d_i
f(t)	Perturbation variable associated with F(t)
$f_x(x), f(x)$	Probability density function of random variable 'x'
$f_{x\|y}(x\|y)$, $f(x\|y)$	Probability density function of random variable 'x', given 'y'
F(x)	Probability distribution function of random variable 'x'
F(t)	Flow rate as a function of time
F_1	Absolute value of stripped MEA flow rate
$\tilde{F}_1$	Absolute value of spent MEA flow rate
F_2	Absolute value of cooler c/w flow rate
FX	Flow loop
$F\{\ \}$	Arbitrary function
g	Input matrix for t.i., d.t. scalar system

G(k)	Input matrix at time 'k' for d.t. state space system (time index dropped if time invariant)
$G\{\ \}$	Arbitrary function
$G(k;\theta)$	Failure signature matrix
GLR	Generalized likelihood ratio (algorithm)
h	Observation matrix for t.i., d.t. scalar system
H(k)	Observation matrix at time 'k' for d.t. state space system (time index dropped if time invariant)
H(t-k)	Heaviside unit step function
H	Hypothesis
I_n	Identity matrix of dimension 'n'
J	Cost function
k	Time index for discrete time system
$\underline{k}$	Vector of heat transfer coefficients
K_{xx}	Heat transfer coefficient
K(k)	Kalman gain at time 'k'. Time index dropped if constant
ℓ,L	Length
$\ell(k)$	χ^2 r.v. derived from r-dimensional innovation vector $\gamma(k)$
$\ell_i(k)$	χ^2 r.v. derived from component $\gamma_i(k)$ of vector $\gamma(k)$
llr	Log-likelihood ratio
LLR	Log-likelihood ratio (algorithm)
$\ell n\Lambda(\gamma)$	Log-likelihood ratio
LX	Level loop
m	Dimension of u(k), mass, (as subscript) mean
$\underline{m}$	Mean value of vector
MEA	Monoethanolamine
n	Dimension of x(k)
n_i	Time delay, seconds
n(k)	Measurement noise on input u(k) at time 'k' (d.t. system)
N	Number of data points, window length
$N(H)$	Null space of matrix H
$\underline{0}$	Null matrix
p	Steady state a posteriori error covariance for scalar system
P( ),Pr( )	Probability
P_D	Probability of correct decision
P_F	Probability of false alarm
P_M	Probability of miss alarm
P_X	Probability of cross-detection
P_U	Probability of non-definite decision

P_s	Steady state degradation in estimation error covariance
P^+	Steady state a priori error covariance
P(k+1|k)	A priori estimation error covariance at time 'k+1'
P(k+1|k+1)	A posteriori estimation error covariance at 'k+1'
q	Variance of system noise for scalar system
q_{ij}	Element of matrix Q
q_{ab}	Rate of heat transfer from 'a' to 'b'
Q	Covariance of process noise vector w(k)
Q_h	Rate of heat transfer
r	Variance of measurement noise for scalar system
r_{ij}	Element of matrix R
rtd	Resistance temperature detector
R	Real line, covariance of output measurement noise vector v(k)
R_o	Observability matrix (Rosenbrock)
s	Seconds, parameter for Laplace transform
ss,s/s	Steady state
s.l.	Significance level
S	Covariance of input measurement noise vector n(k)
SGLR	Simplified generalized likelihood ratio (algorithm)
t	Time, time index for c.t. systems
$t_{c1}(0)$	Perturbation variable associated with $T_{c_1}(0)$
t.i.	Time invariant
T_{110},T110	Absolute value of actual temperature whose measured value is TX110
TX	Temperature loop
TX110	Measured temperature
$\overline{TX177}$	Measured value of T177 at stable operating point
$T_{c1}(0)$	Actual temp. T174 whose measured value is TX174
$T_{c1}(L)$	T110 TX110
$T_{c2}(0)$	T177 TX177
$T_{c2}(L)$	T176 TX176
$T_{x1}(0)$	T173 TX173
$T_{x1}(L)$	T174 TX174
$T_{x2}(0)$	T172 TX172
$T_{x2}(L)$	T175 TX175
u(k)	Input to d.t. system at time 'k'
$\underline{u}_f(i)$	Hypothesized input fault number 'i'
$u_m(k)$	Apparent (i.e. measured) value of u(k)
v(k)	Measurement noise on output at time 'k' (d.t. system)
V(k)	Covariance of innovation vector $\gamma(k)$, k dropped if constant
V(x)	Quadratic function

$w(k)$	Process (or 'system') noise at time 'k' (d.t. system)
$x(k)$	State vector at time 'k'
$\hat{x}(k+l\|k)$	Estimate of 'x' at time 'k+l' given information up to and including time 'k'
$y(k)$	Output of d.t. system at time 'k'
$\underline{y}_f(i)$	Hypothesized output fault number 'i'
β	Bias
$\gamma(k)$	Innovation vector corresponding to measurement y(k)
γ_i	ith component of $\gamma(k)$
Γ_o	Observability matrix (Kalman)
δ	Error, small increment
δ_{jk}	Kronecker delta
Δ	Sampling period, difference between actual/optimal Kalman gains
ΔT	Change in 'T'
ε	Error, alarm threshold
$\eta,\tilde{\eta}$	Alarm thresholds
θ	Time index of first sample following fault, temperature difference, angle
$\underline{\kappa}$	Eigenvector
κ_I,κ_P	Integral, proportional control terms for 3 term algorithm
λ	Eigenvalue
Λ	Likelihood ratio
ν	Fault magnitude
ν_1	Coefficient of skewness
ν_2	Coefficient of kurtosis
ρ	Density
ρ_i	Most likely magnitude of fault in Direction 'i'
ρ_i^*	Actual magnitude of fault in Direction 'i'
$\sum_i$	Summation over all available values of 'i'
τ_r	Residence time
τ_i	Time constant associated with state x_i
ϕ	System matrix for t.i., d.t. scalar system
$\Phi(k)$	System matrix at time 'k' for d.t. state space model (time index dropped if system time invariant)
χ^2 r.v.	Chi-squared random variable
Ψ	Filter transition matrix

CHAPTER 1

INTRODUCTION

1.0 Motivation

One of the most important tasks of the control room personnel on a chemical plant is to accurately diagnose and rectify plant failures on the basis of instrument readings gathered from various parts of the plant. The first line of defence is usually the alarm annunciator which gives the alert that a measured variable has moved outside its normal limits. The operator must use his detailed knowledge of the plant operating manual and his own experience to decide just what is implied by any particular combination of alarms and indications from the plant, or indeed whether an alarm is spurious. In a modern plant with a central control panel 2m high and in excess of 10m long the simultaneous occurrence of several perhaps seemingly unrelated alarms can be bewildering and may tempt the operator into believing that they are caused by a fault in the measurement system itself.

In 1977 a symposium on 'Human Operators and Simulation' included the results of an experiment in which two dozen experienced operators from the petrochemical industry were invited to attempt diagnosis of a range of simulated plant faults from the indications on a control panel. The report of Marshall and Shepherd [1] concluded that there was a disappointing lack of systematic fault finding procedures among the operators. Distrust of the plant instrumentation was reflected in the fact that many operators considered the probability of instrument failure on their own plants so high that, having scanned the alarm lights, they would leave the control room to make a direct check out on the plant.

In recent years, loss prevention has become an important subject in its own right. Safety of personnel and the protection of capital investment by preventing damage to expensive equipment are no less dependent on reliable instrumentation than the loss

of saleable product due to inefficient operation. Clearly a comprehensive instrument maintenance programme is indicated but may be difficult to carry out due to a lack of suitably trained personnel.

In June 1978 The Sunday Times [2] reported that ICI at Wilton, Teeside were losing instrument artificers at an alarming rate. At that time only 230 were employed out of an ideal total of 350, necessitating shutdown of some plants and delaying the start-up of new ones. Many skilled men had been lured away by large salaries in the Middle East and the North Sea and the problem was exacerbated by the refusal of the Wilton craft based unions to allow their members to retrain as artificers without substantial pay increases. In addition the Wilton men, who had served four-year apprenticeships, would not work alongside Government Skillcentre trainees fresh from their twelve month courses.

The need for reliable instrumentation and the difficulties in keeping it reliable point towards the desirability of self-checking in control and monitoring systems. While an ideal system could detect and diagnose a fault of any kind it is clear from the foregoing that a system capable of detecting and isolating faults on the instruments alone is a useful tool and could substantially increase plant safety and reliability while reducing the manpower required for maintenance. This thesis describes the work done in designing and testing such a system for part of an existing plant.

1.1 Literature Survey

The last two decades have seen a tremendous upsurge in the use of computers in all facets of engineering and the appearance of the Kalman filter in the early 1960's was well timed for its development to run in parallel with the falling cost of computing power. Kalman's work has figured extensively in the design of computer based fault detection systems, not least because the innovations sequence generated by the Kalman filter is sensitive to departures of the system from 'normal'. Filtering cannot proceed until a suitable state-space model has been obtained for the system under observation. This has proved more of a

stumbling block in the case of chemical processes than for aerospace applications where the dynamics are often very well defined and where the vast majority of successful filtering work has been carried out.

For this project a survey of the available literature falls into three sections: the Kalman filter, modelling and filtering of chemical processes and fault detection.

1.1.1 The Kalman Filter

Since the original papers of Kalman [3] and Kalman and Bucy [4] hundreds of papers and dozens of books have appeared on the development and applications of the Kalman (or Kalman-Bucy) filter. This project employs the straightforward linear filter applied to a linearized system: the necessary theory is adequately covered by text books and a handful of papers as follows.

Much use is made of Jazwinski [5] (particularly Chapters 7 and 8 on linear filtering theory and its applications), with Sage and Melsa [6] another useful reference. State space modelling is well covered by Kwakernaak and Sivan [7], which includes discretization and, specifically for applications in Chemical Engineering, Seinfeld and Lapidus [8].

Filter design necessitates the prior specification of the process and measurement noise covariance matrices Q and R and the estimation error covariance P(0|0). The effect of error in these parameters is discussed in a paper by Bellingham and Lees [9], while Q and R can, at least in theory, be estimated by the use of an algorithm proposed by Mehra [10] and subsequently modified by Godbole [11].

The work of Martin and Stubberud [12] claims to allow estimation of unknowns in the matrices required for state space modelling followed by estimation of Q and R. However, by dealing with only a part of an existing plant, the model used in this project includes several inputs

which cannot be controlled. These inputs are dictated by conditions elsewhere on the plant and violate the basic assumption of [12] that the input or 'control' vector can be set to zero to allow the estimation to proceed.

The behaviour of suboptimal filters has received much attention. Jazwinski [5] covers the use of filters with constant gain while the effects of suboptimal gain on the estimation accuracy is discussed by Heffes [13] and by Friedland [14]. Uncertain parameters such as bias can be estimated by the use of augmented filters (see [5], [6]) while Friedland has developed in [15] a bias filter which operates on the innovations of an optimal filter to correct the state estimates.

1.1.2 Modelling and filtering of chemical processes

While the potential of the Kalman filter was quickly recognised for aerospace applications, its use in chemical engineering problems has been limited. On line computers are relatively common on modern chemical plants but few of these are doing much more than scanning, logging and d.d.c. by simulation of classical 3-term controllers. Apart from the difficulties in specifying the statistics Q, R, $\hat{x}(0|0)$ and P(0|0) (see [5] for definition) chemical processes are often extremely difficult to model and can give rise to sets of complex differential equations which are not readily amenable to the repetitive calculations entailed by the filter.

Simulation work is fairly well represented in the literature and a comprehensive selection is referenced in [9]. Coggan and Noton [16] carried out simulations on two nonlinear systems, a blending process and a furnace. These processes were linearized for filtering and the filter Q and R matrices were matched to the statistics of the computer generated noise used to obtain simulated data. Attempts to obtain a heat transfer coefficient for the furnace by augmenting the state vector resulted in a biased estimate despite various modifications to the filter.

Goldmann and Sargent [17] also simulated two processes, a binary distillation column and an industrial reactor. For the first example, as in [16], the model used for the filter was the same as that used to generate the data but it was assumed for both processes that there was no process noise, i.e. Q = 0. The results indicated that as long as the model was accurate the filter was reasonably insensitive to errors in the statistics R, $\hat{x}(0|0)$ and $P(0|0)$ and that no appreciable degradation was caused by filtering data contaminated by non-Gaussian or autocorrelated noise. The second example was used to investigate the effects of model inaccuracy. An important conclusion was that there was a limit to the amount by which the state vector could be augmented to estimate parameters such as biases. As the number of parameters increased convergence became slower and eventually broke down as multiple solutions became possible.

In a further simulation study, Joffe and Sargent [18] applied optimal control theory to an adiabatic tubular reactor to maximize product yield. It was shown that good control could be maintained using a control policy based on filter estimates despite manipulation of Q over a wide range.

Not surprisingly studies of 'real' systems are mostly limited to pilot scale plants or laboratory rigs. In [19], Newell and Fisher modelled a pilot scale double-effect evaporator using a modular approach. These building blocks could be linked together in various ways to develop models of differing complexity which were later used by Hamilton, Seborg and Fisher [20] to test the Kalman filter on the plant. In common with many chemical plants, the measurement noise levels on the pilot plant were quite low. This can cause difficulties because the Kalman filter does not work well with extremely low noise levels, although theoretically it breaks down only if R = 0. In [20] it is claimed that artificial measurement noise was added 'in order to provide a more severe test of the Kalman filter'

and it is unfortunate that no comparison was made of performance with and without added noise. From their results Hamilton et al advocated that Q and R were best treated as tuning parameters selected to improve filter performance.

Jo and Bankoff [21] carried out experimental work on the polymerization of vinyl acetate in a small glass reactor. They tried out most of the filter variants to be found in Chapter 8 of Jazwinski [5] and also tested the filter with the state vector augmented by different numbers of variables. Some improvement in filter performance was obtained by estimating one parameter, but no significant change was obtained by adding further parameters. Since parameter augmentation markedly increased the computational load of the filter it was concluded that each case had to be considered on its merits: for the example in [21] the best compromise was the augmentation of the one most uncertain parameter.

Jo and Bankoff tried varying Q and R and found that if Q was specified too small the filter diverged rapidly. A valuable contribution of [21] was the simulation study carried out as a comparison. Here measurements were generated from the model used for the filter monitoring the real system. It was found that the estimation from the simulation was a considerable improvement over the experimental results despite the fact that the same Q and R were used by the filter in each case. This is an example of overly optimistic filtering results from a simulation study.

Several filter variants were also tried out by Litchfield et al [22] on a laboratory chemical reactor whose instrumentation was designed to be essentially noise-free. Artificial measurement noise was added to test the various filters and, in agreement with [17], correlated measurement noise was found to have minimal effect on the filter estimates.

There are few examples of applications in industry. Wells and Wismer [23] used the Kalman filter to estimate temperature and carbon concentration in a steelmaking process, their work illustrating several of the practical difficulties in using the filter for real systems. Modelling was hindered by the fact that the metallurgists did not agree on the chemical mechanisms dominating the process and the delay in sampling and analyzing the waste gases made estimation very difficult.

1.1.3 Fault detection

Much data on the failure rates of chemical plant instrumentation is classified information, but a feel for the problem can be gained from papers by Anyakora, Engel and Lees [24] and Lees [25]. At one plant 'definite failures' were taken arbitrarily as 2% full scale or 2 deg.C or 0.1 pH. These outnumbered smaller errors, classed as 'incidents', by a factor of about 3:1. The following failure rates are taken from [24] which averages over three plants the faults per instrument per year:-

Flow:	Differential pressure transmitter	1.73
Level:	Differential pressure transmitter	1.71
Temperature:	Resistance thermometer	0.41

Reference [25] gives information on the types of fault encountered. On a resistance thermometer the connections may come loose or the resistance bulb and/or thermowell may become loose or damaged. Differential pressure transmitters commonly suffer from blocked or airlocked pressure connections and the transmitters themselves may freeze up or be damaged by vibration or by dripping water or process fluid. The data in [24] leads to the conclusion that instruments out on the plant are up to four times as likely to fail as those located in the control room.

Detailed coverage of chemical plant fault detection from monitoring plant records is to be found in Himmelblau [26] which also introduces statistical techniques including some based on the Kalman filter. Design methods for

on-line fault detection were reviewed in a comprehensive 1976 survey paper by Willsky [27], who divided the various techniques into a number of categories which are used here.

Willsky divides the failure detection problem into three tasks - alarm, isolation and estimation. The first of these is simply to determine whether or not a fault has occurred while the second involves the narrowing down of the source of failure to a particular device or group of devices. The estimation problem is that of determination of the extent of failure and may allow the continued use of a piece of equipment albeit in a degraded mode. Willsky also discusses the probabilities of false alarms and missed detections for the various techniques and points out that one might be more willing to tolerate false alarms in a highly redundant system configuration than in a system without substantial back-up capabilities.

Another important issue is the tradeoff between the usually conflicting requirements of good fault detection properties and acceptable system operation under no-failure conditions. This is particularly true when a Kalman filter is being used simultaneously for state estimation for control purposes and for fault detection.

At the time of publication, most of the contributions described in Willsky's paper had been at a theoretical level with very few real applications of techniques. Of the nine 'real system' references given in [27], eight cover work in the aerospace industry: chemical engineering applications are conspicuous by their absence. In the following sections the various types of failure detection technique are briefly reviewed, more detail being given for those papers that have appeared since Willsky's survey. Willsky's comment that some techniques could be placed in more than one category is equally true of these more recent contributions.

(i) Failure-sensitive filters

One of the simplest ways of detecting failures using a Kalman filter is to monitor the state estimate, based on the premise that a sudden change in $\hat{x}$ reflects a failure. The state vector can also be augmented by failure modes such as system biases which can then be compared with their nominal values. These methods may be foiled by the 'oblivious filter' problem [5] where the precomputed error covariance P(k|k) and the Kalman gain K(k) become very small. The filter effectively relies on old measurements and is at best sluggish in its response to new data; at worst it may diverge if the model is sufficiently in error. The filter can be kept sensitive to new information by throwing away the older data either gradually, as in the exponentially age-weighted filters of Fagin [28] and Tarn and Zaborsky [29], or in blocks as in the limited memory filter of Jazwinski [30]. Another way is simply to fix the filter gain as discussed in [5].

A variation on the theme is a class of failure sensitive filters developed initially by Beard [31]. His paper is concerned with the design, for a linear deterministic plant with feedback, of detector-filters which are formulated to respond in a known way to certain failures. Beard showed that for his system an actuator failure or a change in a parameter in the dynamic equations of the system produced an error signal in a fixed vector direction. For sensor failures the error vector was constrained to lie in a two-dimensional invariant plane. Willsky [27] describes Beard's later work with Jones on the design of filters which are suboptimal from a state estimation point of view but which respond to a wide variety of failures. The approach is limited to time-invariant systems.

(ii) Voting systems

Voting is a well established method in which a system is provided with (at least) three sets of identical instruments. For a given measurement the instrument readings are compared and if one signal differs markedly from the others

then it is eliminated from consideration. The method is clearly expensive from a hardware point of view but provides fast detection of large failures. Such systems may have difficulties in detecting small bias shifts and are vulnerable to power supply or thermal variations which may affect all instruments equally.

Two techniques which hover between this category and the next are those of Labarrere et al [32] and Clark et al [33]. The first of these required only two identical sensors per measurement, the third being replaced by an estimate obtained from a bank of Kalman filters. The technique was applied in [32] to a simulated automatic landing of the AIRBUS.

In [33], Clark, Fosth and Walton simulated the flight control system for a hydrofoil boat. The form of the deterministic system equations rendered the states observable by using any one of the four sensors. Four Luenberger observers were run in parallel, one for each sensor, and the state estimates compared in a voting scheme. Such a method cuts down on hardware redundancy and could be used with Kalman filters for stochastic systems. It is, however, dependent on the system being observable,if not from individual measurements then at least from several subsets of the total number of instruments available.

(iii) Multiple hypothesis filter-detectors

In this class of adaptive estimation and failure detection schemes it is hypothesized that the system can only be operating in one of a finite number of modes. For fault detection purposes, all bar one of these would reflect system failures. The technique is based on identification of the hypothesis which gives the closest fit to the observations, a task usually achieved by monitoring the innovations generated by a bank of Kalman filters - one per hypothesis. This gives the conditional probability that each hypothesis is the true one.

Simulations using this method have been carried out by Montgomery and Caglayan [34] for an orbiting space shuttle represented by linear equations and the work is paralleled for a nonlinear system by Montgomery and Price [35]. That the method also has applications in the field of adaptive control is demonstrated by its use in conjunction with the F-8C digital-fly-by-wire aircraft as described by Athans et al in [36]. Multiple hypothesis methods for estimation, smoothing and prediction have been proposed by Athans and Chang [37].

Closely related to the work of Athans and Chang is the application of a multiple hypothesis method to fault detection in oil pipelines by Digernes [38]. The requirement was for a system that could readily distinguish between actual process failures such as leaks and less serious sensor failures and the method was tested by simulation using data from the Ekofisk-Teeside pipeline. The system required no less than twenty-five parallel Kalman filters but could reliably detect, isolate and estimate a leak even if it was accompanied by an instrument failure on the affected pipeline section.

Also falling into the 'multiple hypothesis' category are methods based on the sequential probability ratio test (SPRT) devised by Wald [39] and described in detail by Hancock and Wintz [40]. This test compares the logarithm of the ratio of the a posteriori probabilities for two modes of operation, 'failed' and 'unfailed', with upper and lower thresholds. The test terminates when one of the thresholds is crossed and the whole process is repeated. For fault detection purposes the SPRT has been used in its original form by Newbold and Ho [41] and in a modified form by Chien and Adams [42]. The latter application was aimed at the detection of moderate biases in inertial navigation systems and the SPRT was chosen because it bases its decision on the complete sensor measurement history. Wald's SPRT does not always respond well to a failure occurring in mid test, but the algorithm of Chien and

Adams overcomes this by employing a feedback loop and by specifying that a switch can only occur in one direction, i.e. from 'normal' to 'failed'.

A final technique in this section is based on the work of Buxbaum and Haddad [43] which was motivated by the difficulties of using Kalman filters in the face of non-Gaussian process noise. The density of such noise is approximated in [43] by a sum of Gaussian terms and the potential of this for fault detection was recognised by Willsky, Deyst and Crawford [44], [45]. In its complete form the 'BH' algorithm requires an exponentially growing bank of filters but these references give approximations which keep the number of filters constant yet gave quite promising results for a simulated inertial system.

(iv) Jump process formulations

In this section potential failures are modelled as jumps characterized by a priori distributions which reflect initial information concerning failure rates. Chien [46] has devised a method for the detection of a jump or ramp in a gyro bias in which the steady state effect of each of these faults is determined. A failure rate and a nominal bias size must be hypothesized in order to compute an approximate stochastic differential equation to which the normal-mode filter residual is input. The scheme can only be used to detect biases larger than nominal and the use of the steady state effect of the fault on the filter residual may cause an unacceptably long delay to detection.

(v) Innovations-based detection systems

This section would appear to include all of the recent work on 'real' chemical plants although, as in Section 1.1.2, this is limited almost exclusively to pilot scale plants and laboratory rigs.

If a Kalman filter is operating completely in accordance with the theory, then the error (or residual) sequence it generates is a zero mean,Gaussian white noise sequence with

known covariance. This sequence, first called the 'innovations' by Kailath [47], will depart from some or all of these properties if a part of the filter formulation is (or subsequently becomes) incorrect. Innovation monitoring thus suggests itself as a method for fault detection bearing in mind that the innovations can be tested for each of the above properties using the techniques given by Mehra and Peschon [48].

A simple method for detecting faults in flow loops was tested on a laboratory rig by Bellingham and Lees [49]. A relatively constant system flow/pressure drop characteristic was assumed for the valve and a two-component innovation vector was generated by a recursive least squares estimator. Fairly large errors were detectable by monitoring the innovations for shifted mean using Student's t test but could not often be isolated.

The results obtained by Bellingham and Lees for a more general control loop are presented in [50]. Here a state space model was derived for a laboratory level control rig which was held at the same setpoint throughout. The algorithm of Mehra/Godbole [10], [11] was used to estimate the noise statistics, but it was found that the method failed due to the low level of measurement noise: artificial noise was added to compensate. Bellingham and Lees employed Friedland's bias filter to estimate measurement bias and used either this estimate or the shift in mean of the two component innovation vector (again via the Student t test) to detect and partially isolate faults.

Another simple detection method with limited isolation capability is the χ^2 test. This has been tested in simulation by Willsky, Deyst and Crawford [44], [45] who concluded that improved isolation might be obtained by generating χ^2 random variables from individual components of the innovation vector.

For plants with many interconnected flow and inventory measurements an innovations based detection method was presented by Rooney et al in 1978 [51]. The algorithm obtained an unbiased minimum variance estimate of a vector of true flows from measurements on some of the flows plus material balances (termed 'pseudo-measurements') at each node. In the steady state each component of the innovation vector was tested at each time step by means of the χ^2 test before using the associated measurement to update the estimate. This allowed detection of leaks and sensor faults.

It was shown by Newman and Perkins [52] that improved reliability could be obtained by testing the whole innovation vector using the χ^2 test at every time step instead of by testing individual components. In [52] a method is also proposed for diagnosing faults by means of monitoring the direction of the post-fault innovation vector. Research in this area, including testing on the same Imperial College pilot plant that is the subject of this thesis, formed a part of Newman's PhD thesis [53], published in 1982 but not reviewed here.

The simpler innovations based techniques rely on the fact that under normal operation the innovations are 'small' while under fault conditions they become in some sense 'larger'. There is however one technique that attempts to maximize the amount of information extracted from the innovations - the Generalized Likelihood Ratio method, or 'GLR'. This approach attempts to isolate different faults by using knowledge of the differing effects that such failures have on the system innovations.

Consider a linear discrete-time system modelled in the standard state-space form as presented in [27]

$$x(k+1) = \Phi(k)\, x(k) + G(k)u(k) + w(k) \quad \ldots \quad (1.1)$$

$$y(k) = Hx(k) + v(k) \quad \ldots \quad (1.2)$$

The algorithm has to be matched to a particular type of fault, such as a jump or step in the dynamics or in a sensor output. A sensor step (constant measurement bias) ν occurring at time θ is modelled as

$$y(k) = Hx(k) + v(k) + \nu\sigma_{k,\theta} \qquad \ldots \quad (1.3)$$

where ν is a vector and $\sigma_{i,j}$ is the unit step:

$$\sigma_{i,j} = \begin{cases} 1 & i \geq j \\ 0 & i < j \end{cases}$$

The linearity of system and filter allow the post fault innovation $\gamma'(k)$ to be split into the part $\gamma(k)$ that would have occurred without the fault and the part due to the fault ν alone

$$\gamma'(k) = G(k;\theta)\nu + \gamma(k) \qquad \ldots \quad (1.4)$$

G is termed the 'failure signature matrix' because it determines the way in which the fault propagates through the system. It is different for each type of fault and can be precomputed.

The GLR technique now uses G to estimate the fault vector ν and the time of occurrence θ. When a new innovation is generated the algorithm has to decide between two hypotheses, H_0 - that there is no fault (innovation $\gamma(k)$) or H_1 - that there is a fault (innovation $\gamma'(k)$). The decision is based on a statistical test that determines whether the innovations belong to the H_0 or the H_1 distribution. If the two distributions are exactly known then the log-likelihood ratio (LLR) test can be used (Van Trees [54]). If, however, the parameters governing H_1 are not known, as ν and θ in this case, it is necessary to use an extension to the theory which has become known as the generalized likelihood ratio. The GLR is defined by

$$\Lambda(\gamma) = \frac{f(\gamma(1),\ldots,\gamma(k)\,|\,H_1,\theta=\hat{\theta}(k),\nu=\hat{\nu}(k))}{f(\gamma(1),\ldots,\gamma(k)\,|\,H_0)} \qquad \ldots \quad (1.5)$$

where the numerator and denominator are respectively the probability densities for the observed innovation history given the two hypotheses H_1 and H_0. The problem that the numerator cannot be obtained unless both θ and ν are known is overcome by assuming that H_1 is true and obtaining from the innovations the maximum likelihood estimates for θ and ν. It can be shown that $\hat{\nu}(k)$ is an explicit function of $\hat{\theta}(k)$ and so the procedure for the full-blown GLR method basically involves maximizing the numerator of (1.5) over all the innovations since the commencement of filtering. Clearly the task of processing the innovations grows linearly with time.

In order to avoid this the estimate of θ can be restricted to a moving window

$$k - N \leq \theta \leq k - M \qquad \ldots \quad (1.6)$$

and there are various other simplifications such as constraining the fault vector ν to lie in one of a number of possible failure directions, i.e.

$$\nu = \alpha d_i \qquad \ldots \quad (1.7)$$

where α is a scalar, or completely specifying the fault

$$\nu = \nu_0 \qquad \ldots \quad (1.8)$$

The algorithms employing (1.7) and (1.8) are termed, respectively, constrained GLR (CGLR) and simplified GLR (SGLR). All variants normally employ the optimal Kalman filter resulting in a non-degraded state estimate under no-fault conditions.

The GLR technique is of course rather more complex than other innovations based techniques, but it does take full account of the transient effect of a fault through the time varying signature matrix, G. This matrix will eventually reach a steady value and, in some applications where the transient effects are limited, another possible

simplification is to use the steady state signature throughout.

GLR for fault-detection first appeared on the scene in the early 1970's, the most general formulation of the approach being given by Willsky and Jones [55], [56]. These papers describe an algorithm designed to look for jumps in state variables and illustrate the technique by a simulation for a vehicle subject to sudden jumps of unknown magnitude in position or velocity. An extension to the theory allows compensation of the state estimate $\hat{x}$ following a fault, making the algorithm suitable for adaptive filtering.

Subsequent work has increased the number of different types of fault which can be isolated by the GLR method. Liu and Jones [57] describe an application to the situation of state jumps on a linear manifold, i.e. constrained to lie among a fixed subset of states, while the disjoint problem of using GLR for degradation in either process or measurement noise is tackled by Liu [58].

The complexity of GLR is due in part to the number of matrix inversions required. Under favourable conditions the Kalman filter itself can be simplified by sequential processing (Sorenson [59]) and it is shown by Chang and Dunn [60], [61] that if a sequential filter is used in conjunction with a new recursive form of GLR then the requirement for matrix inversion in the previously known GLR algorithms can be reduced or avoided.

In his PhD thesis, Pouliezos [62] carried out simulations on a scalar system to test an innovations based scheme partially reliant on GLR techniques. Different types of fault affect the innovation statistics in different ways and Pouliezos showed that the type of fault could be narrowed down by testing for mean, variance and whiteness. This partial fault isolation overcomes to some extent the

difficulty with GLR of having to select the failure signature matrix in accordance with a particular fault type. The algorithm presented in [62] tested the innovation statistics and then switched to fault identification via GLR using the appropriate failure signatures. By concentrating on a scalar system, Pouliezos was able to develop recursive schemes for most aspects of his work resulting in a high computational efficiency.

1.2 Problem statement

It is apparent from the literature survey that many recent papers on fault detection are theoretical, although some include a simple illustrative example. This project aims to tackle the subject the other way round, starting with part of an existing plant and attempting to design for it a suitable fault detection system. It takes its cue from Willsky [27]: "At this time most of the work has been at a theoretical level with only a few real applications of techniques. Much work is yet to be done in the development of implementable systems complete with a variety of design tradeoffs."

The contributions of Bellingham and Lees, particularly [50], are of course a step in this direction. This project can perhaps be viewed as a logical extension to their work in that it considers part of a real plant rather than an isolated loop built as a laboratory rig. It is however intended that rather more instruments should be monitored than in [50] and that fault detection algorithms should be tested at setpoints other than those at which they were set up.

1.2.1 Choice of plant

The Department of Chemical Engineering at Imperial College has available two pilot plants, a fractional crystallization plant and a gas separation plant. The former, which separates an aqueous solution of potassium nitrate and sulphate, takes several hours to reach steady state. There is also a tendency for some of the pipework to become clogged with crystals, making this plant appear rather an

unattractive proposition. The other plant, which separates a mixture of Carbon Dioxide and Nitrogen, is used extensively for both undergraduate and graduate work and takes less than an hour to reach steady state. This appeared much more suitable for a detailed study involving experimental work and formed the basis for the research work presented in this thesis.

The first task was to delineate a part of the plant for further study. This project was carried out under the auspices of the Control Section of the Department of Electrical Engineering with laboratory facilities made available by the Department of Chemical Engineering. It was not intended that the work should include modelling of complex chemical reactions and accordingly the research was confined to a part of the plant involving purely physical processes. This involves no real loss of generality since much of the equipment in a chemical plant is necessary purely to 'condition' the reacting substances as regards their temperature, pressure, flow rate, etc.

The plant is described in Appendix I where Fig A1.1, a simplified Piping and Instrumentation Diagram (P.& I.D.), is to be found. With regard to instrument failure and the safe running of the plant, the most critical loops are those given in the table accompanying the P.& I.D, i.e. the column pressures, the MEA and cooling water flow rates and the absorber level. Since modelling of either column involves chemical reactions it was decided that attention should be focussed on the instrumentation in the area of the heat exchanger and cooler (Section 'A' of Fig A1.1). If time permitted a possible extension was to include Section 'B', the absorber level control loop.

1.2.2 Faults considered

Himmelblau [26] discusses many faults associated with plants to be found in the chemical industry. These fall broadly into three categories: plant, measurement and control. The

first of these includes blockages, leaks and mechanical failure while the second and third cover the two facets of every control loop whether manual or automatic. The major part of the 'control' category concerns actuator failures, including sticking or leaking valves.

This research is limited to the second category, namely faults in the measuring instruments whether used merely as indicators or incorporated into control loops. There is considerably more to a measurement loop than just the measuring element. The Section 'A' instrumentation includes resistance temperature detectors (r.t.d.'s), orifice plates, R/I transducers and differential pressure transmitters, the process variables being transmitted to the computer as 4-20 mA analog signals. By the time a process variable becomes available to the c.p.u. it has travelled via several pieces of equipment including a real-time interface and an analog-to-digital converter. This project seeks to detect a fault and to isolate it wherever possible to a particular measurement loop. The tracing of a fault to a certain 'instrument' is not intended to imply anything further than the identification of the faulty loop and the words 'fault' and 'failure' are used interchangeably.

Four types of faults are considered and these are shown diagrammatically in Fig.1. Types (a) - (c) can be associated with any instrument while type (d) is applicable only to a temperature loop where a break or loose connection in an r.t.d. lead is interpreted as a high resistance causing the temperature variable to stick at the top of the range. In common with previous work attention is concentrated on 'step' faults where a sudden bias appears on the instrument output. The sharp step is of course idealized; in practice such a fault may be due to the formation of air bubbles in the piping to a pressure transmitter or associated with mechanical damage.

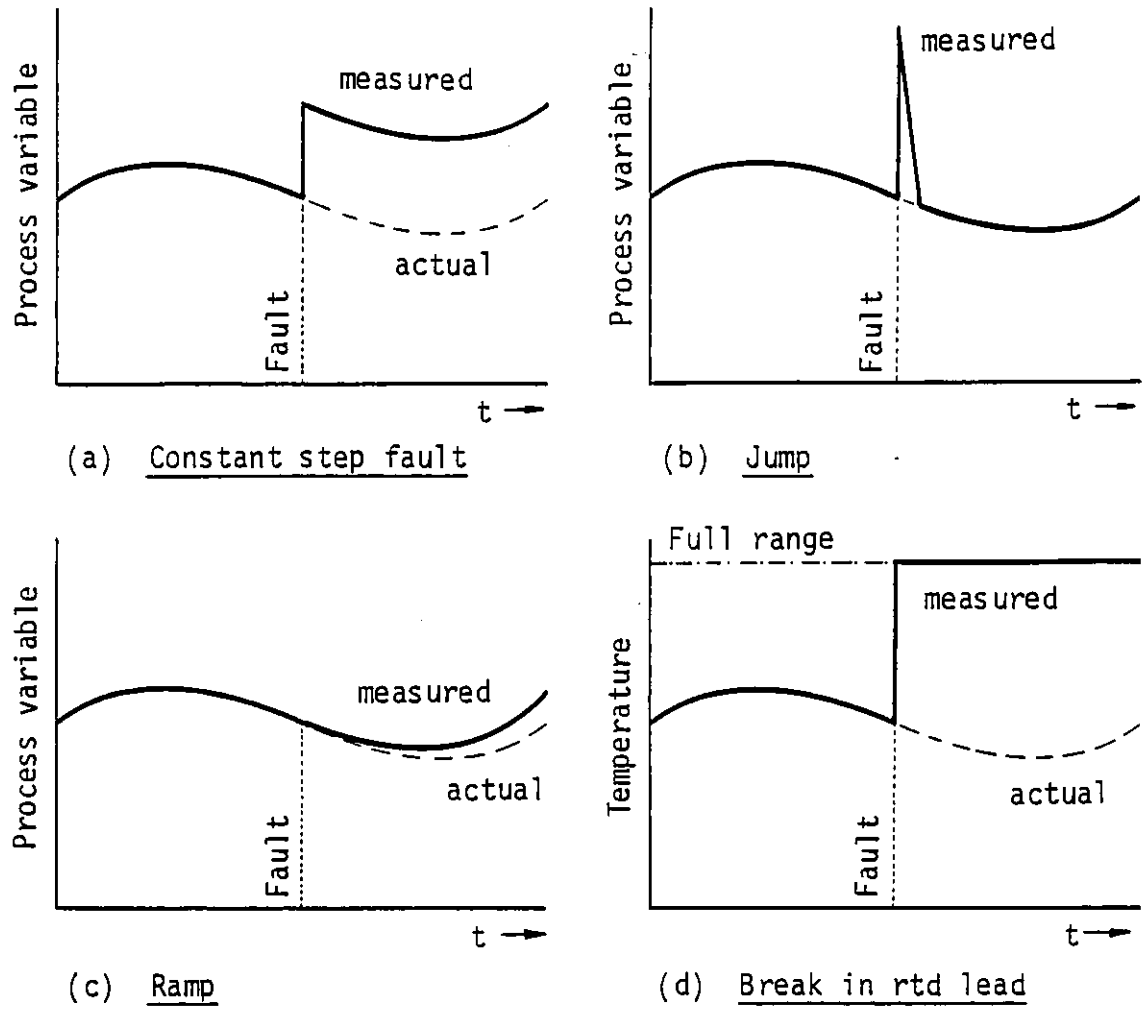

Fig.1 Instrument faults

1.2.3 Approach to the problem

The literature survey indicates that Kalman filters have been used in a variety of ways to detect and isolate faults. It must be borne in mind that some of these techniques, notably the multiple hypothesis methods and GLR, are heavily model dependent and that a real plant may not be sufficiently amenable to accurate mathematical representation.

Continuing on the theme of this project as a logical extension of the work of Bellingham and Lees [50] it seems reasonable to stay with the innovations based techniques since the innovation sequence seems tailor made for fault detection. The innovation vector for a model based on Section 'A' of the plant (Fig A1.1) will have more than

the two components of [50] and leads to the possibility of extracting more information from the innovations than just a shift in mean. Several researchers, notably Beard [31], have utilized the direction of the post-fault innovation vector for fault identification while the steady state innovation direction, used by Chien [46] and touched upon as a possible simplification of GLR by Willsky [27], may well be suitable for the pilot plant which is designed to run in the steady state for long periods.

It would also be possible to estimate instrument biases either by augmenting the state vector or by employing Friedland's bias filter [15], but with several instruments to choose from it is difficult to decide which biases should be estimated. In any case such augmentation adds considerably to the computational load and, with the accent on designing an implementable system, such a refinement is to be avoided if at all possible. Another source of added computational loading is the addition of artificial measurement noise. Clearly an existing plant is 'realistic' without the addition of such noise (cf.[20], [22] and [49]) but the addition of noise to make the filter work at all is quite a different matter and may be unavoidable (see e.g. [9], [50]).

It was decided that work should concentrate on obtaining the simplest (i.e. lowest order) model possible for Section 'A' of the plant, with no state vector augmentation and minimal addition of refinements. The only design criterion would be that at the end of the day the model should be suitable for fault detection purposes, with accurate state estimation a secondary consideration. To quote Newell and Fisher [19]: "In engineering applications, the value of a model is not usually judged by its mathematical rigour or the elegance of the derivation but rather how well it fulfills a specific need in comparison with other alternatives".

It was further decided that all modelling work and testing of fault detection algorithms would be carried out with

real plant data. In order to allow the comparison of different algorithms under identical conditions the plant data was recorded on paper tape and the algorithms tested off-line with superimposed instrument faults.

1.3 Contributions

The main contributions of this work are:-

(i) The development of a new steady state representation for a heat exchanger based on a nonlinear three-fluid model and verified with real plant data.

(ii) Proof that the three-fluid approach becomes mathematically intractable when applied to the transient case.

(iii) A simplified approach to transient heat exchanger modelling, based on partial derivatives obtained from the steady state three fluid model and verified with real plant data.

(iv) Determination of the transient and steady state effects of input and output step faults on the Kalman filter.

(v) Design of a suboptimal filter with enhanced fault detection capabilities by the manipulation of the constant Kalman gain.

(vi) Derivation of the expected value and error covariance of the estimate of fault magnitude.

(vii) Testing of two log-likelihood ratio (LLR) fault detection algorithms for a 6-state system using real plant data.

(viii) Suggestions for extension of the system to include a level control loop.

while miscellaneous minor contributions include:-

(ix) A new proof by linear algebra of the equivalence of the deterministic observability criteria of Kalman and Rosenbrock.

(x) Extension to the discrete-time case of Friedland's work on the estimation error and innovation covariances for the suboptimal filter.

(xi) Analysis of false and miss alarm probabilities for a system with one possible fixed fault and indication that the analysis breaks down when applied to the LLR algorithms.

1.4 Claim of originality

All of the work contained within this thesis is original work unless otherwise stated. In particular this research was carried out independently of work on fault detection in progress concurrently in the Department of Chemical Engineering at Imperial College.

CHAPTER 2

PLANT MODELLING IN THE STEADY STATE

2.0 Introduction

The underlying purpose of the project is to take a specific plant and to design, for at least a part of it, a system capable of detection and isolation of measurement faults. The introductory chapter discussed the selection of a suitable plant and delineated a section of it for detailed study. If the suggested Kalman filter approach is to be adopted then the initial task is to build a state space model for this subsystem.

The APV Paraflow "Junior" is a plate-type heat exchanger consisting of a number of metal plates clamped together in such a way that the hot and cold liquids pass in counter flow through alternate plates. The pilot plant heat exchanger is built up from 105 of these 258cm^2 plates while the cooler has only 19. In view of the similarity of the units it seems reasonable to suppose that the same model could be used for either, simply by employing two different sets of physical constants (cf. the modular approach of Newell and Fisher in [19]).

This chapter takes as a basic process unit a single counter flow heat exchanger and attempts under steady state conditions to relate the outlet temperatures of the two liquids to the inlet temperatures and the flow rates by consideration of heat balances. Consistent with the declared aims of Chapter 1 each model is judged solely by its ability to reproduce the observed plant measurements. We start with the simplest model available making no attempt to represent mathematically the true physical conditions inside the process unit itself. Only if this model proves inadequate is it rejected in favour of a more complex representation.

2.1 Previous work on plant modelling

Information on previous work comes from two sources: published work on plate-type heat exchangers and research work on the pilot plant itself.

2.1.1 The plate-type heat exchanger

This type of heat exchanger has been used in industry in its present form since the 1930's and has many advantages over other types of exchanger, including greater compactness and accessibility of heat transfer surfaces for cleaning purposes (Usher [63]). The plate design causes turbulence in the fluid flow at Reynolds numbers as low as 200, resulting in higher heat transfer coefficients than shell-and-tube units operating at the same Reynolds number. (Lawry [64]).

Most published work is concerned with design methods for determining the number of plates necessary to comply with a certain process fluid temperature specification. Buonopane et al [65] employ empirical methods for calculating the convection coefficients at the plate surfaces and also take account of flow configuration.

From a modelling point of view, it is necessary to make some assumptions regarding the temperature distribution within the unit. Given flow rates and inlet and outlet temperatures, the heat transfer coefficients follow from calculation of the mean temperature difference between fluids. Buonopane's work assumes that heat losses to the surroundings are negligible and employs a logarithmic mean temperature difference used in conjunction with a correction factor dependent on flow rate and configuration.

2.1.2 Previous work on the pilot plant

The pilot plant has been the subject of several research projects over the years and models for many different purposes have been developed. Palmquist [66] utilizes results from several sources, particularly Albrecht [67] and Roberts [68], to develop a simplified 21 state,

5 input state space model for the whole plant. Palmquist's work is mainly concerned with model order reduction and uses borrowed plant data for numerical work.

As far as the heat exchanger units are concerned, Palmquist does not consider the actual flow configuration but uses a simple 'lumped parameter' model. It must be borne in mind that this project does not set out to derive an accurate model for a heat exchanger, rather to develop a model that is 'good enough' to use in conjunction with a Kalman filter. Palmquist's approach is perhaps more attractive than a highly theoretical approach if it can be made to work in practice over a range of operating points.

2.2 Experimental work for modelling purposes

Initial experiments on the plant included two runs for modelling purposes: 'PLANT2' and 'PLANT3', the plant being run in closed loop for these and all other project runs. Only six of the twelve control valves on the plant are shown in Fig. A1.1 (Appendix I) and of these all except CV102 are incorporated into control loops. Of the remaining six, two are not used in the closed loop configuration while four are used in loops for 'utility' flows: Carbon Dioxide and Nitrogen feeds, condenser cooling water flow and steam supply.

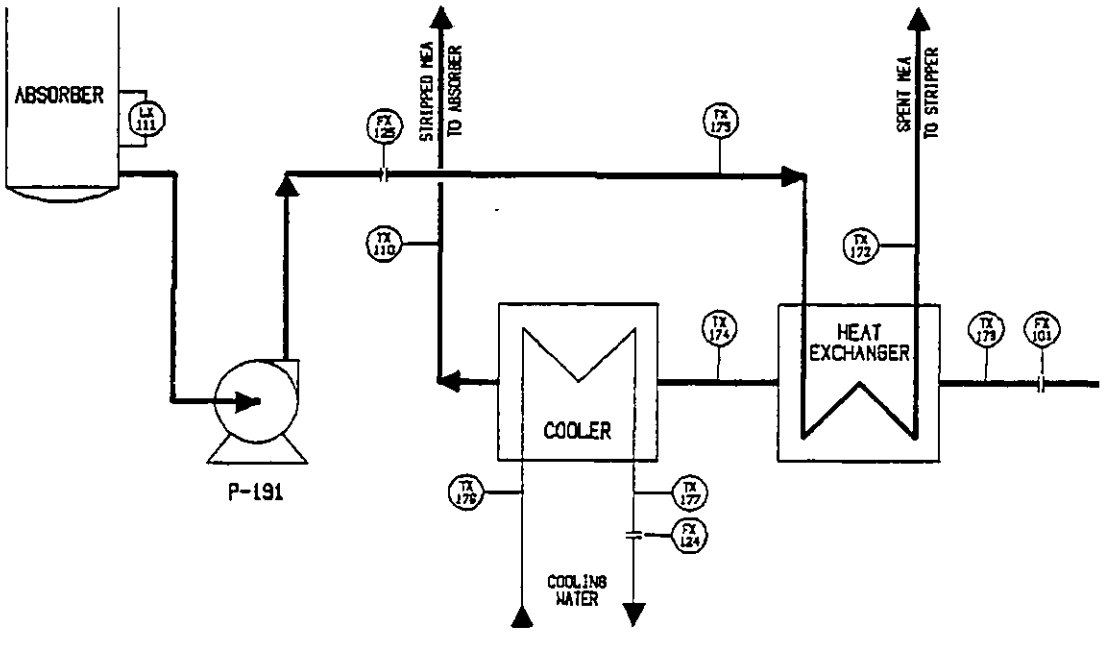

FIG. 2 SCHEMATIC DIAGRAM SHOWING MEASURED VARIABLES FOR RUNS PLANT 2 & 3

It was important to ensure that for consistency the five main loops listed in Fig. A1.1 (Appendix I) were configured in exactly the same way for each plant run. Suitable values for the PID algorithm control terms were obtained from the plant literature and entered via the operator's console. These values were used for all subsequent plant runs and can be found in Appendix I.

Readings from flow instruments FX101, FX124 and FX125 were carefully zeroed before starting up the plant, and on reaching steady state a simple heat balance was performed on each heat exchange unit on each occasion as a rough check on some of the temperature readings. Process variables from the eleven instruments shown in Fig. 2 were recorded on paper tape. The sampling interval was in each case dictated by the purpose of the experiment, but could not be made arbitrarily small due to the finite time taken by the high speed punch to output a group of eleven data points.

2.2.1 Run 'PLANT2'

The purpose of this run was to obtain a steady state data record for analysis of plant and measurement noise statistics (see Chapter 4). The plant was allowed a two hour run up before commencement of data logging to ensure that all temperatures were as steady as possible. For statistical analysis a data set recorded over approximately 1000 time steps is required and a sampling interval of ten seconds was chosen in order to obtain this number of points in a reasonable time.

The plant was set up as shown in Table 1 and the average values of the process variables of interest are summarized in Table 2.

TABLE 1

CONTROL LOOP		Controlled Variable	Setpoint
Valve	Inst.		
CV101	FX101	Stripped MEA flow	0.25 kgs^{-1}
CV104	PX104	Absorber pressure	250 kNm^{-2}
CV107	PX107	Stripper pressure	105 kNm^{-2}
CV110	FX124	Cooler c/w flow	0.25 kgs^{-1}
CV111	LX111	Absorber level	0.3 m

The paper tape ran out after just over two and a half hours so that 924 data sets were in fact recorded.

TABLE 2

Minutes into run:		0-5	149-154		0-5	149-154
FLOW RATE kgs^{-1}	FX101	0.25	0.25	FX124	0.25	0.25
TEMPERATURE °C	TX110	20.0	20.9	TX175	21.69	22.42
	TX172	87.2	87.5	TX176	9.54	10.59
	TX173	101.4	101.6	TX177	23.92	24.72
	TX174	34.7	35.4	Ambient	21.5	21.7

Exchanger heat balance check: the heat gain by the 'cold' liquid should be slightly lower than the heat loss by the 'hot' liquid due to losses to the atmosphere.

Cooler:	cooling water gain	15,042W
	stripped MEA loss	15,376W
Heat exchanger:	spent MEA gain	68,524W
	stripped MEA loss	69,768W

Cooling water for the plant comes from a closed loop system supplying the whole Chemical Engineering laboratory. As the water is piped to a cooler on the roof of the building and then returned to the plant, its temperature is dependent on the outdoor ambient temperature. If the pilot plant is run for a period of several hours, then the temperature (TX176) of the water supplied to the cooler rises slightly, causing other temperatures around the plant to increase by a small amount. This is reflected in the readings obtained, which are quoted in Table 2 as 31 point (5 minute) averages taken from the beginning and the end of the PLANT2 run. Data is quoted to the same number of significant figures as obtained from the paper tape record, this varying with the range of the process variable concerned. PLANT2 data used for steady state modelling is from the beginning of the run.

As the absorber liquid level remains constant, the mean flow rates measured by FX101 and FX125 should be equal, although the latter will have a higher variance. Mean values calculated for PLANT2 are 0.250 kgs^{-1} for FX101 and 0.230 kgs^{-1}, 8% lower, for FX125. This difference may be due to bias in one or both of the measurement loops, but any significant departure from the nominal temperature and pressure used for orifice plate design would also be a contributory factor.

2.2.2 Run 'PLANT3'

It is apparent from Fig. 2 that each heat exchange system has four inputs and two outputs:

Cooler

Inputs:

Stripped MEA inlet temperature TX174 and flow rate FX101.

Cooling water inlet temperature TX176 and flow rate FX124.

Outputs:

Stripped MEA outlet temperature TX110.

Cooling water outlet temperature TX177.

Heat Exchanger

Inputs:

Stripped MEA inlet temperature TX173 and flow rate FX101.
Spent MEA inlet temperature TX175 and flow rate FX125.

Outputs:

Stripped MEA outlet temperature TX174.
Spent MEA outlet temperature TX172.

The purpose of run PLANT3 was to investigate the dynamics of these units by studying responses to step changes in the inputs. This line of study is pursued in Chapter 3, but several points should be noted here:

(i) TX174 is an output of the heat exchanger but is also an input to the cooler.

(ii) All temperature inputs are dictated by operating conditions elsewhere in the plant and, as a consequence, it is not possible to change these inputs suddenly. Experiment is thus limited to applying step changes to the flow rates by changing the flow setpoints at the operator's console (see Appendix I).

(iii) After an MEA or cooling water setpoint change the initial transient dies away after three or four minutes. The change in MEA temperature, however, propagates slowly through the absorber causing temperature drifting which may take half an hour to settle down.

Four step response experiments were carried out as detailed in Table 3, using the same control loop parameters and pressure and level setpoints as for PLANT2 (Table 1). The plant was allowed to return to the steady state after each setpoint change, and each experiment was recorded on a separate paper tape using a sampling interval of ten seconds. These tapes provide data on system transients and a further six sets of steady state temperatures.

TABLE 3

Expt No (ambient)	mins Total	mins expt.	Stripped MEA flow setpoint	Cooler c/w flow setpoint	Remarks	s/s data set
3/E1	0	0	0.2 kgs^{-1}	0.25 kgs^{-1}	Steady	3/1
	2	2	↑ 0.25 kgs^{-1}		Step MEA	
(21.7°C)	28	28			e-o-t	
3/E2	38	0	0.25 kgs^{-1}	0.25 kgs^{-1}	Steady	3/2
	40	2	↑ 0.27 kgs^{-1}		Step MEA	
(22.1°C)	52	14			e-o-t	
	68		0.27 kgs^{-1}	0.25 kgs^{-1}	Steady	3/3
			↓ 0.25 kgs^{-1}	↓ 0.2 kgs^{-1}	'reset'	
3/E3	110	0	0.25 kgs^{-1}	0.2 kgs^{-1}	Steady	3/4
	112	2		↑ 0.25 kgs^{-1}	Step c/w	
(22.1°C)	125	15			e-o-t	
3/E4	150	0	0.25 kgs^{-1}	0.25 kgs^{-1}	Steady	3/5
	154	4		↑ 0.27 kgs^{-1}	Step c/w	
(22.1°C)	166	16			e-o-t	
	179		0.25 kgs^{-1}	0.27 kgs^{-1}	Steady	3/6

e-o-t end of tape. i.e. tape switched off to wait for temperatures to settle down before next experiment.

c/w cooling water.

s/s steady state.

↑,↓ direction of setpoint change, new setpoint.

Heat balance check on data set 3/1

Cooler:	cooling water gain	11966 W
	stripped MEA loss	12050 W
Heat exchanger:	spent MEA gain	55296 W
	stripped MEA loss	55982 W

2.2.3 Summary of steady state data

Steady state operating temperatures from PLANT2 and PLANT3 are summarized in Table 4. Process fluid temperatures quoted for PLANT3 are averaged over the periods immediately prior to flow rate setpoint changes, with the exception of 3/3 and 3/6 which were obtained directly from the operator's console. For steady state modelling purposes cooling water and stripped MEA flow rates are taken to be equal to their respective setpoint values. The steady state spent MEA flow rate is assumed equal to the stripped MEA flow rate.

TABLE 4

run/data set:	2	3/1	3/2	3/3	3/4	3/5	3/6
FX101 kgs^{-1}	0.25	0.2	0.25	0.27	0.25	0.25	0.25
FX124 kgs^{-1}	0.25	0.25	0.25	0.25	0.2	0.25	0.27
TX110 °C	20.0	20.3	22.4	23.3	24.2	21.9	21.3
TX172 °C	87.2	88.6	87.6	87.1	87.8	87.6	87.3
TX173 °C	101.4	101.6	101.4	101.4	101.4	101.4	101.3
TX174 °C	34.7	34.7	36.7	37.6	38.0	36.4	35.9
TX175 °C	21.69	22.52	23.55	24.02	25.04	23.19	22.57
TX176 °C	9.54	12.96	12.48	12.17	12.14	11.76	11.71
TX177 °C	23.92	24.40	26.22	27.00	29.05	25.69	24.66
Ambient °C	21.5	21.7	22.1	22.1	22.1	22.1	22.1

2.3 A simple model

Palmquist [66] models each heat exchange system as a pair of tank reactors with temperature averaging. This idea should not be confused with the more commonly used 'continuously stirred tank reactor' (CSTR) in which it is assumed that the body of liquid in the reactor is at the same temperature as the outlet. Palmquist's reactors could be described as 'partially stirred tank reactors' and will henceforth be referred to as PSTR's. The

following assumptions are taken from [66]:

(i) The mean temperature of the fluid in a PSTR is taken to be the average of the inlet and outlet temperatures. (This is equivalent to assuming a linear temperature profile between inlet and outlet).

(ii) The rate of heat transfer between a pair of PSTR's is proportional to the difference between their mean temperatures.

(iii) The heat loss to the air by the heat exchanger is negligible compared with the heat transfer between fluids due to the large number of plates.

(iv) In the cooler, only the 'hot' MEA loses heat to the air, at a rate proportional to the PSTR temperature excess over ambient.

The rtd's are not located at equal distances from the process unit end plates but no correction is made for this: the heat losses from the connecting pipework to the air are lumped in with the losses from the exchanger itself.

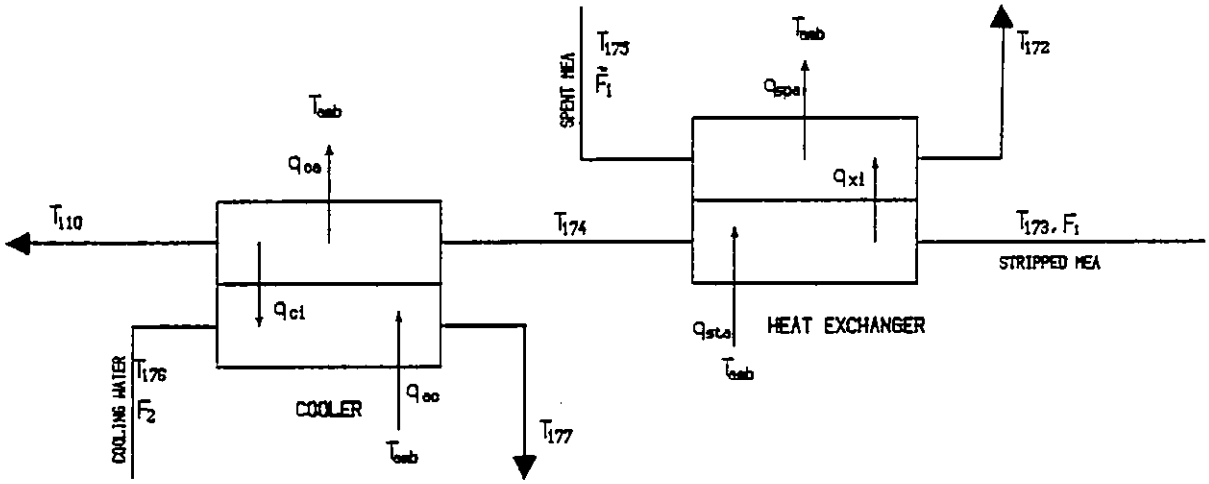

Fig.3 A simple model based on PSTR's

The process variables and heat transfer paths are shown in Fig. 3 where

T_{IJK} = fluid temperature measured by instrument TXIJK.

F_1 = stripped MEA flow rate ($E[F_1]$= setpoint)

$\tilde{F}_1$ = spent MEA flow rate ($E[\tilde{F}_1]$= $E[F_1]$ under s/s conditions)

F_2 = cooler c/w flow rate ($E[F_2]$= setpoint)

2.3.1 Comparison of prediction errors

In order to compare models based on different assumptions it is necessary to introduce a cost function for the prediction errors. Given the ambient temperature, the two liquid flow rates and one input or output temperature for each, the modelling equations can generally be manipulated to allow prediction of the remaining two temperatures (see Fig. 4 and Tables 5 and 7).

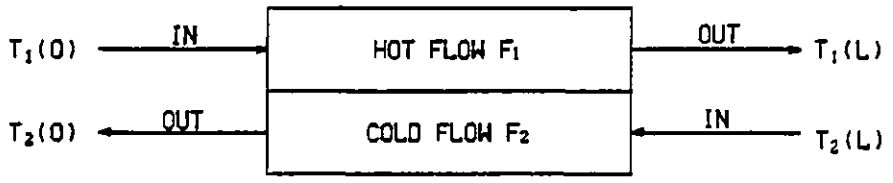

Fig.4 Inlet/outlet temperatures for counter flow heat exchanger

TABLE 5

COOLER			
$T_1(0)$	TX174	$T_1(L)$	TX110
$T_2(0)$	TX177	$T_2(L)$	TX176

For reasons that will become apparent in Section 2.5, the cost function selected is based on prediction of temperatures at the 'cold' end of the exchanger. Writing for the ith data set:

$$\underline{\varepsilon}_i = \begin{bmatrix} (\varepsilon_1)_i \\ (\varepsilon_2)_i \end{bmatrix} = \begin{bmatrix} T_1(L) - \hat{T}_1(L) \\ T_2(L) - \hat{T}_2(L) \end{bmatrix}_i$$

we define for 'n' data sets the cost function:

$$J_1 = \tfrac{1}{2}\,\underline{\varepsilon}^T\underline{\varepsilon} = \sum_{i=1}^{n} \tfrac{1}{2}\{(\varepsilon_1)_i^2 + (\varepsilon_2)_i^2\}$$

2.3.2 A simple cooler model based on a linear temperature distribution

With reference to Fig. 4 and using Palmquist's assumptions (i), (ii) and (iv) a steady state heat balance for the cooler gives:

heat loss by MEA = loss to coolant, $q_{c\ell}$ + loss to air, q_{ca}

$$F_1.C_p(T_{174} - T_{110}) = K_{c\ell}.\tfrac{1}{2}\{T_{174} + T_{110} - (T_{177} + T_{176})\} + K_{cma}\{\tfrac{1}{2}(T_{174} + T_{110}) - T_{amb}\} \ldots (2.1)$$

heat gain by water = gain from MEA, $q_{c\ell}$

$$F_2.C_p(T_{177} - T_{176}) = K_{c\ell}.\tfrac{1}{2}\{T_{174}+T_{110}-(T_{177}+T_{176})\} \ldots (2.2)$$

where K denotes a heat transfer coefficient (Units: WK^{-1})
Each heat exchange unit is of fixed dimensions and so wall thicknesses and areas can be absorbed into coefficient .

subscript 'cℓ': denotes transfer between cooler liquids.
subscript 'cma': denotes transfer between MEA and air.
C_p denotes specific heat (at constant pressure):
value taken to be 4184 $Jkg^{-1}K^{-1}$ for both MEA and water.

At this point a decision must be made as to how best to obtain $K_{c\ell}$ and K_{cma} from the available data. If the cost function J_1 is to be used for model evaluation and comparison then it must be calculated for each model. Furthermore the coefficients should be calculated such that J_1 is minimized, thus presenting the model in the most favourable light.

Study of equations (2.1) and (2.2) reveals that while calculation of J_1 involves a fair degree of manipulation, any attempt to minimize J_1 over $K_{c\ell}$ and K_{cma} is going to be a long and tedious task. While the model may suit the cooler it is possible that it may prove inadequate for the

heat exchanger in which case the effort put into minimizing J_1 is wasted. Clearly there is a case for estimating the coefficients by the simplest means possible to get a quick indication as to the suitability of the model. The values can always be re-estimated at a later stage if justified.

If temperature values are substituted from Table 4 then equation (2.2) yields $K_{c\ell}$ directly allowing (2.1) to be solved for K_{cma}. Coefficients calculated by this means are given in Table 6 where the final estimates are taken to be the mean values over the seven data sets.

TABLE 6

Run	$\hat{K}_{c\ell}$ WK^{-1}	$\hat{K}_{cma}$ WK^{-1}	Run	$\hat{K}_{c\ell}$ WK^{-1}	$\hat{K}_{cma}$ WK^{-1}
2	1416	57.2	3/4	1347	31.6
3/1	1357	14.4	3/5	1398	84.6
3/2	1409	78.6	3/6	1405	98.8
3/3	1428	76.9	mean	1394	63.2

The standard deviation is 28 WK^{-1} in each case. This is reasonable for $\hat{K}_{c\ell}$ (2%) but is a 45% deviation on $\hat{K}_{cma}$. Evaluation of the cost function gives $J_1 = 0.60$ which can be thought of as an upper bound for the model.

2.3.3 A modified linear distribution model for the cooler

In accordance with Palmquist's assumption (iv), Section 2.3.2 presupposes that only the 'hot' MEA, on average some 7°C above ambient, loses heat to the air. The resulting estimated coefficient for this transfer, K_{cma}, has a high standard deviation, suggesting that a modification to the modelling assumptions might be necessary. The cooling water temperature is on average around 3°C below ambient and so it is reasonable to suppose that heat is gained from the air. Equation (2.2) becomes:

heat gain by water = gain from MEA, $q_{c\ell}$ + gain from air, q_{ac}

$$F_2.C_p(T_{177} - T_{176}) = K_{c\ell}\tfrac{1}{2}\{T_{174} + T_{110} - (T_{177} + T_{176})\} + K_{cwa}\{T_{amb} - \tfrac{1}{2}(T_{177} + T_{176})\} \ldots \quad (2.3)$$

where K_{cwa} is the new 'air to water' heat transfer coefficient.

It is no longer possible to calculate coefficients for each data set as the pair of equations (2.1) and (2.3) contains three unknowns. Minimization of J_1 is clearly no easier than it was in the previous case and continuing the policy of taking the line of least resistance we look for an alternative method of obtaining a quick evaluation. Estimates can be obtained by defining a new cost function, J_2, and minimizing it by means of the following theorem.

Theorem 2.1

Consider the minimization of the quadratic function

$$V(\underline{x}) = p + \langle \underline{\sigma}, \underline{x} \rangle + \tfrac{1}{2} \langle \underline{x}, C\underline{x} \rangle$$

with $p \in R$; $\underline{x}, \underline{\sigma} \in R^n$ and $C = C^T > 0 \in R^{nxn}$ (the set of nxn matrices with finite real elements).

We require the point $\hat{\underline{x}} \in R^n$ which minimizes $V(\underline{x})$ on R^n.

Besides ensuring that C is nonsingular, the condition $C > 0$ implies that $V(\underline{x})$ is strictly convex and therefore has a unique local minimum and a unique globally minimizing $\hat{\underline{x}}$ given by:

$$\arg\min_{\underline{x} \in R^n} V(\underline{x}) = \{-C^{-1}\underline{\sigma}\}$$

■

This is a standard result and may be found in [69]

Equations (2.1) and (2.3) are of the form

$$aK_{cma} + bK_{c\ell} = g \quad \ldots \quad (2.4)$$

$$dK_{cwa} + bK_{c\ell} = h \quad \ldots \quad (2.5)$$

where

$$a = \{\tfrac{1}{2}(T_{174} + T_{110}) - T_{amb}\} \quad \ldots \quad (2.6a)$$

$$b = \tfrac{1}{2}\{T_{174} + T_{110} - (T_{177} + T_{176})\} \quad \ldots \quad (2.6b)$$

$$d = \{T_{amb} - \tfrac{1}{2}(T_{177} + T_{176})\} \quad \ldots \quad (2.6d)$$

$$g = F_1.C_p\,(T_{174} - T_{110}) \quad \ldots \quad (2.6g)$$

$$h = F_2.C_p\,(T_{177} - T_{176}) \quad \ldots \quad (2.6h)$$

We now define a prediction error for the power loss terms of (2.4) and (2.5): $\hat{g}_i$ and $\hat{h}_i$ are predicted power losses calculated from coefficient estimates $\hat{K}_{c\ell}$, $\hat{K}_{cma}$ and $\hat{K}_{cwa}$ and the temperature values from data set 'i'

$$(\delta_1)_i = \hat{g}_i - g_i = a_i \hat{K}_{cma} + b_i \hat{K}_{c\ell} - g_i$$

$$(\delta_2)_i = \hat{h}_i - h_i = d_i \hat{K}_{cwa} + b_i \hat{K}_{c\ell} - h_i$$

The problem is to choose the value of $\underline{k}^T = [\hat{K}_{cma}\ \hat{K}_{cwa}\ \hat{K}_{c\ell}]$ such that these errors are minimized in some sense.

Defining a new cost function for 'n' data sets:

$$J_2 = \sum_{i=1}^{n} \tfrac{1}{2}\{(\delta_1)_i^2 + (\delta_2)_i^2\}$$

we require

$$\underline{\hat{k}} = \arg\min_{\underline{k} \in R^3} J_2(\underline{k})$$

$$= \arg\min_{\underline{k} \in R^3} \sum_{i=1}^{n} \tfrac{1}{2}\{a_i\hat{K}_{cma}+b_i\hat{K}_{c\ell}-g_i\}^2+\tfrac{1}{2}\{d_iK_{cwa}+b_i\hat{K}_{c\ell}-h_i\}^2 \quad \ldots (2.7)$$

The cost function can be written in matrix form as

$$J_2(\underline{k}) = p + \langle\underline{\sigma},\underline{k}\rangle + \tfrac{1}{2}\langle\underline{k},C\underline{k}\rangle \quad \ldots (2.8)$$

where, for data sets $i = 1,\ldots,n$

$$p = \tfrac{1}{2}\Sigma_i g_i^2 + \tfrac{1}{2}\Sigma_i h_i^2$$

$$\underline{\sigma}^T = -\begin{bmatrix} \Sigma a_i g_i & \Sigma d_i h_i & \Sigma b_i (g_i + h_i) \end{bmatrix}$$

$$C = \begin{bmatrix} \Sigma a_i^2 & 0 & \Sigma a_i b_i \\ 0 & \Sigma d_i^2 & \Sigma b_i d_i \\ \Sigma a_i b_i & \Sigma b_i d_i & 2\Sigma b_i^2 \end{bmatrix}$$

and $\underline{k}^T = \begin{bmatrix} \hat{K}_{cma} & \hat{K}_{cwa} & \hat{K}_{c\ell} \end{bmatrix}$

Clearly $C = C^T$ and provided that $C > 0$, the vector $\underline{\hat{k}}$ that minimizes $J_2(\underline{\hat{k}})$is given by Theorem 2.1 as

$$\underline{\hat{k}} = -C^{-1}\underline{\sigma} \quad \ldots (2.9)$$

Using this method for data sets PLANT2, PLANT3/j, j=1,...6 we obtain

$$\underline{\hat{k}} = \begin{bmatrix} \hat{K}_{cma} \\ \hat{K}_{cwa} \\ \hat{K}_{c\ell} \end{bmatrix} = \begin{bmatrix} 41.0 \\ 53.0 \\ 1374 \end{bmatrix} \quad WK^{-1}$$

Evaluation of the 'comparison' cost function for these coefficients gives the value $J_1 = 0.75$. Note that had Sections 2.3.2 and 2.3.3 actually minimized J_1 over the coefficient vector $\underline{k}$ then the latter would have generated a J_1 value less than or equal to that generated by the former because of the additional parameter. As it is the J_1 values are only approximately minimized and the slightly higher value for J_1 in this case suggests that the modification is unlikely to bring about any great improvement.

2.3.4 A simple nonlinear model for the cooler

The models described in 2.3.2 and 2.3.3 both assume that the temperature profile of each liquid is linear between inlet and outlet. For the purpose of calculating the mean temperature difference between fluids ('b' of equations (2.4) and (2.5)), a tubular heat exchanger is usually modelled as a distributed system rather than as a pair of PSTR's. While it is true that the pilot plant exchangers are not of the tubular type there is no reason why such an approach should not be tried. A possible modification to the approach of 2.3.3 is to retain the assumption that there is heat transfer between each cooler fluid and the air, but to add that the temperature profile is governed only by the heat transfer between liquids. The distributed system theory could then be extended to the calculation of the mean temperature difference between each liquid and ambient (i.e. 'a' and 'd' of equations (2.4) and (2.5)) to account for losses.

Expressions are derived in Appendix II for mean temperatures θ_m, T_{1m} and T_{2m}. Symbols are as shown in

Fig. 5 and correspond to the cooler instrumentation tag numbers given in Table 5.

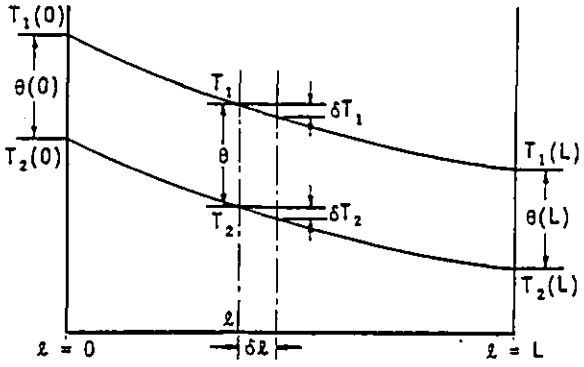

$T_1(\ell)$ = hot fluid temperature at 'ℓ'
$T_2(\ell)$ = cold fluid temperature at 'ℓ'
$\theta(\ell) = T_1(\ell) - T_2(\ell)$
T_{1m} = mean temperature hot fluid
T_{2m} = mean temperature cold fluid
θ_m = mean temperature difference

Fig. 5 Temperature profiles for counter flow heat exchanger

$$\theta_m = \frac{\theta(L) - \theta(0)}{\ell n\left[\frac{\theta(L)}{\theta(0)}\right]} \quad \ldots \quad (2.10)$$

$$T_{1m} = \frac{T_1(0)\theta(L) - T_1(L)\theta(0) - \theta_m\{T_1(0)-T_1(L)\}}{\theta(L) - \theta(0)} \quad \ldots \quad (2.11)$$

$$T_{2m} = \frac{T_1(0)\theta(L) - T_1(L)\theta(0) - \theta_m\{T_2(0)-T_2(L)\}}{\theta(L) - \theta(0)} \quad \ldots \quad (2.12)$$

Equations (2.6a, b & d) are thus replaced by (2.13a,b & d) as follows:

$$a = T_{1m} - T_{amb} \quad \ldots \quad (2.13a)$$

$$b = \theta_m \quad \ldots \quad (2.13b)$$

$$d = T_{amb} - T_{2m} \quad \ldots \quad (2.13d)$$

It should be noted that for runs PLANT2 and PLANT3/j, j = 1,...6, the value of θ_m is very nearly equal to 'b' as originally defined in (2.6b). Values of 'a' and 'd' tend to be marginally lower (less than 1°C) than their counterparts defined in (2.6a & d). The three heat transfer coefficients are calculated in exactly the same way as in 2.3.3 yielding

$$\underline{\hat{k}} = \begin{bmatrix} \hat{R}_{cma} \\ \hat{R}_{cwa} \\ \hat{K}_{c\ell} \end{bmatrix} = \begin{bmatrix} 65.5 \\ 19.7 \\ 1396 \end{bmatrix} \quad WK^{-1}$$

Evaluation of cost function J_1 for this model is much less straightforward than for the previous two cases because $T_1(L)$ and $T_2(L)$ cannot be obtained explicitly in terms of the other variables. Predicted values for $T_1(L)$ and $T_2(L)$ are obtained by a graphical technique as follows:

Given F_1, F_2, $T_1(0)$, $T_2(0)$ and T_{amb}, a computer is used to find, by trial and error, values of $T_1(L)$ that satisfy equation (2.4) for a range of $T_2(L)$ values extending to about half a degree on either side of the measured $T_2(L)$ value. The $\{T_1(L), T_2(L)\}$ pairs so obtained are plotted on graph paper giving a curve of possible solutions to (2.4). If the process is repeated for equation (2.5) over the same $T_2(L)$ range, a second curve can be plotted, the intersection of the two curves yielding the unique $\hat{T}_1(L)$ and $\hat{T}_2(L)$ values that simultaneously satisfy (2.4) and (2.5).

Temperature prediction by this means leads to a cost function value $J_1 = 0.42$, a 30% reduction on the previous 'best' value of 0.6 obtained with the original (Palmquist) assumptions. At this stage no one model stands out as the obvious choice: J_1 is only approximately minimized in each case and the one with the smallest prediction error as measured by J_1 has the disadvantage that its structure makes it difficult to work with. As it would be desirable to use the same model for cooler and heat exchanger, the choice must in any case be delayed pending evaluation of these approaches for heat exchanger modelling.

2.3.5 Suitability of simple methods for heat exchanger modelling

Although Palmquist's assumption (iii) (Section 2.3) neglects heat transfer from the heat exchanger to the air, the check heat balances show that both cooler and heat exchanger lose to atmosphere a similar percentage of the heat actually transferred between fluids.

Both the hot liquid (stripped MEA) and the 'cold' liquid (spent MEA) are at a higher temperature than the surrounding air and so it seems reasonable to suppose that each loses heat to the atmosphere. Following a parallel development to that of Section 2.3.3 and referring to Fig. 3:

Stripped MEA heat loss = loss to spent MEA, $q_{x\ell}$

+ loss to air, q_{sta}

$$F_1 . C_p(T_{173} - T_{174}) = K_{x\ell}\tfrac{1}{2}\{T_{173} + T_{174} - (T_{172} + T_{175})\} + K_{sta}\{\tfrac{1}{2}(T_{173} + T_{174}) - T_{amb}\} \quad \ldots (2.14)$$

Spent MEA heat gain = gain from stripped MEA, $q_{x\ell}$

- loss to air, q_{spa}

$$F_1 . C_p(T_{172} - T_{175}) = K_{x\ell}\tfrac{1}{2}\{T_{173} + T_{174} - (T_{172} + T_{175})\} - K_{spa}\{\tfrac{1}{2}(T_{172} + T_{175}) - T_{amb}\} \quad \ldots (2.15)$$

where the K - subscripts are

$x\ell$: transfer between heat exchanger liquids
sta : transfer between stripped MEA and air
spa : transfer between spent MEA and air

These equations, as (2.1) and (2.3), are of the form

$$a\,K_{sta} + b\,K_{x\ell} = g \quad \ldots (2.16)$$

$$-d\,K_{spa} + b\,K_{x\ell} = h \quad \ldots (2.17)$$

where

$$a = \{\tfrac{1}{2}(T_{173} + T_{174}) - T_{amb}\} \quad \ldots \quad (2.18a)$$

$$b = \tfrac{1}{2}\{T_{173} + T_{174} - (T_{172} + T_{175})\} \quad \ldots \quad (2.18b)$$

$$d = \{\tfrac{1}{2}(T_{172} + T_{175}) - T_{amb}\} \quad \ldots \quad (2.18d)$$

$$g = F_1.C_p\,(T_{173} - T_{174}) \quad \ldots \quad (2.18g)$$

$$h = \tilde{F}_1.C_p\,(T_{177} - T_{176}) \quad \ldots \quad (2.18h)$$

Using Theorem 2.1 once again for data sets PLANT2, PLANT3/j, j = 1, ... 6 we obtain

$$\underline{\hat{k}} \qquad \begin{bmatrix} \hat{K}_{sta} \\ \hat{K}_{spa} \\ \hat{K}_{x\ell} \end{bmatrix} = \begin{bmatrix} 13.0 \\ -0.4 \\ 4933 \end{bmatrix} \quad WK^{-1}$$

That there are problems associated with this method is evident from the negative value obtained for coefficient K_{spa}. Cost function J_1 comes out at 76.7 although this figure is distorted by very large prediction errors (over 8°) for $T_1(L)$ and $T_2(L)$ in data set PLANT3/1. Subtracting out the 3/1 errors still leaves J_1 at 4.73, very much higher than the value of 0.75 obtained using the same model for the cooler.

TABLE 7

HEAT EXCHANGER			
$T_1(0)$	TX173	$T_1(L)$	TX174
$T_2(0)$	TX172	$T_2(L)$	TX175

Turning now to the 'logarithmic mean' method of Section 2.3.4, 'a', 'b' and 'd' of equations (2.13a, b & d) are once again redefined, (2.19d) reflecting the fact that T_{2m} is now above ambient:

$$a = T_{1m} - T_{amb} \quad \ldots \quad (2.19a)$$

$$b = \theta_m \quad \ldots \quad (2.19b)$$

$$d = T_{2m} - T_{amb} \quad \ldots \quad (2.19d)$$

θ_m, T_{1m} and T_{2m} are calculated from (2.10, 2.11 and 2.12) bearing in mind that temperatures $T_1(0)$, $T_2(0)$ etc. now correspond to the heat exchanger instrumentation tag numbers in Table 7. The coefficients obtained are:

$$\underline{\hat{k}} = \begin{bmatrix} \hat{K}_{sta} \\ \hat{K}_{spa} \\ \hat{K}_{x\ell} \end{bmatrix} = \begin{bmatrix} -1341.9 \\ 1907.6 \\ 9637 \end{bmatrix} \quad WK^{-1}$$

For the seven data sets available, substitution of the logarithmic mean for the linear mean has no effect on the value of 'b'. Matrix 'C' and vector '$\underline{\sigma}$' equation (2.8), are also little altered, the maximum difference between the logarithmic and the linear case being a reduction of just 1.5% in $\sum_i d_i^2$. The new $\hat{K}$ values which minimize cost function $J_2(\underline{\hat{k}})$ are, however, not even approximately equal to those obtained for the linear model. The physical significance of the negative value for $\hat{K}_{sta}$ is that the stripped MEA (mean temperature nearly 70°C) is taking in heat from the air! Clearly there is now little point in re-estimating the cooler coefficients to minimize J_1.

The numerical instability can be explained by the use of an analogy. The cost function can be thought of as a very shallow dish in the x-y plane with the cost $J_2(\underline{\hat{k}})$ plotted in the vertical z-direction. For given parameters in equation (2.8), the lowest point on the dish surface corresponds to 'optimum' co-ordinates $\hat{x}$ and $\hat{y}$. Small changes in matrix C and vector $\underline{\sigma}$ of (2.8) cause the dish to tip up slightly and because it is so shallow this causes the co-ordinates of the lowest point on the surface of the dish, corresponding to coefficient estimates $\hat{K}$, to shift dramatically.

The fact that the two process units are physically similar begs the question as to why the linear and logarithmic approximations should be reasonably successful with the cooler but fail when applied to the heat exchanger. The reason is almost certainly connected with the fact that

these simple models neglect the influence of the heat loss to the air in shaping the fluid temperature profiles. The prime differences between the units are the temperatures of the fluids relative to ambient: clearly the influence of the heat loss is likely to be stronger for the heat exchanger than for the cooler which operates fairly close to the ambient temperature.

In the following development, which is original work, the exchanger is remodelled as a fully distributed three-fluid system in order to try and take account of the effects of the heat loss on the temperature profile for each channel It should be noted that this is not an attempt to model the true flow configuration inside the exchanger, merely an attempt to find a better representation.

2.4 A distributed steady state model for a counter flow heat exchanger

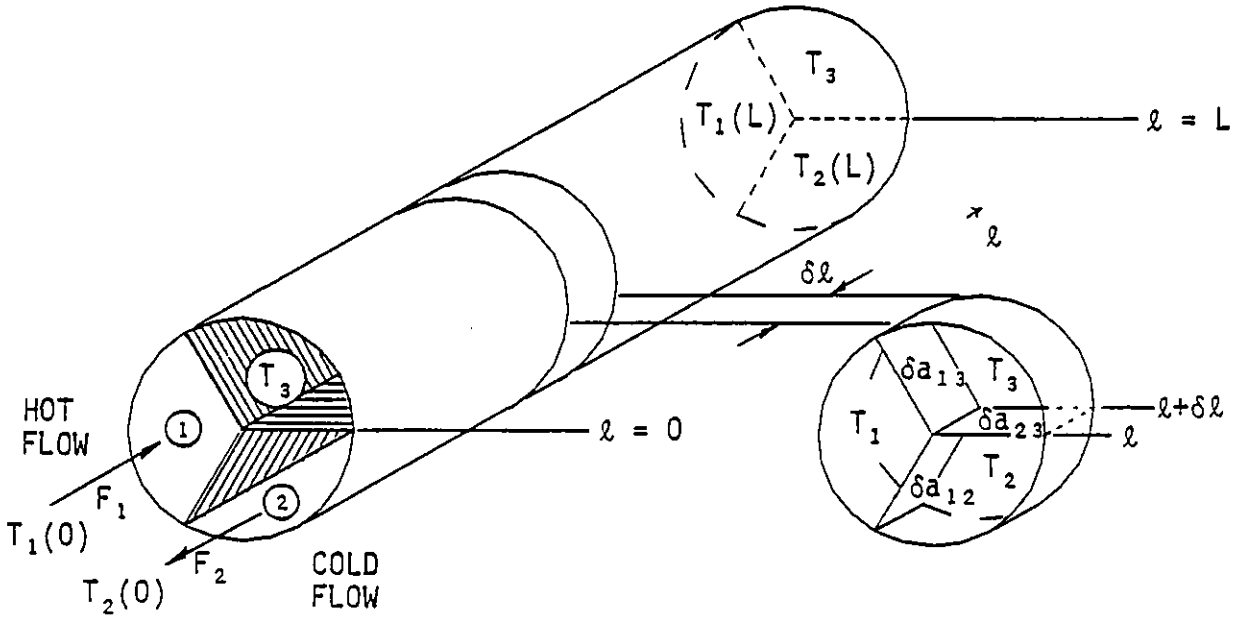

Fig. 6 A three-fluid model

Consider Fig. 6, in which the exchanger is modelled as a hollow cylinder, perfectly insulated from its surroundings and divided longitudinally into three separate channels. The two fluids pass in counter flow through channels 1 and 2, while channel 3 carries an air flow to represent the air surrounding the exchanger. This "three-fluid" approach was suggested by Kerschenbaum [70].

We make the following assumptions:

(i) Fluid temperatures vary axially but are constant along a radius.

(ii) The air flow is so fast that its temperature remains constant at T_3 during its passage through the exchanger.

and over the length $\delta\ell$ of a small element:

(iii) Heat transfer between channels 'i' and 'j' through area δa_{ij} is proportional to the area and to the mean temperature difference between the channels

i.e. δq_{ij} = heat transfer <u>from</u> 'i' <u>to</u> 'j'

$$= U_{ij}\, \delta a_{ij}\, (T_i - T_j)$$

where U_{ij} is a heat transfer coefficient for transfer from 'i' to 'j' expressed in $Wm^{-2}\ K^{-1}$

but $\delta a_{ij} = A_{ij} \frac{\delta\ell}{L}$

where A_{ij} is the total area of the dividing wall of length L between channel 'i' and channel 'j'. U_{ij} and A_{ij} can be combined into a single coefficient, K_{ij}, expressed in WK^{-1}.

(cf. equations (2.1 and 2.2)

hence $$q_{ij} = K_{ij}\, (T_i - T_j)\, \frac{\delta\ell}{L} \qquad \ldots \quad (2.20)$$

Consider now a steady state heat balance for the segmental 'wedges' of fluid in channels 1 and 2 between ℓ and $\ell + \delta\ell$ (Fig. 7).

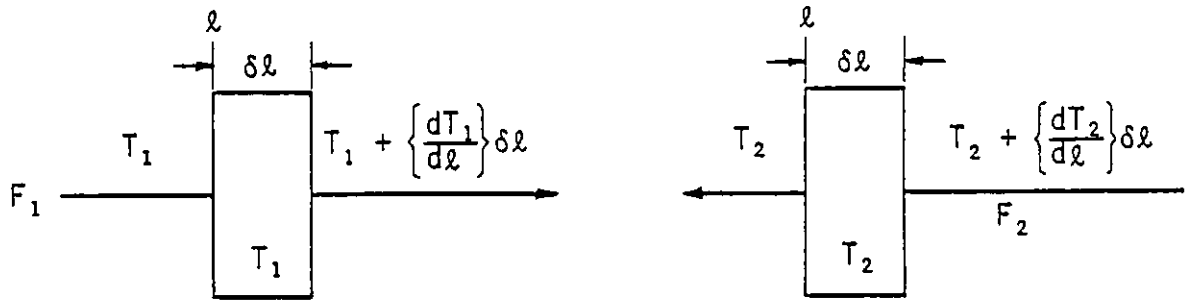

Fig.7 Three fluid model: temperature and flow conventions

	Channel 1	Channel 2
Temperature at ℓ	T_1	T_2
Temperature at $\ell + \delta\ell$	$T_1 + \left[\frac{dT_1}{d\ell}\right]\delta\ell$	$T_2 + \left[\frac{dT_1}{d\ell}\right]\delta\ell$
Temperature drop	$T_1(\ell) - T_1(\ell+\delta\ell)$	$T_2(\ell) - T_2(\ell+\delta\ell)$
	$= -\left[\frac{dT_1}{d\ell}\right]\delta\ell$	$= -\left[\frac{dT_2}{d\ell}\right]\delta\ell$
Flow rate	F_1	$-F_2$ (counter flow)
Heat loss by element	$-F_1C_{p1}\left[\frac{dT_1}{d\ell}\right]\delta\ell$	$F_2C_{p2}\left[\frac{dT_1}{d\ell}\right]\delta\ell$

Heat losses by conduction

Channel 1 to 2	$K_{12}(T_1 - T_2)\frac{\delta\ell}{L}$	2 to 1	$K_{12}(T_2 - T_1)\frac{\delta\ell}{L}$
Channel 1 to 3	$K_{13}(T_1 - T_3)\frac{\delta\ell}{L}$	2 to 3	$K_{23}(T_2 - T_3)\frac{\delta\ell}{L}$

Equating the heat loss terms:

$$-F_1C_{p1}\left[\frac{dT_1}{d\ell}\right]\delta\ell = K_{12}(T_1 - T_2)\delta\ell + K_{13}(T_1 - T_3)\delta\ell \quad \ldots \quad (2.21)$$

$$F_2C_{p2}\left[\frac{dT_2}{d\ell}\right]\delta\ell = K_{12}(T_2 - T_1)\delta\ell + K_{23}(T_2 - T_3)\delta\ell \quad \ldots \quad (2.22)$$

and by re-arranging we obtain a pair of ordinary differential equations:

$$\frac{dT_1}{d\ell} = -\frac{1}{L}\left[\frac{K_{12}}{F_1 C_{p1}} + \frac{K_{13}}{F_2 C_{p2}}\right] T_1 + \frac{1}{L}\frac{K_{12}}{F_1 C_{p1}} T_2 + \frac{1}{L}\frac{K_{13}}{F_1 C_{p1}} T_3 \quad \ldots \quad (2.23)$$

$$\frac{dT_2}{d\ell} = -\frac{1}{L}\frac{K_{12}}{F_2 C_{p2}} T_1 + \frac{1}{L}\left[\frac{K_{12}}{F_2 C_{p2}} + \frac{K_{23}}{F_2 C_{p2}}\right] T_2 - \frac{1}{L}\frac{K_{23}}{F_2 C_{p2}} T_3 \quad \ldots \quad (2.24)$$

These can be expressed in matrix form, writing temperatures formally as functions of length

$$\begin{bmatrix} \dot{T}_1(\ell) \\ \dot{T}_2(\ell) \end{bmatrix} = \frac{B}{L}\begin{bmatrix} T_1(\ell) \\ T_2(\ell) \end{bmatrix} - \frac{B}{L}\begin{bmatrix} T_3 \\ T_3 \end{bmatrix} \quad \ldots \quad (2.25)$$

where $\dot{T}$ denotes a derivative with respect to 'ℓ'

and

$$B = \begin{bmatrix} -\frac{K_{12} + K_{13}}{F_1 C_{p1}} & \frac{K_{12}}{F_1 C_{p1}} \\ -\frac{K_{12}}{F_2 C_{p2}} & \frac{K_{12} + K_{23}}{F_2 C_{p2}} \end{bmatrix}$$

Since B is a constant matrix, the solution to (2.25) is

$$\begin{bmatrix} T_1(\ell) \\ T_2(\ell) \end{bmatrix} = e^{\frac{B\ell}{L}}\begin{bmatrix} T_1(0) \\ T_2(0) \end{bmatrix} - \left[\int_0^{\ell} e^{\frac{B}{L}(\ell-\omega)}\, d\omega\right]\frac{B}{L}\begin{bmatrix} T_3 \\ T_3 \end{bmatrix} \quad \ldots \quad (2.26)$$

Providing that B is nonsingular, $\int e^{\frac{B\omega}{L}} = LB^{-1} e^{\frac{B\omega}{L}}$, leading to

$$\begin{bmatrix} T_1(\ell) \\ T_2(\ell) \end{bmatrix} = e^{\frac{B\ell}{L}}\begin{bmatrix} T_1(0) \\ T_2(0) \end{bmatrix} + e^{\frac{B\ell}{L}}\left[e^{-\frac{B\ell}{L}} - I_2\right]\begin{bmatrix} T_3 \\ T_3 \end{bmatrix} \quad \ldots \quad (2.27)$$

where I_2 is a 2 x 2 identity matrix, and finally

$$\begin{bmatrix} T_1(\ell) \\ T_2(\ell) \end{bmatrix} = e^{\frac{B\ell}{L}}\begin{bmatrix} T_1(0) - T_3 \\ T_2(0) - T_3 \end{bmatrix} + \begin{bmatrix} T_3 \\ T_3 \end{bmatrix} \quad \ldots \quad (2.28)$$

2.5 Estimation of heat transfer coefficients

If the flow rates F_1 and F_2 are known, along with coefficients K_{12}, K_{13} and K_{23} and temperatures $T_1(0)$, $T_2(0)$ and T_3, equation (2.28) can be used to predict the temperatures at end 'L'.

$$\begin{bmatrix}\hat{T}_1(L)\\ \hat{T}_2(L)\end{bmatrix} = e^{B}\begin{bmatrix}T_1(0) - T_3\\ T_2(0) - T_3\end{bmatrix} + \begin{bmatrix}T_3\\ T_3\end{bmatrix} \quad \ldots \quad (2.29)$$

We now define for the ith data set the prediction error

$$\underline{\varepsilon}_i = \begin{bmatrix}(\varepsilon_1)_i\\ (\varepsilon_2)_i\end{bmatrix} = \begin{bmatrix}T_1(L) - \hat{T}_1(L)\\ T_2(L) - \hat{T}_2(L)\end{bmatrix}_i$$

$$= e^{B}\begin{bmatrix}T_3 - T_1(0)\\ T_3 - T_2(0)\end{bmatrix}_i + \begin{bmatrix}T_1(L) - T_3\\ T_2(L) - T_3\end{bmatrix}_i \quad \ldots \quad (2.30)$$

so that for 'n' data sets we again arrive at the cost function

$$J_1(\underline{k}) = \sum_{i=1}^{n} \underline{\varepsilon}_i^{T}\underline{\varepsilon}_i \quad \ldots \quad (2.31)$$

Given the flow rates and temperatures, the heat transfer coefficients can be estimated by finding the values of K_{12}, K_{13} and K_{23} which minimize $J_1(\underline{k})$. This cost function, which here arises naturally, gives direct comparison with the linear and logarithmic models.

2.5.1 A numerical algorithm for minimization of $J_1(\underline{k})$

Unlike expression (2.8), (2.31) does not have a closed form solution for the vector $\underline{k}$ that minimizes $J_1(\underline{k})$, necessitating the use of an iterative technique.

Of the many Numerical Algorithm Group (NAG) routines available to computer users at Imperial College, E04JAF is described as 'a quasi-Newton algorithm for finding the minimum of a function $F(X_1, X_2 \ldots X_N)$ subject to fixed upper and lower bounds on independent variables X_1, $X_2 \ldots X_N$ using function values only.' The user must supply a subroutine to calculate the value of $F(\underline{X})$ at any point $\underline{X}$.

From a starting point supplied by the user there is generated on the basis of estimates of the gradient and the curvature of $F(\underline{X})$ a sequence of feasible points intended to converge to a local minimum of the constrained function.

For the parameter estimation covered by the remainder of Chapter 2, this algorithm was employed with the constraint that the coefficients K_{12}, K_{13} and K_{23} were estimated with a lower bound of zero.

2.5.2 A note on matrix exponentials

Cost function $J_1(\underline{k})$ requires evaluation of matrix exponential e^B where B is a 2 x 2 matrix. This can be expressed in terms of matrix B and its eigenvalues in a direct application of Corollary 2.14 of Chen [71], as shown in the following theorem.

Theorem 2.2

We define the following functions of λ, where λ is an eigenvalue of B

$$f(\lambda) = e^{\lambda} \quad \ldots (2.32)$$

$$g(\lambda) = c_1 + c_2\lambda \quad \ldots (2.33)$$

Constants c_1 and c_2 are to be found by equating f and g for distinct eigenvalues and by equating their derivatives for repeated eigenvalues of B.

Case (i): Distinct eigenvalues

For λ_1 $\quad c_1 + c_2\lambda_1 = e^{\lambda_1} \quad \ldots (2.34)$

λ_2 $\quad c_1 + c_2\lambda_2 = e^{\lambda_2} \quad \ldots (2.35)$

From (2.34) $\quad c_1 = e^{\lambda_1} - c_2\lambda_1 \quad \ldots (2.36)$

and by substitution into (2.35)

$$e^{\lambda} - c_2\lambda_1 + c_2\lambda_2 = e^{\lambda_2} \quad \ldots (2.37)$$

giving $\quad c_2 = \dfrac{e^{\lambda_1} - e^{\lambda_2}}{\lambda_1 - \lambda_2} \quad \ldots (2.38)$

From (2.36)

$$c_1 + \frac{\lambda_1(e^{\lambda_1} - e^{\lambda_2})}{\lambda_1 - \lambda_2} = e^{\lambda_1} \qquad \ldots \quad (2.39)$$

leading to $$c_1 = \frac{\lambda_1 e^{\lambda_2} - \lambda_2 e^{\lambda_1}}{\lambda_1 - \lambda_2} \qquad \ldots \quad (2.40)$$

thus

$$e^B = \frac{\lambda_1 e^{\lambda_2} - \lambda_2 e^{\lambda_1}}{\lambda_1 - \lambda_2} I_2 + \frac{e^{\lambda_1} - e^{\lambda_2}}{\lambda_1 - \lambda_2} B \qquad \ldots \quad (2.41)$$

Case (ii): Repeated eigenvalues

$$f(\lambda) = g(\lambda) \qquad c_1 + c_2\lambda = e^{\lambda} \qquad \ldots \quad (2.42)$$

$$f'(\lambda) = g'(\lambda) \qquad c_2 = e^{\lambda} \qquad \ldots \quad (2.43)$$

where f' is the derivative with respect to 'λ'.

Substituting from (2.43) into (2.42)

$$c_1 = (1 - \lambda)e^{\lambda} \qquad \ldots \quad (2.44)$$

and $$e^B = (1 - \lambda)e^{\lambda} I_2 + e^{\lambda} B \qquad \ldots \quad (2.45)$$

Note that Theorem 2.2 is valid only for 2 x 2 matrices.

2.5.3 Heat exchanger coefficients using ambient air temperature

Approximation techniques for modelling performed reasonably well on the cooler but Section 2.3.5 saw the failure of two of these methods for heat exchanger modelling. Of prime interest, therefore, is whether or not the distributed model of Section 2.4 can cope with the heat exchanger problem.

The theory requires the specification of the temperature of the air passing through channel 3. In line with assumption (ii), Section 2.4, this temperature is taken to be constant along the length of the exchanger, bearing in mind that in reality this is a plate type exchanger with complex intermingled flow paths. The most obvious choice for T_3

is to use the ambient air temperature, measured incidentally some 3-4 metres away from the plant.

Taking this and the liquid temperatures from Table 4 and using NAG routine E04JAF for the seven data sets available we obtain:

$$\underline{\hat{k}} = \begin{bmatrix} \hat{K}_{x\ell} \\ \hat{K}_{sta} \\ \hat{K}_{spa} \end{bmatrix} = \begin{bmatrix} \hat{K}_{12} \\ \hat{K}_{13} \\ \hat{K}_{23} \end{bmatrix} = \begin{bmatrix} 6133 \\ 0 \\ 125.7 \end{bmatrix} \quad WK^{-1}$$

The value of $J_1(\underline{\hat{k}})$ is supplied by routine E04JAF as 30.7. While lower than the 76.7 of Section 2.3.5 this is clearly still entirely unacceptable. The coefficient of zero for heat transfer from the stripped MEA to the air indicates that this model is still based on at least one incorrect assumption.

2.5.4 Cooler coefficients using ambient air temperature

Repeating the process of the previous section for the cooler and again specifying $T_3 = T_{amb}$ we obtain:

$$\underline{\hat{k}} = \begin{bmatrix} \hat{K}_{c\ell} \\ \hat{K}_{cma} \\ \hat{K}_{cwa} \end{bmatrix} = \begin{bmatrix} \hat{K}_{12} \\ \hat{K}_{13} \\ \hat{K}_{23} \end{bmatrix} = \begin{bmatrix} 1405 \\ 77.6 \\ 10.9 \end{bmatrix} \quad WK^{-1}$$

With a cost function of $J_1(\underline{\hat{k}})$ of 0.39 this cooler model is actually marginally better than the simple nonlinear model of Section 2.3.4 ($J_1(\underline{\hat{k}}) = 0.42$). That the distributed model should work well with the cooler but fail with the heat exchanger suggests that the problem lies in the heat transfer to the air and,in particular, in the way in which T_3 is specified.

2.6 Modifications to assumptions regarding the air temperature

As far as the cooler is concerned, the mean liquid temperatures are fairly close to ambient and the air surrounding the unit does not warm up appreciably when the plant is running. In contrast the air around the heat exchanger feels distinctly warm: a thermometer placed a few inches above the unit recorded temperature increases of 15-20°C over ambient. This suggests that the effective value of T_3 is in some way connected with the liquid temperatures and, at least for the heat exchanger, should be considerably higher than the ambient air temperature.

An experiment was tried with the heat exchanger data involving a small change to the program used for the coefficient estimation of Section 2.5.3. Instead of optimizing $J_1(\underline{k})$ over the three coefficients K_{12}, K_{13} and K_{23}, a fourth independent variable T_{b3} was added, this being a constant bias on T_3 such that

$$(T_3)_i = (T_{amb})_i + T_{b3} \qquad \forall \text{ data sets } i \qquad \ldots \quad (2.46)$$

There was no guarantee that this would produce a meaningful result, but in fact E04JAF generated:

$$\underline{\hat{k}} = \begin{bmatrix} \hat{K}_{12} \\ \hat{K}_{13} \\ \hat{K}_{23} \end{bmatrix} = \begin{bmatrix} 7194 \\ 841 \\ 0 \end{bmatrix} \quad WK^{-1} \qquad \hat{T}_{b3} = 40.9°C \qquad J_1(\underline{\hat{k}}) = 8.2$$

This result is encouraging: not only does it represent a 73% reduction in $J_1(\underline{\hat{k}})$ but also the bias T_{b3} brings the air temperature T_3 up to around 62°C.

For run PLANT2 the linear mean temperature of fluid 1 is 68.1°C and of fluid 2, 54.5°C. The average of these temperatures, 61.3°C, can be thought of as the mean temperature of the liquids and hence of the unit as a whole. This result suggests that the air in the region of the exchanger plates is at the same mean temperature as the unit itself and that the effective value of T_3 should thus be specified as equal to the mean liquid temperature.

To test this assumption further the coefficient estimation program was further modified to calculate T_3 as the linear mean of the liquid temperatures for each data set:

$$(T_3)_i = \tfrac{1}{4}[T_1(0) + T_2(0) + T_1(L) + T_2(L)]_i$$
$$\forall \text{ data sets } i \qquad \ldots \quad (2.47)$$

This was tried on both heat exchanger and cooler (appropriate instrument tag numbers from Tables 7 and 5 respectively, data from Table 4).

Heat exchanger

$$\underline{\hat{k}} = \begin{bmatrix} \hat{K}_{12} \\ \hat{K}_{13} \\ \hat{K}_{23} \end{bmatrix} = \begin{bmatrix} 6764 \\ 571 \\ 219 \end{bmatrix} \quad WK^{-1}$$

$$J_1(\underline{\hat{k}}) = 2.13$$

Cooler

$$\underline{\hat{k}} = \begin{bmatrix} \hat{K}_{12} \\ \hat{K}_{13} \\ \hat{K}_{23} \end{bmatrix} = \begin{bmatrix} 1366 \\ 392 \\ 285 \end{bmatrix} \quad WK^{-1}$$

$$J_1(\underline{\hat{k}}) = 0.18$$

These figures represent cost function reductions of 74% and 54% for heat exchanger and cooler respectively and justify further analysis to derive the true mean liquid temperature for the distributed model of Section 2.4.

2.6.1 Derivation of the mean liquid temperature for the distributed model

The mean liquid temperatures are given by equation (A3.6) [Appendix III]:

$$\begin{bmatrix} T_{1m} \\ T_{2m} \end{bmatrix} = B^{-1} \begin{bmatrix} T_1(L) - T_1(0) \\ T_2(L) - T_2(0) \end{bmatrix} + \begin{bmatrix} T_3 \\ T_3 \end{bmatrix} \quad \ldots \quad (2.48)$$

The overall mean liquid temperature, T_m, is thus given by:

$$T_m = \tfrac{1}{2}(T_{1m} + T_{2m}) \quad \text{or} \quad \tfrac{1}{2}[1 \;\; 1] \begin{bmatrix} T_{1m} \\ T_{2m} \end{bmatrix} \qquad \ldots \quad (2.49)$$

Equating T_m to T_3

$$T_m = T_3 = \tfrac{1}{2}[1 \;\; 1]\, B^{-1} \begin{bmatrix} T_1(L) - T_1(0) \\ T_2(L) - T_2(0) \end{bmatrix} + T_3 \ldots \quad (2.50)$$

Clearly T_3 disappears from this equation, but by re-arranging (2.28) with $\ell = L$

$$\begin{bmatrix} T_1(L) \\ T_2(L) \end{bmatrix} = e^B \begin{bmatrix} T_1(0) \\ T_2(0) \end{bmatrix} + (I_2 - e^B) \begin{bmatrix} T_3 \\ T_3 \end{bmatrix} \qquad \ldots \quad (2.51)$$

and substituting into (2.50) we obtain:

$$[1 \;\; 1]\, B^{-1}(e^B - I_2) \begin{bmatrix} T_1(0) - T_3 \\ T_2(0) - T_3 \end{bmatrix} = 0 \qquad \ldots \quad (2.52)$$

Writing $[\psi_1 \;\; \psi_2] = [1 \;\; 1]\, B^{-1}(e^B - I_2)$ we have

$$[\psi_1 \;\; \psi_2] \begin{bmatrix} T_1(0) - T_3 \\ T_2(0) - T_3 \end{bmatrix} = 0 \qquad \ldots \quad (2.53)$$

and hence $$T_3 = \frac{\psi_1 T_1(0) + \psi_2 T_2(0)}{\psi_1 + \psi_2} \qquad \ldots \quad (2.54)$$

2.6.2 An iterative technique for coefficient estimation

A problem arises in redefining T_3 in this way because its value is now dependent on the entries of matrix B (equation (2.25)), which in turn are dependent on the heat transfer coefficients that are being estimated.

The program based on NAG routine E04JAF requires a user supplied initial estimate of the coefficients along with the liquid flow rates, the four liquid inlet and outlet temperatures and a value for T_3 to calculate optimum values

for K_{12}, K_{13} and K_{23}. Only then can it use these estimated coefficients to arrive at a value for T_3 via equation (2.54). Clearly the user must also supply an initial estimate for T_3 to start the estimation process. This could be done by calculating T_3 from the initial estimates for the heat transfer coefficients, but it is easier to use the linear mean as defined by equation (2.47). This results in the iterative estimation technique shown as a flow diagram in Fig. 8.

No analysis has been done to prove that this iterative procedure will cause the estimates to converge to optimum values. Because of this, rather than incorporating a stopping condition as implied in Fig. 8, a program was written to print out $(T_3)_i$, $i = 1,\ldots 7$, $\hat{K}_{12}$, $\hat{K}_{13}$ and $\hat{K}_{23}$ and the cost function at each iteration. At each iteration, routine E04JAF outputs an 'IFAIL' parameter which indicates the degree of confidence as to whether the point found is actually a minimum.

IFAIL	Remarks
0	Preferred value: point found is a minimum.
3	Conditions for minimum not all met but no lower point found: unsatisfactory.
5, 6, 7, 8	Some doubt as to whether point found is a minimum. Degree of confidence decreases as IFAIL increases. IFAIL = 5: reasonable estimate, IFAIL = 8: unlikely to be a minimum.

The value of this parameter was also printed out along with the above.

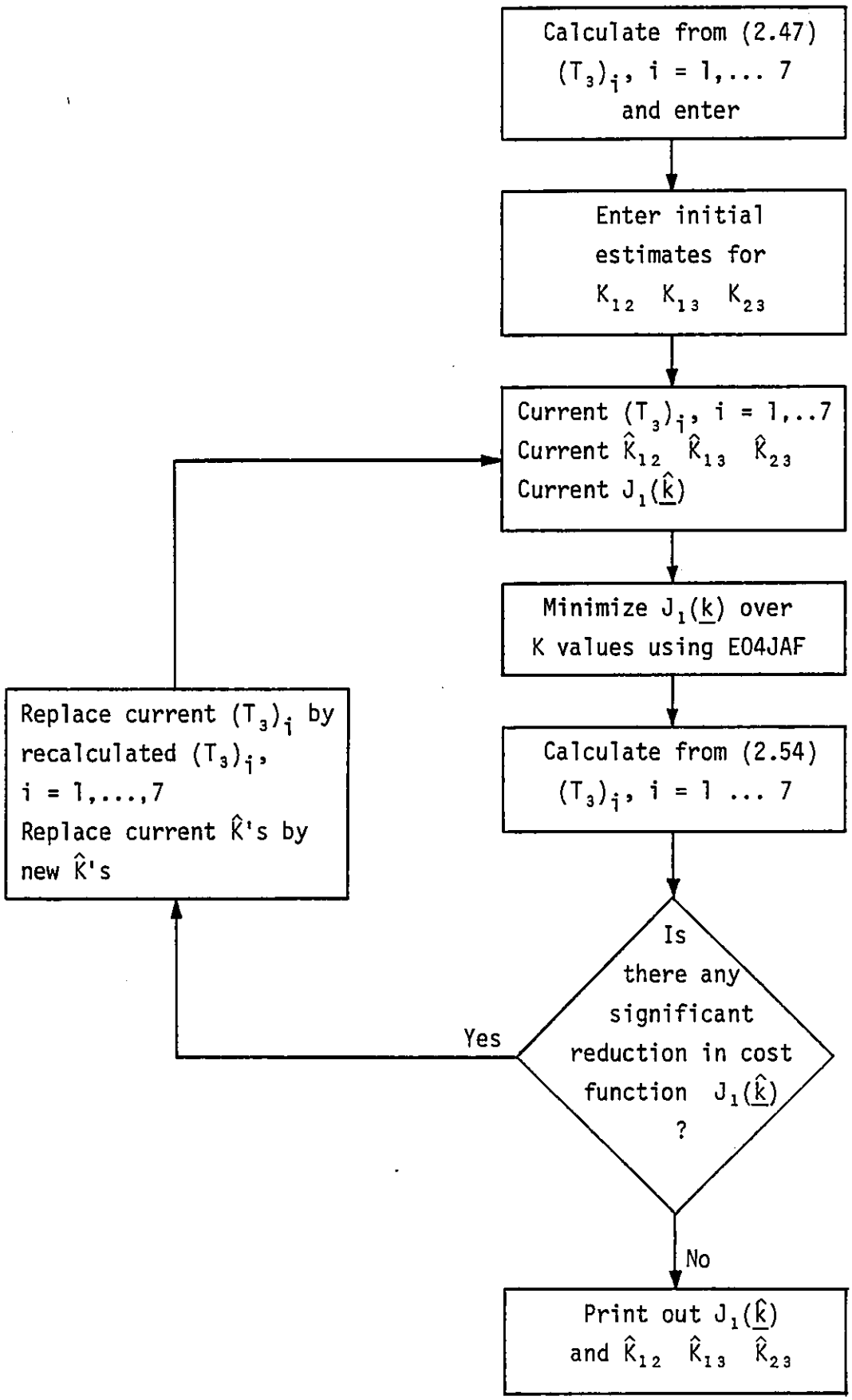

FIG. 8 FLOW DIAGRAM FOR ITERATIVE ESTIMATION TECHNIQUE

2.6.3 Heat exchanger coefficients using modified air temperature

The iterative estimation program was run with the seven data sets, printing out $\hat{K}$ values to one decimal place and cost function $J_1(\hat{\underline{k}})$ to six decimal places.

The coefficient estimates became steady after 22 iterations and any reduction in $J_1(\hat{\underline{k}})$ after this point was less than 0.0001. The IFAIL parameter was however erratic, jumping around from 3 to 7 or 8. This casts some doubt on the results, but continuation of the run over a total of 46 iterations brought no better value than IFAIL = 7.

If the estimation is judged by the prediction error cost function alone, the algorithm produced the lowest figure to date, $J_1(\hat{\underline{k}}) = 0.38$.

The coefficient estimates were:

$$\hat{\underline{k}} = \begin{bmatrix} \hat{K}_{12} \\ \hat{K}_{13} \\ \hat{K}_{23} \end{bmatrix} = \begin{bmatrix} 6528.5 \\ 435.4 \\ 283.6 \end{bmatrix} \quad WK^{-1}$$

2.6.4 Cooler coefficients using modified air temperature

The algorithm performance was better on the cooler and the coefficient estimates became steady after only 11 iterations. The IFAIL parameter was again erratic but jumped only from zero to 5, 6 or 7. The value of zero at iteration 11 implies that $J_1(\hat{\underline{k}})$ at this point is a true minimum. The coefficients were estimated at:

$$\hat{\underline{k}} = \begin{bmatrix} \hat{K}_{12} \\ \hat{K}_{13} \\ \hat{K}_{23} \end{bmatrix} = \begin{bmatrix} 1348.5 \\ 524.7 \\ 417.8 \end{bmatrix} \quad WK^{-1}$$

with a cost function value of $J_1(\hat{\underline{k}}) = 0.14$, again the lowest to date.

2.7 Use of model to predict output temperatures

The effective air temperature T_3 can be expressed in terms of $T_1(0)$ and $T_2(0)$ as in equation (2.54). In conjunction with equation (2.29) this allows prediction of $T_1(L)$ and $T_2(L)$ from the liquid flow rates and the temperatures $T_1(0)$ and $T_2(0)$. As this model concerns a counter flow exchanger with inputs at opposite ends, some manipulation is required to enable outputs $T_1(L)$ and $T_2(0)$ to be predicted from inputs $T_1(0)$, $T_2(L)$, F_1 and F_2 (or $\tilde{F}_1$).

For $\ell = L$ equation (2.28) can be written

$$\begin{bmatrix} T_1(L) \\ T_2(L) \end{bmatrix} = e^B \begin{bmatrix} T_1(0) \\ T_2(0) \end{bmatrix} + (I_2 - e^B) \begin{bmatrix} T_3 \\ T_3 \end{bmatrix} \quad \ldots \quad (2.55)$$

and from (2.52) and (2.54)

$$T_3 = \frac{1}{\alpha} [1 \quad 1] B^{-1}\{e^B - I_2\} \begin{bmatrix} T_1(0) \\ T_2(0) \end{bmatrix} \quad \ldots \quad (2.56)$$

where $\alpha = \psi_1 + \psi_2$

Substituting for T_3 in (2.55)

$$\begin{bmatrix} T_1(L) \\ T_2(L) \end{bmatrix} = \left[e^B - \frac{1}{\alpha}\{e^B - I_2\} \begin{bmatrix} 1 & 1 \\ 1 & 1 \end{bmatrix} B^{-1}\{e^B - I_2\} \right] \begin{bmatrix} T_1(0) \\ T_2(0) \end{bmatrix} \ldots \quad (2.57)$$

or

$$\begin{bmatrix} T_1(L) \\ T_2(L) \end{bmatrix} = M \begin{bmatrix} T_1(0) \\ T_2(0) \end{bmatrix} \quad \ldots \quad (2.58)$$

where

$$M = \begin{bmatrix} \mu_{11} & \mu_{12} \\ \mu_{21} & \mu_{22} \end{bmatrix} = e^B - \frac{1}{\alpha}\{e^B - I_2\} \begin{bmatrix} 1 & 1 \\ 1 & 1 \end{bmatrix} B^{-1}\{e^B - I_2\}$$

Multiplying out equation (2.58) gives

$$T_1(L) = \mu_{11} T_1(0) + \mu_{12} T_2(0) \quad \ldots \quad (2.59)$$

$$T_2(L) = \mu_{21} T_1(0) + \mu_{22} T_2(0) \quad \ldots \quad (2.60)$$

and by re-arranging (2.60)

$$T_2(0) = \frac{1}{\mu_{22}} T_2(L) - \frac{\mu_{21}}{\mu_{22}} T_1(0) \quad \ldots \quad (2.61)$$

and substituting for $T_2(0)$ in (2.59)

$$T_1(L) = \left[\mu_{11} - \frac{\mu_{12}\,\mu_{21}}{\mu_{22}} \right] T_1(0) + \frac{\mu_{12}}{\mu_{22}} T_1(L) \quad \ldots \quad (2.62)$$

we obtain an expression for the output temperatures in terms of the input temperatures and flow rates:

$$\begin{bmatrix} T_1(L) \\ T_2(0) \end{bmatrix} = \frac{1}{\mu_{22}} \begin{bmatrix} \mu_{11}\,\mu_{22} - \mu_{12}\,\mu_{21} & \mu_{12} \\ -\mu_{21} & 1 \end{bmatrix} \begin{bmatrix} T_1(0) \\ T_2(L) \end{bmatrix} \quad \ldots \quad (2.63)$$

Matrix M is calculated from the coefficient set of Section 2.6.3 for the heat exchanger and from that of Section 2.6.4 for the cooler. If (2.63) is used for each steady state data set the results, including prediction errors, are as given in Tables 8 and 9.

TABLE 8

COOLER						
RUN	$T_1(L)$	$\hat{T}_1(L)$	$\hat{T} - T$	$T_2(0)$	$\hat{T}_2(0)$	$\hat{T} - T$
PLANT2	20.0	19.95	- .05	23.92	23.81	- .11
PLANT3/1	20.3	20.08	- .28	24.40	24.26	- .14
3/2	22.4	22.50	+ .10	26.22	26.22	0
3/3	23.3	23.44	+ .14	27.00	26.96	- .04
3/4	24.2	24.00	- .20	29.05	29.03	- .02
3/5	21.9	21.95	+ .05	25.69	25.73	+ .04
3/6	21.3	21.38	+ .08	24.66	24.71	+ .05

TABLE 9

HEAT EXCHANGER						
RUN	$T_1(L)$	$\hat{T}_1(L)$	$\hat{T} - T$	$T_2(0)$	$\hat{T}_2(0)$	$\hat{T} - T$
PLANT2	34.7	35.12	+ .42	87.2	87.23	+ .03
PLANT3/1	34.7	34.74	+ .04	88.6	88.65	+ .05
3/2	36.7	36.66	- .04	87.6	87.53	- .07
3/3	37.6	37.53	- .07	87.1	87.17	+ .07
3/4	38.0	37.91	- .09	87.8	87.83	+ .03
3/5	36.4	36.36	- .04	87.6	87.47	- .13
3/6	35.9	35.84	- .06	87.3	87.30	0

2.8 Sensitivity of the model to errors in the input data

A system model is of limited use if small errors in the input data cause disproportionately large errors in the output. A program based on equation (2.63) was used to check the variation in the predicted outputs for small increases in individual input variables.

For run PLANT2 the nominal inputs (Table 4) are:

Cooler $T_1(0) = 34.7°C/T_2(L) = 9.54°C/F_1 = F_2 = 0.25 kgs^{-1}$

Heat exchanger $T_1(0) = 101.4°C/T_2(L) = 21.69°C/F_1 = \tilde{F}_1 = 0.25 kgs^{-1}$

Table 10 gives the model-predicted change in each output variable when one of the input variables is altered, the other inputs remaining at their nominal values. Note that for the heat exchanger it is assumed that $\tilde{F}_1 = F_1$ in the steady state, and so these input variables are altered at the same time.

TABLE 10

COOLER			HEAT EXCHANGER		
Change in input	$\Delta\hat{T}_1(L)$	$\Delta\hat{T}_2(0)$	Change in input	$\Delta\hat{T}_1(L)$	$\Delta\hat{T}_2(0)$
$T_1(0)$ + 5%	+ 3.6%	+ 4.1%	$T_1(0)$ + 5%	+ 2.4%	+ 4.8%
$T_2(L)$ + 5%	+ 1.4%	+ 0.9%	$T_1(0)$ + 5%	+ 2.6%	+ 0.2%
F_1 + 5%	+ 2.4%	+ 1.0%	$F_1, \tilde{F}_1$ + 5%	+ 0.9%	- 0.3%
F_2 + 5%	- 1.1%	- 2.0%			

Clearly the predicted output temperatures are more sensitive to some input errors than others, but in general a given percentage error in the input produces an output error of similar order.

2.9 Summary

Steady state data from two plant runs has been extensively analyzed in this chapter. Two similar process units were initially represented as pairs of PSTR's, an approach which gave reasonable results with the cooler but failed when applied to the heat exchanger.

This necessitated a more detailed analysis involving the modelling of each unit as a fully distributed 'three fluid' system. Expressions were derived for the temperature distributions of the 'hot' and 'cold' flows, and it was shown that the effective temperature of the air surrounding the heat exchanger could be approximated by substitution of the mean liquid temperature. An iterative technique was devised to estimate heat transfer coefficients for the two units, but the heat exchanger caused some difficulty in that the NAG routine was not fully confident that it had found a true minimum of the cost function. This is offset by the ability of the model to produce good estimates of the output temperatures when supplied with the input temperatures and flow rates. It should also be noted that the ratio of $\hat{K}_{12}$ for the heat exchanger to $\hat{K}_{12}$ for the cooler, about 5 : 1, is consistent with the ratio of the numbers of plates and hence the areas available for heat transfer between fluids.

In the light of experience with the three fluid model it seems likely that the earlier approaches assuming a linear or logarithmic temperature distribution could have been improved for heat exchanger modelling by using an effective air temperature in place of the true ambient. The three fluid model is however a neat, effective and easily handled solution to the steady state modelling problem and seems unlikely to be bettered for this application by any other model employing a similar number of parameters.

The development and testing with real data of a distributed three fluid model for a plate type heat exchanger is an original contribution.

CHAPTER 3

MODELLING OF SYSTEM TRANSIENTS

3.0 Introduction

Investigation of transients by applying flow rate step changes was outlined in Section 2.2.2. The system responses obtained from run PLANT3 are presented in this chapter and an attempt is made to extend the three-fluid analysis to deal with the transient case.

A state space model requires the derivation of a system of first order o.d.e's containing time derivatives only. The most obvious approach is to return to the method of Section 2.4, writing instantaneous heat balances in terms of partial derivatives with respect to length and time. It is shown, however, that the equations so obtained cannot be solved by conventional Laplace Transform techniques, necessitating a different approach to the modelling problem.

The remainder of Chapter 3 covers the development of a 'semi-lumped' model for prediction of transient behaviour. The steady state distributed model is used to predict the settled out effect of an input change, while the transient itself is modelled by returning to the assumption that the liquid channels behave as stirred tanks. Although relatively straightforward, this chapter is original work in so far as it is based on an original approach to heat exchanger modelling.

3.1 Instantaneous heat balances for the three fluid model

Consider Fig. 9 which shows a small element in the jth channel of the three fluid model. If the cross sectional area is S_j then for an element of length $\delta\ell$ the volume is given by

$$\delta V_j = S_j \delta\ell$$

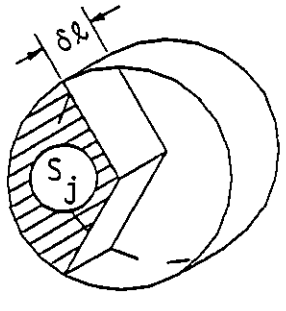

Fig.9

and if the jth channel carries fluid of density ρ_j then the mass of fluid contained in the elemental volume is

$$\delta m_j = \rho_j S_j \delta \ell$$

Writing flow rates as functions of time and temperatures T_1 and T_2 as functions of length and time, the instantaneous heat balances are:

$$(\rho_1 S_1 \delta\ell) C_{p1} \left\{\frac{\partial T_1(\ell,t)}{\partial t}\right\} = -F_1(t) C_{p1} \left\{\frac{\partial T_1(\ell,t)}{\partial \ell}\right\} \delta\ell$$
$$-K_{12}\frac{\delta\ell}{L}\left[T_1(\ell,t)-T_2(\ell,t)\right] - K_{13}\frac{\delta\ell}{L}\left[T_1(\ell,t)-T_3(t)\right] \quad \ldots (3.1)$$

and

$$(\rho_2 S_2 \delta\ell) C_{p2} \left\{\frac{\partial T_2(\ell,t)}{\partial t}\right\} = F_2(t) C_{p2} \left\{\frac{\partial T_2(\ell,t)}{\partial \ell}\right\} \delta\ell$$
$$-K_{12}\frac{\delta\ell}{L}\left[T_2(\ell,t)-T_1(\ell,t)\right] - K_{23}\frac{\delta\ell}{L}\left[T_2(\ell,t)-T_3(t)\right] \quad \ldots (3.2)$$

Note that T_3 is assumed to be constant over the length of the exchanger and is therefore a function of time only.

Dividing through by $(\delta\ell/L)$ and noting that $\rho_j S_j L = m_j$, the mass of fluid in the jth channel

$$m_1 C_{p1} \left\{\frac{\partial T_1(\ell,t)}{\partial t}\right\} = -F_1(t) C_{p1} L \left\{\frac{\partial T_1(\ell,t)}{\partial \ell}\right\}$$
$$- K_{12}\left[T_1(\ell,t)-T_2(\ell,t)\right] - K_{13}\left[T_1(\ell,t)-T_3(t)\right] \quad \ldots (3.3)$$

$$m_2 C_{p2} \left\{\frac{\partial T_2(\ell,t)}{\partial t}\right\} = F_2(t) C_{p2} L \left\{\frac{\partial T_2(\ell,t)}{\partial \ell}\right\}$$
$$- K_{12}\left[T_2(\ell,t)-T_1(\ell,t)\right] - K_{23}\left[T_2(\ell,t)-T_3(t)\right] \quad \ldots (3.4)$$

3.2 Attempted solution of heat balance equations

A full solution to the heat balance equations (3.3) and (3.4) would yield a pair of equations of the form of (3.5) and (3.6).

$$T_1(L,t) = F_1\left\{T_1(0,t),\ T_2(L,t),\ F_1(t),\ F_2(t),\ t\right\} \quad \ldots (3.5)$$

$$T_2(0,t) = F_2\left\{T_1(0,t),\ T_2(L,t),\ F_1(t),\ F_2(t),\ t\right\} \quad \ldots (3.6)$$

From these it would be possible to predict the transient behaviour of output temperatures $T_1(L,t)$ and $T_2(0,t)$ for any time function of the input temperatures or the flow rates.

Further, a pair of equations of the form of (3.7) and (3.8) could be obtained to model the system dynamics. By considering the output temperatures to be the states of the system (see Chapter 4) such a pair of o.d.e's would be suitable for state space modelling.

$$\frac{dT_1(L,t)}{dt} = G_1\left\{T_1(0,t),T_1(L,t),T_2(0,t),T_2(L,t),F_1(t),F_2(t),t\right\} \quad \ldots \quad (3.7)$$

$$\frac{dT_2(0,t)}{dt} = G_2\left\{T_1(0,t),T_1(L,t),T_2(0,t),T_2(L,t),F_1(t),F_2(t),t\right\} \quad \ldots \quad (3.8)$$

It is shown in Appendix IV that by the use of certain substitutions and by defining a Laplace Transform with respect to the time variable, equations (3.3) and (3.4) reduce to matrix-vector equation (3.9) where the derivative is with respect to 'ℓ'.

$$\dot{\underline{t}}(\ell,s) = \frac{1}{L}(sT + B)\,\underline{\bar{t}}(\ell,s) - W(s)e^{B\frac{\ell}{L}}\underline{\theta} + \underline{k}(s)\bar{t}_3(s) \quad \ldots \quad (3.9)$$

where $\underline{\bar{t}}(\ell,s) = \mathcal{L}\{\underline{t}(\ell,t)\}$ and 2 x 2 matrix $W(s)$ and 2 x 1 vectors $\underline{\theta}$ and $\underline{k}(s)$ are independent of 'ℓ'.

The solution to this equation is given as equation (A4.14) in Appendix IV. It is rather messy and includes one term that cannot be inverted to the time domain.

Matrix T, defined in Appendix IV as

$$T = \begin{bmatrix} -\frac{m_1}{F_1} & \\ & \frac{m_2}{F_2} \end{bmatrix} \quad \text{can also be written} \quad T = \begin{bmatrix} -\tau_{r1} & \\ & \tau_{r2} \end{bmatrix}$$

where τ_{rj} is the residence time of the fluid in channel 'j'.

Equation (A4.14) contains the term $e^{(sT + B)\frac{\ell}{L}}$. At first glance it would appear that

$$e^{(sT + B)\frac{\ell}{L}} = e^{sT\frac{\ell}{L}}.e^{B\frac{\ell}{L}} \quad \ldots \quad (3.10)$$

where $\mathcal{L}^{-1}\left\{ e^{sT\frac{\ell}{L}} \; F(s) \right\} \rightarrow H(t - T\frac{\ell}{L})F(t - T\frac{\ell}{L})$

and $H(t - x)$ is the Heaviside unit step function.

Indeed this appears reasonable from a physical standpoint. Substituting ($\ell = L$) in (3.10), the first term would imply that a temperature change at $\ell = 0$ does not manifest itself at $\ell = L$ until τ_r seconds later, i.e. until the liquid has passed through the exchanger.

Unfortunately Stephenson [72] informs us that (3.10) holds only if the two matrices commute, i.e.

$$e^{(A+B)} = e^{A}e^{B} \quad \text{only if } AB = BA \qquad \ldots \quad (3.11)$$

Clearly the opposite signs of the (1,1) and (2,2) entries of matrix T ensure that it cannot commute with B as defined in (2.25). Equation (3.10) does <u>not</u> hold and the inverse L.T. of this exponential term is not defined.

As a consequence the solution to (3.9) cannot be inverted to the time domain to give a solution corresponding to equations (3.5) and (3.6). Any attempt to obtain equations of the form of (3.7) and (3.8) is also thwarted by the same underlying problem.

3.3 <u>An alternative approach to the modelling of transients</u>

If equations corresponding to (3.5) and (3.6) could have been obtained then for a step change in any one input variable, the output variable change would have been given as a function of time by an expression similar, in essence, to (3.12)

$$\Delta \text{ output}(t) = \left[\frac{\Delta \text{ output}}{\Delta \text{ input}}\right]_{ss} \times \text{input step size} \times \left[1 - \zeta(t)\right] \qquad \ldots \quad (3.12)$$

Here the first term on the right hand side is the steady state change in the output variable per unit change in the input variable, i.e. the change in output that remains when all the transients have died away. The term $\zeta(t)$ represents a transient term which tends to zero as $t \rightarrow \infty$.

Equation (3.12) expresses the required result in a very simple form but if the first and third terms on the right hand side can be approximated in some way then it does provide the basis for an alternative approach to modelling.

If the system nonlinearity is not too severe (see 3.3.1) then the first term on the r.h.s. of equation (3.12) can be regarded as a partial derivative with respect to a single input variable. This could be evaluated under the operating conditions existing immediately prior to the change in input.

For a real plant the third term, which includes the function $\zeta(t)$, is very complex and representing it mathematically is a tradeoff between number of parameters and goodness of fit. The difficulties of Section 3.2 mean that an approximation cannot be obtained via the three fluid model and an alternative must be sought. This is further discussed in Section 3.5.3.

3.3.1 Linearization about the operating point

The data for Fig.10 was calculated from equation (2.63) for the steady state data set PLANT3/4. All of the inputs were held at their nominal values except for the cooling water flow rate which was varied over the range 0.15-0.29 kgs^{-1}. This graph, which is typical, shows that the nonlinearity is not too severe for a linear approximation to be used for small jumps in liquid flow rate.

In Section 3.4 partial derivatives are found for each input/output pair directly from the steady state results of Chapter 2. The transient itself is then modelled in Section 3.5 by using curves drawn from recorded plant data to obtain an approximation to the term $\zeta(t)$.

3.4 Steady state partial derivatives

In Chapter 2 a single model structure was adopted for use with either cooler or heat exchanger. As a result the partial derivative analysis need be performed only once, as derivative values for either unit can be obtained by substitution of suitable parameter values. Section 3.4.1 deals with derivatives with respect to input temperature while the lengthier analysis to obtain flow rate derivatives is covered in Section 3.4.2.

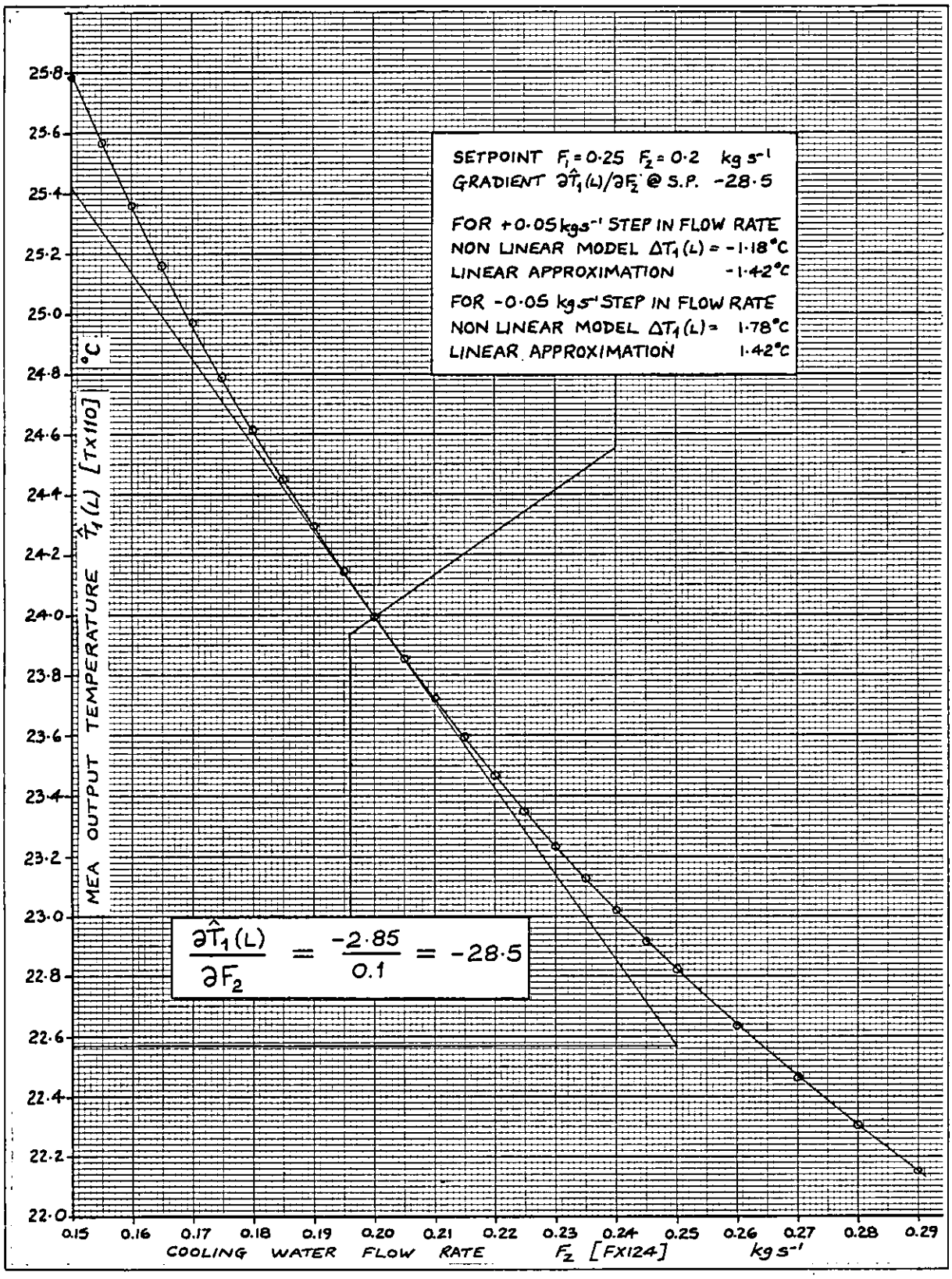

Fig.10 Variation with cooling water flow rate of the estimated temperature of the MEA leaving the cooler. All other input variables constant:

$T_1(0)$ TX174 = 38.0 C F_1 = 0.25 kgs^{-1}

$T_2(L)$ TX176 = 12.14 C Data: PLANT3/4

3.4.1 Changes in input temperature

Equations (2.62) and (2.61) related output temperatures to those at the inputs as follows:

$$T_1(L) = \left[\frac{\mu_{11}\mu_{22}-\mu_{12}\mu_{21}}{\mu_{22}}\right] T_1(0) + \left[\frac{\mu_{12}}{\mu_{22}}\right] T_2(L) \quad \ldots \quad (3.13)$$

$$T_2(0) = \left[-\frac{\mu_{21}}{\mu_{22}}\right] T_1(0) + \left[\frac{1}{\mu_{22}}\right] T_2(L) \quad \ldots \quad (3.14)$$

where μ_{ij} is dependent on both fluid flow rates and on the heat transfer coefficients.

At constant flow the partial derivatives required are thus given by:

$$\frac{\partial T_1(L)}{\partial T_1(0)} = \left[\frac{\mu_{11}\mu_{22} - \mu_{12}\mu_{21}}{\mu_{22}}\right] \qquad \frac{\partial T_1(L)}{\partial T_2(L)} = \left[\frac{\mu_{12}}{\mu_{22}}\right]$$

$$\frac{\partial T_2(0)}{\partial T_1(0)} = \left[-\frac{\mu_{21}}{\mu_{22}}\right] \qquad \frac{\partial T_2(0)}{\partial T_2(L)} = \left[\frac{1}{\mu_{22}}\right] \quad \ldots \quad (3.15)$$

3.4.2 Changes in flow rate

Equations (3.13) and (3.14) can be written

$$T_1(L) = \xi_{11}T_1(0) + \xi_{12}T_2(L) \quad \ldots \quad (3.16)$$

$$T_2(0) = \xi_{21}T_1(0) + \xi_{22}T_2(L) \quad \ldots \quad (3.17)$$

At constant input temperature the partial derivatives with respect to flow rate F_j are thus given by

$$\frac{\partial T_1(L)}{\partial F_j} = \frac{\partial \xi_{11}}{\partial F_j} T_1(0) + \frac{\partial \xi_{12}}{\partial F_j} T_2(L) \qquad j = 1,2 \quad \ldots \quad (3.18)$$

$$\frac{\partial T_2(0)}{\partial F_j} = \frac{\partial \xi_{21}}{\partial F_j} T_1(0) + \frac{\partial \xi_{22}}{\partial F_j} T_2(L) \qquad j = 1,2 \quad \ldots \quad (3.19)$$

The terms μ_{mn} were defined as elements of the 2 x 2 matrix M in equation (2.58). We define Ξ as the 2 x 2 matrix whose elements are ξ_{ik}, i = 1,2, k = 1,2. Since each element ξ_{ik} is a function of μ_{mn}, m = 1,2, n = 1,2, it follows that the flow derivatives of M must be calculated before the flow derivatives of Ξ can be found.

Differentiating (2.58) we obtain

$$\frac{\partial}{\partial F_j}\begin{bmatrix}\mu_{11} & \mu_{12}\\ \mu_{21} & \mu_{22}\end{bmatrix} = \frac{\partial}{\partial F_j}\left[e^B - \frac{1}{\alpha}\{e^B - I_2\}\begin{bmatrix}1 & 1\\ 1 & 1\end{bmatrix} B^{-1}\{e^B - I_2\}\right] \qquad j = 1,2 \ldots \quad (3.20)$$

recalling that $\alpha = \psi_1 + \psi_2 = [1\ 1]\, B^{-1}(e^B - I_2)\begin{bmatrix}1\\1\end{bmatrix}$

Clearly even the calculation of the flow derivative of M must be preceded by calculation of flow derivatives of several terms involving matrices. Simplifying the approach as much as possible we write (3.20) in the form:

$$M = \left[e^B - \frac{1}{\alpha}(e^B - I_2)U\right] \qquad \ldots \quad (3.21)$$

where (i) from (2.52) $[\psi_1\ \psi_2] = [1\ 1]\, B^{-1}(e^B - I_2)$

and (ii) $$U = \begin{bmatrix}\psi_1 & \psi_2\\ \psi_1 & \psi_2\end{bmatrix}$$

Thus, differentiating (3.21) and defining

$$\tilde{U} = (I_2 - \frac{I}{\alpha}U) = \frac{1}{\alpha}\begin{bmatrix}\psi_2 & -\psi_2\\ -\psi_1 & \psi_1\end{bmatrix}$$

$$\frac{\partial M}{\partial F_j} = \frac{\partial e^B}{\partial F_j}\tilde{U} - \frac{I}{\alpha}(e^B - I_2)\frac{\partial U}{\partial F_j} + \frac{1}{\alpha^2}(e^B - I_2)\, U\, \frac{\partial \alpha}{\partial F_j} \qquad \ldots \quad (3.22)$$

$j = 1,2$

Theorem 2.2 allows calculation of e^B from the expression

$$e^B = c_1 I_2 + c_2 B \qquad \ldots \quad (3.23)$$

where $c_1 = \dfrac{\lambda_1 e^{\lambda_2} - \lambda_2 e^{\lambda_1}}{\lambda_1 - \lambda_2}$, $c_2 = \dfrac{e^{\lambda_1} - e^{\lambda_2}}{\lambda_1 - \lambda_2}$

and λ_1, λ_2 are the eigenvalues of B (assumed distinct).

Flow derivatives are calculated in the following order:

(i) Calculate $\dfrac{\partial \lambda_1}{\partial F_j}$, $\dfrac{\partial \lambda_1}{\partial F_j}$ and $\dfrac{\partial}{\partial F_j}(\lambda_1 - \lambda_2)$

(ii) Use results of (i) to calculate $\dfrac{\partial c_1}{\partial F_j}$ and $\dfrac{\partial c_2}{\partial F_j}$

(iii) Use results of (ii) to calculate $\dfrac{\partial U}{\partial F_j}$ and $\dfrac{\partial \alpha}{\partial F_j}$

(iv) Calculate $\dfrac{\partial B}{\partial F_j}$ and use this and the results of (ii) to calculate $\dfrac{\partial e^B}{\partial F_j}$

(v) Use $\dfrac{\partial e^B}{\partial F_j}$, $\dfrac{\partial U}{\partial F_j}$ and $\dfrac{\partial \alpha}{\partial F_j}$ to calculate $\dfrac{\partial \mu_{mn}}{F_j}$ and hence $\dfrac{\partial \xi_{ik}}{\partial F_j}$

In the following analysis the two fluid flow rates are termed F_1 and F_2. For the heat exchanger read $F_2 = \tilde{F}_1$

(i) <u>Flow derivatives of the eigenvalues of B</u>

The characteristic equation of B is

$$\Delta(\lambda) = \begin{vmatrix} \lambda + \dfrac{K_{12} + K_{13}}{F_1 C_{p1}} & -\dfrac{K_{12}}{F_1 C_{p1}} \\ \dfrac{K_{12}}{F_2 C_{p2}} & \lambda - \dfrac{K_{12} + K_{13}}{F_2 C_{p2}} \end{vmatrix} \qquad \ldots \quad (3.24)$$

$$= \lambda^2 + \left[\frac{K_{12}+K_{13}}{F_1 C_{p1}} - \frac{K_{12}+K_{23}}{F_2 C_{p2}} \right] \lambda + \frac{K_{12}^2 - (K_{12}+K_{13})(K_{12}+K_{23})}{F_1 F_2 C_{p1} C_{p2}}$$

$$\ldots \quad (3.25)$$

The eigenvalues are given by

$$\lambda_i = -\tfrac{1}{2}y - (-1)^i z^{\frac{1}{2}} \qquad i = 1,2 \qquad \ldots \quad (3.26)$$

where $y = \left[\frac{K_{12} + K_{13}}{F_1 C_{p1}} - \frac{K_{12} + K_{23}}{F_2 C_{p2}} \right]$

and $z = y^2 - 4\left[\frac{K_{12}^2 - (K_{12} + K_{13})(K_{12} + K_{13})}{F_1 F_2 C_{p1} C_{p2}} \right]$

$$= \left[\frac{K_{12} + K_{13}}{F_1 C_{p1}} + \frac{K_{12} + K_{23}}{F_2 C_{p2}} \right]^2 - \frac{4K_{12}^2}{F_1 F_2 C_{p1} C_{p2}}$$

From (3.26) $\qquad \lambda_1 - \lambda_2 = z^{\frac{1}{2}} \qquad \ldots \quad (3.27)$

and by differentiating with respect to flow rate F_j

$$\frac{\partial \lambda_i}{\partial F_j} = -\tfrac{1}{2}\frac{\partial y}{\partial F_j} - (-1)^i \tfrac{1}{2} z^{-\frac{1}{2}} \frac{\partial z}{\partial F_j} \qquad i = 1,2 \quad j = 1,2$$

$$= -\tfrac{1}{2}\frac{\partial y}{\partial F_j} - (-1)^i \frac{1}{2(\lambda_1 - \lambda_2)} \frac{\partial z}{\partial F_j} \qquad \ldots \quad (3.28)$$

The required results follow by differentiating 'y' and 'z' with respect to the two flow rates and substituting into (3.28)

$$\frac{\partial \lambda_i}{\partial F_1} = \tfrac{1}{2}\left[\frac{K_{12}+K_{13}}{C_{p1} F_1^2} \right] + (-1)^i \frac{1}{2(\lambda_1 - \lambda_2)} \left\{ \left[\frac{K_{12}+K_{13}}{F_1 C_{p1}} + \frac{K_{12}+K_{23}}{F_2 C_{p2}} \right] \frac{K_{12}+K_{13}}{F_1^2 C_{p1}} - \frac{2K_{12}^2}{F_1^2 F_2 C_{p1} C_{p2}} \right\} \qquad \ldots \quad (3.29)$$

$i = 1,2$

$$\frac{\partial \lambda_i}{\partial F_2} = -\tfrac{1}{2}\left[\frac{K_{12}+K_{23}}{C_{p2} F_2^2} \right] + (-1)^i \frac{1}{2(\lambda_1 - \lambda_2)} \left\{ \left[\frac{K_{12}+K_{13}}{F_1 C_{p1}} + \frac{K_{12}+K_{23}}{F_2 C_{p2}} \right] \frac{K_{12}+K_{23}}{F_2^2 C_{p2}} - \frac{2K_{12}^2}{F_1 F_2^2 C_{p1} C_{p2}} \right\} \qquad \ldots \quad (3.30)$$

$i = 1,2$

also

$$\frac{\partial}{\partial F_1}(\lambda_1 - \lambda_2) = -\frac{1}{\lambda_1 - \lambda_2} \left\{ \left[\frac{K_{12}+K_{13}}{F_1 C_{p1}} + \frac{K_{12}+K_{23}}{F_2 C_{p2}} \right] \frac{K_{12}+K_{13}}{F_1^2 C_{p1}} + \frac{2K_{12}^2}{F_1^2 F_2 C_{p1} C_{p2}} \right\} \qquad \ldots \quad (3.31)$$

$$\frac{\partial}{\partial F_2}(\lambda_1-\lambda_2) = \frac{1}{\lambda_1-\lambda_2}\left\{\left[\frac{K_{12}+K_{13}}{F_1C_{p1}} + \frac{K_{12}+K_{23}}{F_2C_{p2}}\right]\frac{K_{12}+K_{23}}{F_2^2C_{p2}} + \frac{2K_{12}^2}{F_1F_2^2C_{p1}C_{p2}}\right\} \quad \ldots \quad (3.32)$$

(ii) Flow derivatives of exponential coefficients 'c_1' and 'c_2'

From (3.23) $\quad c_1 = \dfrac{\lambda_1 e^{\lambda_2} - \lambda_2 e^{\lambda_1}}{\lambda_1 - \lambda_2}$

Derivatives are obtained directly

$$\frac{\partial c_1}{\partial F_j} = \frac{(\lambda_1-\lambda_2)\frac{\partial}{\partial F_j}\{\lambda_1 e^{\lambda_2}-\lambda_2 e^{\lambda_1}\} - \{\lambda_1 e^{\lambda_2}-\lambda_2 e^{\lambda_1}\}\frac{\partial}{\partial F_j}(\lambda_1-\lambda_2)}{(\lambda_1-\lambda_2)^2}$$

$$= \frac{(e^{\lambda_2}-\lambda_2 e^{\lambda_1})\frac{\partial\lambda_1}{\partial F_j} - (e^{\lambda_1}-\lambda_1 e^{\lambda_2})\frac{\partial\lambda_2}{\partial F_j} - c_1\frac{\partial}{\partial F_j}(\lambda_1-\lambda_2)}{(\lambda_1-\lambda_2)}$$

$$j = 1,2 \quad \ldots \quad (3.33)$$

similarly $\quad c_2 = \dfrac{e^{\lambda_1} - e^{\lambda_2}}{\lambda_1 - \lambda_2}$

and $$\frac{\partial c_2}{\partial F_j} = \frac{\left\{e^{\lambda_1}\frac{\partial\lambda_1}{\partial F_j} - e^{\lambda_2}\frac{\partial\lambda_2}{\partial F_j}\right\} - c_2\frac{\partial}{\partial F_j}(\lambda_1-\lambda_2)}{\lambda_1-\lambda_2}$$

$$j = 1,2 \quad \ldots \quad (3.34)$$

(iii) Flow derivatives of 'U' and 'α'

$$[\Psi_1 \quad \Psi_2] = [1 \quad 1]\,B^{-1}\{e^B - I_2\}$$

and from (3.23) $= [1 \quad 1]\,B^{-1}\{(c_1-1)I_2 + c_2B\} \quad \ldots \quad (3.35)$

$$= [1 \quad 1]\,\{(c_1-1)B^{-1} + c_2I_2\} \quad \ldots \quad (3.36)$$

Now

$$B^{-1} = \frac{1}{\det B}\begin{bmatrix} \frac{K_{12}+K_{23}}{F_2C_{p2}} & -\frac{K_{12}}{F_1C_{p1}} \\ \frac{K_{12}}{F_2C_{p2}} & -\frac{K_{12}+K_{13}}{F_1C_{p1}} \end{bmatrix} \quad \ldots \quad (3.37)$$

where det B $= \dfrac{K_{12}^2 - (K_{12} + K_{13})(K_{12} + K_{23})}{F_1 F_2 C_{p1} C_{p2}}$

leading to

$$[1 \quad 1]\, B^{-1} = (c_1 - 1)\,\frac{1}{\det B}\left[\frac{2K_{12}+K_{23}}{F_2 C_{p2}} - \frac{2K_{12}+K_{13}}{F_1 C_{p1}}\right] \quad \ldots (3.38)$$

and by writing

$$\eta_1 = \frac{(2K_{13}+K_{23})\, C_{p1}}{K_{12}^2-(K_{12}+K_{13})(K_{12}+K_{23})}$$

and

$$\eta_2 = \frac{(2K_{12}+K_{13})C_{p2}}{K_{12}^2-(K_{12}+K_{13})(K_{12}+K_{23})}$$

$$[\psi_1 \; \psi_2] = \left[(c_1-1)\eta_1 F_1 + c_2 \quad -(c_1-1)\eta_2 F_2 + c_2\right] - \quad \ldots (3.39)$$

But from (3.21) $\quad U = \begin{bmatrix} \psi_1 & \psi_2 \\ \psi_1 & \psi_2 \end{bmatrix}$

and the required flow derivatives are

$$\frac{\partial U}{\partial F_1} = \begin{bmatrix} \eta_1(c_1-1)+\eta_1 F_1 \frac{\partial c_1}{\partial F_1} + \frac{\partial c_2}{\partial F_1} & -\eta_2 F_2 \frac{\partial c_1}{\partial F_1} + \frac{\partial c_2}{\partial F_1} \\ \eta_1(c_1-1)+\eta_1 F_1 \frac{\partial c_1}{\partial F_1} + \frac{\partial c_2}{\partial F_1} & -\eta_2 F_2 \frac{\partial c_1}{\partial F_1} + \frac{\partial c_2}{\partial F_1} \end{bmatrix} \quad \ldots (3.40)$$

$$\frac{\partial U}{\partial F_2} = \begin{bmatrix} \eta_1 F_1 \frac{\partial c_1}{\partial F_2} + \frac{\partial c_2}{\partial F_2} & -\eta_2(c_1-1)-\eta_2 F_2 \frac{\partial c_1}{\partial F_2} + \frac{\partial c_2}{\partial F_2} \\ \eta_1 F_1 \frac{\partial c_1}{\partial F_2} + \frac{\partial c_2}{\partial F_2} & -\eta_2(c_1-1)-\eta_2 F_2 \frac{\partial c_1}{\partial F_2} + \frac{\partial c_2}{\partial F_2} \end{bmatrix} \quad \ldots (3.41)$$

Also $\alpha = \psi_1 + \psi_2 = (c_1-1)\left[\eta_1 F_1 - \eta_2 F_2\right] + 2c_2 \quad \ldots (3.42)$

so that

$$\frac{\partial \alpha}{\partial F_1} = \eta_1(c_1-1) + (\eta_1 F_1 - \eta_2 F_2)\frac{\partial c_1}{\partial F_1} + 2\frac{\partial c_2}{\partial F_1} \quad \ldots (3.43)$$

and

$$\frac{\partial \alpha}{\partial F_2} = -\eta_2(c_1-1) + (\eta_1 F_1 - \eta_2 F_2)\frac{\partial c_1}{\partial F_2} + 2\frac{\partial c_2}{\partial F_2} \quad \ldots (3.44)$$

(iv) Flow derivatives of B and e^B

Flow derivatives of matrix B are obtained directly from the definition of B in equation (2.25)

Hence

$$\frac{\partial B}{\partial F_1} = \begin{bmatrix} \frac{K_{12}+K_{13}}{F_1{}^2C_{p1}} & -\frac{K_{12}}{F_1{}^2C_{p1}} \\ 0 & 0 \end{bmatrix} \quad \text{and} \quad \frac{\partial B}{\partial F_2} = \begin{bmatrix} 0 & 0 \\ \frac{K_{12}}{F_2{}^2C_{p2}} & -\frac{K_{12}+K_{23}}{F_2{}^2C_{p2}} \end{bmatrix}$$

... (3.45) ... (3.46)

Now $e^B = c_1 I_2 + c_2 B$, and taking the derivative with respect to F_j

$$\frac{\partial}{\partial F_j}[e^B] = \frac{\partial c_1}{\partial F_j} I_2 + c_2 \frac{\partial B}{\partial F_j} + \frac{\partial c_2}{\partial F_j} B, \quad j = 1,2 \qquad \ldots \quad (3.47)$$

(v) Flow derivative of M and hence of Ξ

Once stages (i) - (iv) have been completed, $\frac{\partial M}{\partial F_j}$ is calculated from equation (3.22).

This furnishes $\frac{\partial \mu_{11}}{\partial F_j}$ $\frac{\partial \mu_{12}}{\partial F_j}$ $\frac{\partial \mu_{21}}{\partial F_j}$ and $\frac{\partial \mu_{22}}{\partial F_j}$, $j = 1,2$

By comparing (3.13) and (3.14) with (3.16) and (3.17)

$$\Xi = \begin{bmatrix} \xi_{11} & \xi_{12} \\ \xi_{21} & \xi_{22} \end{bmatrix} = \begin{bmatrix} \frac{\mu_{11}\mu_{22} - \mu_{12}\mu_{21}}{\mu_{22}} & \frac{\mu_{12}}{\mu_{22}} \\ \frac{\mu_{21}}{\mu_{22}} & \frac{1}{\mu_{22}} \end{bmatrix} \qquad (3.48)$$

The required flow derivatives of output temperatures $T_1(L)$ and $T_2(0)$ are thus given by substituting for the derivatives of ξ_{ik} in (3.13) and (3.14).

$$\frac{\partial T_1(L)}{\partial F_j} = \left\{ \frac{\partial \mu_{11}}{\partial F_j} - \frac{\mu_{22}\left[\mu_{12}\frac{\partial \mu_{21}}{\partial F_j} + \mu_{21}\frac{\partial \mu_{12}}{\partial F_j}\right] - \mu_{12}\mu_{21}\frac{\partial \mu_{22}}{\partial F_j}}{\mu_{22}^2} \right\} T_1(0)$$

$$+ \left\{ \frac{\mu_{22}\frac{\partial \mu_{12}}{\partial F_j} - \mu_{12}\frac{\partial \mu_{22}}{\partial F_j}}{\mu_{22}^2} \right\} T_2(L) \quad \ldots \quad (3.49)$$

$$j = 1,2$$

$$\frac{\partial T_2(0)}{\partial F_j} = \left\{ \frac{-\mu_{22}\frac{\partial \mu_{21}}{\partial F_j} + \mu_{21}\frac{\partial \mu_{22}}{\partial F_j}}{\mu_{22}^2} \right\} T_1(0) - \left\{ \frac{\frac{\partial \mu_{22}}{\partial F_j}}{\mu_{22}^2} \right\} T_2(L) \ldots (3.50)$$

$$j = 1,2$$

3.5 Transient Modelling

This section sets out to model the cooler and heat exchanger fluid temperature responses to step changes in either cooling water or MEA flow rate. The ideas formulated in this section are further developed in Chapter 4 with the aim of generating o.d.e's of the form of (3.7) and (3.8) for state space modelling. Approximations are used to cut down the number of time constants used to model the system dynamics, thus yielding a low order model which is relatively easy to handle.

Although for filter development the plant is to be modelled as a stochastic system with noisy measurements, it is typical of many plants in the process industry in that it exhibits very low noise levels. Most variables of interest in this section of the plant are generally quite smooth functions of time and permit the analysis to be carried out in a deterministic setting.

Each flow jump was timed to fall just after a sampling instant. This was done by entering the setpoint change at the operator's console (see Appendix I) and pressing the 'execute' button immediately after the high speed punch had output a set of measurements. After an initial transient lasting from three to four minutes, any such change in flow rate causes temperature drifting around the plant that may take half an hour to settle down. In the short term, however, input temperatures governed by conditions elsewhere in the plant may be considered steady so that the transients obtained are in response to step changes in flow input only.

3.5.1 Step changes in the cooling water flow rate

From the experimental work of run PLANT3 it would appear that on a change in setpoint the response of control valve CV110 and hence of the cooler c/w flow rate approximates to a simple exponential. The flow rate setpoint change is itself a true step function and the actual flow rate change may be thought of as the output of a first order delay to which the setpoint is input.

With the proportional and integral control terms set at the values given in Appendix I, additional experiments were carried out on the FX124/CV110 control loop with the flow rate recorded on tape at a 2 second sampling interval. Assuming the flow measurement loop time constant to be negligible in comparison with the valve delay, the time constant for the cooling water flow rate change was found to vary between 7 and 10 seconds irrespective of step size. The shape of the leading edge could not be improved by adjustment of the proportional gain.

3.5.2 Step changes in the MEA flow rate

As explained in Appendix I, although it is the stripped MEA flow rate that is held to a setpoint, any change in flow F_1 propagates through the absorber so that after a delay there is a corresponding jump in spent MEA flow rate $\tilde{F}_1$. It follows that for the heat exchanger it is not possible to obtain experimentally the response to a step change in F_1 in isolation.

MEA flow characteristics are dependent on two control loops, FX101/CV101 and LX111/CV111. Typical experimental results are shown in Fig.11 for which the control terms were as given in Appendix I. Changes in F_1 are approximately exponential and, with a time constant of around 3 seconds, valve CV101 has a rather faster response than CV110 controlling the cooling water flow. This is due to the fact that in common with CV111 but unlike CV110, valve CV101 is fitted with a booster.

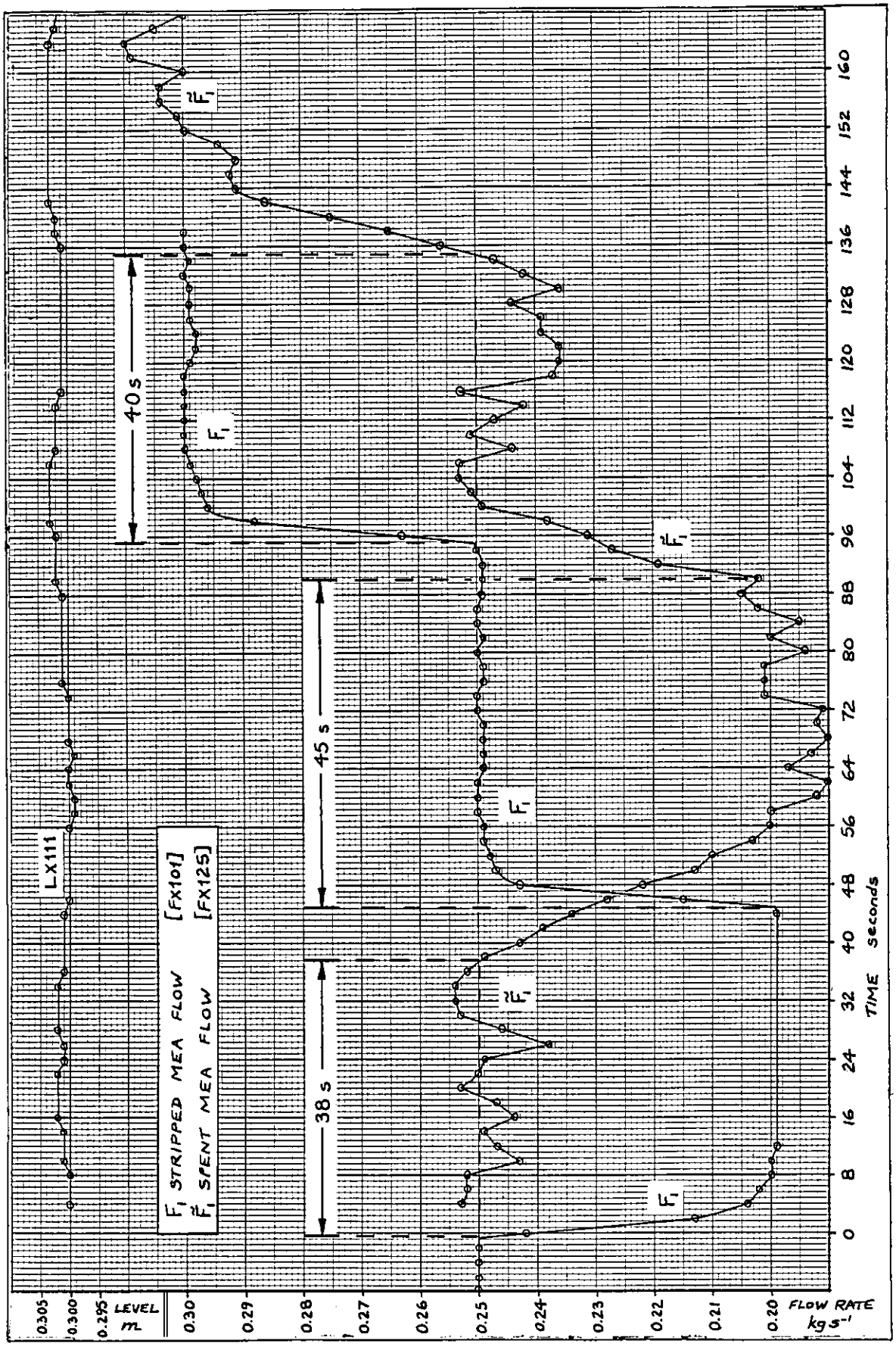

Fig.11 Absorber level and MEA flow response to step changes in F_1, showing transport delay introduced by absorber packing

The transport delay introduced by the absorber was found to depend mainly on the flow at the time of the flow setpoint change. The delay is difficult to estimate from Fig. 11 because of the extremely noisy $\tilde{F}_1$ readings, but it is clear that at $F_1 = 0.25$ kgs^{-1} the delay is about 40 seconds for a 0.05 kgs^{-1} step in either direction; varying the step size did not have a marked effect. At $F_1 = 0.25$ kgs^{-1} there is less liquid hold up in the absorber column and flow rate changes take longer to propagate; about 45 seconds in this example. Measurements of $\tilde{F}_1$ (FX125) were found to be extremely noisy at all times with a standard deviation of 0.01 - 0.02 kgs^{-1} compared with 0.001 - 0.003 kgs^{-1} for F_1 (FX101). The noise precludes accurate determination of a time constant for the change in $\tilde{F}_1$ following a step change in F_1 and, in any case, the flow-time curves for $\tilde{F}_1$ were not found to be reliably repeatable under identical experimental conditions.

3.5.3 Reduction of the number of time constants

From the outset the aim has been to build a model suitable for an implementable fault detection system. The computational load imposed by the Kalman filter rises dramatically with increasing model order and so the emphasis must be on the derivation of a low order model. This is balanced by the need to obtain a 'reasonable' approximation to the function $\zeta(t)$ of Section 3.3. In this section methods are discussed for the approximation of $\zeta(t)$ by first and second order exponentials.

The response of a delay of order 'n' to a step input can be represented by an nth order o.d.e. In state space form this would be replaced by a system of 'n' first order o.d.e.'s or, equivalently, 'n' system states would be required. Clearly the number of time constants must be kept to a minimum by neglecting or lumping together the many secondary effects that exist on a real plant. For flow rate setpoint step changes applied to the process units in question, the three main sources of delay are the control valves, the system dynamics and the measuring devices, all of which must be considered separately for each channel.

Valve delays were discussed in Sections 3.5.1 and 3.5.2 and clearly cannot be neglected. Section 3.5.4 includes discussion of a method for avoiding the introduction of a valve time constant by assuming the existence of a fictitious zero-order hold condition.

The transients obtained from run PLANT3 indicate that some responses, particularly those connected with the heat exchanger, approximate to second order delays. In these cases the two time constants required can conveniently be classified as system and measurement delays. It is important to realise that two time constants are used simply because this would appear to be the lowest number required to adequately represent certain responses. By labelling them 'system' and 'measurement' time constants we have identified the dominant delay in each case but must not lose sight of the fact that these terms are 'catch-alls' for unmodelled secondary effects.

The 'system' time constant represents the thermal inertia of the system itself and includes the delays in changing the temperature of the process fluid in each channel, the exchanger metalwork and the pipework between the exchanger and the rtd's. The heat exchanger has five times the capacity and metalwork of the cooler and so we would expect the effects of the system dynamics to be more in evidence with the former than with the latter. It is assumed that the delay parameter is constant with flow rate and that all second and higher order effects can be neglected.

The 'measurement' time constant represents the thermal and electrical delays in the measurement loop and includes the delay in transferring heat to the thermowell, the thermal inertia of the thermowell and of the resistance bulb itself plus any delays introduced by other devices in the loop such as the R/I converter. The coefficient of heat transfer between process fluid and thermowell varies slightly with fluid flow rate, but it is assumed that over a limited flow range this and the other delays can be approximated by a single, constant delay parameter. All second and higher order effects are again neglected.

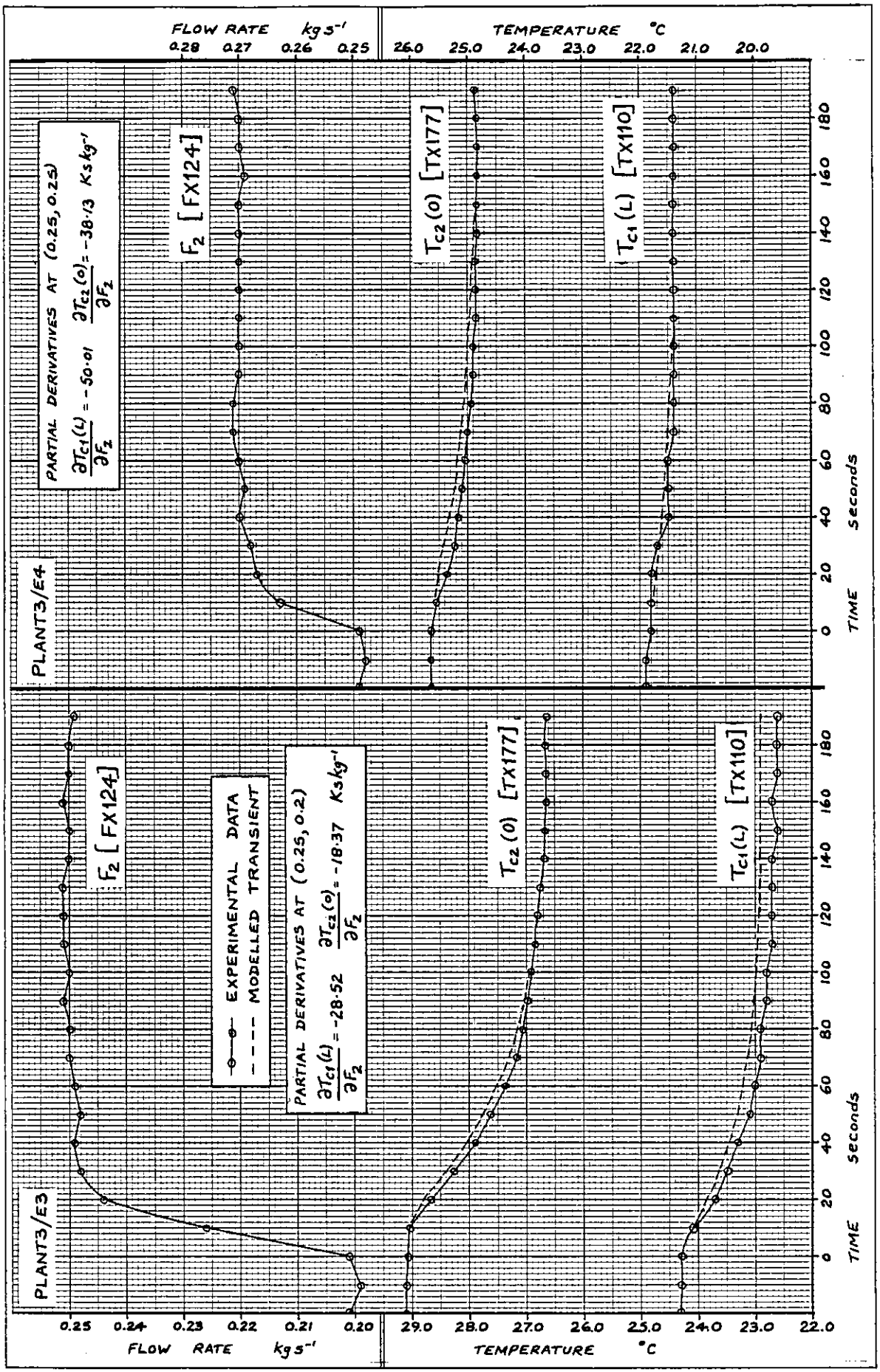

Fig.12 Effect on the cooler of a step change in cooling water flow rate

Data: PLANT3

3.5.4 Effect on the cooler of a step change in cooling water flow rate

Fig. 12 shows the results of applying cooling water flow step changes of +0.05 kgs^{-1} (experiment 3/E3) and +0.02kgs^{-1} (3/E4) as listed in Table 3. Note that the 'end' temperature symbols now carry the additional suffix 'c' for 'cooler' (e.g. $T_{c2}(0)$ to distinguish them from similar symbols used for the heat exchanger which will carry the suffix 'x'. TX174 can be referred to as $T_{c1}(0)$ or $T_{x1}(L)$ depending on context.

The 3/E3 traces for temperatures $T_{c1}(L)$ and $T_{c2}(0)$ approximate to first order exponentials and the curves are well defined for $t \geq 20$ seconds allowing graphical estimation of time constants. These were found to be:

for	$T_{c1}(L)$	$\tau_1 = 36s$
	$T_{c2}(0)$	$\tau_2 = 45s$

The process fluid capacity of the cooler is given on the plant drawings as "1 pint" implying that at a flow rate of $F_1 = 0.25$ kgs^{-1} the residence time is about 2 seconds. The transient response of a platinum resistance thermometer is very fast, but this short time constant will always be swamped in practice by the thermal delay introduced by the thermowell. The short residence time implies that the cooler dynamics are virtually instantaneous in comparison with the thermal lags due to the measurement loops. For the cooler the responses are effectively first order, with 'measurement' time constants τ_1 and τ_2 and 'system' time constants zero.

For each output temperature a true step function (the flow setpoint) is effectively applied to a system comprising two first order delays in series. Delay 'a' is valve CV110 with τ_a about 10 seconds, 'b' is thermal lag τ_1 or τ_2 and the system 'gain' is partial derivative $\partial T_x(\cdot)/\partial F_2$. With τ_b rather longer than τ_a it is easily shown that the theoretical response to the input step approximates to a simple exponential with time constant τ_b but delayed by τ_a

seconds. Assuming that the flow setpoint was altered at t = 0, inspection of Fig. 12 reveals that neither temperature is affected until approximately t = 10 seconds ($=\tau_a$), but then each changes exponentially, with time constant τ_1 or τ_2, in accordance with the theory.

In Chapter 4 the continuous-time framework of this chapter gives way to a discrete-time model consistent with the discrete nature of the measurements available to the computer system. A basic assumption of such a transformation is that system inputs remain constant between sampling instants ('zero-order hold'), a condition clearly not satisfied by F_2 immediately following a setpoint change. Rather than using the flow measurement FX124 it would be possible to constrain each setpoint change to occur immediately prior to a sampling instant and to model the cooling water flow by passing the flow setpoint through a first order delay with time constant τ_a. However, by introducing a fictitious zero-order hold condition the inclusion of τ_a in the model can be avoided.

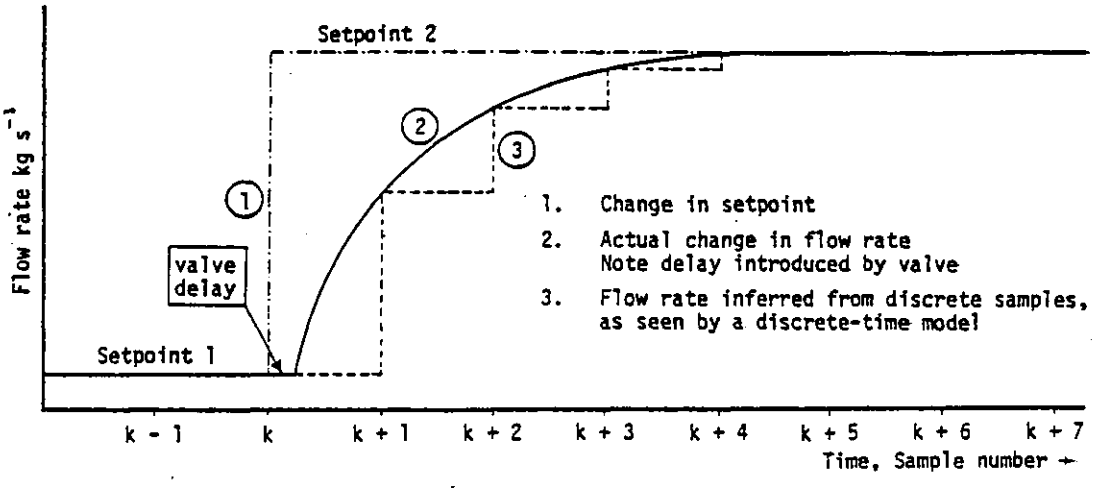

Fig.13 Flow setpoint change showing actual and inferred flow rates

Suppose that F_2 is at setpoint '1' (Fig. 13). If a setpoint change is timed to fall just after sampling instant 'k' then a discrete time model assumes that $F_2 = F_2(k)$ for $k \leq t < k+1$, even though by t = k+1 the actual flow $F_2(t)$ is two thirds of the way to its new value at s.p. '2'. At 'k+1' the computer 'sees' a value $F_2(k+1)$ which it interprets as a step of height $\{F_2(k+1)-F_2(k)\}$ occurring at t = k+1. Further steps of diminishing size

occur at k+2, k+3, etc, until F_2 has become steady at s.p.2. The cooler can thus be modelled by representing channels 1 and 2 as first order delays with time constants τ_1 and τ_2 and applying inputs $F_2(n)$ at discrete times $n = \ldots k-1, k, k+1 \ldots$ etc.

By using sampled values of F_2,a setpoint change at t=0 is applied to the model in stages starting at t = 10 seconds. This takes advantage of the fact that τ_a is approximately equal to the sampling interval and means that the modelled temperatures do not begin to change until t = 10, as required. The effect of this modification is to cause the modelled transients, shown dashed in Fig.12, to lag slightly behind the true responses. These curves are quite a reasonable fit to the experimental data, the 0.3°C discrepancy in the settled out value of $T_{C1}(L)$ in 3/E3 being due to linearization error as is apparent from Fig.10.

3.5.5 Effect on the cooler of a step change in MEA flow rate

The effect of changing the MEA setpoint is summarized by Fig. 14 in which instantaneous cooler dynamics are assumed. In this section the actual fluid temperature whose measured value is TX1xx is denoted by 'T1xx'.

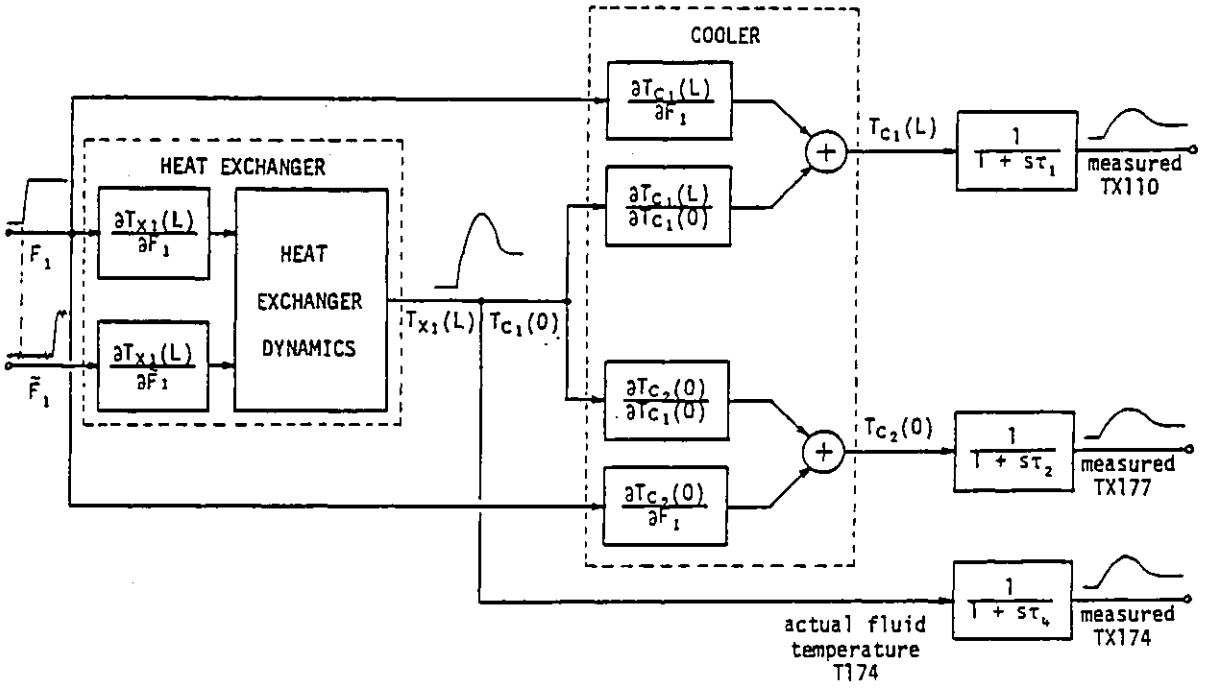

Fig.14 Block schematic showing how a step change in F_1 affects temperatures throughout the heat exchanger/cooler subsystem

The 'measurement' time constant, due primarily to the thermowell, affects every temperature measurement on the plant and must be evaluated for each of the process unit output temperatures. For the cooler the system time constant is negligible and the step responses of TX110 and TX177 readily allow extraction of measurement time constants τ_1 and τ_2. This section shows how time constant τ_4, associated with TX174, can be obtained by considering the effect on the cooler of a change in MEA flow rate.

The system time constant for the heat exchanger cannot be neglected: the response of TX174 to an MEA flow step is second order. The measurement time constant cannot therefore be obtained directly from this response without prior knowledge of τ_3, the system time constant for the stripped MEA channel of the heat exchanger. A measurement time constant could be obtained by removing TX174 (both rtd and thermowell) from the plant and testing the assembly in isolation by using water baths at different temperatures. The result of such an experiment could however be misleading because the water bath cannot reproduce the actual plant conditions, particularly with regard to heat transfer between fluid and thermowell. This method is in any case not necessary because there is a way of obtaining the required value from existing PLANT3 data.

Recall that TX174 is an output from the heat exchanger $[T_{X1}(L)]$ as well as an input to the cooler $[T_{C1}(0)]$. An MEA flow rate step causes a transient in the heat exchanger which in turn gives rise to a transient in TX174. The cooler is thus affected by simultaneous changes in two inputs, the MEA flow rate F_1 and the (stripped) MEA inlet temperature $T_{C1}(0)$. If the changes in the cooler output temperatures due to each cause are separated out then that due to the change in $T_{C1}(0)$ alone allows τ_4 to be estimated as follows.

A 'small' step change ΔF_1 causes a steady state change of $\Delta T_{C1}(0)$ in $T_{C1}(0)$ which is measured by TX174. The overall cooler output temperature changes are thus given by:

$$\Delta T_{c1}(L) = \frac{\partial T_{c1}(L)}{\partial T_{c2}(0)} \Delta T_{c1}(0) + \frac{\partial T_{c1}(L)}{\partial F_1} \Delta F_1 \quad \ldots \quad (3.51)$$

$$\Delta T_{c2}(0) = \frac{\partial T_{c2}(0)}{\partial T_{c1}(0)} \Delta T_{c1}(0) + \frac{\partial T_{c2}(0)}{\partial F_1} \Delta F_1 \quad \ldots \quad (3.52)$$

Because of system nonlinearity, equations (3.51) and (3.52) give good but not exact agreement between predicted and observed overall changes in temperature. All available plant data was processed to find the data set in which the actual and predicted values from either equation were closest. In every case (3.52) gave better prediction than (3.51) and a data set from run PLANT7 (described in Chapter 6) was selected. A jump of +0.05 kgs^{-1} in F_1 resulted in an observed $\Delta T_{c2}(0)$ of +2.1°C. ΔT174 was +0.75°C resulting in a 0.46° predicted rise in $T_{c2}(0)$ and this, coupled with a predicted 1.75° rise due to the flow jump itself, gave an overall predicted temperature change of +2.21°C.

The estimation procedure is laid out in Fig. 15 and makes use of the fact that the actual fluid temperature T and the observed value TX are related by the equation

$$\frac{dTX}{dt} = -\frac{1}{\tau_m} TX + \frac{1}{\tau_m} T \quad \ldots \quad (3.53)$$

where τ_m is the measurement time constant.

Hence the actual temperature can be estimated from

$$T = \tau_m \frac{dTX}{dt} + TX \quad \ldots \quad (3.54)$$

or, if both T and TX are known, τ_m can be estimated:

$$\tau_m = \frac{T - TX}{(dTX/dt)} \quad \ldots \quad (3.55)$$

The smoothing of TX177 in Step 1 ensures a smooth curve from Step 2, which uses (3.54) to obtain an estimate of T177 from TX177 via $\tau_m = \tau_2 = 45$ secs. Having isolated that part of

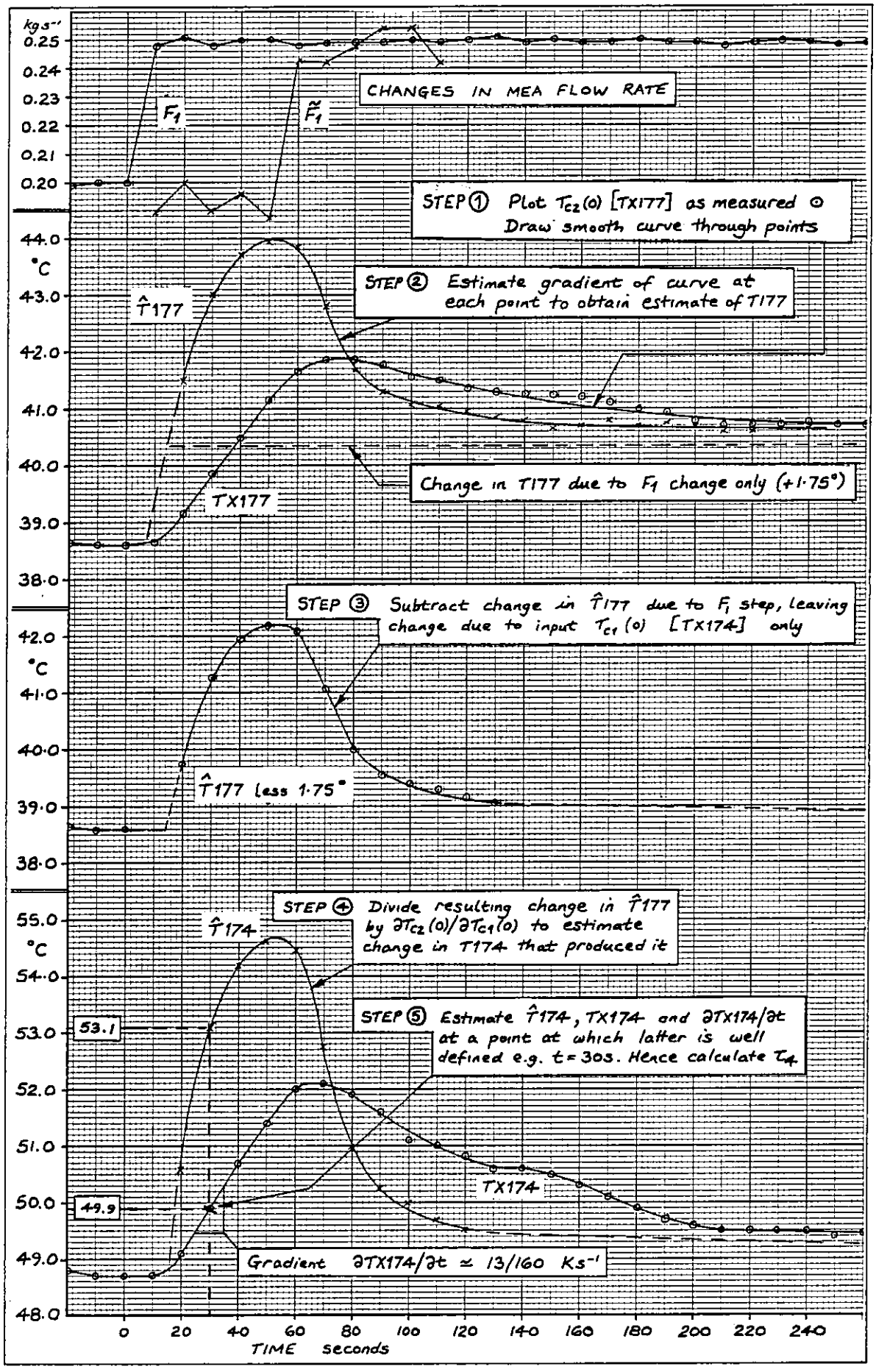

Fig.15 Method of obtaining an approximation to τ_4 Data: PLANT7

the change in T177 that is due to the change in T174 only, the latter can be calculated as in Step 4. In Step 5 values are obtained at a particular point for T174 and TX174, enabling τ_m (i.e. τ_4) to be estimated from (3.55).

$$\tau_4 = \frac{53.1 - 4.99}{13/160} \simeq 40 \text{ s}$$

For $0 \leq t < 50$ s the curve for T174 produced in Step 4 represents the actual fluid temperature response to a step change in F_1 only. Without the corresponding $\tilde{F}_1$ jump at $t \simeq 50$ s the temperature would eventually rise by 7.1° to 55.8°C, since $\Delta F_1 = +0.05$ kgs^{-1} and $\partial T_{X1}(L)/\partial F_1 = +142.2$ Kskg^{-1} at this operating point. While the cooler can be considered to exhibit instantaneous dynamics, the heat exchanger contains five times as much process fluid and five times as many plates. From the leading edge of the Step 4 curve it is apparent that the rise in T174 is governed by a time constant τ_3 of approximately 22 seconds, which can be thought of as representing the delay in heating the process fluid and exchanger metalwork.

3.5.6 Flow rates as model inputs

In section 3.5.3, problems concerning the timing of cooling water flow step changes for modelling were circumvented by assuming that the sampled flow inputs were generated by a zero-order hold.

While selecting a part of the plant for study, data from a preliminary run PLANT1 was run through a filter based on equations derived by Palmquist [66]. These experiments showed that the zero-order hold assumption worked well with F_1[FX101] values, but that the high variance of the $\tilde{F}_1$ values caused instability in the estimates if the readings from FX125 were used as model inputs.

Following an MEA flow setpoint change, the step in $\tilde{F}_1$ is of the same magnitude as the step in F_1. For discrete time modelling, $\tilde{F}_1$ jumps can therefore be approximated by storing

F_1 values for an integral number of time steps and re-using them in place of the measured $\tilde{F}_1$ values.

3.5.7 Effect on the heat exchanger of a step change in MEA flow rate

The section of Fig. 14 that deals with the heat exchanger can now be redrawn as Fig. 16 to include output $T_{X2}(0)$ and to show the constants that remain to be estimated.

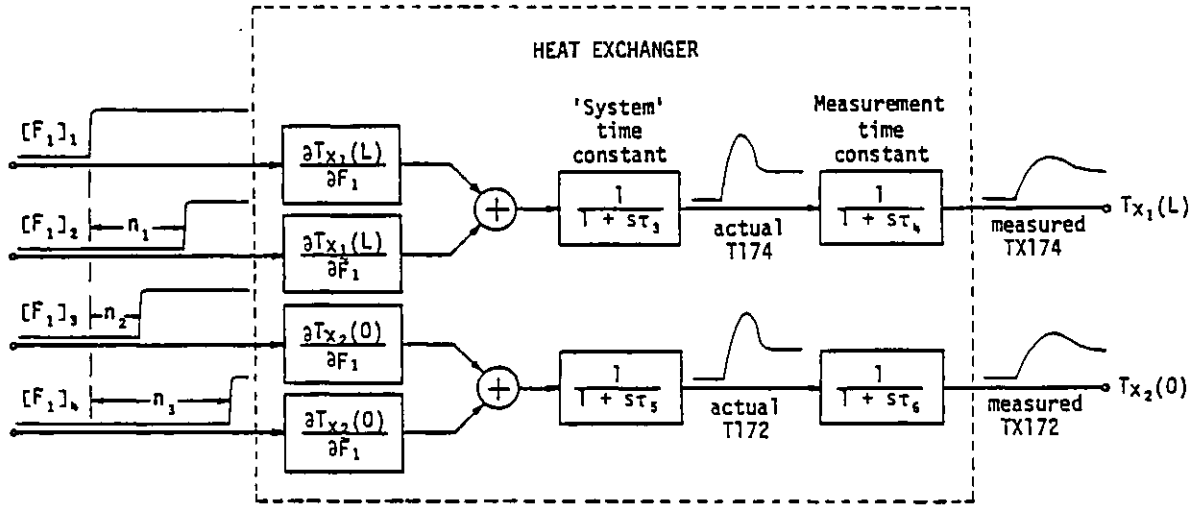

Fig.16 Block schematic showing heat exchanger model with $\tilde{F}_1$ flow input replaced by stored F_1 input

All available data was again processed to find the data sets giving the closest agreement between experiment and equations (3.56) and (3.57) predicting overall temperature change:

$$\Delta T_{X1}(L) = \left\{ \frac{\partial T_{X1}(L)}{\partial F_1} + \frac{\partial T_{X1}(L)}{\partial \tilde{F}_1} \right\} \Delta F_1 \qquad \ldots \quad (3.56)$$

$$\Delta T_{X2}(0) = \left\{ \frac{\partial T_{X2}(0)}{\partial F_1} + \frac{\partial T_{X2}(0)}{\partial \tilde{F}_1} \right\} \Delta F_1 \qquad \ldots \quad (3.57)$$

bearing in mind that $\Delta\tilde{F}_1 = \Delta F_1$. Data sets from PLANT3/E1 and from PLANT7 were selected and transients are plotted in Fig. 17.

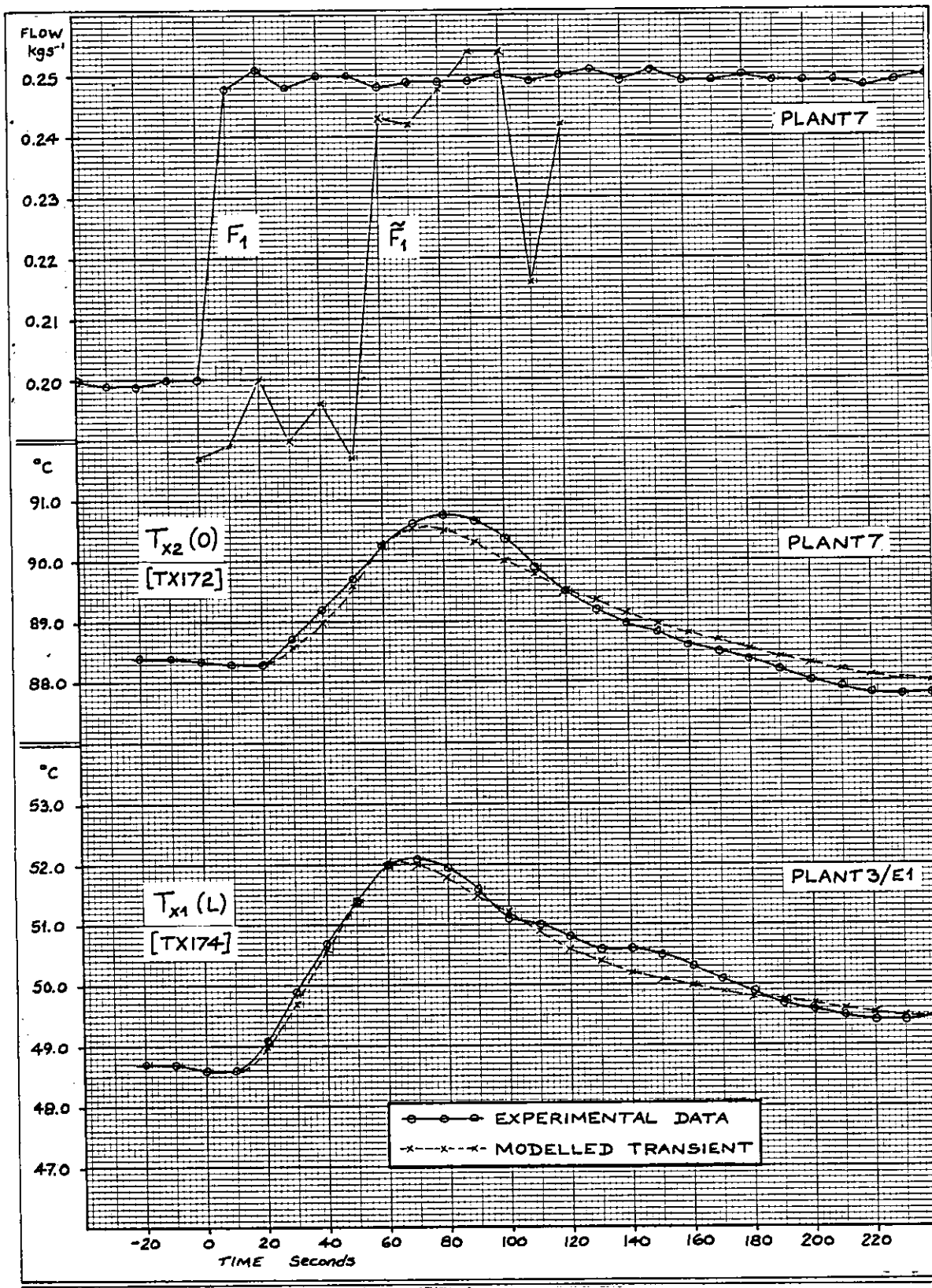

Fig.17 Effect on the heat exchanger of a step change in MEA flow rate

Data: PLANT3 & PLANT7

Having estimated τ_3 and τ_4, the flow response of TX174 is completely modelled by estimating the artificial delay n_1 associated with the stored value $[F_1]_2$ replacing $\tilde{F}_1$. Experiment shows that with a step change in F_1 occurring at t = 0, TX174 begins to change at about t = 10 and TX172 at about t = 20 (see Fig. 17). The delay of one sampling period relating to TX174 is handled by applying the zero order hold assumption to $[F_1]_1$ as with the cooling water jumps in section 3.5.4. An estimate for n_1 is obtained by finding the value w_1 for which curve (3.58) best fits the experimental curve from the PLANT3/E1 data.

$$\Delta TX174 = \Delta F_1\left[1+\nu_3 e^{-t/\tau_3} - \nu_4 e^{-t/\tau_4}\right] \frac{\partial T_{X1}(L)}{\partial F_1}$$

$$+ \Delta F_1 H(t-w_1\Delta)\left[1+\nu_3 e^{-(t-w_1\Delta)/\tau_3} - \nu_4 e^{(t-w_1\Delta)/\tau_4}\right] \frac{\partial T_{X1}(L)}{\partial \tilde{F}_1} \quad \ldots \quad (3.58)$$

where $\nu_3 = \tau_3/(\tau_4 - \tau_3)$ $\quad$ $\nu_4 = \tau_4/(\tau_4 - \tau_3)$

$H(t-x)$ is the Heaviside step function

and Δ is the sampling period, here 10 seconds.

A value of 4 for w_1 gave the 'modelled' curve for TX174 in Fig. 17. This was found to be a closer fit than w_1 = 3 or 5, hence $n_1 = 4\Delta = 40$ seconds.

The change in TX172 occurs about 20 seconds after an F_1 step change. This is conveniently about 10 seconds, or one sampling period, after the change in TX174. This delay can be handled by using as the third flow input in Fig. 16 not $[F_1]_1$ as in reality but $[F_1]_3$ such that $[F_1]_3(k) = [F_1]_1(k-1)$, i.e. n_2 = 10 seconds.

The final stage is to estimate τ_5, τ_6 and n_3, thus enabling the flow response of TX172 to be modelled. It is not possible to separate the effects of these constants and approximations can only be obtained by finding a set of values for which curve (3.59) is a reasonable fit to the experimental curve from the PLANT7 data of Fig. 17.

$$\Delta TX172 = \Delta F_1\left[1+\nu_5 e^{-t/\tau_5} - \nu_6 e^{-t/\tau_6}\right]\frac{\partial T_{X_2}(0)}{\partial F_1}$$

$$+ \Delta F_1 H(t-w_3\Delta)\left[1+\nu_5 e^{-(t-w_3\Delta)/\tau_5} - \nu_6 e^{(t-w_3\Delta)/\tau_6}\right]\frac{\partial T_{X1}(L)}{\partial \tilde{F}_1} \quad \ldots \quad (3.59)$$

where $\nu_5 = \tau_5/(\tau_6 - \tau_5)$ $\qquad$ $\nu_6 = \tau_6/(\tau_6 - \tau_5)$

$H(t-x)$ and Δ as in (3.58) and $n_3 = w_3\Delta$

An attempt was made to find sets of values for τ_5, τ_6 and w_3 by trial and error, but in practice it proved impossible to obtain a unique set of estimates from the PLANT7 data alone. Extending the analysis to TX172 flow responses from experiments PLANT3/E1 and PLANT8 (see Chapter 6) also failed to give consistent results. Eventually the values

$\tau_5 = 12s$ $\qquad$ $\tau_6 = 100s$ and $n_3 = 50s$

were selected. These values were chosen because they are of the same order as the 'system' and 'measurement' time constants τ_3 and τ_4 for TX174 and because when substituted into equation (3.59) they gave a reasonable approximation to the PLANT7 data as shown by the 'modelled transient' of Fig. 17.

3.6 Constants for transient modelling

The nine constants obtained in section 3.5 are thus as follows:

Constant	Value,s	Description
τ_1	36	Measurement delay for TX110
τ_2	45	Measurement delay for TX177
τ_3	22	System delay for T174
τ_4	40	Measurement delay for TX174
τ_5	12	System delay for T172
τ_6	100	Measurement delay for TX172
n_1	40	Flow input delay, i.e. $[F_1]_2(k)=[F_1]_1(k-4)$
n_2	10	Flow input delay, i.e. $[F_1]_3(k)=[F_1]_1(k-1)$
n_3	50	Flow input delay, i.e. $[F_1]_4(k)=[F_1]\ (k-5)$

3.7 Summary

It has been shown in this chapter that the steady state analysis of the three fluid model performed in Chapter 2 cannot be extended to the transient case. A simple equation that is representative of the full solution can, however, be used to model the system by considering it as a series of steady state gains together with time delays governed by system and measurement time constants.

The main theoretical contribution of this chapter is the derivation of partial derivatives for the process unit output temperatures with respect to flow and temperature input variables. A model that is new for this particular plant is developed around six time constants, four of which can be individually estimated in a logical sequence. The extremely noisy $\tilde{F}_1$ spent MEA flow input is dispensed with, the measured F_1 input at each time 'k' being stored and used four times at k, k + 1, k + 4 and k + 5.

The lumping of so many transient effects into the two 'system' and 'measurement' time constants is of course a vast oversimplification. This is balanced by the small number of parameters required to represent the system in this way, which will in the next chapter give rise to a low order model and a Kalman filter with modest computational requirements. The model must be judged solely by its performance when incorporated into a fault detection algorithm in Chapter 6.

In common with the work of Chapter 2, all the results of this chapter are based on real data from experimental work on the pilot plant.

CHAPTER 4

FILTER DESIGN AND SIMPLE FAULT DETECTION

4.0 Introduction

This chapter moulds the work of the previous two chapters into a six state discrete-time linear model suitable for Kalman filtering and restates the fault detection problem in detail. Proceeding along similar lines to Bellingham and Lees [9], [50] this is followed by an attempt at identification of the measurement noise covariance and optimal Kalman gain using Godbole's modification [11] of the algorithm of Mehra [10].

Similar difficulties to those discussed in [9] and [50] are experienced with the algorithm but the decision is taken not to add artificial measurement noise. Innovations generated by running real plant data through a Kalman filter are tested for normality by means of the Kolmogorov-Smirnov test and the chapter concludes with some simple examples to examine by simulation the feasibility of some ideas for fault detection algorithms.

4.1 The continuous-time state space model

The first stage in filter design is to obtain a model in the standard state space form (see, for example, Chapter 1 of Kwakernaak and Sivan [7]). Rather than using absolute values of process variables we employ 'perturbation variables' in order to make use of the equations of Chapter 3 which relate changes in flow and temperature. When the plant has reached steady state, the variables of interest at this 'stable operating point' can be taken as the nominal values for calculation of perturbation variables. For regulated flow rates the base value is the setpoint, while temperatures can be averaged over a number of data points.

Perturbation variables are simply deviations from the nominal values at the selected stable operating point. Suppose at this point the cooling water outlet temperature is $\overline{TX177}$. At any subsequent time 't' the perturbation variable associated with TX177, which turns out to be state variable x_2, is defined as:

$$x_2(t) = TX177(t) - \overline{TX177}$$

The states of the system arise naturally as those (perturbation) variables whose rates of change can be expressed in terms of other plant variables by means of first order o.d.e's. The measurements of the cooler outlet temperatures are related to flow and temperature changes via single measurement time constants and are included as x_1 and x_2. The step responses of the heat exchanger outlet temperatures are second order and intermediate variables must be introduced to split these into pairs of first order o.d.e's. This is done by including the measured outlet temperatures as states x_4 and x_6 and relating these to the actual liquid outlet temperatures via the measurement time constants. By definition these 'actual' temperatures cannot be measured but they can still be included as states and are designated x_3 and x_5. These are in turn related to flow and temperature changes via the system time constants. The state variables (x), inputs (u) and outputs (y) used for filter design are summarized in Table 11.

TABLE 11

STATE	SYMBOL	PROCESS VARIABLE	OUTPUT	INPUT	SYMBOL	PROCESS VARIABLE
x_1	$t_{c1}(L)$	TX110	y_1	u_1	$[f_1]_1$	FX101
x_2	$t_{c2}(0)$	TX177	y_2	u_2	$[f_1]_2$	FX101 delayed n_1
x_3	-	T174	-	u_3	f_2	FX124
x_4	$t_{c1}(0)$ / $t_{x1}(L)$	TX174	y_3	u_4	$t_{x1}(0)$	TX173
				u_5	$t_{x2}(L)$	TX175
x_5	-	T172	-	u_6	$t_{c2}(L)$	TX176
x_6	$t_{x2}(0)$	TX172	y_4	u_7	$[f_1]_3$	FX101 delayed n_2
				u_8	$[f_1]_4$	FX101 delayed n_3

4.1.1 Form of equations

For a system with a first order step response, the state x_a is related via time constant τ_j either to one other state x_b, as in equation (4.1), or to an 'input' u(t), as in equation (4.2). Note that $\alpha_j = 1/\tau_j$ in each case.

$$\dot{x}_a(t) = -\alpha_j x_a(t) + \alpha_j x_b(t) \quad \ldots \quad (4.1)$$

$$\dot{x}_a(t) = -\alpha_j x_a(t) + \alpha_j u(t) \quad \ldots \quad (4.2)$$

The term u(t) may include a number of different inputs and/or other states.

4.1.2 Cooler output temperatures TX110 and TX177

Since the cooler dynamics are assumed to be instantaneous the actual output temperatures vary with input flow and temperature as follows (assuming a linear system):

$$\Delta T110(t) = \frac{\partial T_{C_1}(L)}{\partial F_1}.u_1(t) + \frac{\partial T_{C_1}(L)}{\partial F_2}.u_3(t) + \frac{\partial T_{C_1}(L)}{\partial T_{C2}(L)}.u_6(t) + \frac{\partial T_{C_1}(L)}{\partial T_{C1}(0)}.x_3(t) \quad \ldots \quad (4.3)$$

$$\Delta T174(t) = \frac{\partial T_{C_2}(0)}{\partial F_1}.u_1(t) + \frac{\partial T_{C2}(0)}{\partial F_2}.u_3(t) + \frac{\partial T_{C2}(0)}{\partial T_{C2}(L)}.u_6(t) + \frac{\partial T_{C2}(0)}{\partial T_{C1}(0)}.x_3(t) \quad \ldots \quad (4.4)$$

Note the appearance in these equations of state x_3. This is the actual outlet temperature of the stripped MEA from the heat exchanger but is also $t_{C1}(0)$ which is a cooler input. Clearly it is the actual temperature x_3 which is input to the cooler rather than its measured value x_4: the two coincide only in the steady state.

A first order o.d.e. for x_1 is obtained by substituting $\Delta T110(t)$ from equation (4.3) for u(t) in (4.2). That for x_2 is similarly obtained by substitution of $\Delta T174(t)$ from equation (4.4).

4.1.3 Heat exchanger output temperatures TX174 and TX172

The results of Chapter 3 indicate that the responses of the actual heat exchanger outlet temperatures to step changes in MEA flow rate are governed by system time constants τ_3 and τ_5. In practice it is not possible to obtain responses to step changes in inlet temperature but it is assumed here that these responses would be governed by the same time constants. The actual fluid temperatures vary with flow inputs u_1, u_2, u_7 and u_8 and temperature inputs u_4 and u_5 as shown in Fig.16. The effects of the appropriate inputs are substituted for u(t) in equation (4.2) to obtain ordinary differential equations (4.5) and (4.6) for x_3 and x_5.

$$\dot{x}_3(t) = -\alpha_3 x_3(t) + \alpha_3\left\{\frac{\partial T_{x_1}(L)}{\partial F_1}.u_1(t) + \frac{\partial T_{x_1}(L)}{\partial T_{x_1}(0)}.u_4(t) + \frac{\partial T_{x_1}(L)}{\partial T_{x_2}(L)}.u_5(t) + \frac{\partial T_{x_1}(L)}{\partial F_1}.u_7(t)\right\} \quad \ldots \quad (4.5)$$

$$\dot{x}_5(t) = -\alpha_5 x_5(t) + \alpha_5\left\{\frac{\partial T_{x_2}(0)}{\partial F_1}.u_2(t) + \frac{\partial T_{x_2}(0)}{\partial T_{x_1}(0)}.u_4(t) + \frac{\partial T_{x_2}(0)}{\partial T_{x_2}(L)}.u_5(t) + \frac{\partial T_{x_2}(0)}{\partial F_1}.u_8(t)\right\} \quad \ldots \quad (4.6)$$

The measured temperatures x_4 and x_6 are related to the actual temperatures x_3 and x_5 by using equation (4.1).

$$\dot{x}_4(t) = -\alpha_4 x_4(t) + \alpha_4 x_3(t) \quad \ldots \quad (4.7)$$

$$\dot{x}_6(t) = -\alpha_6 x_6(t) + \alpha_6 x_5(t) \quad \ldots \quad (4.8)$$

4.1.4 The model in matrix form

The differential equations for x_j, $j = 1,\ldots 6$ can now be expressed in the form

$$\dot{x}(t) = A_c x(t) + B_c u(t) \quad \ldots \quad (4.9)$$

$$y(t) = C_c x(t) \quad \ldots \quad (4.10)$$

where the state vector $x(t) = [x_1\ x_2\ x_3\ x_4\ x_5\ x_6](t)^T$

input vector $u(t) = [u_1\ u_2\ u_3\ u_4\ u_5\ u_6\ u_7\ u_8](t)^T$

and output vector $y(t) = [y_1\ y_2\ y_3\ y_4](t)^T$

The subscript 'c' emphasizes that $\{A_c, B_c, C_c\}$ is a continuous time system.

Matrices A_C, B_C and C_C are as follows. Note that $\alpha_j = 1/\tau_j$, $j = 1,\ldots 6$.

'System' Matrix A_C

$-\alpha_1$		$\alpha_1 \frac{\partial T_{C_1}(L)}{\partial T_{C_1}(0)}$			
	$-\alpha_2$	$\alpha_2 \frac{\partial T_{C_2}(0)}{\partial T_{C_1}(0)}$			
		$-\alpha_3$			
		α_4	$-\alpha_4$		
				$-\alpha_5$	
				α_6	$-\alpha_6$

'Input' Matrix B_C

$\alpha_1 \frac{\partial T_{C_1}(L)}{\partial F_1}$		$\alpha_1 \frac{\partial T_{C_1}(L)}{\partial F_2}$			$\alpha_1 \frac{\partial T_{C_1}(L)}{\partial T_{C_2}(L)}$		
$\alpha_2 \frac{\partial T_{C_2}(0)}{\partial F_1}$		$\alpha_2 \frac{\partial T_{C_2}(0)}{\partial F_2}$			$\alpha_2 \frac{\partial T_{C_2}(0)}{\partial T_{C_2}(L)}$		
$\alpha_3 \frac{\partial T_{X_1}(L)}{\partial F_1}$			$\alpha_3 \frac{\partial T_{X_1}(L)}{\partial T_{X_1}(0)}$	$\alpha_3 \frac{\partial T_{X_1}(L)}{\partial T_{X_2}(L)}$		$\alpha_3 \frac{\partial T_{X_1}(L)}{\partial F_1}$	
	$\alpha_5 \frac{\partial T_{X_2}(0)}{\partial F_1}$		$\alpha_5 \frac{\partial T_{X_2}(0)}{\partial T_{X_1}(0)}$	$\alpha_5 \frac{\partial T_{X_2}(0)}{\partial T_{X_2}(L)}$			$\alpha_5 \frac{\partial T_{X_1}(L)}{\partial F_1}$

'Observation' Matrix C_C

The observations are the measured output temperatures x_1, x_2, x_4 and x_6. (The 'actual' temperatures x_3 and x_5 cannot be observed directly).

$$C_C = \begin{bmatrix} 1 & 0 & 0 & 0 & 0 & 0 \\ 0 & 1 & 0 & 0 & 0 & 0 \\ 0 & 0 & 0 & 1 & 0 & 0 \\ 0 & 0 & 0 & 0 & 0 & 1 \end{bmatrix}$$

Consistent with the comments made in Section 3.5, the model has been developed in a deterministic setting. System and measurement noise levels are discussed in Sections 4.5 and 4.6.

4.2 Conversion to an 'equivalent discrete-time system'

The continuous-time model must now be converted to an equivalent discrete-time form to provide a basis for a discrete-time Kalman filter to operate on sampled plant data. The development followed here is identical to that to be found in Chapter 6 of Kwakernaak & Sivan [7] and is based on the 'zero-order hold' principle. It is assumed that after an input is sampled the value of that input stays constant until the next sample is taken. This is only strictly true if inputs are altered only at sampling instants, but in Chapter 3 it was seen that the assumption of a zero-order hold condition could be advantageous in modelling the effects of flow input changes. The approach in [7] assumes that all inputs comply with the zero hold condition, not only the flow inputs already considered.

Instability of filter estimates, characterized by bias and high error variance, can be caused by applying the zero-order hold assumption to inputs that in reality change appreciably between samples. Use of FX125 for $\tilde{F}_1$ (see Section 3.5.5) is a prime example of this problem and the rates of change of u_4[TX173], u_5[TX175] and u_6[TX176] must now be considered.

As a rule, TX173, the temperature of the stripped MEA from the reboiler is fairly steady, although slight instability may occur if too much steam is used. Being in a closed loop, the cooling

water input temperature to the cooler, TX176, does rise a little over a long run but the rate of change, about 1 degree C per hour, is insufficient to cause problems. TX175, the temperature of the MEA leaving the absorber, does drift following a setpoint change but quite slowly as rapid fluctuations are smoothed out by the absorber packing. The steady nature of these temperatures implies that the zero-order hold assumption is a reasonable approximation and a further consequence is that the effects of the input measurement time constants can be safely neglected.

4.2.1 Choice of sampling period

In control problems, such as that of Newell and Fisher [73], the degree of control improves as the sampling period is reduced and the discrete time equations become a better approximation to the continuous time system. In the present application the choice of sampling period does not affect the running of the plant and can be made entirely to suit the fault detection algorithm. For detection purposes there are two reasons for making the sampling period as short as possible. An instrument fault occurring just after a sampling instant cannot be detected at the very earliest until the next sample is collected. The detection system may also need several samples exhibiting the fault to make a reliable diagnosis and the higher the sampling rate the shorter the time in which this is achieved.

If the data were to be processed in real time then the minimum sampling period would be dictated by the time taken by the computer to complete all the necessary calculations on each set of data. Algorithms run in real time by Newman [53] on the pilot plant with its relatively limited computing facilities needed, for example, a sampling period of over a minute.

The research for this project was, however, done by recording plant data on paper tape and later simulating faults on a larger computer. The minimum sampling period is in this case dictated by the time taken by the tape punch to output all the required points. Due regard must also be paid to the time constants employed in the model; a time

constant that is negligible in comparison with the sampling period is effectively instantaneous and may permit model order reduction (see e.g. Marshall [74]).

The modelling work of Chapter 3 suggests that, in the present case, the sampling period must divide exactly into 10 seconds in order to store the FX101 readings for F_1 by n_1 (40s), n_2 (10s) and n_3 (50s) to obtain inputs u_2, u_7 and u_8. With time constants ranging from 12-100 seconds a sampling period of 10 seconds, as used for runs PLANT2 and PLANT3, was adopted.

4.2.2 The discrete-time system matrix, Φ

From [7], the discrete-time system matrix is the transition matrix defined for the time period between sample k and sample k + 1.

$$\Phi(t_{k+1}, t_k) = e^{A_c\Delta} \qquad \ldots (4.11)$$

where $\Delta = t_{k+1} - t_k$ = sample period $\qquad \ldots (4.12)$

The new matrix will be denoted by Φ, it being understood that this is defined over the length of the sampling period. From Section 4.1.4 and equation (4.11) matrix Φ is calculated as shown in Fig. 18.

4.2.3 The discrete-time input matrix, G

The input matrix now follows using equation (4.13) also from [7]

$$G = \left[\int_0^{\Delta} e^{A_c\tau}d\tau\right] B_c \qquad \ldots (4.13)$$

Evaluating the integral for nonsingular A_c

$$\int_0^{\Delta} e^{A_c\tau}d\tau = A_c^{-1}\left[e^{A_c\tau}\right]_0^{\Delta} = A_c^{-1}\left[e^{A_c\Delta} - I_6\right] \qquad \ldots (4.14)$$

$e^{-\alpha_1\Delta}$		$\frac{\alpha_1(e^{-\alpha_1\Delta}-e^{-\alpha_3\Delta})\frac{\partial T_{C1}(L)}{\partial T_{C1}(0)}}{\alpha_3 - \alpha_1}$			
	$e^{-\alpha_2\Delta}$	$\frac{\alpha_2(e^{-\alpha_2\Delta}-e^{-\alpha_3\Delta})\frac{\partial T_{C1}(L)}{\partial T_{C1}(0)}}{\alpha_3 - \alpha_2}$			
		$e^{-\alpha_3\Delta}$			
		$\frac{\alpha_4(e^{-\alpha_3\Delta}-e^{-\alpha_4\Delta})}{\alpha_4 - \alpha_3}$	$e^{-\alpha_4\Delta}$		
				$e^{-\alpha_5\Delta}$	
				$\frac{\alpha_6(e^{-\alpha_5\Delta}-e^{-\alpha_6\Delta})}{\alpha_6 - \alpha_5}$	$e^{-\alpha_6\Delta}$

Fig. 18 Discrete-time system matrix Φ

$\beta_1 \frac{\partial T_{C1}(L)}{\partial F_2}$ + $\left[\left\{\frac{\alpha_3\beta_1-\alpha_1\beta_3}{\alpha_3-\alpha_1}\right\}\frac{\partial T_{C1}(L)}{\partial T_{C1}(0)}\right]\frac{\partial T_{X1}(L)}{\partial F_1}$		$\beta_1 \frac{\partial T_{C1}(L)}{\partial F_2}$	$\left[\left\{\frac{\alpha_3\beta_1-\alpha_1\beta_3}{\alpha_3-\alpha_1}\right\}\frac{\partial T_{C1}(L)}{\partial T_{C1}(0)}\right]\frac{\partial T_{X1}(L)}{\partial T_{X1}(0)}$	$\left[\left\{\frac{\alpha_3\beta_1-\alpha_1\beta_3}{\alpha_3-\alpha_1}\right\}\frac{\partial T_{C1}(L)}{\partial T_{C1}(0)}\right]\frac{\partial T_{X1}(L)}{\partial T_{X2}(L)}$	$\beta_2 \frac{\partial T_{C1}(L)}{\partial T_{C2}(L)}$	$\left[\left\{\frac{\alpha_3\beta_1-\alpha_1\beta_3}{\alpha_3-\alpha_1}\right\}\frac{\partial T_{C1}(L)}{\partial T_{C1}(0)}\right]\frac{\partial T_{X1}(L)}{\partial F_1}$	
$\beta_2 \frac{\partial T_{C2}(0)}{\partial F_1}$ + $\left[\left\{\frac{\alpha_3\beta_2-\alpha_2\beta_3}{\alpha_3-\alpha_2}\right\}\frac{\partial T_{C2}(0)}{\partial T_{C1}(0)}\right]\frac{\partial T_{X1}(L)}{\partial F_1}$		$\beta_2 \frac{\partial T_{C2}(0)}{\partial F_2}$	$\left[\left\{\frac{\alpha_3\beta_2-\alpha_2\beta_3}{\alpha_3-\alpha_2}\right\}\frac{\partial T_{C2}(0)}{\partial T_{C1}(0)}\right]\frac{\partial T_{X1}(L)}{\partial T_{X1}(0)}$	$\left[\left\{\frac{\alpha_3\beta_2-\alpha_2\beta_3}{\alpha_3-\alpha_2}\right\}\frac{\partial T_{C2}(0)}{\partial T_{C1}(0)}\right]\frac{\partial T_{X1}(L)}{\partial T_{X2}(L)}$	$\beta_2 \frac{\partial T_{C2}(0)}{\partial T_{C2}(L)}$	$\left[\left\{\frac{\alpha_3\beta_2-\alpha_2\beta_3}{\alpha_3-\alpha_2}\right\}\frac{\partial T_{C2}(0)}{\partial T_{C1}(0)}\right]\frac{\partial T_{X1}(L)}{\partial F_1}$	
$\beta_1 \frac{\partial T_{X1}(L)}{\partial F_1}$			$\beta_3 \frac{\partial T_{X1}(L)}{\partial T_{X1}(0)}$	$\beta_3 \frac{\partial T_{X1}(L)}{\partial T_{X2}(L)}$		$\beta_3 \frac{\partial T_{X1}(L)}{\partial F_1}$	
$\left\{\frac{\alpha_4\beta_1-\alpha_1\beta_4}{(\alpha_4-\alpha_3)}\right\}\frac{\partial T_{X1}(L)}{\partial F_1}$			$\left\{\frac{\alpha_4\beta_1-\alpha_1\beta_4}{\alpha_4-\alpha_3}\right\}\frac{\partial T_{X1}(L)}{\partial T_{X1}(0)}$	$\left\{\frac{\alpha_4\beta_1-\alpha_1\beta_4}{\alpha_4-\alpha_3}\right\}\frac{\partial T_{X1}(L)}{\partial T_{X2}(L)}$		$\left\{\frac{\alpha_4\beta_1-\alpha_1\beta_4}{\alpha_4-\alpha_3}\right\}\frac{\partial T_{X1}(L)}{\partial F_1}$	
	$\beta_5 \frac{\partial T_{X2}(0)}{\partial F_1}$		$\beta_5 \frac{\partial T_{X2}(0)}{\partial T_{X1}(0)}$	$\beta_5 \frac{\partial T_{X2}(0)}{\partial T_{X2}(L)}$			$\beta_5 \frac{\partial T_{X2}(0)}{\partial F_1}$
	$\left\{\frac{\alpha_6\beta_5-\alpha_5\beta_6}{\alpha_6-\alpha_5}\right\}\frac{\partial T_{X2}(0)}{\partial F_1}$		$\left\{\frac{\alpha_6\beta_5-\alpha_5\beta_6}{\alpha_6-\alpha_5}\right\}\frac{\partial T_{X2}(0)}{\partial T_{X1}(0)}$	$\left\{\frac{\alpha_6\beta_5-\alpha_5\beta_6}{\alpha_6-\alpha_5}\right\}\frac{\partial T_{X2}(0)}{\partial T_{X2}(L)}$			$\left\{\frac{\alpha_6\beta_5-\alpha_5\beta_6}{\alpha_6-\alpha_5}\right\}\frac{\partial T_{X2}(0)}{\partial F_1}$

Fig.19 Discrete-time input matrix, G

$$\therefore \quad G = A_C^{-1}\left[e^{A_C\Delta} - I_6\right]B_C \qquad \ldots \quad (4.15)$$

The evaluation of G is 'straightforward but tedious' and the result is given in Fig.19, where

$$\beta_j = (1 - e^{-\alpha_j\Delta}) \qquad j = 1, \ldots, 6 \qquad \ldots \quad (4.16)$$

4.2.4 The discrete-time observation matrix, H

For the special case where the sampling period for inputs equals the sampling period for outputs and the sampling instants coincide, the continuous-time matrix C_C is unchanged in the discrete-time case, i.e.

$$H = \begin{bmatrix} 1 & 0 & 0 & 0 & 0 & 0 \\ 0 & 1 & 0 & 0 & 0 & 0 \\ 0 & 0 & 0 & 1 & 0 & 0 \\ 0 & 0 & 0 & 0 & 0 & 1 \end{bmatrix}$$

4.3 The fault detection problem in detail

Having arrived at a model with eight inputs, six states and four outputs (i.e. measurements) the possible instrumentation faults can be listed.

Four fault types were considered in Chapter 1 and illustrated in Fig. 1. These were

(a) Step in instrument output (a constant bias)
(b) Jump in instrument output (a 'spike')
(c) Ramp in instrument output (gradually increasing bias)
(d) Instrument output full scale (break in r.t.d. lead)

4.3.1 Output faults

Biases of any of the above types can occur in four different fault 'directions', each related to a single instrument in measurement vector $\underline{y} = [y_1\ y_2\ y_3\ y_4]^T$

$$\underset{(TX110)}{\underline{y}_f(1)}\begin{bmatrix}\pi_1\\0\\0\\0\end{bmatrix}\quad\underset{(TX177)}{\underline{y}_f(2)}\begin{bmatrix}0\\\pi_2\\0\\0\end{bmatrix}\quad\underset{(TX174)}{\underline{y}_f(3)}\begin{bmatrix}0\\0\\\pi_3\\0\end{bmatrix}\quad\underset{(TX172)}{\underline{y}_f(4)}\begin{bmatrix}0\\0\\0\\\pi_4\end{bmatrix}\quad\ldots\quad(4.17a,b,c,d)$$

The magnitude, time of occurrence and duration of π_j depends on which of the fault types (a) - (d) is under consideration.

4.3.2 Input faults where input is controlled at a setpoint

Flow rate inputs FX101 (MEA) and FX124 (cooling water) are both held to setpoints (see Appendix I). Assume that one of these is at setpoint 1. If the flow measuring instrument output should suddenly exhibit a constant bias $+\Delta F$, the control system interprets this as an error of $+\Delta F$ in the flow control loop and reduces the actual flow by ΔF so that the instrument output is again at setpoint. Because of this the input signal to the fault detection system departs only briefly from normal, and after a short time does not reflect the fact that the setpoint is now ΔF lower than setpoint 1. Meanwhile the actual flow is ΔF less than the flow value being used by the model, which predicts output temperatures in line with the original flow (setpoint 1). On comparison with the model predictions, the output temperatures being received from the plant look as if they are in error by the amount they would change if the flow rate were decreased by ΔF (assuming linearity). Faults in the MEA and cooling water flow measurement loops therefore look like multiple rtd biases and are accordingly classified as 'output' rather than 'input' faults.

Note that a bias in FX101 affects inputs u_1, u_2, u_7 and u_8 while a bias in FX124 affects input u_3 only. The steady state fault directions $\underline{y}_f(5)$ for a bias in FX101 and $\underline{y}_f(6)$ for a bias in FX124 are thus as follows:

$$\underline{y}_f(5) = \begin{bmatrix} \left[\frac{\partial T_{C_1}(L)}{\partial F_1} + \frac{\partial T_{C_1}(L)}{\partial T_{C_1}(0)}\left\{\frac{\partial T_{X_1}(L)}{\partial F_1} + \frac{\partial T_{X_1}(L)}{\partial \tilde{F}_1}\right\}\right] \Delta F_1 \\ \left[\frac{\partial T_{C_2}(0)}{\partial F_1} + \frac{\partial T_{C_2}(0)}{\partial T_{C_1}(0)}\left\{\frac{\partial T_{X_1}(L)}{\partial F_1} + \frac{\partial T_{X_1}(L)}{\partial \tilde{F}_1}\right\}\right] \Delta F_1 \\ \left[\frac{\partial T_{X_1}(L)}{\partial F_1} + \frac{\partial T_{X_1}(L)}{\partial \tilde{F}_1}\right] \Delta F_1 \\ \left[\frac{\partial T_{X_2}(0)}{\partial F_1} + \frac{\partial T_{X_2}(0)}{\partial \tilde{F}_1}\right] \Delta F_1 \end{bmatrix} \quad \ldots \quad (4.18)$$

$$\underline{y}_f(6) = \begin{bmatrix} \frac{\partial T_{C_1}(L)}{\partial F_2} \Delta F_2 \\ \frac{\partial T_{C_2}(0)}{\partial F_2} \Delta F_2 \\ 0 \\ 0 \end{bmatrix}$$

where the comments regarding π_j in Section 4.3.1 apply also to ΔF_1 and ΔF_2

$$\ldots \quad (4.19)$$

4.3.3 Other input faults

Five of the eight components of the input vector are flow rates and are included in Section 4.3.2. Any of the four bias types can occur in the instruments measuring inputs u_4, u_5 and u_6.

$$\underline{u}_f(1) = [0 \ 0 \ 0 \ \upsilon_1 \ 0 \ 0 \ 0 \ 0]^T \quad (TX173) \quad \ldots \quad (4.20)$$

$$\underline{u}_f(2) = [0 \ 0 \ 0 \ 0 \ \upsilon_2 \ 0 \ 0 \ 0]^T \quad (TX175) \quad \ldots \quad (4.21)$$

$$\underline{u}_f(3) = [0 \ 0 \ 0 \ 0 \ 0 \ \upsilon_3 \ 0 \ 0]^T \quad (TX176) \quad \ldots \quad (4.22)$$

where υ_1, υ_2 and υ_3 are specified in the same way as the biases π_j in Section 4.3.1.

4.3.4 Fault simulation

Faults $\underline{y}_f(1)$ - (4) and $\underline{u}_f(1)$ - (3) cause no physical changes to the system and can therefore be simulated by superimposing faults onto recorded plant data. For these fault directions it is thus possible to investigate the detection of all four fault types. A fault $\underline{y}_f(5)$ or (6) on a flow measuring

instrument, however, causes a change in a setpoint. These faults can only be studied by physically altering the setpoint while the plant is running, and as a consequence only faults of type (a) can be investigated for these two instruments.

The problem can now be precisely defined: to design a fault detection system which can detect that one of the above faults has occurred, which can isolate the fault provided that it is a fault on an individual instrument and which under favourable circumstances can estimate the magnitude of the fault.

4.4 The Kalman Filter equations

The filters employed are based on a time-invariant linear stochastic model in the standard state space form.

$$x(k+1) = \Phi x(k) + Gu(k) + w(k) \quad \ldots (4.23)$$

$$y(k) = Hx(k) + v(k) \quad \ldots (4.24)$$

where x(k) and w(k) are n-vectors, u(k) is an m-vector and y(k) and v(k) are r-vectors, all at sampling instant 'k'.

'u' is a known input and w ('process' or 'system' noise) and v ('measurement' noise) are zero-mean, independent, white Gaussian sequences with covariances defined by

$$E[w(k)w^T(j)] = Q\delta_{kj} \qquad E[v(k)v^T(j)] = R\delta_{kj} \quad \ldots (4.25a,b)$$

where δ_{kj} is the Kronecker delta.

The optimal filter is then described by the following steps. The notation is that of Willsky [27], except for the input matrix where 'B' is replaced by 'G'. $\hat{x}(k|j)$ denotes the estimate of x at time 'k' using information received up to and including time 'j'. Recall also that $\Phi = \Phi(k+1, k)$

(1) Store current estimate and estimation error covariance

$$\hat{x}(k|k) \qquad P(k|k)$$

(2) Predict state at k + 1

$$\hat{x}(k+1|k) = \Phi\,\hat{x}(k|k) + Gu(k) \qquad \ldots \quad (4.26)$$

(3) Predict error covariance at k + 1

$$P(k+1|k) = \Phi P(k|k)\Phi^T + Q \qquad \ldots \quad (4.27)$$

(4) Compute innovation covariance

$$V(k+1) = HP(k+1|k)H^T + R \qquad \ldots \quad (4.28)$$

(5) Compute Kalman Gain

$$K(k+1) = P(k+1|k)H^T V^{-1}(k+1) \qquad \ldots \quad (4.29)$$

(6) Calculate innovation

$$\gamma(k+1) = y(k+1) - H\hat{x}(k+1|k) \qquad \ldots \quad (4.30)$$

(7) Update state estimate

$$\hat{x}(k+1|k+1) = \hat{x}(k+1|k) + K(k+1)\gamma(k+1) \qquad \ldots \quad (4.31)$$

(8) Update estimation error covariance

$$P(k+1|k+1) = [I-K(k+1)H]P(k+1|k)[I-K(k+1)H]^T + K(k+1)RK^T(k+1) \qquad \ldots \quad (4.32)$$

(9) Set k = k + 1 and return to step (1).

4.5 Filtering prerequisites

Prerequisites for filtering are concerned with the stability of the system and of the filter. The system itself is seen to be stable from physical considerations; the input temperatures and flows must remain bounded and it is not possible for the four temperatures chosen as states to become unbounded. Mathematically, system stability could be guaranteed by demonstrating that the eigenvalues of the system matrix A_c all lie in the left hand half

plane or equivalently that those of Φ, the discrete-time system matrix, lie inside the unit disc.

The original work of Kalman and Bucy [4] indicates that for uniform asymptotic stability of the optimal filter certain conditions must be satisfied. In addition to bounding the norms of the system matrix and the noise covariance matrices the system must be both uniformly completely observable and uniformly completely controllable (see, for example, Jazwinski [5] for definitions of these terms).

Of prime interest for fault detection purposes is the concept of observability. This can be approached from several different angles: uniform complete observability as defined by Jazwinski, for example, implies stochastic observability as defined by Aoki [75]. Furthermore, checking for uniform complete observability requires knowledge of the measurement noise covariance matrix R, at this stage unknown.

Having modelled a specific plant we are now in a position to see if there are any aspects of this particular system which can be exploited for fault detection purposes. One possibility is that we may be able to run two or more filters in parallel, each utilizing different subsets of the available instrumentation (cf Clark et al [33]). The options open to us are determined by system observability but we have seen that this issue is not as clear cut as it might be. In the system under consideration, however, there is a good case for looking only at the deterministic observability, which simplifies matters considerably. It is easily proved (and intuitively obvious) that a system which is unobservable in a deterministic sense cannot be observable in any stochastic sense. Deterministic observability criteria can therefore be used to weed out those instrument subsets which render the system unobservable. For the subsets which remain, the deterministic check obviously cannot guarantee stochastic observability, but is a fairly reliable guide. The noise levels on the process plant are very low and if the system is observable in a deterministic sense then it seems unlikely that it will become unobservable in the presence of a small amount of noise.

For constant coefficient systems the uniformity requirement is always satisfied. As a test for (uniform) complete observability

of such systems, Kalman [76] introduced the 'observability matrix', defined for any n-state, r-(noise free) measurement system as

$$\Gamma_O = \begin{bmatrix} H \\ H\Phi \\ H\Phi^2 \\ \vdots \\ H\Phi^{n-1} \end{bmatrix} \quad \ldots \quad (4.33)$$

This is an n x nr matrix and the system is observable if Γ_O has full rank, i.e. rank(Γ_O) = n. It is, of course, only necessary to compute sufficient rows to obtain n that are linearly independent, but in cases where n is large this may be tedious. A second test, equivalent to the above and proposed by Rosenbrock [77] is to check that the (n + r) x n matrix

$$R_O = \begin{bmatrix} s_i I_n - \Phi \\ H \end{bmatrix} \quad \ldots \quad (4.34)$$

has full rank for all eigenvalues of Φ, i.e. rank(R_O) = n $\forall$ s_i. The system is observable if there are no eigenvectors of Φ in the null space of H.

Here (Fig.18) the eigenvalues of Φ are displayed on the diagonal. If the eigenvectors for eigenvalues λ_1 - λ_6 are written as the columns of matrix T we have, designating non-zero values by 'x'

$$T = \begin{bmatrix} 1 & 0 & 1 & 0 & 0 & 0 \\ 0 & 1 & X & 0 & 0 & 0 \\ 0 & 0 & X & 0 & 0 & 0 \\ 0 & 0 & X & 1 & 0 & 0 \\ 0 & 0 & 0 & 0 & 1 & 0 \\ 0 & 0 & 0 & 0 & X & 1 \end{bmatrix} \quad \ldots \quad (4.35)$$

With direct state measurements, Rosenbrock's method enables us to see at a glance which combinations of measurements result in system observability. Clearly if we retain the four measurements on states x_1, x_2, x_4 and x_6, then no eigenvector falls in $N(H)$ and

the system is observable. Observability is lost, however, if any one of these measurements is dropped; if, for example x_1 is not measured then the first column of $T \in N(H)$. Thus, in this case, the only feasible filter is one employing all the available measurements.

Rosenbrock proves that the R_0 criterion implies complete observability by making use of the fact that the matrices $(sI_n - \Phi, H)$ are 'relatively right prime'. It is also possible, however, to prove that the R_0 criterion is equivalent to Kalman's criterion based on the rank of Γ_0: see Appendix V. This proof, an original contribution, uses linear algebra and does not introduce the concept of relative primeness of matrices.

4.6 Identification of variances

Implementation of the optimal Kalman filter requires an exact knowledge of the process noise covariance matrix Q and the measurement noise covariance matrix R. These are usually unknown in practice, the gas separation plant being no exception.

Identification of Q and R can be carried out using a method developed by Mehra [10]. The basic algorithm requires batch processing of data and works only in the case in which the form of Q is known and the number of unknown elements in Q is less than $n \times r$ where n is the dimension of the state vector and r the dimension of the measurement vector. Q is required for computation of the Kalman gain (equations 4.27 to 4.29), but a modification also given in Mehra's paper allows direct estimation of R and the steady state optimal gain K_{op} by an iterative technique which is used here. Mehra's method does not allow for the case where the system and measurement noises have non-zero mean caused by unknown biases particularly in measuring instruments. Although these can cause the method to fail the difficulty can be overcome by using a modification proposed by Godbole [11].

4.6.1 Initial estimates for Q and R

System equation (4.23) includes process noise w(k) but assumes that u(k) is known exactly. In practice u has to be measured and is subject to measurement noise, i.e.

$$u_m(k) = u(k) + n(k) \quad \ldots (4.36)$$

where $u_m(k)$ is the measured input and n(k) is a zero-mean white Gaussion sequence that is assumed to be independent of w and v. Now

$$x(k+1) = \Phi x(k) + Gu(k) + w(k) \quad \ldots (4.23)$$
$$= \Phi x(k) + G[u_m(k)-n(k)] + w(k) \quad \ldots (4.37)$$
$$= \Phi x(k) + Gu_m(k) + \tilde{w}(k) \quad \ldots (4.38)$$

where $\tilde{w}(k) = w(k) - Gn(k)$ ... (4.39)

we have also

$$E[\tilde{w}(k)\tilde{w}^T(j)] = E[(w(k)-Gn(k))(w(j)-Gn(j))^T] \ldots (4.40)$$
$$= Q + GSG = \tilde{Q} \quad \ldots (4.41)$$

where $E[n(k)n^T(j)] = S\delta_{kj}$ ... (4.42)

We now require initial estimates of R and, to obtain $\tilde{Q}$, Q and S.

Approximate plant noise levels can be gauged with the aid of steady state data from the 2½ hour run PLANT2 (see 2.2.1). Four outputs and three inputs are temperatures and can reasonably be expected to be subject to similar degrees of measurement noise. TX176 is the temperature least affected by plant influences and over the first 6.2/3 minutes (40 samples) of the PLANT2 record its mean is 9.54° with a variance of approximately 3×10^{-4}. There is no reason to suspect any correlation between noise sequences on different measurements and so the initial estimate for R is taken to be

$$R(0) = r\, I_4 \text{ with } r = 3.0 \times 10^{-4} \quad \ldots (4.43)$$

This value of 'r' can also be used as the initial estimate for the variance of the measurement noise on input temperatures u_4, u_5 and u_6. For flow measurements FX101 (u_1, u_2, u_7 and u_8) and FX124 (u_3) the first 40 samples of PLANT2 yielded variances of 5.0×10^{-6} and 1.0×10^{-6} respectively. It is not possible to tell how much of this variance is due to actual ripple in the flow rate and how much to true measurement noise, and so we assume for the initial estimate that is all due to the latter, giving

$$S(0) = \text{diag}\{5 \quad 5 \quad 1 \quad 300 \quad 300 \quad 300 \quad 5 \quad 5\} \times 10^{-6} \qquad \ldots \quad (4.44)$$

Note that although the measured value of F_1 is used four times, the covariance matrix S is still a diagonal matrix. This is because S is defined at time 'k' and the four entries are recorded at different sampling instants. Thus, provided that the measurement noise on FX101 is a white noise sequence, the noise samples at time 'k' on each of the four are uncorrelated. The repeated use of F_1 does, however, violate the assumption that n(k) is a white vector sequence. This would require that $E[n(k)n^T(j)] = S\delta_{kj}$ (cf. 4.25 a & b). Clearly there is correlation between the measurement noise sequences on u_1, u_2, u_7 and u_8 for $j \neq k$ and from a purely theoretical viewpoint the Kalman filter equations do not hold. Consider however the simulation work carried out on a model of a distillation column by Goldmann and Sargent [17]. They showed that autocorrelated measurement noise did not degrade the filter performance for their example. While not corresponding exactly to their case, our problem is closely related and in the light of the findings of [17] it was decided that the correlation present could be safely neglected.

The process noise covariance matrix Q cannot be reliably estimated directly from the process data and any initial value Q(0) is at best a 'guesstimate'. System output TX177 (x_2, y_2) has a variance over the first 40 samples of PLANT2 of about 3.3×10^{-3}. Assuming that the actual flow and temperature inputs to the cooler are steady, then this figure

represents the process noise associated with x_2 plus the measurement noise associated with y_2. The latter is already supposed to have a variance of about 3×10^{-4} and so the process noise variance must be of the order of 3×10^{-3}. Since all four outputs are temperatures an initial value for matrix Q is

$$Q(0) = q.I_4 \quad \text{with} \quad q = 3 \times 10^{-3} \qquad \ldots \quad (4.45)$$

Note that there is no theoretical justification for taking Q(0) to be diagonal; this simply reflects the lack of knowledge concerning the nature of the process noise.

4.6.2 The steady state Kalman gain

The procedure for calculation of the optimal Kalman gain K(k) and the estimation error covariance P(k|k) is given by equations (4.27, 4.28, 4.29 and 4.32). After a certain number of time steps both K(k) and P(k|k) will reach steady state values independent of the choice of P(0|0). As these matrices depend only on the model and not on the actual observations their behaviour can be studied off line.

A program PDERIV, written to calculate the partial derivatives obtained in Chapter 3, was run with the stable operating point values given for run PLANT2 in Table 2. Matrices Φ and G were then calculated using the expressions given in Figs 18 and 19 respectively and $\tilde{Q}$ calculated from equation (4.41) using Q(0) from (4.45) and S(0) from (4.44). Replacing Q by $\tilde{Q}$ in equation (4.27) and using R(0) from (4.43) in (4.28) and (4.32), program FILCALC was run to investigate the behaviour of K(k) and P(k|k) for various values of P(0|0).

The choice of the latter, which reflects the uncertainty in the initial state estimate $\hat{x}(0|0)$, was not found to influence greatly the number of iterations taken to reach a steady Kalman gain. Even working to seven decimal places the gain was found to become steady after about ten time steps for any P(0|0). Φ, G and steady state values for K(k) and P(k|k) are given for the PLANT2 operating point in

System matrix, Φ

$$\begin{bmatrix} 0.758 & & 0.080 & & & \\ & 0.801 & 0.066 & & & \\ & & 0.635 & & & \\ & & 0.176 & 0.779 & & \\ & & & & 0.435 & \\ & & & & 0.064 & 0.905 \end{bmatrix}$$

Input matrix, G

$$\begin{bmatrix} 12.311 & & -4.548 & 0.004 & 0.017 & 0.142 & -2.401 & \\ 7.115 & & -7.754 & 0.004 & 0.019 & 0.086 & -2.679 & \\ 51.393 & & & 0.062 & 0.304 & & -42.638 & \\ 6.349 & & & 0.008 & 0.038 & & -5.267 & \\ & 69.535 & & 0.465 & 0.101 & & & -82.934 \\ & 3.817 & & 0.026 & 0.006 & & & -4.553 \end{bmatrix}$$

Steady state Kalman gain, K_{ss}

KGAINX

$$\begin{bmatrix} 0.929 & 0.010 & 0.012 & 0.000 \\ 0.010 & 0.921 & 0.009 & 0.000 \\ 0.851 & 0.587 & 0.960 & 0.000 \\ 0.012 & 0.009 & 0.932 & 0.000 \\ 0.000 & 0.000 & 0.001 & 1.305 \\ 0.000 & 0.000 & 0.000 & 0.926 \end{bmatrix}$$

Steady state estimation error covariance, P(k|k)

$$\begin{bmatrix} 0.0003 & 0.0000 & 0.0003 & 0.0000 & 0.0000 & 0.0000 \\ 0.0000 & 0.0003 & 0.0002 & 0.0000 & 0.0000 & 0.0000 \\ 0.0003 & 0.0002 & 0.0231 & 0.0003 & 0.0000 & 0.0000 \\ 0.0000 & 0.0000 & 0.0003 & 0.0003 & 0.0000 & 0.0000 \\ 0.0000 & 0.0000 & 0.0000 & 0.0000 & 0.0675 & 0.0004 \\ 0.0000 & 0.0000 & 0.0000 & 0.0000 & 0.0004 & 0.0003 \end{bmatrix}$$

Fig.20 Discrete-time model, steady state Kalman gain and estimation error covariance at the PLANT2 operating point

Fig. 20. Note that this steady state gain is not the optimal steady state gain, K_{op} because $\tilde{Q}$ and R are imprecisely known. Note also that the estimation error variances for states x_3 and x_5 are much higher than those for the other states which are directly measured.

4.6.3 Testing for optimality

If the filter is optimal, the innovation sequence generated by equation (4.30) is a zero mean Gaussian white noise. If the model is correct and all measuring devices are unbiased then any departure from these properties is caused by erroneous values of Q and R, and hence K.

For j = 0 the autocorrelation function $C_j = E[\gamma(i)\gamma^T(i-j)]$ is the predicted innovation covariance V given by equation (4.28). Like K and P(k|k) this too reaches a steady state value. For the optimal filter $C_j = 0$ for non-zero 'lag' number 'j' but with incorrect Q and R the innovation sequence becomes non-white, a property that can be detected by statistical means.

The C_j's can be estimated from a batch of N samples by

$$\hat{C}_j = \frac{1}{N}\sum_{i=j}^{N} \gamma(i)\gamma^T(i-j) \qquad \ldots \quad (4.46)$$

The diagonal entries of the C_j's give information regarding the whiteness of each component in the innovation vector. Normalized autocorrelation coefficients for these entries can be obtained from

$$\hat{\rho}_{mj} = \frac{[\hat{C}_j]_{mm}}{[\hat{C}_0]_{mm}} \qquad \ldots \quad (4.47)$$

If the innovations are white then the coefficients ρ are, like the C_j's, asymptotically independent and normal with zero mean and covariance (1/N). For each m, ρ_{mj}, j = 1,2... can be regarded as samples from the same normal distribution and therefore the 95% confidence limits for ρ_{mj}, j > 0

are $\pm(1.96/\sqrt{N})$. The batch size N should be statistically significant, i.e. N ≃ 1000, and the autocorrelation function evaluated for lags up to about j = 40.

4.6.4 Mehra's estimation algorithm

Mehra's algorithm is given without proof (see Mehra [10]). Bellingham and Lees [9], [50] found that the algorithm would not work on real data without the modification of Godbole [11] and accordingly this is included as step (5). The algorithm requires that both system and filter have reached steady state conditions and run PLANT2 was designed for this purpose, consisting of 924 data points. The initial estimate of the gain, K_1, which is given as K_{SS} in Fig. 20, corresponds to noise covariances Q(0), R(0) and S(0). 'P' is the steady state a posteriori error covariance P(k|k) and $\hat{PH}^T$ is the estimate of PH^T.

Program KALF02

Subtracts stable operating point values from PLANT2 data to obtain perturbation variables. Uses constant gain in place of equations (4.27, 4.28, 4.29 and 4.32). Initial state estimates all taken as zero. Set i = 1.

(1) Read in PLANT2 data. Read gain K_i from file KGAINX.

(2) Run filter. Discard first 10 innovations to allow for transients, then write remaining 913 4-component innovation vectors to file RESLT.

Program WHITE

(3) Read in RESLT and check all four components for whiteness.
If all components white, K_i is optimal. STOP.
If some components non-white, K_i is suboptimal.
Proceed to (4).

Program MEHRA

(4) Read KGAINX. Read RESLT and calculate innovation mean.

(5) Subtract mean from innovations (Godbole's modification).

(6) Calculate $\hat{C}_o$ and $\hat{C}_j$, $j = 1, \ldots n$ from (4.46). Here 'n', the number of states, is 6.

(7) Use K_i from KGAINX with H and Φ to calculate Λ

$$\Lambda = \begin{bmatrix} H\Phi \\ H\Phi(I - K_iH)\Phi \\ \vdots \\ H[\Phi(I - K_iH)]^{n-1}\Phi \end{bmatrix} \quad \ldots \quad (4.48)$$

(8) Find the generalized inverse of Λ, Λ^*

$$\Lambda^* = (\Lambda^T\Lambda)^{-1}\Lambda^T \quad \ldots \quad (4.49)$$

(9) Estimate $\hat{PH}^T$ from

$$\hat{PH}^T = K_i\hat{C}_o + \Lambda^* \begin{bmatrix} \hat{C}_1 \\ \vdots \\ \hat{C}_n \end{bmatrix} \quad \ldots \quad (4.50)$$

(10) Estimate R from

$$\hat{R} = \hat{C}_o - H\hat{PH}^T \quad \ldots \quad (4.51)$$

(11) Calculate ΔK_i, correction to K_i from

$$\Delta K_i = \Lambda^* \begin{bmatrix} \hat{C}_1 \\ \vdots \\ \hat{C}_n \end{bmatrix} \hat{C}_o^{-1} \quad \ldots \quad (4.52)$$

(12) Set $K_{i+1} = K_i + \Delta K_i$ ... (4.53)
and overwrite data file KGAINX with new value

(13) Set i = i + 1 and return to step (1).

The algorithm whitens the innovations at each iteration until the test in step (3) is passed.

4.6.5 Estimation of R and K_{op} for run PLANT2

The algorithm was run using raw PLANT2 data and the initial Kalman gain, K_1, given in Fig. 20. For the innovation sequence to be white at step 3 not more than 5% of the normalized autocorrelation coefficients must lie outside the band $\pm(1.96/\sqrt{N})$ or ± 0.0649. Coefficients were calculated for lag numbers up to 40 as suggested by Mehra [10], i.e. 5% = 2.

At iteration 1 : Points outside band at step 3.

seq 1 : 10 seq 2 : 9 seq 3 : 7 seq 4 : 5

Innovations non-white : K_1 is suboptimal

$$\Delta K_1 = \begin{bmatrix} -0.251 & 0.445 & 0.102 & -0.002 \\ 0.076 & -0.031 & 0.074 & 0.015 \\ -0.349 & 3.475 & -0.632 & -1.099 \\ 0.170 & -0.380 & 0.112 & 0.257 \\ 3.773 & 18.961 & 0.263 & -3.550 \\ -0.173 & -0.844 & -0.035 & 0.276 \end{bmatrix} \quad \ldots \quad (4.54)$$

and the diagonal entries of $\hat{R}$

$$\hat{r}_{jj},\ j = 1,..4 = \{0.0003\ -0.0004\ -0.0005\ -0.0005\} \quad \ldots(4.55)$$

Note the very large corrections to some entries in the ΔK_1 matrix and the negative covariances obtained for three components of the measurement noise 'v'.

At iteration 10 : Points outside band at step 3.

seq 1 : 7 seq 2 : 9 seq 3 : 6 seq 4 : 6

$$K_{10} + \Delta K_{10} = K_{11} = \begin{bmatrix} 0.561 & 0.598 & 0.160 & -0.081 \\ 0.152 & 0.829 & 0.068 & -0.040 \\ 0.792 & 3.252 & -0.411 & -0.012 \\ 0.066 & -0.152 & 1.167 & -0.092 \\ 0.217 & 21.374 & -2.851 & -6.444 \\ 0.025 & -1.094 & 0.276 & 1.213 \end{bmatrix} \quad \ldots(4.56)$$

and the diagonal entries of $\hat{R}$

$$\hat{r}_{jj},\ j = 1,...4 = \{0.0041\ 0.00002\ -0.00032\ -0.00097\} \quad \ldots(4.57)$$

After ten iterations it is clear that the algorithm has failed. The estimated 'optimal' Kalman gain bears no resemblance to the original but the large 'corrections' have not resulted in any marked whitening of the innovations. Furthermore the estimated R matrix contains two physically unrealisable negative variances.

It was just possible that the failure was caused by the fact that there is a slight drift in temperature over the 924 points of run PLANT2 due to a slight rise in the cooling water inlet temperature. To test this theory the change in expected value of each variable from the beginning to the end of the run was estimated. The drifts, assumed to be proportional to time, were subtracted from each temperature record to generate data set PLANT2X.

The algorithm was run again using PLANT2X data and initial Kalman gain K_1. The performance was no better with this doctored data and the comments on the first run apply equally here.

A more likely reason for the algorithm's failure is that the process and measurement noises, as reflected by the temperature measurements, are not Gaussian. The noise sequences may well be Gaussian in reality but they are at a very low level on this particular plant, and the state measurements in degrees are rounded off to just one decimal place (two for TX177). The continuous Gaussian distribution will be effectively replaced by a distribution in which perhaps only two or three discrete temperature values can occur.

Exactly the same problem was reported by Bellingham and Lees [9], [50] who overcame the difficulty by adding computer generated Gaussian white noise to their measurements. This was tried in order to confirm the source of the problem and to check the operation of the computer programs.

A NAG routine was used to generate 3696 points from a N(0,0.3) distribution. The first 924 were added to the y_1 readings from PLANT2X, the second to y_2 and so on to produce a third data set PLNT2XX. Program FILCALC, used to obtain the matrices of Fig.20, was re-run with the original Q(0) and S(0) but with $R(0) = 0.009I_4$. These gave a new initial steady state Kalman gain which was used with PLNT2XX to run Mehra's algorithm for a third time.

The results, which are summarized in Table 12, show how much more successfully the algorithm is able to whiten the innovations and arrive at a realistic estimate for R. The diagonal entries of the latter are close to the variances of the artificial noise added, bearing in mind that the original noise is still present.

TABLE 12

Itn. No.	Coeffs. outside band				Estimated R			
	1	2	3	4	$\hat{r}_{11}$	$\hat{r}_{22}$	$\hat{r}_{33}$	$\hat{r}_{44}$
1	3	3	0	6	.094	.092	.085	.072
2	3	3	0	4	.093	.091	.085	.075
3	3	2	0	4	.093	.091	.086	.075
4	3	2	0	4	.093	.091	.086	.075

4.6.6 Artificial measurement noise : to add or not to add?

White, Gaussian innovations with covariance equal to that predicted by equation (4.28) indicate filter optimality. It is clear from the experimental work that with the nature and low level of the plant noise in this case, any filter designed to work on the raw data will be suboptimal.

It must be decided at this point whether there is a case for adding artifical measurement noise. Bellingham and Lees [9], [50] added noise to obtain a reliable estimate of K_{op} via Mehra's algorithm. Litchfield et al [22] designed their instrumentation to be "essentially noise free", then added Gaussian noise to test several filters, while Hamilton et al [20] added artificial measurement noise "to

provide a more severe test" of the filter considering the "relatively low" plant noise levels.

By adding such noise it is possible to mask the true plant noise and to obtain a good approximation to an optimal filter. For state estimation there are advantages in this because some credence is given to the computed estimation error covariance, P(k|k). The filter faces a stiffer test in instances where noise is not added and the operation is outside the conditions laid down in the theory.

Three considerations tip the balance in favour of using the raw data. Firstly, if the filter is to be used for fault detection and not for state estimation the reliability of P(k|k) is irrelevant. What is more important is whether the innovations still convey information on the nature of any faults present and whether their statistical nature allows this information to be extracted. Secondly, having to add artificial noise decreases the computational efficiency of a filtering algorithm and thirdly the decision ensures that a different direction is taken from that followed by Bellingham and Lees resulting in a more original piece of research into fault detection on a real process plant.

4.7 Innovation statistics for a suboptimal filter

This section examines the statistical nature of the innovation sequence generated by running the raw PLANT2 data through a filter with a constant Kalman gain KGAINX (Fig. 20). The sequence, shown to be non-white at the first iteration of Mehra's algorithm at the beginning of Section 4.6.5, was tested for mean, covariance and distribution.

The sample mean (913 4-vectors) was found to be

$$E[\gamma] = \{-0.0131 \quad -0.0400 \quad 0.0225 \quad -0.0082\}^T$$

which is close to zero. The variance of each component can be compared with its theoretical steady state variance given by the program generating the matrices of Fig. 20:

Theoretical v_{ii}, i = 1,4 {0.0045 0.0039 0.0046 0.0040}

Actual $E[\gamma\gamma^T]_{ii}$, i = 1,4 {0.0036 0.0016 0.0032 0.0045}

A program was written to generate the distribution functions $F_n(x)$ for each component of the innovation vector. When plotted these were found to be approximately Gaussian and were further investigated by means of the Kolmogorov-Smirnov (K-S) statistic (see, for example, Lindgren [78]).

This statistic is "distribution-free", i.e. it can be used to test a given sample distribution function $F_n(x)$ against the "null" or H_0 hypothesis that the samples are drawn from any given distribution function F(x). The K-S statistic, D_n, is based on the numerical difference between the actual and the H_0 distributions and is defined by

$$D_n = \sup_x | F_n(x) - F(x) | \quad \ldots \quad (4.58)$$

In this one-sample two-tailed test D_n is compared with a threshold,so that if $F_n(x)$ and F(x) differ by too much the H_0 hypothesis is rejected at a given level of significance.

The sample distribution for each component of the innovation vector was tested against the H_0 hypothesis that it was a Gaussian distribution with the sample mean and variance. An attempt was made in each case to reduce the K-S statistic by keeping the mean constant but altering the variance of the H_0 distribution. The computational work was carried out by Wellings [79] using a program developed by him as a part of his PhD thesis and employing the "large sample" thresholds for D_n given by White, Yeats and Skipworth [80]. The second component of the innovation vector was found to be the closest fit to the Gaussian distribution and the fourth component the worst. These two examples are plotted in Fig. 21.

As a further indication of the shape of the actual distributions obtained, coefficients of skewness (ν_1) and kurtosis (ν_2) were calculated (see, for example, Wetherill [81]).

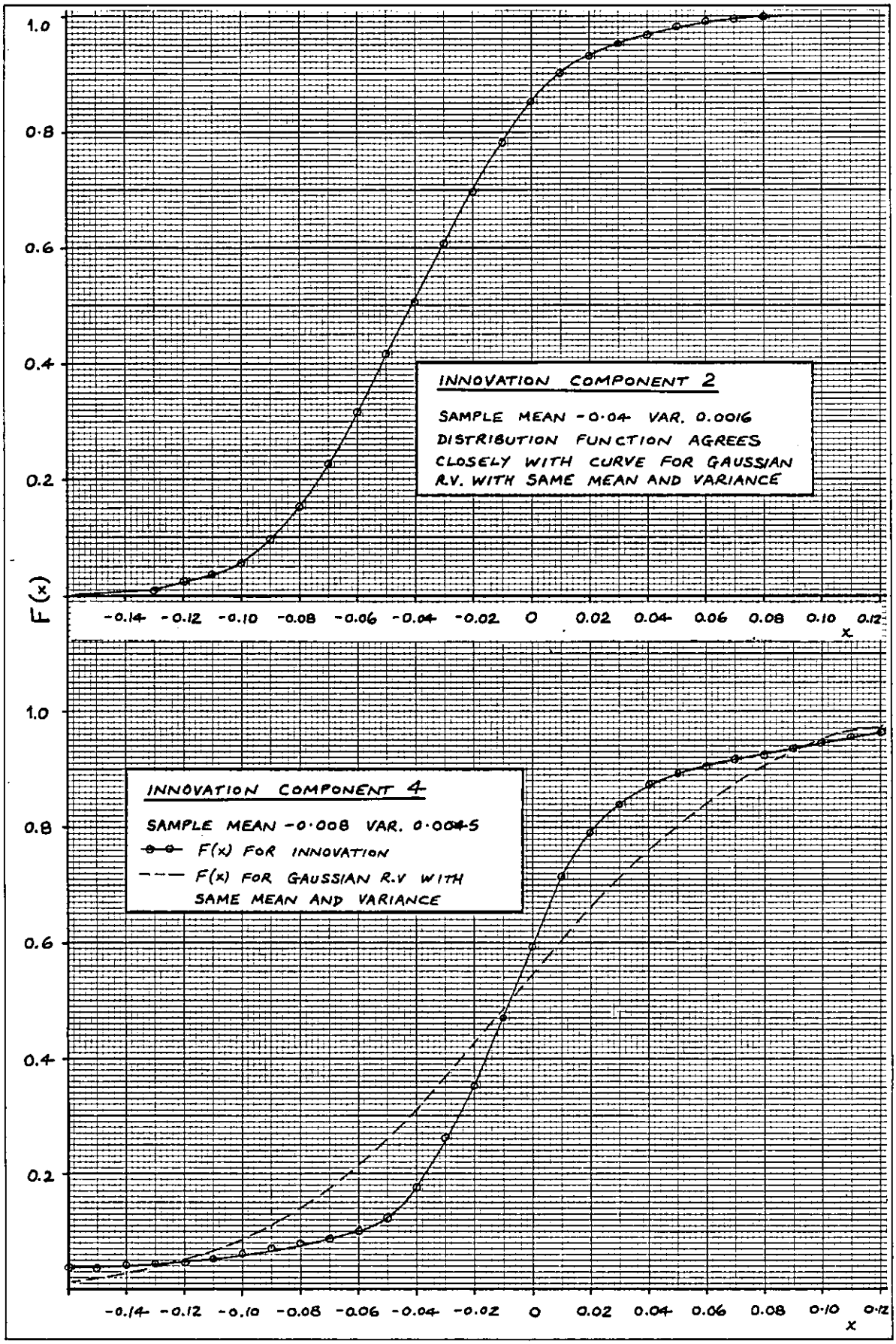

Fig.21 Probability distribution functions for two components of the innovation vector

These are defined by

$$\nu_1 = \frac{E[x - \mu]^3}{\{E[x - \mu]^2\}^{3/2}} \qquad \nu_2 = \frac{E[x - \mu]^4}{\{E[x - \mu]^2\}^2} - 3$$

(where $\mu = E[x]$) ... (4.59 a,b)

and are both zero for the normal distribution. Coefficient ν_2 is defined only for distributions that are symmetrical and unimodal and should therefore be calculated after a check on skewness has been made. Results obtained are summarized in Table 13 and show that only sequence 4 is markedly non-Gaussian, exhibiting a fair degree of lepto-kurtosis.

TABLE 13

seq.	mean	std.devn.	var.	ν_1	ν_2
1	-0.0131	0.0596	0.0036	0.0194	0.4830
2	-0.0400	0.0399	0.0016	0.1592	0.0205
3	0.0225	0.0566	0.0032	-0.0399	2.0485
4	-0.0082	0.0670	0.0045	-0.3708	5.5915

seq.	H_o mean	H_o s.devn.	D_n	result of test
1	-0.0131	0.0596	0.0325	H_o accepted
1	-0.0131	0.055	0.0234	H_o accepted
2	-0.0400	0.0399	0.0166	H_o accepted
2	-0.0400	0.04	0.0164	H_o accepted
3	0.0225	0.0566	0.0520	H_o rejected at 2% s.l.
3	0.0225	0.049	0.0305	H_o accepted
4	-0.0082	0.0670	0.1456	H_o rejected at 1% s.l.
4	-0.0082	0.0420	0.0575	H_o rejected at 1% s.l.

4.8 An idea for an innovations based fault detection algorithm

The work of Beard and Jones (see Willsky [27]) on the design of detector filters for linear time-invariant systems was examined briefly in the introductory chapter. Rather than designing a filter for accurate state estimation they sought to accentuate the effects of certain failures in the filter residual. By suitable choice of filter gain, particular failure modes could be made to manifest themselves as residuals which remained in a fixed direction or plane.

The original work was carried out in a deterministic setting, and the question arises as to whether a similar method could be used for a stochastic time-invariant system. The remainder of this chapter looks at the feasibility of this idea.

4.8.1 The innovation direction

Under normal operation, the expected value of the r-dimensional innovation vector is a null vector, i.e $E[\gamma]$ is a point at the origin of r-space. If a fault occurs so that in some way equations (4.23) and (4.24) no longer accurately model the process, there will be a change in the expected value that is dependent on the type and magnitude of the fault.

The innovations can be monitored for this shift in mean by the use of the Student t test, giving rise to the detection algorithm used by Bellingham and Lees [49], [50]. This does not, however, make use of the fact that the post fault innovation may point in a characteristic direction in r-space. If the likely fault sources are reasonably few and if each source drives the innovation in a unique direction, then fault isolation may be possible by testing the innovations against each of these 'reference' directions in turn.

4.9 Innovation monitoring

Statistical means for innovation monitoring in the literature are developed on the assumption that the innovations are generated by optimal filters and are therefore Gaussian. As experiment has shown that near-Gaussian innovations can be obtained by filtering plant data even when the filter is known to be suboptimal, these techniques can be applied with some confidence.

Letting H_o be the hypothesis that system operation is normal, each of the 'q' likely fault sources gives rise to hypothesis H_i, $i = 1,....q$ that the fault is due to source 'i'. For each fault source it is possible to calculate reference vector d_i, the value of $E[\gamma]$ for a unit step fault from source 'i'. For simplicity we will assume for the remainder of this chapter that d_i is constant.

Under no-fault conditions the probability density of $\gamma(k)$ forms a symmetrical pattern around the origin of r-space. The occurrence of a fault from source 'i' distorts this pattern so that a 'lobe' of increased probability extends along d_i. The algorithm must decide whether a given innovation $\gamma(k)$ belongs to the symmetrical distribution (implies H_o) or an asymmetrical distribution (implies H_i).

Vector $\gamma(k)$ will have a component $\rho_i d_i$ along each direction d_i which can be found from Lemma 4.1. For each direction d_i, $i = 1,....q$, the value ρ_i can be thought of as the most likely magnitude for a fault from source 'i'.

Lemma 4.1

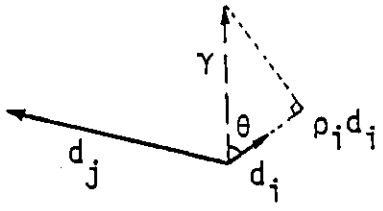

Fig.22

$$\rho_i d_i = |\gamma| \cos\theta$$

$$\rho_i |d_i|^2 = |\gamma| \cdot |d_i| \cos\theta = \gamma^T d_i$$

$$\rho_i = \frac{\gamma^T d_i}{d_i^T d_i}$$

Every $\gamma(k)$ will in general have a finite ρ_i for all values of 'i' whether or not a fault exists. These ρ values will generally be 'small' under no fault conditions, but one or more will increase in magnitude if there is a fault. Three tests, each assuming Gaussian innovations, are proposed for monitoring purposes.

4.9.1 The χ^2 test

In its simplest form the χ^2 or weighted sum-squared residual (WSSR) test is very much a detection only method and relies on the increase in innovation magnitude under fault conditions. The detection criterion is:

$$\ell(k) = \sum_{j=k-N+1}^{k} \gamma^T(j) V^{-1}(j) \gamma(j) \underset{H_o}{\overset{H_1}{\gtrless}} \varepsilon \qquad \ldots \quad (4.60)$$

where H_1 is a composite 'fault' hypothesis. If the system operation is correctly given by equations (4.23) and (4.24) then $\ell(k)$ is a chi-squared random variable with Nr degrees of freedom, where r = dim (γ).

Willsky, Deyst and Crawford [44], [45] found that improved fault detection and isolation performance could be obtained by generating 'r' χ^2 r.v.'s, one from each component of the innovation vector γ, and comparing these individually with thresholds ε_i, i = 1,....r

$$\text{i.e.} \quad \ell_i(k) = \sum_{j=k-N+1}^{k} \gamma_i^2(j)/v_{ii}(j) \quad i = 1,....r \quad ...(4.61)$$

Note that the "window length" N and the threshold ε are design parameters and that under steady state conditions, V(k) is a constant matrix.

4.9.2 The log-likelihood ratio (LLR) test

'Small' ρ values in all reference directions d_i will be generated by Lemma 4.1 even under normal conditions. A test is required to decide whether the implied shift in mean in any particular direction is statistically significant for a given innovation vector $\gamma(k)$.

The calculation of ρ for each d_i fixes the mean of $\gamma(k)$ for hypothesis H_i at $\rho_i d_i$. The choice of hypothesis now rests on deciding whether $\gamma(k)$ belongs to a population with zero mean (H_o) or mean $\rho_i d_i$, i = 1,....q (H_i).

Given the distribution functions of γ under two hypotheses H_o and H_1, Van Trees [54] defines the likelihood ratio $\Lambda(\gamma)$ as

$$\Lambda(\gamma) = \frac{f_{\gamma|H_1}(\gamma|H_1)}{f_{\gamma|H_o}(\gamma|H_o)} \quad ... \quad (4.62a)$$

and a likelihood ratio test with threshold $\tilde{\eta}$

$$\Lambda(\gamma) \underset{H_o}{\overset{H_1}{\gtrless}} \tilde{\eta} \quad ... \quad (4.62b)$$

Because the natural logarithm is a monotonic function and both sides of (4.62b) are positive, an equivalent test is the log-likelihood ratio (LLR) test

$$\ell n\Lambda(\gamma) \underset{H_o}{\overset{H_1}{\gtrless}} \ell n\ \tilde{\eta} = \eta \qquad \ldots \quad (4.63)$$

The probability density for r-dimensional Gaussian γ with mean $\underline{m}$ and non-singular covariance matrix V is given by

$$f_\gamma(\gamma) = \frac{1}{2\pi^{r/2}|V|^{1/2}} \cdot \exp\{-\tfrac{1}{2}(\gamma-\underline{m})^T V^{-1}(\gamma-\underline{m}) \quad \ldots \quad (4.64)$$

giving rise to the LLR statistic

$$\ell n\Lambda(\gamma) = \gamma^T V^{-1}\gamma - (\gamma-\rho_i d_i)^T V^{-1}(\gamma-\rho_i d_i) \underset{H_o}{\overset{H_i}{\gtrless}} \eta \quad \ldots \quad (4.65)$$

For each innovation the statistic should be calculated for all directions 'i', with each llr being tested, in principle, against the same threshold. It is, however, quite possible that the ratios generated from $\gamma(k)$ may exceed the threshold for more than one 'i' value, in which case the test fails to completely isolate the fault. The uncertainty can be reduced by employing some other policy in the case where more than one fault hypothesis is significant against H_o. One possibility is to declare the 'i' value generating the maximum value of $\ell n\Lambda(\gamma)$ to be the fault direction. This is further discussed in Chapter 6.

4.9.3 A note on alarm thresholds

If the innovation mean corresponding to each hypothesis H_i were known exactly (implying a fixed fault size) then a suitable value for η could be determined from statistical theory for any desired significance level. The means in equation (4.65) have, however, been estimated from Lemma 4.1. The proposed LLR test is strictly speaking a form of the Generalized Likelihood Ratio (GLR) test, in which the parameters governing $f(\gamma|H_i)$ are estimated assuming H_i to be true. It is shown in Chapter 5 that this makes the calculation of suitable thresholds very difficult. In this case η is perhaps best considered a design parameter to avoid misleading false alarms at the expense of sensitivity.

4.9.4 The recursive conditional probability (RCP) test

Intuitively, a possible shortcoming of the LLR test is that it considers only the evidence provided by a single innovation $\gamma(k)$, i.e. at time (k) the test is not influenced by its decision at time (k-1).

Consider Bayes' theorem for 'n' mutually exclusive events $B_1,\ldots B_n$, of which some one must occur in a given trial, and A which is any event for which $P(A)\neq 0$ (see, for example, Alder & Roessler [82]). The conditional probability $P(B_i|A)$ for any B_i given that A has occurred is given by

$$P(B_i|A) = \frac{P(A|B_i)P(B_i)}{\sum_{i=1}^{n} P(A|B_i)P(B_i)} \qquad \ldots (4.66)$$

If the B_i's are replaced by hypotheses H_i, i = 0,1,....q, and A by γ then (4.66) is directly applicable to the problem of finding the conditional probability that each hypothesis is 'true', given the innovation $\gamma(k)$. Equation (4.66) can be made recursive by modifying the $P(H_i)$ terms to $P(H_i|k-1)$ where the latter is the probability that H_i is true given all information up to and including time (k-1).

To start off, a priori probabilities must be used: $P(H_i)$, i = 0,1....q, must sum to 1 and could be chosen such that $P(H_o)>>P(H_i)$, i = 1,....q. Probability $P(H_i|k)$ is then given for each i by the recursion

$$P(H_i|k) = \frac{f(\gamma(k)|H_i)P(H_i|k-1)}{\sum_{j=0}^{q} f(\gamma(k)|H_j)P(H_j|k-1)} \qquad \ldots (4.67)$$

where the probability densities $f(\gamma|H)$ are as given in (4.64). This method gives the relative probabilities of each hypothesis being the true one and enables a decision to be reached over several innovations.

4.10 A simplified filter

In order to assess the feasibility of these ideas by simulation we now construct a simplified filter based on the pilot plant. The full model is described by the equations:

$$x(k+1) = \Phi x(k) + Gu(k) + w(k) \quad \ldots \quad (4.68)$$

$$y(k) = Hx(k) + v(k) \quad \ldots \quad (4.69)$$

where Φ and G are as shown in Figs.18 and 19. For a feasibility study we can cut down on computational effort by employing a reduced order model. This is obtained by increasing the sampling period Δ until it is substantially longer than the plant time constants τ_1-τ_6 and by constraining flow setpoint changes to occur at sampling instants only. If Δ is set at 240 seconds then, neglecting long term temperature drifting, the effect of a change in input at sample 'k' will have reached steady state by 'k + 1'. There is now no need to model transients and x_3 and x_5 can be dropped leaving four states which are directly measurable. Furthermore, if the MEA flow setpoint (F_1) is changed then the associated step change in $\tilde{F}_1$ occurs well before the next observation so that inputs u_1, u_2, u_7 and u_8 can be combined into a single MEA flow input. To a good approximation, equations (4.68) and (4.69) become:

$$x(k+1) = Gu(k) + w(k) \quad \ldots \quad (4.70)$$

$$y(k) = x(k) + v(k) \quad \ldots \quad (4.71)$$

where G is now a 4x5 matrix of steady state gains, Φ has disappeared because it approximates to a null matrix and H has become a 4x4 identity matrix. The output vector 'y' is a 4x1 vector of noisy measurements on the four states. These and the five components of the input vector are perturbation variables associated with the instruments as follows:

$$y^T = [y_1\ y_2\ y_3\ y_4] = [\text{TX110}\ \ \text{TX177}\ \ \text{TX174}\ \ \text{TX172}]$$

$$u^T = [u_1\ u_2\ u_3\ u_4\ u_5] = [\text{FX101}\ \ \text{FX124}\ \ \text{TX173}\ \ \text{TX175}\ \ \text{TX176}]$$

The partial derivatives required for evaluation of G are again obtained from program PDERIV. These are calculated at the stable operating point given below, which is from an actual plant run.

TX110 = 24.2 °C	TX172 = 87.8°C	TX173 = 101.4°C
TX177 = 29.05°C	FX101 = 0.25 kgs^{-1}	TX175 = 25.04°C
TX174 = 38.0 °C	FX124 = 0.2 kgs^{-1}	TX176 = 12.14°C

As the sampling interval increases, G becomes independent of Δ and is given for this operating point by

$$G = \begin{bmatrix} 50.311 & -28.524 & .077 & .382 & .541 \\ 34.536 & -50.005 & .110 & .544 & .346 \\ 22.968 & & .169 & .832 & \\ -22.709 & & .822 & .178 & \end{bmatrix} \quad \ldots \quad (4.72)$$

Turning now to the filter, steps (3), (4), (5) and (8) (Sections 4.4 and 4.6.1) simplify to constant terms as a consequence of the fact that Φ is now a null matrix:

$$(3) \quad P(k+1|k) = \tilde{Q} \quad \ldots \quad (4.73)$$

$$(4) \quad V(k) = \tilde{Q} + R \quad \ldots \quad (4.74)$$

$$(5) \quad K(k) = \tilde{Q}(\tilde{Q} + R)^{-1} \quad \ldots \quad (4.75)$$

$$(8) \quad P(k|k) = (I - K)\tilde{Q} \quad \ldots \quad (4.76)$$

Under normal operation the innovations are seen to have zero mean and constant covariance $(\tilde{Q} + R)$. We now consider the effects on these innovations of two simple step faults to determine the associated reference vectors 'd_i', defined in Section 4.9. The innovation biases are not formally derived here because a full reference vector analysis is carried out in Chapter 5.

4.10.1 Output fault

Suppose a constant step fault '$\underline{b}$' appears on the measurement system between samples 'k' and 'k + 1', i.e:

$$y(k+1) = x(k+1) + v(k+1) + \underline{b} \quad \ldots \quad (4.77)$$

For the simplified system the bias is mirrored by the innovations, i.e:

$$E[\gamma(j)] = \underline{b} \qquad \forall j \geq k+1$$

Taking as an example fault direction $\underline{y}_f(1)$ (Section 4.3.1), the reference vector is the innovation bias resulting from a unit step fault in temperature measurement TX110

$$\text{i.e:} \quad d_1 = \underline{b} = [1 \;\; 0 \;\; 0 \;\; 0]^T \quad \ldots \quad (4.78)$$

Note that d_1 is defined for a positive unit step, i.e: $+1^{\circ}C$.

4.10.2 Input fault

Suppose a constant step fault $\underline{\sigma}$ appears on an input measurement between samples 'k - 1' and 'k', i.e:

$$u_m(k) = u(k) + n(k) + \underline{\sigma} \qquad \ldots \quad (4.79)$$

The filter uses the erroneous measurement at step (2):

$$\hat{x}(k+1|k) = Gu(k) + G\underline{\sigma} \qquad \ldots \quad (4.80)$$

leading to

$$E[\gamma(j)] = -G\underline{\sigma} \qquad \forall j \geq k+1$$

Taking as an example fault direction $\underline{u}_f(2)$ (Section 4.3.3), the reference vector is the innovation bias resulting from a unit step fault in temperature measurement TX175.

i.e: $d_8 = -G\underline{\sigma} = [-0.382 \quad -0.544 \quad -0.832 \quad -0.178]^T$ ... (4.81)

Note that TX175 is u_4 for the simplified filter and that the $+1^{\circ}C$ fault picks out the negative of the fourth column of G. The reference vector associated with this instrument is numbered 'd_8' for consistency with later work.

The innovation covariance is unaffected by step faults in either input or output measurements.

4.10.3 System simulation

For simulation purposes u(k) was taken to be identically zero so that the system was driven by zero mean white noise w(k) only. White noise sequences at realistic levels were computer generated as follows:

(i) Sequence w(k) 4-dimensional, zero mean, $Q = 0.0009I_4$

(ii) Sequence v(k) 4-dimensional, zero mean, $R = 0.0004I_4$

(iii) Sequence n(k) 5-dimensional, zero mean with

$$S = \text{diag}\,[4 \quad 1 \quad 400 \quad 400 \quad 400] \times 10^{-6}$$

These sequences were then used to create new data files as follows:

(iv) File of actual states. With u(k) = 0 $\forall k$, these are given by equation (4.70): $x(k+1) = w(k)$

(v) File 'OBSERVE' containing noisy measurements of the actual states obtained via equation (4.71), i.e. $y(k) = x(k) + v(k)$.

(vi) File 'CONTROL' containing apparent inputs. With $u(k) = 0\ \forall k$, these are given by equation (4.36): $u_m(k) = n(k)$

Input and output faults could then be simulated by adding suitable biases to selected instruments in files CONTROL and OBSERVE respectively. All files were 100 time steps in length.

4.10.4 Fault simulation and filtering

Filter construction was greatly simplified for this example because the Kalman gain K, given in equation (4.75), did not have to be recalculated at every time step. For each experiment a fault was superimposed onto either CONTROL or OBSERVE before running both files through the filter to generate an innovation file 'RESID'. The data file could then be analyzed using the proposed tests and the results compared. Examples are given in Fig. 23.

(a) χ^2 test

With no faults superimposed, single component χ^2 r.v.'s were generated using equation (4.61) with N = 3. For three degrees of freedom, 99% of these values should be less than 11.35; the maximum was in fact found to be 11.03.

With the alarm threshold set at 11.35, Example 1 shows a $+1^0$C step fault on TX110 occurring between k = 50 and k = 51. As expected from Section 4.10.1 this affects $\ell_1(k)$ only and is detected at k = 51. Example 2 shows a $+1^0$C step fault on TX175 occurring between k = 9 and k = 10. The fault mainly affects $\ell_3(k)$ but,as expected for an input fault, matrix G distributes the effect and all four χ^2 r.v.'s exceed the alarm threshold. Detection is delayed until k = 11 because $\gamma(10)$ is unaffected.

These results indicate that in principle the χ^2 test can differentiate between input and output faults and can isolate the latter. This is based on the premise that a fault on y_j affects $\ell_j(k)$ only whereas an input fault

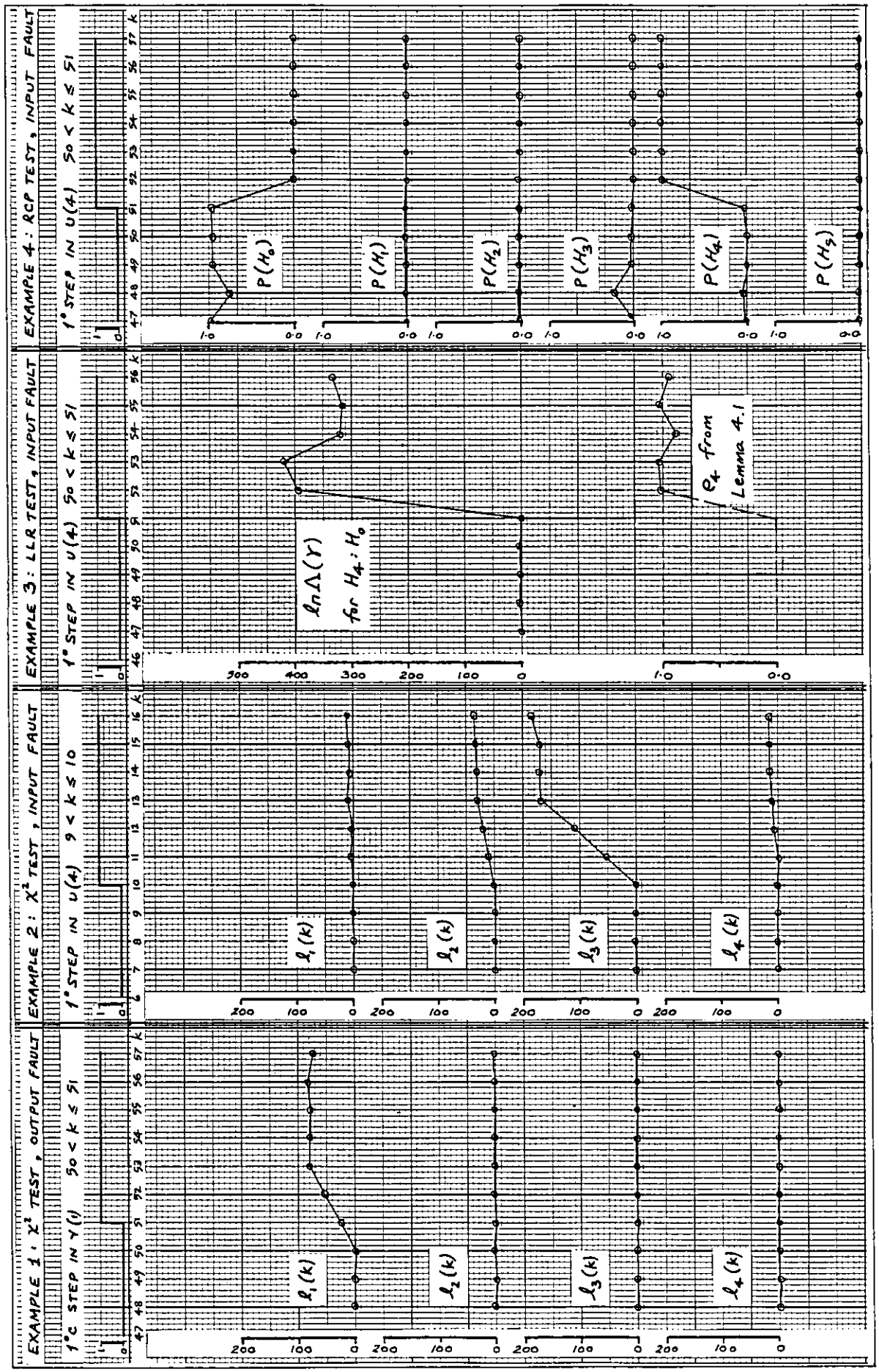

Fig.23 Fault simulations for the simplified system

affects more than one of the $\ell_j(k)$'s. Example 2 shows that this may not always work in practice: a very small fault on TX175 might drive only $\ell_3(k)$ over the alarm threshold which would be misinterpreted as a fault on y_3 (TX175).

The χ^2 test cannot isolate input faults and more sophisticated methods are required.

(b) LLR test

This test was first tried on undoctored data to ascertain the normal level of the llr statistic and to set the alarm threshold. For every innovation, $\ell n\Lambda(\gamma)$ was calculated for each of the five hypothesized input faults using reference vectors such as (4.81) together with Lemma 4.1 and equation (4.65). The maximum llr, which never exceeded 5.2, was printed out at each time step together with the corresponding fault hypothesis. Each failure direction was found to generate the maximum value with about the same frequency, as might be expected for a zero mean innovation sequence.

For the second run, a +1°C step fault on TX175 was injected between k = 50 and k = 51. The alarm threshold was set at 10.0 but as can be seen from Example 3, $\ell n\Lambda(\gamma)$ for i = 4 leapt to around 400 at k = 52. The llr's for some of the other directions also exceeded 10.0 but all were negligible in comparison with the value for $H_4:H_0$. Fig. 23 also shows the estimate of fault magnitude: prior to k = 52 H_0 is declared true and ρ_i, i = 1,...5 are not defined. The fault is detected at k = 52 whereupon Lemma 4.1 estimates the fault to within 10% of the correct value.

(c) RCP test

This test was also used to look for faults on input measurements and the a priori failure probabilities for use with equation (4.67) were initially set at

$$P(H_0) = 0.975 \qquad P(H_i) = 0.005,\ i = 1,\ldots 5$$

Under no-fault conditions, $P(H_0)$ fell to zero after about 28 time steps and by k = 48 the algorithm had locked onto a non-existent fault in u_3, i.e. $P(H_3) = 1.0$. After this the algorithm was oblivious to faults introduced on any other instrument. Changing the a priori probabilities did not cure the problem but merely postponed the inevitable.

Better results were obtained by modifying equation (4.67) to utilise the a priori probabilities at every step, although this negates the argument given in Section 4.9.4 about reaching a 'considered' decision over several innovations. The modified algorithm was used to detect the same TX175 fault as in Example 3. As shown in Example 4 it succeeded, with $P(H_4)$ jumping from near zero to 1.0 at k = 52. As the RCP test also uses Lemma 4.1, the estimate of fault magnitude is the same as that supplied by LLR.

4.11 Summary

A six state discrete-time linear state space model has been derived for the heat exchanger/cooler subsystem and a set of possible faults was defined for further study. The standard Kalman filter equations were presented and system observability, including a new proof of equivalence between two tests for deterministic observability, was discussed.

Identification of noise statistics was attempted via Mehra's algorithm but was unsuccessful due to the low noise levels on this particular plant. The decision was taken not to add artificial measurement noise but it was shown by means of the Kolmogorov-Smirnov test that the filter innovations were still approximately Gaussian.

A method for simultaneous fault detection, isolation and approximate estimation was proposed as a development of techniques used by Beard and Jones for deterministic systems. Two algorithms based on this principle were tested for feasibility using a simple example and were compared with the well known χ^2 test.

For the LLR algorithm, fault decisions were based on individual innovations while the RCP algorithm was designed in an attempt to reach a considered decision over several innovations. Rather than improving matters the latter algorithm proved unstable, showing a marked tendency to generate a false alarm while becoming insensitive to new data. Both the LLR algorithm and a modified version of the RCP algorithm performed well under ideal simulation conditions.

CHAPTER 5

THEORETICAL ASPECTS OF FAULT DETECTION

5.0 Introduction

The idea of monitoring the innovation direction and magnitude for fault detection purposes is in itself not new. Willsky [27] describes the work of Beard and Jones on continuous-time deterministic systems and suggests how noise might be taken into account in certain simple cases. The work covered by this chapter is original in that it parallels the deterministic case by assuming from the outset that the system is stochastic and that innovations are to be generated by a discrete-time Kalman filter. Chapter 6 carries the work a stage further than Beard and Jones by applying the theory to a real system and testing algorithms with real data.

Initially the Kalman filter is analyzed for the general case to determine the effects on the innovations of step faults on input and output measurements. This leads to the possibility of using suboptimal filters with enhanced fault detection properties but raises important questions regarding degradation of performance, stability and divergence of estimates.

As with any fault detection algorithm the possibility of false alarms and incorrect fault isolation decisions must be studied. Since the algorithms of Chapter 4 also claim, via Lemma 4.1, to provide an approximation to the fault magnitude it is also necessary to look at the accuracy that might be expected of this estimate.

5.1 The Kalman Filter

The standard equations for the time-invariant linear discrete-time filter are presented in Section 4.4 but are repeated here for ease of reference.

$$\hat{x}(k+1|k) = \Phi\hat{x}(k|k) + Gu(k) \quad \ldots \quad (5.1)$$

$$P(k+1|k) = \Phi P(k|k)\Phi^T + Q \quad \ldots \quad (5.2)$$

$$V(k+1) = HP(k+1|k)H^T + R \quad \ldots \quad (5.3)$$

$$K(k+1) = P(k+1|k)H^T V^{-1}(k+1) \quad \ldots \quad (5.4)$$

$$\gamma(k+1) = y(k+1) - H\hat{x}(k+1|k) \quad \ldots \quad (5.5)$$

$$\hat{x}(k+1|k+1) = \hat{x}(k+1|k) + K(k+1)\gamma(k+1) \quad \ldots \quad (5.6)$$

$$P(k+1|k+1) = \left[I-K(k+1)H\right]P(k+1|k)\left[I-K(k+1)H\right]^T + K(k+1)RK^T(k+1) \quad \ldots \quad (5.7)$$

5.1.1 The filter transition matrix, Ψ

Consider the case where the filter has reached steady-state, i.e. $K(k+1) = K(k) = K$. Equations (5.1), (5.5) and (5.6) can be combined to give

$$\hat{x}(k+1|k+1) = (I-KH)\Phi\hat{x}(k|k) + (I-KH)Gu(k) + Ky(k+1) \quad \ldots \quad (5.8)$$

or

$$\hat{x}(k+1|k+1) = \Psi\hat{x}(k|k) + (I-KH)Gu(k) + Ky(k+1) \quad \ldots \quad (5.9)$$

where $\Psi = (I - KH)\Phi$ is the filter transition matrix.

Note that the filter is stable iff all the eigenvalues of Ψ lie inside the unit disc.

5.2 The effect of sudden bias on the Kalman Filter

In this section the effect on the filter of a sudden step bias on an output or input measurement is to be determined. Although this analysis requires the Kalman gain K(k) at each step it does not consider the way in which the gain is computed and therefore does not imply that the filter is necessarily optimal. Neither is it assumed that the system was free of measurement bias before the step bias under consideration; the analysis deals only with the effect of a 'new' step which is assumed to occur in the interval $\theta - 1 < k \leq \theta$.

Variables affected by the fault are shown primed, e.g. $\gamma'(\theta)$. Each is expressed as a function of the variable that would have

occurred with no fault, shown unprimed, plus a term due to the fault alone.

It will be shown that the post-fault innovations and state estimates can be expressed in terms of the no-fault variables plus the fault vector $\underline{b}$ premultiplied by a bias matrix B, i.e.

$$\gamma'(k) = \gamma(k) + B(\gamma;k)\underline{b} \quad \ldots \quad (5.10)$$
$$\hat{x}'(k|k) = \hat{x}(k|k) + B(\hat{x};k)\underline{b}$$

Similar bias matrices are used in the analysis of GLR detection algorithms (see, for example, Willsky and Jones [55]) but they are presented in a different way and termed 'failure signature matrices'. Theorems 5.1 and 5.3 are original work having been derived from first principles. Theorems 5.2 and 5.4 are original extensions.

Theorem 5.1 Step bias in the y vector

The instrument step is modelled as

$$y(k) = Hx(k) + v(k) + \underline{b}\sigma_{k,\theta} \quad \ldots \quad (5.12)$$

where $\underline{b}$ is the fault vector and $\sigma_{k,\theta} \begin{cases} = 0; & k < \theta \\ = 1; & k \geq \theta \end{cases}$

At the end of time step $k = \theta-1$, $\hat{x}(\theta-1|\theta-1)$ is stored.

Time step θ

Predict state: $\hat{x}(\theta|\theta-1) = \Phi\hat{x}(\theta-1|\theta-1) + Gu_m(\theta-1) \quad \ldots \quad (5.13)$

Output contains bias, $\underline{b}$, i.e. $y'(\theta) = y(\theta) + \underline{b} \quad \ldots \quad (5.14)$

Innovation: $\gamma'(\theta) = y'(\theta) - H\hat{x}(\theta|\theta-1)$

$$= \gamma(\theta) + \underline{b} \quad \ldots \quad (5.15)$$

State estimate update:

$$\hat{x}'(\theta|\theta) = \hat{x}(\theta|\theta-1) + K(\theta)\Upsilon'(\theta)$$

$$= \hat{x}(\theta|\theta-1) + K(\theta)\left[\Upsilon(\theta) + \underline{b}\right]$$

but $\hat{x}(\theta|\theta) = \hat{x}(\theta|\theta-1) + K(\theta)\Upsilon(\theta)$

i.e. $\hat{x}'(\theta|\theta) = \hat{x}(\theta|\theta) + K(\theta)\underline{b}$ ... (5.16)

Innovation bias $B_y(\Upsilon;\theta)\underline{b} = \underline{b}$ i.e. $B_y(\Upsilon;\theta) = I$

State estimate bias $B_y(\hat{x};\theta)\underline{b} = K(\theta)\underline{b}$ i.e. $B_y(\hat{x};\theta) = K(\theta)$

The 'y' suffix carried by B_y indicates that it refers to a step in the 'y' vector.

Store $\hat{x}'(\theta|\theta)$

Time step $\theta + 1$

Predict state: $\hat{x}'(\theta+1|\theta) = \Phi\hat{x}'(\theta|\theta) + Gu_m(\theta)$

$$= \Phi\hat{x}(\theta|\theta) + \Phi K(\theta)\underline{b} + Gu_m(\theta)$$

$$= \hat{x}(\theta+1|\theta) + \Phi K(\theta)\underline{b}$$

which can be written $= \hat{x}(\theta+1|\theta) + \Phi.B_y(\hat{x};\theta)\underline{b}$ ... (5.17)

Innovation: $\Upsilon'(\theta+1) = y'(\theta+1) - H\hat{x}'(\theta+1|\theta)$

$$= y(\theta+1) + \underline{b} - H\left[\hat{x}(\theta+1|\theta) + \Phi B_y(\hat{x};\theta)\underline{b}\right]$$

$$= \Upsilon(\theta+1) + \left[I_r - H\Phi B_y(\hat{x};\theta)\right]\underline{b} \quad \ldots \quad (5.18)$$

i.e. $B_y(\Upsilon;\theta+1) = \left[I_r - H\Phi B_y(\hat{x};\theta)\right]$

State estimate update:

$$\hat{x}'(\theta+1|\theta+1) = \hat{x}'(\theta+1|\theta) + K(\theta+1)\Upsilon'(\theta+1)$$

$$= \hat{x}(\theta+1|\theta) + \Phi B_y(\hat{x};\theta)\underline{b} + K(\theta+1)\left[\Upsilon(\theta+1) - \{I_r - H\Phi B_y(\hat{x};\theta)\}\underline{b}\right]$$

$$= \hat{x}(\theta+1|\theta+1) + \Phi B_y(\hat{x};\theta)\underline{b} + K(\theta+1)\{I_r - H\Phi B_y(\hat{x};\theta)\}\underline{b}$$

$$= \hat{x}(\theta+1|\theta+1) + B_y(\hat{x};\theta+1)\underline{b} \quad \ldots \quad (5.19)$$

where $B_y(\hat{x};\theta+1) = \Phi B_y(\hat{x};\theta) + K(\theta+1)\{I_r - H\Phi B_y(\hat{x};\theta)\}$

$$= \Phi B_y(\hat{x};\theta) + K(\theta+1)B_y(\Upsilon;\theta+1) \quad \ldots \quad (5.20)$$

Clearly the propagation of the bias through the filter is now given by the following recursions:

$$B_y(\hat{x};\ \theta\text{-}1) = 0 \qquad \ldots \quad (5.21)$$

$$\left.\begin{aligned} B_y(\Upsilon;\ j\text{+}1) &= \left[I_r - H\Phi B_y(\hat{x};j)\right] \\ B_y(\hat{x};\ j\text{+}1) &= \Phi B_y(\hat{x};j) + K(j\text{+}1)B_y(\Upsilon;j\text{+}1) \end{aligned}\right\}\forall j \geq \theta\text{-}1 \qquad \begin{aligned} &\ldots \quad (5.22) \\ &\ldots \quad (5.23) \end{aligned}$$

Innovation bias = $B_y(\Upsilon;j)\underline{b}$

State estimate bias = $B_y(\hat{x};j)\underline{b}$ ∎

Lemma 5.1 If the filter is stable, the matrix $[I_n - \Psi]$ is non-singular.

The equation

$$|sI_n - \Psi| = 0$$

is satisfied by values of 's' which are eigenvalues of Ψ. The filter is stable so all eigenvalues lie within the unit disc, i.e. '1' is not an eigenvalue, and hence

$$|I_n - \Psi| \neq 0 \quad \text{and} \quad [I_n - \Psi]^{-1} \text{ exists.} \qquad ∎$$

Theorem 5.2 Settling out of the 'y' bias effect.
Theorem 5.1 can be further developed if we assume that the Kalman gain is constant, i.e. $K(j) = K\ \forall j$. This could be engineered by using a constant K from the outset or by assuming that no faults occur until the filter has reached a steady state.

Equations (5.21-3) now become:

$$B_y(\hat{x};\ \theta\text{-}1) = 0 \qquad \ldots \quad (5.24)$$

$$\left.\begin{aligned} B_y(\Upsilon;\ j\text{+}1) &= I_r - H\Phi B_y(\hat{x};j) \\ B_y(\hat{x};\ j\text{+}1) &= \Phi B_y(\hat{x};j) + KB_y(\Upsilon;j\text{+}1) \end{aligned}\right\}\forall j \geq \theta\text{-}1 \qquad \begin{aligned} &\ldots \quad (5.25) \\ &\ldots \quad (5.26) \end{aligned}$$

From (5.25) and (5.26)

$$\begin{aligned} B_y(\hat{x};\ j\text{+}1) &= \Phi B_y(\hat{x};j) + K\left[I_r - H\Phi B_y(\hat{x}:j)\right] \\ &= K + (I_n\text{-}KH)\Phi B_y(\hat{x};j) \\ &= K + \Psi B_y(\hat{x};j) \qquad \ldots \quad (5.27) \end{aligned}$$

By applying (5.27) repeatedly to the initial condition (5.24),

$$B_y(\hat{x};\ \theta+j) \ = \ \sum_{m=o}^{j} \Psi^m K \qquad \ldots \quad (5.28)$$

where $\Psi^o = I_n$

This is a geometric series and can be summated to 'N' terms

$$B_y(\hat{x};\ \theta+N) \ = \ [I_n-\Psi]^{-1}\ [I_n-\Psi^N]K \qquad \ldots \quad (5.29)$$

The existence of $[I-\Psi]^{-1}$ is guaranteed by Lemma 5.1. Furthermore, with a stable filter all eigenvalues of Ψ lie within the unit disc and so

$$\lim_{N\to\infty}(\Psi^N) \ \to \ 0$$

and the bias matrix assumes a steady state value given by

$$B_y(\hat{x}) \ = \ [I_n - \Psi]^{-1}K \qquad \ldots \quad (5.30)$$

The steady-state innovation bias matrix follows directly from this together with (5.25):

$$B_y(\gamma) \ = \ I_r - H\Phi[I_n - \Psi]^{-1}K \qquad \ldots \quad (5.31)$$

■

The process can now be repeated for a step bias on an input measurement.

Theorem 5.3 Step bias in the 'u' vector

The instrument step is modelled as:

$$x(k+1) \ = \ \Phi x(k) + G\left[u_m(k) + \underline{b}.\sigma_{k,\theta}\right] + \tilde{w}(k) \qquad \ldots \quad (5.32)$$

where $\underline{b}$ and $\sigma_{k,\theta}$ are defined as for Theorem 5.1. Measurement $u_m(\theta)$ is the first to contain the fault which therefore affects the estimate at step $\theta + 1$.

At the end of time step $k = \theta$, $\hat{x}(\theta|\theta)$ is stored.

Time step $\theta + 1$

Predict state: $\hat{x}'(\theta+1|\theta) = \Phi\hat{x}(\theta|\theta) + G\left[u_m(\theta) + \underline{b}\right]$

$$= \hat{x}(\theta+1|\theta) + G\underline{b} \quad \ldots \quad (5.33)$$

Innovation: $\gamma'(\theta+1) = y(\theta+1) - H\hat{x}'(\theta+1|\theta)$

$$= \gamma(\theta+1) - HG\underline{b} \quad \ldots \quad (5.34)$$

i.e. $B_u(\gamma;\theta+1) = -HG$

State estimate update:

$$\hat{x}'(\theta+1|\theta+1) = \hat{x}'(\theta+1|\theta) + K(\theta+1)\gamma'(\theta+1)$$

$$= \hat{x}(\theta+1|\theta+1) + \left[I_n - K(\theta+1)H\right]G\underline{b} \quad \ldots \quad (5.35)$$

i.e. $B_u(\hat{x};\theta+1) = \left[I_n - K(\theta+1)H\right]G$

Store $\hat{x}'(\theta+1|\theta+1)$

Time step $\theta + 2$

Predict state: $\hat{x}'(\theta+2|\theta+1) = \Phi\hat{x}'(\theta+1|\theta+1) + G\left[u_m(\theta+1) + \underline{b}\right]$

$$= \hat{x}(\theta+2|\theta+1) + B_u(\hat{x};\theta+1)\underline{b} + G\underline{b} \quad \ldots \quad (5.36)$$

Innovation: $\gamma'(\theta+2) = y(\theta+2) - H\hat{x}'(\theta+2|\theta+1)$

$$= \gamma(\theta+2) - H\Phi B_u(\hat{x};\theta+1)\underline{b} - HG\underline{b} \quad \ldots \quad (5.37)$$

State estimate update:

$$\hat{x}'(\theta+2|\theta+2) = \hat{x}'(\theta+2|\theta+1) + K(\theta+2)\gamma'(\theta+2)$$

$$= \hat{x}(\theta+2|\theta+2) + \left[I_n - K(\theta+2)H\right]\left[G + \Phi B_u(\hat{x};\theta+1)\right]\underline{b} \quad \ldots \quad (5.38)$$

leading to the recursions:

$$B_u(\hat{x};\theta) = 0 \quad \ldots \quad (5.39)$$

$$B_u(\gamma,j+1) = -HG - H\Phi B_u(\hat{x};j) \quad \ldots \quad (5.40)$$

$$B_u(\hat{x},j+1) = \left[I_n - K(j+1)H\right]\left[G + \Phi B_u(\hat{x};j)\right] \quad \ldots \quad (5.41)$$

$\forall\, j \geq \theta$

Theorem 5.4 Settling out of the 'u' bias effect.

With constant K, equations (5.40 and 5.41) become

$$B_u(\gamma;j+1) = -HG - H\Phi B_u(\hat{x};j) \quad \ldots \quad (5.42)$$

$$B_u(\hat{x};j+1) = (I_n-KH)[G + \Phi B_u(\hat{x};j)] \quad \ldots \quad (5.43)$$

By applying (5.43) repeatedly to the initial condition (5.39)

$$B_u(\hat{x};\theta+j) = \sum_{m=0}^{j} \Psi^m(I_n-KH)G \quad \ldots \quad (5.44)$$

and summating to N terms

$$B_u(\hat{x},\theta+N) = [I_n-\Psi]^{-1}[I_n-\Psi^N] (I_n-KH)G \quad \ldots \quad (5.45)$$

As $N \to \infty$ this approaches a steady state value

$$B_u(\hat{x}) = [I_n - \Psi]^{-1} (I_n - KH)G \quad \ldots \quad (5.46)$$

The steady state innovation bias matrix follows directly from this together with (5.42):

$$B_u(\gamma) = -H\left[G + \Phi[I - \Psi]^{-1} (I - KH)G\right] \quad \ldots \quad (5.47)$$

■

5.3 The effect of jumps ('bad data points')

Bad data points are not uncommon in industrial plants where 'spikes' may occur on measured variables from time to time due to electromagnetic interference. A sudden measurement jump may affect only a single sample and can then be modelled as a step at $k = \theta$ followed by a step in the opposite sense at $k = \theta + 1$. Clearly if the filter is stable the effect on both the state estimate and the innovations will eventually die away to zero. Whether or not the spike will be picked up by a fault detection algorithm will depend on the magnitude and rate of decay of its effect on the innovations that follow. This type of fault is studied experimentally in Chapter 6.

5.4 A scalar example

The possibility of using a constant, perhaps suboptimal Kalman gain has already been mooted. The effect this would have on the steady state bias matrices of Theorems 5.2 and 5.4 is more readily understood with the aid of a computer simulation based on a scalar example.

Consider the system

$$x(k+1) = \phi x(k) + gu(k) + w(k) \qquad \ldots \quad (5.48)$$

$$y(k) = hx(k) + v(k) \qquad \ldots \quad (5.49)$$

with $h = g = 1.0$ $\quad q = E[ww^T] = 1.0$

$\phi = 0.4$ $\quad r = E[vv^T] = 0.2$

Taking u(k) to be identically zero for all k, Gaussian process and measurement noise files QNOISE and RNOISE, each containing 1000 data points, were generated by using computer NAG routines. QNOISE was then run through the model (5.48) to generate a file of states to which was added RNOISE to create an observation file.

The observations were used in conjunction with constant gain filters which utilized filter equations (5.1, 5.5 and 5.6) only. The effects of altering K over a wide range were noted.

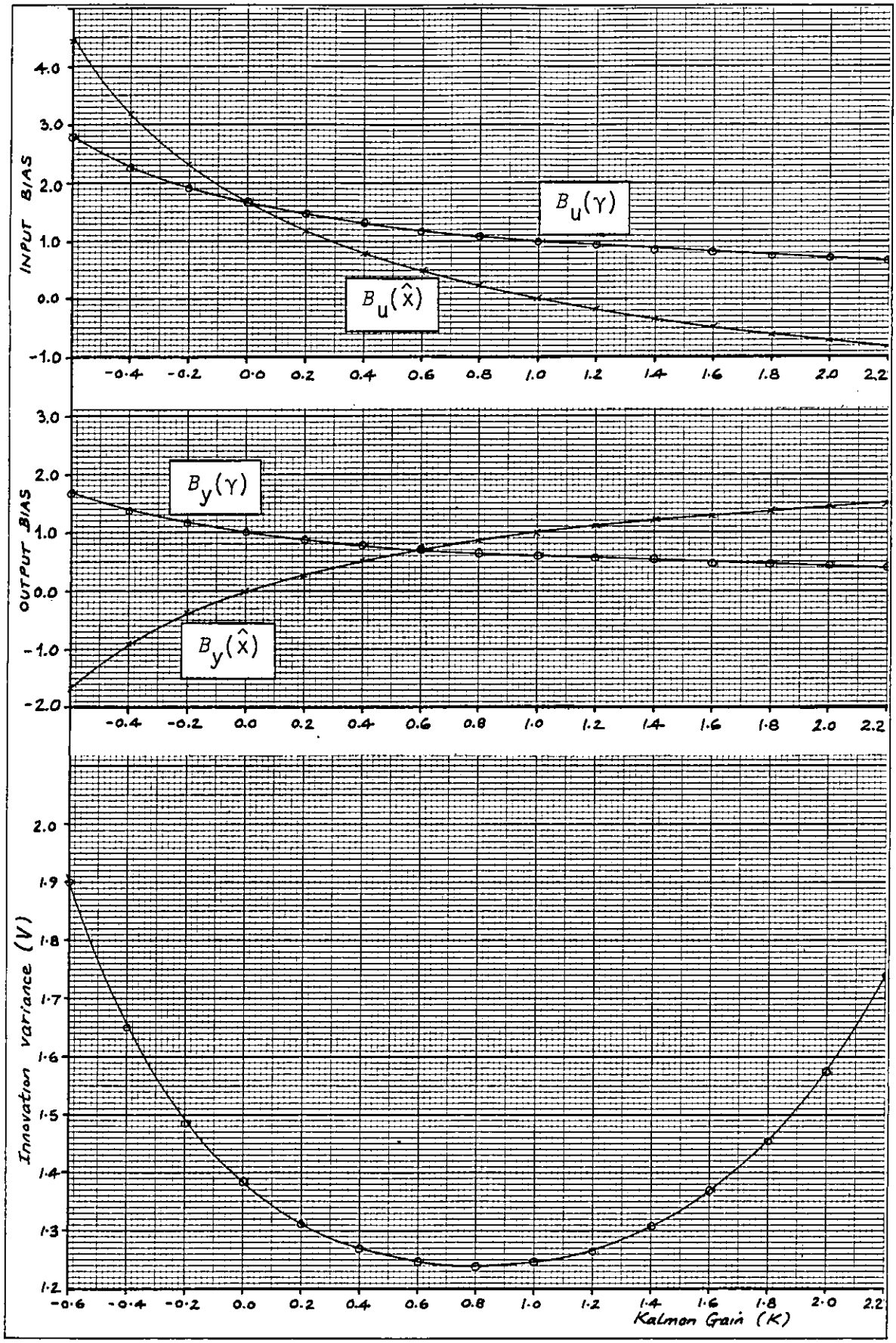

Fig.24 Innovation variance and bias matrices as functions of K for a scalar example

By using equations (5.2, 5.3, 5.4 and 5.7) it is clear that the steady state a posteriori error covariance 'p' is the solution of

$$p = \frac{p\phi^2 r + qr}{p\phi^2 + q + r} \qquad \text{i.e. } p = 0.168 \qquad \ldots \quad (5.50)$$

The optimal steady state Kalman gain is therefore given by

$$K = \frac{p\phi^2 + q}{p\phi^2 + q + r} = 0.837 \qquad \ldots \quad (5.51)$$

The effect of K on the innovation variance is plotted in Fig 24. As might be expected, this variance is at a minimum at around the optimal value of K. This is of course also true of the error variance 'p'.

Also shown in Fig 24 as functions of K are bias matrices (here scalars) calculated from equations (5.31) and (5.47), i.e.

$$B_y(\gamma) = h\left\{ g + \frac{\phi(1-Kh)}{1-\psi} \right\} \qquad \ldots \quad (5.52)$$

$$B_u(\gamma) = \left\{ 1 - \frac{h\,\phi\,K}{1-\psi} \right\} \qquad \ldots \quad (5.53)$$

Two points from Fig 24 should be noted:

(i) As K approaches zero the effect on the state estimate of a step in y also approaches zero.

(ii) As K decreases the effect on the innovations of a step in either y or u is increased.

This example illustrates several important points.

5.4.1 The oblivious filter

When the full filtering equations (5.1) to (5.7) are used, covariance matrices Q and R must be specified. Although Q is defined as the process noise covariance it can be manipulated to reflect the accuracy of the model (see

Hamilton et al [20] for discussion). A Q that is 'low' compared with R implies a somewhat higher degree of confidence in the model than in the measurements and will result in a 'small' steady state Kalman gain. Conversely the use of a (constant) small gain implies a low Q (and/or a relatively high R).

A filter using a small gain relies almost completely on the model to produce estimates. If there are substantial unmodelled phenomena then the filter may diverge and become useless as a state estimator because it is oblivious to the new information it receives. Techniques for keeping the filter sensitive to new data include several in which P(k|k), and hence K(k), are prevented from becoming too small (see Fagin [28] and Tarn and Zaborsky [29]). Fixing the gain at a suitable value has already been mentioned and is discussed briefly by Jazwinski [5].

The designer of fault detection systems seeks a quick response to sudden measurement biases: Kerr [83] considered an augmented filter in which certain failure modes were included as state variables. With a small gain, note (i) indicates that a sudden measurement bias will have minimal effect on the state estimate and may go undetected.

5.4.2 The innovation bias matrix

Decreasing K is clearly undesirable for fault detection methods relying on state estimation. Note (ii), however, suggests that such a decrease could improve the sensitivity of an innovations based detection algorithm, particularly as such a move would appear to amplify the effect of step biases in both input and output measurements. This is explained as follows:

A 'small' K implies that Q is 'low' relative to R and hence that the model is more reliable than the measurements.

At a step bias in y: The filter trusts the model rather than the observations, y. It therefore doesn't let the change in y influence the estimates and $B_y(\hat{x})$ stays small. Because the estimates do not follow the change in the observations, the second term in equation (5.5) is left behind by the first and the innovation bias $B_y(\gamma)$ is high.

At a step bias in u: The filter considers model equation (5.1) to be reliable and so makes full use of the incorrect u values, altering the estimate accordingly: $B_u(\hat{x})$ is large. The second term in (5.5) is now incorrect while the observations y are unaffected: $B_u(\gamma)$ is high also.

5.4.3 The available range of K

Another point raised by this example is the range of K values that can be obtained by manipulation of q and r. For stability, ψ must lie in the range $-1 < \psi < +1$ so that K is constrained to $-1.5 < K < +3.5$

For the scalar case K is dependent on the ratio q/r. This ratio must lie in the range $0 \leq q/r < \infty$ so that for an optimal filter K must lie in the range $0 \leq K < +1$. Evidently there are ranges of K values

$$-1.5 < K < 0.0 \qquad \text{and} \qquad 1.0 \leq K < 3.5$$

for which the filter is stable but which could not be obtained by specifying the q/r ratio.

5.4.4 Summary

The scalar example indicates that in general a 'small' Kalman gain increases the effect of a fault on the innovations, be it an input or an output fault. A suboptimal gain also has the effect of increasing the innovation and estimation error (co)variances. Suitable Kalman gains can be obtained by specifying fictitious Q and R matrices, but such an approach precludes the use of other K values for which the eigenvalues of ψ lie within

the unit disc but which cannot be obtained from any combination of Q and R. Such gains are therefore not representative of physically realisable systems but may yet produce stable and possibly useful filters.

5.5 Discussion on the LLR algorithm of Sections 4.8 & 4.9.2

Consider a step fault constrained to occur in one of the nine hypothesized failure directions given in Section 4.3. Theorems 5.1 and 5.3 give for each direction the trajectory of the expected value of the innovation vector in r-space for $k \geq \theta$, where θ is the time of the first post-fault sample. These theorems can be used to obtain a characteristic innovation time-pattern for each failure direction. For a set of innovations, $\gamma(j) \ldots \gamma(j+N)$, which is believed to reflect an instrument fault, a detection algorithm could be constructed from the following heuristic argument.

Starting with the first innovation in the set, we assume that a fault has just occurred, i.e. that $\theta = j$. We compare innovations $\gamma(j) \ldots \gamma(j+N)$ with the characteristic pattern for direction 1, then go on to do exactly the same for directions 2 to 9. The next step is to drop $\gamma(j)$ and to assume that $\theta = j+1$, this time comparing innovations $\gamma(j+1) \ldots \gamma(j+N)$ with the characteristic patterns for directions 1 to 9. The process is repeated by dropping the oldest innovation at each step, the final check being to compare just $\gamma(j+N)$ with the characteristic $\gamma(\theta)$ for each failure direction.

We have now checked all the innovations for the possibility that a fault in one of the nine hypothesized directions has occurred at some stage during the monitored time span. The next step is to estimate from all these comparisons firstly the time at which the fault, if any, was most likely to have occurred and secondly the failure direction in which it was most likely to have occurred. Having reached the decision that the innovations reflect a particular fault at a particular time, the final task is to decide by means of a suitable statistical test whether the innovations have departed sufficiently from normal to justify the declaration of the estimated (i.e. the most likely) fault as 'true'.

Such a method is clearly very complex but what we have in fact just described is, in essence, the CGLR algorithm mentioned briefly in Section 1.1.3(v). We now discuss the LLR technique proposed in Chapter 4, highlighting the areas in which the algorithm could be designed to make substantial savings in computational effort in comparison with CGLR.

The (C)GLR formulation allows the use of a time-varying Kalman gain because the innovation time-patterns are effectively calculated on-line as required. If, as already suggested, we employ a constant Kalman gain, then the effect on the innovations of a step fault asymptotically approaches a constant bias and could be precomputed. By going a stage further and neglecting the transients altogether we can reduce the storage requirements to just the steady state reference vectors d_i , $i = 1, \ldots 9$, which can be obtained from Theorems 5.2 and 5.4.

From the discussion on the previous page it is clear that if the full blown CGLR algorithm is run continuously then the linearly growing innovation set implies a similarly increasing work-load. This is the area in which the LLR method can make the greatest computational savings over CGLR, although it remains to be seen whether this is accompanied by unacceptable limitations in performance. LLR does not optimize $\hat{\theta}$ at all and estimates the fault magnitude from a single innovation via Lemma 4.1.

A direct consequence of this one-sample estimation is that the log-likelihood ratio (llr) can only be calculated from one sample, which removes the need to store past innovations. The llr is normally evaluated over a number of innovations which, under the fault hypothesis, are viewed as observations on a random process characterized by some fault parameter. This parameter need not be constant but any time variation must be accounted for. By using Lemma 4.1, however, the innovation bias is re-estimated at every innovation for each failure direction. Furthermore, the use of steady state reference vectors precludes correction for transients and means that the innovations cannot be strung together for the purposes of log-likelihood ratio calculation.

We therefore propose to implement an LLR-based algorithm employing steady state reference vectors for use with Lemma 4.1 and working in conjunction with a constant gain filter.

5.6 The manipulation of K

Section 5.4 showed that,in principle at least,we are free to specify a constant gain K in any way we choose. Before studying the possible ill effects we examine the advantages that might accrue from the use of a constant suboptimal gain.

Fault isolation is limited by the separation of the steady state reference vectors in r-space. If two are close together then the algorithm may not be able to distinguish between the two fault sources. The distribution of the reference vectors in space is, however, governed by the choice of gain and so it may be possible to move such vectors apart by manipulation of K.

Another danger is that if on occurrence of a certain fault the innovation vector swings wildly in r-space then it may pass close to the reference vectors for other faults, causing, at least initially, a misleading diagnosis. Also, if the innovation magnitude fluctuates rapidly or dies away very quickly, then this will limit the accuracy of the estimation of the fault magnitude via Lemma 4.1.

To summarize, the optimal K for this type of algorithm is that which ensures a strong innovation response while minimizing the magnitude variation and rotation of the post fault innovations relative to the reference vectors, which must themselves be evenly distributed in r-space.

5.7 Degradation of filter performance

Having established that there may be considerable advantage in manipulating K for fault detection purposes, it now becomes necessary to study the possible disadvantages of such a step.

5.7.1 Increases in error and innovation covariances

This project has moved away from state estimation towards a filter designed solely for fault detection purposes. With this in mind the loss of estimation accuracy, reflected by the estimation error covariance $P(k|k)$, is of secondary importance provided that it remains at a 'reasonable' level - see Section 5.7.2.

A suboptimal K, however, increases the innovation covariance: an excessive increase could make it very difficult to extract meaningful fault information from the innovations. The degradation of the error and innovation covariances are closely related since the latter is derived from the a priori error covariance in equation (5.3).

In Chapter 7 of [5], Jazwinski derives recursions for $P_a(k+1|k)$ and $P_a(k|k)$, the 'actual' estimation error covariances, for a suboptimal filter. The actual degradation in performance, $P_s(k|k)$, could be calculated by subtracting the optimal and actual covariances, i.e.

$$P_s(k|k) = P_a(k|k) - P(k|k) \quad \ldots \quad (5.54)$$

For the constant gain case and where the optimal steady state innovation covariance is known, the steady state P_s can be calculated directly for any Kalman gain K from (5.55).

$$P_s = [I - K_a H]P_s^+[I - K_a H]^T + \Delta V \Delta^T \quad \ldots \quad (5.55)$$

where K_a = actual (constant) Kalman gain used

$P_s^+ = \Phi P_s \Phi^T$

$\Delta = K_a - K$ where K is the optimal s/s gain

V = optimal s/s innovation covariance

The corresponding increase in innovation covariance, V_s, is given by

$$V_s = HP_sH^T \quad \ldots \quad (5.56)$$

Equations (5.55) and (5.56) are original extensions of the work of Friedland [14] who derived a similar result for the continuous time case. The proof is given in Appendix VI.

5.7.2 Filter divergence

The manipulation and possible 'reduction' of K bring with them the danger of filter divergence. Consider the Kalman filtering equations (5.1) to (5.7). If the model $\{\Phi, G, H\}$ is precise and Q, R are correctly specified then the actual estimation error covariance obtained will be in close agreement with that predicted by equation (5.7). Filter divergence is caused by inaccuracies in modelling, with overconfidence in the model often a contributory factor. Under certain circumstances, particularly in problems of navigation in nearly circular orbits, it has been found that the actual estimation errors increase with time and the filter diverges.

Fitzgerald [84] defines true (or 'mathematical') divergence, in which the mean square errors can actually be shown to approach infinity with increasing time, and apparent (or 'practical') divergence where the steady state errors are bounded but are too large for the estimates to be useful.

Fitzgerald shows for the continuous-time case that if A_c and C_c are precisely specified then, except under one particular system condition, true divergence cannot occur however small P (and hence K) are allowed to become. If Φ were known exactly then Fitzgerald's theory could perhaps be extended to show that a similar result exists for the discrete-time case, with a view to showing that a stable filter based on the pilot plant model will not exhibit true divergence whatever the value of K used.

This, however, would not guarantee immunity from apparent divergence. The pilot plant model is known to be approximate, not only because it was obtained by linearization but also because of the rather crude estimation of time constants and transport delays in Chapter 3. Apparent divergence can be detected only by simulation and in the circumstances the additional analysis required to even attempt to prove that true divergence will not take place is not justified.

Both Jazwinski [5] and Fitzgerald [84] discuss the addition of fictitious process noise (i.e. specifying Q larger than its true value) in order to prevent divergence in certain cases. In the light of this it must be borne in mind that if there is any likelihood of filter divergence with the pilot plant model then the suggested reduction of K can only exaggerate it. Clearly the possibility requires investigation by extensive and prolonged simulation.

5.8 Incorrect decision probabilities for LLR algorithms

In common with Section 4.9, this analysis is based on hypothesis testing via a single innovation. For a system with two or more possible faults there are three categories of incorrect decision for which probabilities can be defined. Using the notation of Section 4.9:

H_0 true	algorithm declares H_i	false alarm
H_i true	algorithm declares H_0	miss alarm
	algorithm declares $H_j, j \neq i$	cross-detection

We define

P_D probability of correct decision

P_F probability of false alarm

P_M probability of miss alarm

P_X probability of cross-detection

P_U probability of non-definite decision

5.8.1 Geometric interpretation

Each of these probabilities can be related to the probability of finding an innovation in a given region of r-space. Consider Fig 25(a) in which, for a two dimensional example, there are two possible fault directions d_1 and d_2. Using Lemma 4.1 and expression (4.65) for direction d_1, 'cea' is a contour of constant log-likelihood ratio and an innovation falling in area A_1 will be declared as significant when testing H_1 against H_0.

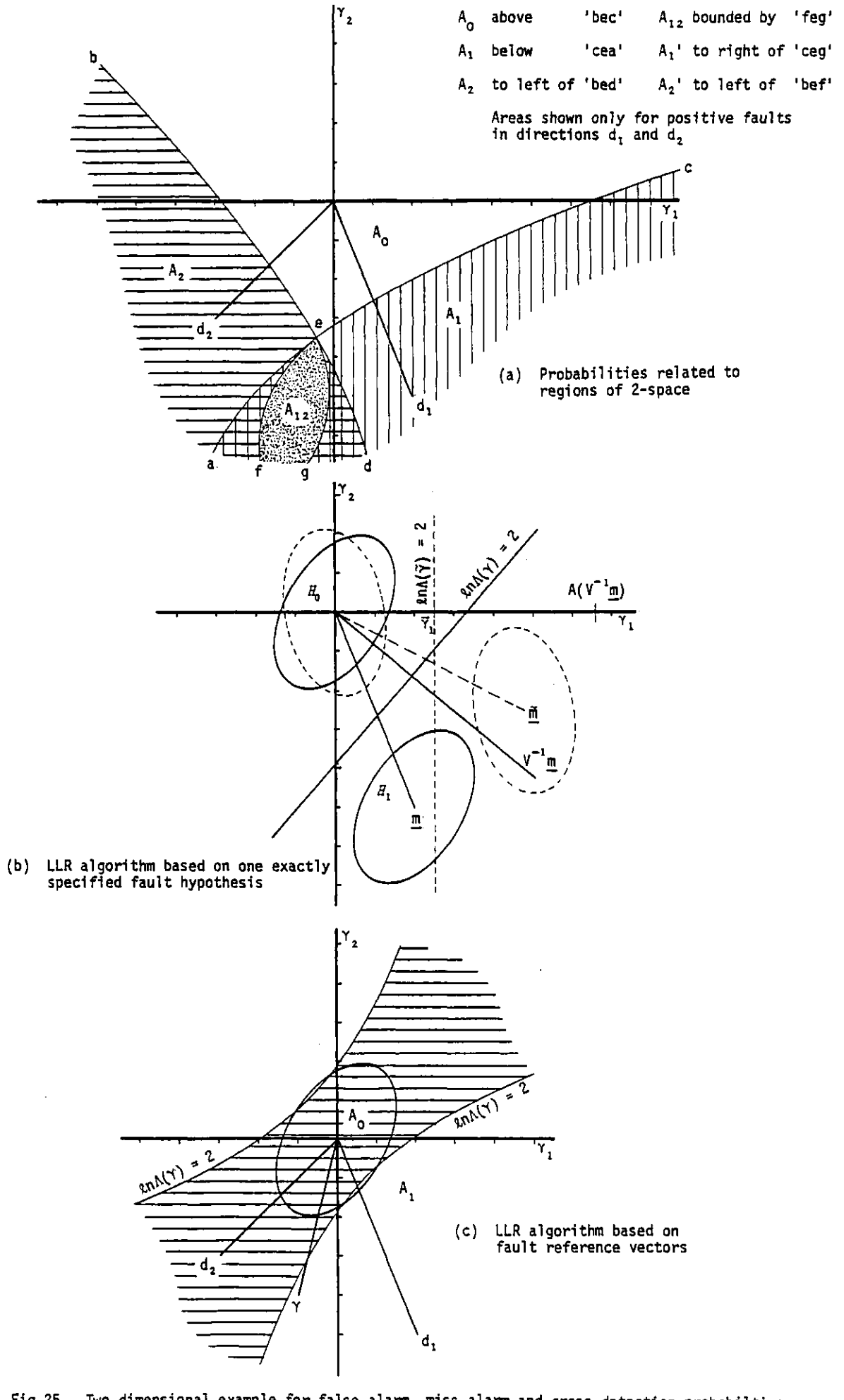

Fig.25 Two dimensional example for false alarm, miss alarm and cross-detection probabilties

Similarly an innovation falling in A_2 will be declared significant when testing H_2 against H_0. Low magnitude innovations fall in area A_0 and are not significant for either fault hypothesis. $\overline{A}$ is 'not A', i.e. the whole of 2-space except for A.

H_0 true

$$P_F = Pr(\Upsilon \in A_1 \cup A_2 \mid H_0)$$

$$P_D = Pr(\Upsilon \in A_0 \mid H_0)$$

H_1 true

$$P_M = Pr(\Upsilon \in A_0 \mid H_1)$$

$$P_D = Pr(\Upsilon \in \overline{A}_0 \cap \overline{A}_2 \mid H_1) \quad \text{area to right of 'ced'}$$

$$P_X = Pr(\Upsilon \in \overline{A}_0 \cap \overline{A}_1 \mid H_1) \quad \text{area to left of 'bea'}$$

There is uncertainty if $\Upsilon \in A_1 \cap A_2$, i.e. Υ is significant for both H_1 and H_2 against H_0. For H_1 true:

$$P_U = Pr(\Upsilon \in A_1 \cap A_2 \mid H_1)$$

Should $\Upsilon \in A_1 \cap A_2$, it is possible to reduce the possibility of uncertainty by testing H_2 against H_1 for the same innovation. An innovation falling in the area bounded by 'ged' has Υ significant for both H_1 and H_2. The second test shows that Υ is significant for H_1 against H_2, and H_1 is declared. For H_1 true this extends the area corresponding to P_D so that

$$P_D' = Pr(\Upsilon \in A_1' \mid H_1) \qquad P_D' > P_D$$

Uncertainty then exists only if $\Upsilon \in A_{12}$ (where $A_{12} \subset (A_1 \cap A_2)$, shown speckled in the diagram): Υ is significant for both H_1 and H_2 against H_0 but not significant for H_1 against H_2 or vice versa. P_X and P_U are revised as follows for H_1 true:

$$P_X' = Pr(\Upsilon \in A_2' \mid H_1) \qquad P_X' > P_X$$

$$P_U' = Pr(\Upsilon \in A_{12} \mid H_1) \qquad P_U' < P_U$$

Note that P_U is reduced at the expense of increasing P_X.

5.8.2 Probabilities for a completely specified fault

To begin with, consider the two dimensional system shown in Fig 25(b) for which there is one completely specified fault (H_1) which drives $E[\underline{\gamma}]$ instantaneously to $\underline{m} = [2\ -5]^T$. For this example $\underline{\gamma} = [\gamma_1\ \gamma_2]^T$ where γ_1, γ_2 are jointly normal random variables with correlation coefficient 0.5 and covariance

$$V = \begin{bmatrix} 1 & 1/\sqrt{2} \\ 1/\sqrt{2} & 2 \end{bmatrix} \qquad \ldots \quad (5.57)$$

The solid ellipses shown in the diagram are contours of constant probability density $f(\gamma_1, \gamma_2)$ under H_0 and H_1. Specifying an llr threshold of $\eta = 2$ we can draw a contour for which η is constant at this value. Its equation, given by (A7.2), Appendix VII is

$$5.024\gamma_1 - 4.276\gamma_2 = 16.72$$

which is a straight line orthogonal to $V^{-1}\underline{m} = [5.024\ \ -4.276]^T$. From Section 5.8.1, P_F is the probability that under H_0 an innovation lies below the constant llr contour, while P_M is the probability that under H_1 an innovation lies above it. In general the llr contour is not parallel to a co-ordinate axis and the variables must be transformed in order to evaluate the required probabilities. Rotating the problem relative to the existing axes until $V^{-1}\underline{m}$ is aligned in the $+\gamma_1$ direction we obtain the situation shown in dashed lines in Fig 25(b). Labelling the transformed variables $\tilde{\gamma}, \tilde{\underline{m}}$ and $\tilde{V}$ the required values are obtained by considering the marginal density of $\tilde{\gamma}_1$ alone using tables for the standard normal distribution.

$$P_F = Pr(\tilde{\gamma}_1 > \bar{\gamma}_1 \mid H_0) = 1 - \Phi(\bar{\gamma}_1/\tilde{\sigma}_1)$$

$$P_M = Pr(\tilde{\gamma}_1 < \bar{\gamma}_1 \mid H_1) = 1 - \Phi((m_1 - \bar{\gamma}_1)/\tilde{\sigma}_1)$$

Using the results of Appendix VII

$$\tilde{V}_{11}^{\,2} = 0.722 \quad (\text{i.e. } \tilde{\sigma}_1 = 0.85)$$

$$\bar{\gamma}_1 = 2.49 \qquad \tilde{m}_1 = 4.76$$

Recalling the definition of $\ell n\Lambda(\gamma)$ from (4.65) we have

$$P_F = Pr(\gamma \text{ s.t. } \ell n\Lambda(\gamma) > \eta | H_0) = 1 - \Phi(2.93) = 0.0018$$

$$P_M = Pr(\gamma \text{ s.t. } \ell n\Lambda(\gamma) > \eta | H_1) = 1 - \Phi(2.67) = 0.0039$$

5.8.3 Probabilities for a fault in a specified direction

Fig 25(c) represents the situation in which two possible faults, H_1 and H_2, drive the innovations in directions d_1 and d_2 respectively. As in Section 4.9, vectors $d_1 = [2\ -5]^T$ and $d_2 = [-3\ -3]^T$ are reference vectors relating to step faults of unit magnitude. We first consider the problem of testing a single innovation via expression (4.65) to decide between H_0 ($E[\gamma] = \underline{0}$) and $H_1(E[\gamma] = \rho_1[2\ -5]^T)$. At the llr threshold we have, in general

$$\gamma^T V^{-1}\gamma - (\gamma - \rho_1 d_1)^T V^{-1}(\gamma - \rho_1 d_1) = \eta \qquad \ldots \quad (5.58)$$

Substituting for ρ_1 from Lemma 4.1

$$\gamma^T V^{-1} d_1 \left[\frac{\gamma^T d_1}{d_1^T d_1}\right] = \tfrac{1}{2}\left[\frac{\gamma^T d_1}{d_1^T d_1}\right]^2 d_1^T V^{-1} d_1 + \tfrac{1}{2}\eta \quad \ldots(5.59)$$

Unlike the previous case this is not a hyperplane but a curved surface in r dimensions. We can investigate further for this two dimensional example by substituting for d_1, V and η. Writing $\gamma = [\gamma_1\ \gamma_2]^T$ and letting $\eta = 2$ as before we obtain from (5.59)

$$228.52\gamma_1^2 - 662.21\gamma_1\gamma_2 + 227.17\gamma_2^2 - 841 = 0 \quad \ldots(5.60)$$

This is of the form $ax^2 + 2hxy + by^2 + c = 0$ with $h^2 - ab > 0$ and is therefore a hyperbola as shown in Fig 25(c). Innovations falling inside the shaded area will be declared as H_0, those falling outside as H_1. It is the fact that ρ_1 can be positive or negative for direction d_1 that constrains the H_0 area to a waisted band symmetrical about the origin. Clearly for the same llr threshold as in Section 5.8.2 ($\eta = 2$) P_F is increased but calculation of actual probabilities is a complex problem

even in the two dimensional case. The above analysis repeated for H_2 would yield a second 'H_0' band superimposed on the first and further increasing P_F.

5.8.4 Discussion

When a fault occurs in one of the anticipated directions, the question of whether the fault will be correctly detected is further complicated by the transient nature of the bias superimposed on the innovations. This means that in the Section 5.8.1 expressions for P_M, P_D and P_X which are defined 'given H_1', the hypothesis H_1 changes at each time step until it eventually reaches a steady mean aligned with vector d_1: these probabilities are therefore different at each time step.

It is the time-varying nature of each fault hypothesis H_i that dictates the use of a single innovation for hypothesis testing. In order to use a 'moving window' of innovations to increase P_D and reduce P_M and P_X each innovation must be treated as an independent observation on a random process whose statistical time variations are included in the llr calculation. A number of innovations could be used for the example of Section 5.8.2 where the word 'instantaneously' is included to imply that there is no transient: H_1 is constant.

In the light of the failure under simulation (Section 4.10.4) of the RCP algorithm as originally specified in Section 4.9.4, it may be an advantage that the decision based on each innovation is unaffected by any previous decision.

5.8.5 Minimum angle versus maximum llr

The discussion in Section 5.6 gives the impression that the reference vector nearest to the current innovation will be the one, if any, to be declared as the true fault direction. While this is true in the majority of cases it is not always the case as is indicated by the following example illustrated in Fig.25(c).

Consider the innovation $\gamma = [-1\ -4]^T$. The angle θ between γ and d_i is given by

$$\theta = \cos^{-1}\left[\frac{d_i^T\gamma}{|d_i||\gamma|}\right]$$

We have $d_1 = [2\ -5]^T$ and $d_2 = [-3\ -3]^T$. For d_1 the angle is 35.8° and for d_2, 30.97°, i.e. the innovation is closer to d_2. Lemma 4.1 gives $\rho_1 = 0.621$ and $\rho_2 = 0.833$. With V from (5.57) the llr's are calculated from (4.65) as follows:

For d_1 $\quad \ell n\, \Lambda(\gamma) = 8.228 - 5.340 = 2.888$

For d_2 $\quad \ell n\, \Lambda(\gamma) = 8.228 - 6.607 = 1.621$

If $\eta = 2$ as before then H_1 is significant against H_0 but H_2 is not. In this case the fault direction with the higher llr is not the direction nearer the innovation in r-space.

The innovation distribution under H_0 has a greater density along d_2 than along d_1 as illustrated by the ellipse of constant density in Fig 25(c). The component of γ lying along d_2 needs to be substantially larger than that along d_1 to achieve the same level of significance over the H_0 hypothesis. It follows that a purely geometric interpretation of results should be treated with caution, particularly if the 'r' innovation variances do not have similar values.

5.9 Accuracy of fault magnitude estimation via Lemma 4.1

Consider the accuracy of estimation from a single innovation. In Lemma 4.1 the fault magnitude ρ_i is estimated as the value that makes $\rho_i d_i$ the orthogonal projection of γ onto a vector aligned with d_i. The value of ρ obtained is clearly a least squares estimate (LSE).

The estimate ρ_i can also be viewed as the value which maximizes the probability density (4.64) of the innovation under the hypothesis that its mean $\underline{m}$ lies along d_i. The value obtained by this means is the Maximum Likelihood Estimate (MLE) and is clearly

the same as the LSE. This is only true because the innovation vector has a (multi)normal distribution.

The accuracy of the estimate is again affected by the transients associated with the post-fault innovation. Reference vector d_i is defined as the steady state bias superimposed on the no-fault innovations due to a unit step fault. Let the actual innovation bias due to a unit step fault be f_i, where f_i tends to d_i with each succeeding time step. If γ_o is the no-fault innovation then on the occurrence of a step fault of magnitude ρ_i^* the observed innovation is given by

$$\gamma = \rho_i^* f_i + \gamma_o \qquad \ldots \quad (5.61)$$

By Lemma 4.1 we estimate the fault magnitude as

$$\rho_i = \frac{\gamma^T d_i}{d_i^T d_i} \qquad \ldots \quad (5.62)$$

Hence
$$\rho_i - \rho_i^* = \frac{[\rho_i^* f_i + \gamma_o]^T d_i}{d_i^T d_i} - \rho_i^* \qquad \ldots \quad (5.63)$$

$$= \rho_i^* \left[\frac{f_i^T d_i}{d_i^T d_i} - 1 \right] + \frac{\gamma_o^T d_i}{d_i^T d_i} \qquad \ldots \quad (5.64)$$

Taking expectations and recalling that $E[\gamma_o] = \underline{0}$ we find that

$$E[\rho_i - \rho_i^*] = \rho_i^* \left[\frac{f_i^T d_i}{d_i^T d_i} - 1 \right] \qquad \ldots \quad (5.65)$$

Clearly the estimate is initially biased but the bias dies away to zero as the effect of the fault on the innovations becomes steady. The error variance is obtained from (5.64) and (5.65), recalling that $E[\overline{\gamma\gamma}^T] = V$

$$\text{var}\,[\rho_i - \rho_i^*] = \frac{d_i^T V d_i}{d_i^T d_i} \qquad \ldots \quad (5.66)$$

5.10 Summary

The main contribution of this chapter is the analysis of the Kalman filter to derive reference vectors for fault detection purposes. A scalar example was used to show how the effects of faults on the innovations could be amplified by the use of a suboptimal Kalman gain.

The degradation of filter performance with a suboptimal gain was examined and the possibility of divergence discussed. With the 'exact' model for the pilot plant unknown, true divergence cannot be ruled out but even if it could then this would not preclude apparent divergence. It was decided that the divergence problem could be studied only by simulation.

The problem of calculating incorrect decision probabilities was examined. It was shown that values could be obtained if the possible faults were completely specified but that explicit solutions could not be obtained for the LLR algorithm proposed in Chapter 4. Finally it was shown that the fault magnitude estimate furnished by Lemma 4.1 is asymptotically unbiased and an expression was derived for the error variance.

CHAPTER 6

IMPLEMENTATION OF FAULT DETECTION ALGORITHMS

6.0 Introduction

Two innovations-based algorithms, LLR and RCP, were proposed in Chapter 4. Each of these estimated a fault magnitude for every hypothesized failure direction but differed in the method used to process the current innovation vector to arrive at a final decision. In Chapter 5 the Kalman filter was analyzed to obtain expressions for the reference vectors required for the implementation of these algorithms on a real plant. It was also shown that algorithm sensitivity could possibly be improved by employing a suboptimal Kalman gain.

In this chapter these algorithms are implemented and tested by simulation with real data and their performance is compared with that of the simpler χ^2 test. Detection thresholds for the LLR algorithms are arrived at empirically due to the difficulties experienced in carrying out a full analysis for P_F and P_D. Also studied are the effects of various constant suboptimal gains on log-likelihood ratio levels during normal operation and on the distribution of the reference vectors in r-space. The remainder of the chapter is devoted to the presentation of results from numerous fault simulations. Attention is focussed on constant step type faults but examples of the other fault types given in Chapter 1 are included.

6.1 Experimental work for algorithm testing

To obtain data for fault simulation and testing of algorithms, two further pilot plant runs 'PLANT7' and 'PLANT8' were carried out. The plant was set up with control loops and proportional and integral control terms identical to those used for PLANT2 and PLANT3 (Section 2.2). The eleven process variables shown in Fig.2 were again recorded on paper tape at ten second intervals. There were, however, important differences between these runs,

carried out during July, and those of Chapter 2 which were completed during the preceding winter.

Reporting of apparent discrepancies in instrument readings, particularly temperature, pressure and flow measurements, is likely to be higher during the winter months when the plant is heavily used for undergraduate work. No such errors had come to light when data sets PLANT2 and PLANT3 were recorded, this being borne out by the satisfactory check heat balances on the exchangers.

While setting up the plant for the new runs the flow loop outputs were again carefully zeroed, i.e. the analog signals at the computer real time interface were checked under no-flow conditions. This is, however, no guarantee that the flow readings will not be biased due to small bubbles in the connecting pipes, and the amount of bias will almost certainly be different from that prevailing eight months previously. Temperature loops also have a tendency to drift, which may go unnoticed during the summer months when the few research students working on the plant are unlikely to be monitoring the many temperature variables required for this project.

The time of year was found to have a marked effect on plant temperatures in general, not so much due to the laboratory ambient temperature, which only varied by a few degrees, as to the cooling water temperature. The cooler inlet temperature (TX176), around 10°C in winter, was found to rise to 18-20°C in the summer months. This made for an increase of 15-20°C in some steady state temperatures, notably TX174, TX175 and TX177, between PLANT2 and PLANT7/8 under identical flow conditions.

It is normal practice when testing a new algorithm to carry out simulation work on 'ideal' data so that any changes to the data can be strictly controlled and their effects on the algorithm noted. Data sets PLANT7 and PLANT8 do not allow this luxury: the algorithms are faced with the stiffer test of being designed from one set of plant data and then being expected to work on the plant under different operating conditions with unknown

errors in the data. The new figures can at least be considered as typical of an industrial type plant and are certainly likely to show up any lack of robustness in the algorithms under test.

With the plant running in the steady state, the purpose of each run was to apply three separate changes in setpoint: MEA flow (FX101), cooler c/w flow (FX124) and absorber level (LX111).

6.1.1 Runs 'PLANT7' and 'PLANT8'

These are summarized in Tables 14 and 15 respectively. The layout and abbreviations are the same as for Table 3 (Chapter 2).

TABLE 14: PLANT7

Data Point	mins	Stripped MEA flow setpoint	Cooler c/w flow setpoint	Absorber level setpoint	Remarks
0	0	0.2 kgs^{-1}	0.2 kgs^{-1}	0.1m	Steady
290	48	↑ 0.25 kgs^{-1}			Step MEA
515	86		↑ 0.25 kgs^{-1}		Step c/w
540	90	Computer 'crashed' and was restarted			e-o-t
0	95	0.25 kgs^{-1}	0.25 kgs^{-1}	0.1m	new tape
43	102			↑ 0.15m	step level
94	111				e-o-t

TABLE 15: PLANT8

Data Point	mins	Stripped MEA flow setpoint	Cooler c/w flow setpoint	Absorber level setpoint	Remarks
0	0	0.22 kgs^{-1}	0.2 kgs^{-1}	0.12m	Steady
34	5	↑ 0.25 kgs^{-1}			Step MEA
192	32		↑ 0.25 kgs^{-1}		Step c/w
347	58			↑ 0.15m	Step level
479	80				e-o-t

The process variables of interest are summarized in Table 16 in which values quoted at a particular data point are averaged over the preceding five samples.

TABLE 16

PLANT'X':data pt	7:289	7:514	7:540	8:33	8:191	8:346
FX101 kgs^{-1}	0.2	0.25	0.25	0.22	0.25	0.25
FX124 kgs^{-1}	0.2	0.2	0.25	0.2	0.2	0.25
TX110 °C	29.7	31.9	30.2	35.4	36.1	32.4
TX172 °C	91.7	90.2	90.2	93.7	92.3	91.7
TX173 °C	104.8	104.0	104.1	104.1	103.6	103.5
TX174 °C	48.7	48.6	48.5	57.4	56.2	53.7
TX175 °C	37.08	35.66	35.58	47.76	45.70	42.35
TX176 °C	18.10	18.24	18.19	20.21	19.54	18.94
TX177 °C	38.65	40.30	37.36	46.02	46.05	40.66
Ambient °C	25.0	25.0	25.0	23.0	23.0	23.0

6.1.2 Discussion

Had it been possible to carry out a full false/miss alarm analysis for the LLR algorithm, alarm thresholds could have been calculated from the innovation statistics for all hypothesized failure directions to obtain reasonable values for P_F, P_M and P_X. These would have been based on the H_0 hypothesis that the innovations have zero mean.

In practice, instrument bias and linearization errors ensure that the innovation mean is never exactly zero even under normal running conditions. That the PLANT7 and PLANT8 data contains bias is apparent from a check heat balance on the cooler. For each set of figures given in Table 16 the heat gain by the cooling water is greater than the heat loss by the spent MEA.

It is likely that thresholds arrived at by a theoretical approach would actually make the algorithm oversensitive

in practice. With a ten second sampling rate, a false alarm probability as low as 0.1% still implies a false alarm once every three hours. On an industrial plant, a fault detection system generating false alarms any more often than, say, once a month (perhaps once every few months) would soon be distrusted by operating personnel. In the author's experience even a conventional annunciator will be ignored if the setpoints are such that the system alarms when operator intervention is not absolutely necessary. On this basis, suitable alarm thresholds for a real system should be obtained by prolonged monitoring of the innovations generated by filtering 'normal'data. It is better for the system to react reliably to faults of a significant size and to ignore very small faults rather than to alarm at the slightest disturbance.

For an installation such as the pilot plant which might be subjected to occasional small changes in setpoint, a detection algorithm should be able to cope without requiring major adjustment at every setpoint change. It was shown in Chapter 2 that Section A (Fig.A1.1) of this particular plant is not strongly nonlinear. An algorithm based on a filter designed for use at a particular operating point might therefore be expected to work at (flow) setpoints slightly above or below nominal. The accuracy of the model has a direct bearing on this. At a setpoint change, the eventual value of each state is governed by the partial derivatives of Chapter 3. If these are inaccurate or if the setpoint change is so large that the linearization is no longer valid then the innovations following the change will be biased and a fault may be registered. The time constants dictate only the trajectories of the states between initial and final values. Inaccuracies in these have an effect immediately after a setpoint change or input disturbance which could well result in a fault being declared during the transient following such a change. If, on the other hand, the alarm thresholds are set sufficiently high to suppress a false

alarm during the transient then the algorithm may be insensitive to faults occurring during periods of running in the steady state.

Alarm thresholds are covered in Section 6.5.3. PLANT7 and PLANT8 were designed to test the ability of algorithms to avoid giving false alarms during setpoint change transients and during steady state running away from the nominal operating point. The level setpoint changes were included to allow extension of the system to include Section B (Fig A1.1) but time did not permit this work to be carried out - see 'suggestions for further work'. It was decided that all the available plant data should be used to decide on alarm thresholds. Following analysis of the PLANT7 and PLANT8 data, thresholds could obviously be chosen so that algorithms using these data sets would never generate false alarms. This is a slight disadvantage in that no idea is gained of the false alarm probability that might be obtained in practice. This would require very much more recorded data than was actually obtained for use with this project.

6.2 Programs for Kalman filtering

Two identically structured programs, KALF07 and KALF08, were written to filter data from PLANT7 and PLANT8 respectively. KALF07 is described here along with programs PDERIV and FILCALC which are required for filter design (see also Section 4.6.2).

6.2.1 Program PDERIV

PDERIV is written around the results of Chapter 3. The program accepts steady state values of inputs FX101, FX124, TX173, TX174, TX175 and TX176 and generates partial derivatives for each output with respect to the relevant flow and temperature inputs. A typical printout from PDERIV for data set PLANT7 is given overleaf. Note that 'D' $\equiv \partial$, 'FT' $\equiv \tilde{F}_1$ and 'TC1(0)' $\equiv T_{C1}(0)$ etc.

STABLE OPERATING POINT/LINEARIZATION POINT:

MONOETHANOLAMINE FLOW F1 = 0.200 KG/S
COOLING WATER FLOW F2 = 0.200 KG/S
COOLER INPUTS TC1(0) = 49.6 TC2(L) = 17.75 DEG.C
HEAT EXCHANGER INPUTS TX1(0) = 103.8 TX2(L) = 38.40 DEG.C

GRADIENT MATRIX:

DTC1(L)/DF1	DTC1(L)/DF2	DTC2(0)/DF1	DTC2(0)/DF2
DTC1(L)/DTC1(0)	DTC1(L)/DTC2(L)	DTC2(0)/DTC1(0)	DTC2(0)/DTC2(L)
DTX1(L)/DF1	DTX1(L)/DFT	DTX2(0)/DF1	DTX2(0)/DFT
DTX1(L)/DTX1(0)	DTX1(L)/DTX2(L)	DTX2(0)/DTX1(0)	DTX2(0)/DTX2(L)
62.267	-34.868	36.499	-62.988
.372	.628	.607	.393
142.198	-125.367	132.794	-149.436
.154	.846	.836	.164

6.2.2 Program FILCALC

FILCALC uses the output from PDERIV and Figs 18 and 19 to calculate Φ and G. From a user supplied P(0|0) it then cycles through filter steps (1, 3-5 and 8; Section 4.4) until a steady state Kalman gain is reached for the system $\{\Phi, G, H, Q, R, S\}$. FILCALC can also be used to produce a suboptimal steady state gain by manipulation of the noise covariance matrices.

6.2.3 Program KALF07 (and KALF08)

KALF07 was written to accept two input data files, PLANT7 and KGAIN. File KGAIN contains a constant Kalman gain which has either been generated by FILCALC or has been specified for fault detection purposes by some other means. Having processed PLANT7 using KGAIN, KALF07 outputs data files RESLT1 (state estimates) and RESLT2 (innovations). The program structure is as follows:-

(a) Set the operating/linearization point (i.e. set the temperatures and flows to their actual values at the start of PLANT7).
(b) Set the partial derivatives (obtained from PDERIV).

(c) Set time constants τ_1 - τ_6 (Section 3.6).
(d) Calculate Φ and G from Figs 18 and 19 respectively.
(e) Read plant data from PLANT7.
(f) Linearize data by subtracting the values (a) for all data points.
(g) Read Kalman gain from KGAIN .
(h) Filter data with $\hat{x}(0|0) = \underline{0}$
(i) Write data to files RESLT1 and RESLT2.

6.3 Reference vectors for LLR and RCP algorithms

The effects of a fault on the innovation vector were analyzed in Chapter 5 to obtain bias matrices $B_y(\gamma;j)$ and $B_u(\gamma;j)$. It was shown that these could be simplified to obtain 'settled out' matrices $B_y(\gamma)$ and $B_u(\gamma)$.

6.3.1 Matrix FMAT

In Section 5.5 it was decided that the settled out reference vectors should be used for fault detection purposes. The bias matrix is defined such that for a step fault $\underline{b}$ the actual innovation bias β_γ is given by

$$\beta_\gamma = B_y(\gamma)\underline{b} \text{ for output step fault '}\underline{b}\text{'} \quad \ldots \quad (6.1a)$$

$$= B_u(\gamma)\underline{b} \text{ for input step fault '}\underline{b}\text{'} \quad \ldots \quad (6.1b)$$

The reference vector d_i for fault direction 'i' was defined in Section 4.9 as the bias vector resulting from a positive step fault of unit magnitude in direction 'i'.

Referring back to Section 4.3, nine failure directions are defined. For output faults $\underline{y}_f(1)$ to $\underline{y}_f(4)$ a step fault of unit magnitude is given by setting π_i, i = 1,...4 to '1' from the 'fault time' θ onwards in equations (4.17a-d). Similarly, for input faults $\underline{u}_f(1)$ - $\underline{u}_f(3)$, υ_j, j= 1,...3 is set to '1' in equations (4.20 - 4.22). In the case of the remaining two output faults $\underline{y}_f(5)$ and $\underline{y}_f(6)$ the flow steps ΔF_1 and ΔF_2 must be set to '1' in equations (4.18) and (4.19) respectively.

Failure directions d_i, i = 1,...9 can now be defined as $\underline{y}_f(1) - \underline{y}_f(6)$, $\underline{u}_f(1) - \underline{u}_f(3)$. We now construct a (4 x 9) matrix FMAT whose columns are the reference vectors obtained from unit step faults as described in the preceding paragraph, i.e.

$$\text{FMAT} = \left[B_y(\Upsilon)\left[\tilde{\underline{y}}_f(1) \ \ldots \ \tilde{\underline{y}}_f(6)\right] \,\middle|\, B_u(\Upsilon)\left[\tilde{\underline{u}}_f(1) \ \ldots \ \tilde{u}_f(3)\right]\right] \quad \ldots \quad (6.2)$$

where the addition of a '~' as in '$\tilde{\underline{y}}_f(1)$' implies a step fault of unit magnitude.

Since $\tilde{\underline{y}}_f(1) - \tilde{\underline{y}}_f(4)$ pick out the four columns of (4 x 4) matrix $B_y(\Upsilon)$ and $\tilde{\underline{u}}_f(1) - \tilde{u}_f(3)$ the 4th, 5th and 6th columns of (4 x 8) matrix $B_u(\Upsilon)$ we can write

$$\text{FMAT} = \left[B_y(\Upsilon) \,\middle|\, B_y(\Upsilon)\left[\tilde{\underline{y}}_f(5), \tilde{\underline{y}}_f(6)\right] \,\middle|\, \text{cols 4,5,6 of } B_u(\Upsilon)\right] \quad \ldots \quad (6.3)$$

6.3.2 Reference vector magnitude

It was shown in Section 5.4.2 that a Kalman gain corresponding to a Q that is set artificially low relative to R could amplify the effect of a step bias on the innovations. This approach is a first step towards choosing a constant suboptimal gain specifically for fault detection purposes.

Experiments were carried out using as a basis for PDERIV variables corresponding to the steady state operating point at the beginning of run PLANT2. Three sets of covariance matrices were used with FILCALC, which was run until a steady Kalman gain was obtained for each set. A new program, BIASCL1, was written to calculate matrix FMAT from equations (5.31), (5.47) and (6.3).

Q, R and S were varied as follows:

Set I: Q, R and S specified as in (4.45), (4.43) and (4.44) respectively. These were the original 'guesstimates' for the plant noise levels and will henceforth be referred to as 'ONA' ('original noise assumptions'). As shown in Section 4.7 the predicted and actual innovation statistics obtained by using ONA covariances were of the same order. The gain computed from this Q, R and S is probably sufficiently close to the optimal value to be used as a benchmark for comparison with algorithms based on suboptimal gains.

Sets II and III:

S = 0. The only reasoning behind this is that it simplifies the structure of the resulting steady state Kalman gain. It is well known that if both Q and R are of the form qI and rI (q, r scalars) then the Kalman gain obtained depends only on the q/r ratio. Two different ratios were tried, each with $q \ll r$.

Set II: q/r = 0.01, generating gain 'KGAINY'.

Set III: q/r = 0.001, generating gain 'KGAINZ'.

The s/s gain KGAINX corresponding to ONA was given in Fig 20, while that for Set II is given below

$$\text{KGAINY} = \begin{bmatrix} 0.023 & 0.001 & 0.002 & \\ 0.001 & 0.027 & 0.002 & \\ 0.002 & 0.001 & 0.004 & \\ 0.002 & 0.002 & 0.028 & \\ & & & 0.001 \\ & & & 0.047 \end{bmatrix}$$

An identifier is added to FMAT to indicate the gain and setpoint used for calculation:

FMATX = gain KGAINX (~ ONA) with PLANT2 data
FMATY2 = gain KGAINY (~ Set II) with PLANT2 data

FMATX

$$\begin{bmatrix} 0.229 & -0.017 & -0.030 & -0.000 & -9.898 & 3.637 & -0.010 & -0.048 & -0.127 \\ -0.025 & 0.200 & -0.025 & -0.000 & -4.826 & 7.322 & -0.009 & -0.045 & -0.072 \\ -0.063 & -0.036 & 0.171 & -0.000 & 0.172 & -2.586 & -0.022 & -0.107 & 0.053 \\ 0.000 & -0.000 & -0.000 & 0.088 & 2.087 & -0.000 & -0.072 & -0.016 & 0.000 \end{bmatrix}$$

FMATY2

$$\begin{bmatrix} 0.932 & -0.003 & -0.007 & 0 & -45.187 & 17.376 & -0.064 & -0.314 & -0.545 \\ -0.003 & 0.902 & -0.007 & 0 & -29.529 & 35.053 & -0.066 & -0.327 & -0.389 \\ -0.007 & -0.007 & 0.905 & 0 & -21.118 & -0.394 & -0.152 & -0.748 & 0.007 \\ 0 & 0 & 0 & 0.692 & 16.392 & 0 & -0.569 & -0.123 & 0 \end{bmatrix}$$

As expected the magnitude of d_i, $i = 1,...9$ is higher for FMAT generated from KGAINY than from KGAINX. The degree of 'amplification' can indeed be calculated by comparing the magnitudes of the d_i's for the three gains for each 'i' value (Table 17).

TABLE 17

i	$\lvert d_i \rvert$ (KGAINX)	$\lvert d_i \rvert$ (KGAINY)	$\frac{\lvert d_i \rvert \text{KGAINY}}{\lvert d_i \rvert \text{KGAINX}}$	$\lvert d_i \rvert$ KGAINZ	$\frac{\lvert d_i \rvert \text{KGAINZ}}{\lvert d_i \rvert \text{KGAINX}}$	% inc. KGAINZ/Y
1	0.239	0.932	3.90	0.992	4.15	6.4
2	0.204	0.902	4.42	0.988	4.84	9.5
3	0.175	0.905	5.17	0.988	5.65	9.3
4	0.088	0.692	7.86	0.916	10.41	32.4
5	11.209	60.237	5.37	66.535	5.94	10.6
6	8.575	39.125	4.56	42.691	4.98	9.2
7	0.076	0.596	7.84	0.778	10.24	30.6
8	0.127	0.883	6.95	0.974	7.67	10.4
9	0.155	0.670	4.32	0.721	4.65	7.6

6.3.3 Reference vector separation in r-space

That reference vectors with a small angle between them can cause resolution problems was mentioned in Section 5.6. The amplification produced by using a gain corresponding to a low q/r ratio will not be of much use if it has the effect of moving any of the reference vectors significantly closer together in r-space.

Program BIASCL1 was extended to calculate the angles between all the reference vectors in FDIREC. Defining θ_{ij} as the angle between d_i and d_j we have

$$\theta_{ij} = \cos^{-1}\left[\frac{d_i^T d_j}{|d_i||d_j|}\right] \qquad \ldots \quad (6.4)$$

BIASCL1 produced results as follows:

ANGLES BETWEEN FAULT DIRECTION VECTORS (DEGREES)

KGAINX

i	9	8	7	6	5	4	3	2
1	34.3	84.2	88.1	66.5	36.2	90.0	66.0	82.3
2	63.4	80.4	86.8	31.2	69.4	90.0	72.7	
3	57.6	44.7	76.2	60.8	76.9	90.0		
4	90.0	82.9	19.4	90.0	79.3			
5	21.9	63.3	89.0	41.7				
6	32.2	78.0	86.0					
7	86.4	63.5						
8	79.2							

KGAINY

i	9	8	7	6	5	4	3	2
1	35.7	69.6	84.0	63.8	41.8	90.0	89.1	89.6
2	54.7	68.7	83.7	26.5	61.0	90.0	89.1	
3	88.8	32.7	75.3	88.8	70.1	90.0		
4	90.0	82.0	17.4	90.0	74.2			
5	26.9	45.0	88.0	39.8				
6	28.1	61.2	81.7					
7	81.4	64.6						
8	60.3							

KGAINZ

i	9	8	7	6	5	4	3	2
1	36.4	69.6	84.9	64.2	43.5	90.0	89.9	89.9
2	53.7	68.1	84.6	25.8	60.7	90.0	89.8	
3	89.8	32.7	77.6	89.8	69.3	90.0		
4	90.0	80.4	14.5	90.0	71.0			
5	28.9	47.1	82.6	40.8				
6	27.9	60.8	82.9					
7	82.7	65.8						
8	59.9							

The ideal distribution would be for all vectors d_i to be orthogonal but clearly this is not possible with nine reference vectors in 4-space and the best that can be hoped for is an 'even' distribution. Directional pairs (5,9), (6,9), (2,6) and especially (4,7) give the greatest cause for concern with KGAINX. Reducing the q/r ratio improves the first of these but reduces the other three, although not dramatically. A lower q/r ratio does improve the angles between pairs (3,9), (3,6) and (1,3).

6.3.4 Discussion

Although the angle tables give an idea of the faults that are likely to be difficult to distinguish, the actual angle below which resolution is unlikely is related to the distribution of the innovations under no-fault conditions, i.e. to the innovation covariance. Further, the use of a low q/r ratio to amplify the effect of a fault on the innovations ('signal') also has the effect of increasing the innovation covariance ('noise'). The alarm thresholds will have to be increased, and if the effective signal to noise ratio is not actually improved then there is no advantage in using KGAINY or KGAINZ. The optimum gain for fault detection purposes can be determined only by simulation.

6.4 The innovation covariance

Both the LLR algorithm, summarized by expression (4.65) and the RCP algorithm (4.67) require the innovation covariance matrix V. Innovation statistics for the three constant gains of Section 6.3.2 were estimated from innovations generated by KALF02 from PLANT2 data, this set being the only one available containing sufficient steady state data points to give reasonable estimates for V.

It has already been suggested (6.3.2) that the ONA filter is fairly close to the optimal. FILCALC was used to generate the theoretical steady state innovation covariance for comparison with the actual value. Results were obtained as follows:

Theoretical V for KGAINX at PLANT2 operating point

$$V = \begin{bmatrix} 0.0045 & 0.0007 & 0.0008 & 0.0000 \\ 0.0007 & 0.0039 & 0.0006 & 0.0000 \\ 0.0008 & 0.0006 & 0.0046 & 0.0000 \\ 0.0000 & 0.0000 & 0.0000 & 0.0040 \end{bmatrix}$$

Actual V for KGAINX/PLANT2 data

$$VX = \begin{bmatrix} 0.0036 & 0.0015 & 0.0012 & 0.0003 \\ 0.0015 & 0.0016 & 0.0009 & 0.0003 \\ 0.0012 & 0.0009 & 0.0032 & 0.0017 \\ 0.0003 & 0.0003 & 0.0017 & 0.0045 \end{bmatrix}$$

Actual V for KGAINY/PLANT2 data

$$VY = \begin{bmatrix} 0.0086 & 0.0058 & 0.0071 & 0.0039 \\ 0.0058 & 0.0055 & 0.0061 & 0.0037 \\ 0.0071 & 0.0061 & 0.0126 & 0.0082 \\ 0.0039 & 0.0037 & 0.0082 & 0.0109 \end{bmatrix}$$

Actual V for KGAINZ/PLANT2 data

$$VZ = \begin{bmatrix} 0.0090 & 0.0062 & 0.0075 & 0.0041 \\ 0.0062 & 0.0058 & 0.0065 & 0.0040 \\ 0.0075 & 0.0065 & 0.0133 & 0.0087 \\ 0.0041 & 0.0040 & 0.0087 & 0.0117 \end{bmatrix}$$

Note that as in Section 6.3 there is very little difference between results using KGAINY and results using KGAINZ. Note also that while filtering PLANT2 data hardly constitutes the 'extensive and prolonged simulation' prescribed in Section 5.7.2, no tendency for the filter to diverge was noted even when using the very low q/r gain KGAINZ.

6.5 LLR algorithm design

We are now in a position to finalise design parameters for an algorithm based on the LLR test. As discussed in Section 6.1.2 these parameters were obtained by using all the available plant

data, the PLANT8 record being cut short at data point 346 to exclude the unmodelled level setpoint change.

The three programs KALF02, 07 and 08 were used to generate innovations from PLANT2, 7 and 8 respectively for analysis. Each run requires three input matrices: the constant Kalman gain, the fault direction matrix FMAT and the innovation covariance.

TABLE 18

Data set:	PLANT2	PLANT7	PLANT8
Noise: ONA Reference directions Innovation covariance	KGAINX FMATX VX	KGAINX7 FMATX7 VX	KGAINX8 FMATX8 VX
Noise: Set II Reference directions Innovation covariance	KGAINY FMATY2 VY	KGAINY FMATY7 VY	KGAINY FMATY8 VY
Noise: Set III Reference directions Innovation covariance	KGAINZ FMATZ2 VZ	KGAINZ FMATZ7 VZ	KGAINZ FMATZ8 VZ

Kalman gain

This is calculated from FILCALC and requires the operating point (linearization point) for the plant data set in question in order to obtain derivatives from PDERIV. Under ONA the gains were calculated individually for each plant run but under Sets II and III the gains were found to vary little with change in setpoint and KGAINY and KGAINZ (PLANT2 setpoint) were used throughout.

Matrix FMAT

Reference vectors were calculated individually for each of the nine combinations of gain and plant operating point.

Innovation covariances

The 'actual' covariances estimated from PLANT2 data were used throughout.

Nine runs were carried out using the plant data and input

matrices as defined in Table 18. For the first run KALF02 was set up to filter the PLANT2 data using gain KGAINX. The innovations were then analyzed using a second program, INVEC, which utilized KGAINX, FMATX and VX to calculate the minimum angle (Section 5.8.5) and maximum llr for each innovation generated by KALF02. The remaining eight runs were carried out in a similar fashion as per Table 18.

6.5.1 A note on divergence

In the course of these experiments the low q/r gain KGAINZ was used with PLANT7 and PLANT8 data. Even after a setpoint change with the filter working away from its design operating point, there was absolutely no tendency for the filter to diverge. While this is not conclusive evidence the indications are that in this particular case it is safe to use the suboptimal gains suggested.

6.5.2 Maximum llr versus minimum angle

INVEC was used to test in practice the frequency of occurrence of the situation discussed in Section 5.8.5. The program was used to count the number of times that for a given innovation the failure direction giving rise to the maximum llr was not the same direction as that lying closest in 4-space to the innovation vector under test. The number of these 'mismatches', given in Table 19 where NDP is the total number of data points, is rather higher than might be expected. This is due to the asymmetry of the innovation distribution (variation in diagonal terms of VX, VY, VZ) and underlines the comments made in Section 5.8.5 regarding purely geometric interpretation of results.

TABLE 19

Data set (NDP)	PLANT2 (913)	PLANT7 (540)	PLANT8 (346)
Noise: ONA	278 (30%)	148 (27%)	50 (14%)
Noise: Set II	278 (30%)	123 (23%)	19 (6%)
Noise: Set III	274 (30%)	134 (25%)	19 (6%)

6.5.3 LLR test thresholds

As discussed in Section 6.1.2 the alarm thresholds are the most critical design parameters for the LLR algorithm. The most important point to be established is whether the llr's increase during transients due to poor modelling. If this is the case then it might pay to 'switch off' the detector for a while following an intentional setpoint change.

The data from the nine runs of Table 18 was used to obtain a set of thresholds corresponding to each of the three sets of noise assumptions (Section 6.3.2). In each of Tables 20-22, column A gives for each of the nine hypothesized failure directions the data set, data point and value of the maximum llr. An asterisk indicates that the value was recorded during a transient (defined as the first four minutes after a setpoint change). If the value in the first column occurred during a transient then the second column gives the highest llr not during a transient. Should the value in column A be from PLANT2 (no transients) then column B gives the highest llr from PLANT7 or 8 whether during a transient or not. Column C gives the highest llr from PLANT2 if not already recorded in column A.

From the tables it is apparent that the maximum llr values for no more than half of the failure directions occur during transients. What is also apparent is that with the exception of Table 20 directions 4 and 7, none of the maximum llr's occur in PLANT2 or prior to the first setpoint change in either PLANT7 or PLANT8. This implies that inaccuracy of the model and/or system nonlinearity have a marked effect on llr's occurring under no-fault conditions when working away from the design operating point.

Clearly, from the values given in Column C of Tables 21 and 22, an LLR algorithm designed to work at a single operating point could utilize lower llr thresholds and

TABLE 20 - Noise: ONA

Fault	Column A			Column B			Column C	
1	8-209	*	54.6	7-450		52.9	2-149	16.7
2	7-296	*	50.9	7-465		47.7	2-701	15.5
3	7-494		57.8				2-105	18.3
4	2-276		53.2	8-134		30.9		
5	7-453		39.1				2-606	21.0
6	7-294	*	35.2	8-342		26.0	2-400	16.8
7	2-277		39.4	8-181		26.2		
8	7-412		35.3				2-861	16.8
9	7-494		49.6				2-606	21.3

TABLE 21 - Noise: Set II

Fault	Column A			Column B			Column C	
1	7-527	*	372.8	8-72		201.7	2-826	21.8
2	7-297	*	260.3	8-67		89.1	2-830	52.0
3	7-511		180.2				2-105	37.6
4	7-304	*	160.0	8-290		38.9	2-276	30.5
5	7-377		125.0				2-276	25.1
6	7-296	*	160.8	8-344		131.5	2-830	58.1
7	7-304	*	107.8	8-290		31.9	2-276	24.5
8	7-413		109.1				2-600	20.6
9	7-347		176.5				2-607	41.1

TABLE 22 - Noise: Set III

Fault	Column A			Column B			Column C	
1	7-308	*	405.3	8-72		218.2	2-826	23.4
2	7-297	*	267.9	8-67		99.3	2-830	57.6
3	7-511		194.1				2-106	41.1
4	7-304	*	192.9	8-290		41.0	2-276	25.0
5	7-377		123.5				2-276	26.4
6	7-296	*	164.6	8-344		148.9	2-830	63.0
7	7-304	*	142.7	8-290		35.5	2-276	21.4
8	7-413		115.5				2-600	21.5
9	7-347		187.7				2-607	45.0

would be more sensitive. The price of making the algorithm oblivious to small setpoint changes is to make it less sensitive to small faults.

As was found in Sections 6.3.3 and 6.4 there is little difference between the results of Table 21 (KGAINY) and Table 22 (KGAINZ). The maximum llr's almost all occur at the same points in the data records. The amount of work necessary to run a simulation example will be apparent from Section 6.8 and it was decided at this juncture that rather than running each example with KGAINY and KGAINZ it was better to concentrate on one of these and to run more examples. KGAINY was selected because, despite the comments in Section 6.5.1, the q/r ratio is lower for KGAINZ and, of the two, this is the more likely to lead ultimately to divergence.

Alarm thresholds were selected for ONA and Set II by raising the maximum llr (Column A Tables 20,21) by about 20% in each case. Values are given in Table 23. The thresholds are different for each direction because of bias in the innovations due to instrument bias, inaccuracy of the model and system nonlinearity

TABLE 23 - ALARM THRESHOLDS

Fault	Noise:ONA	Noise:Set II	Fault	Noise:ONA	Noise:Set II
1	66	450	6	42	193
2	61	312	7	47	130
3	70	216	8	43	131
4	64	192	9	60	212
5	47	150			

6.5.4 Reduction of P_U

As discussed in Section 5.8.1, if a particular innovation generates an llr that is significant ($\ell n \Lambda(\gamma) > \eta$) for more than one failure direction then the algorithm arrives at a 'non-definite' decision with probability P_U. This probability can be reduced by

comparing the llr's obtained for the different H_0-significant directions.

In this case the following intuitive argument is proposed. Faults H_1 and H_2 have thresholds η_1 and η_2 respectively. At a particular innovation we have $[\ell n\Lambda(\gamma)]_1 > \eta_1$ but also $[\ell n\Lambda(\gamma)]_2 > \eta_2$. Suppose $[\ell n\Lambda(\gamma)]_1 > [\ell n\Lambda(\gamma)]_2$:

If $[\ell n\Lambda(\gamma)]_1 - [\ell n\Lambda(\gamma)]_2 > \eta_1$ declare H_1 true
If $[\ell n\Lambda(\gamma)]_1 - [\ell n\Lambda(\gamma)]_2 \leq \eta_1$ declare 'uncertain'

The reasoning for this is that to be 'definite' a fault should be at least as significant over other H_0-significant directions as it is itself over the H_0 hypothesis. The feasibility of this in practice was tested by simulation rather than by repeating the analysis of Section 6.5.3.

6.5.5 Program LOGLRAT

The above named fault detection program was written to implement the LLR algorithm. For each time step there are five possible outcomes which are printed out as follows for data point 271:

DPT	LLR	S	SIG DIRECTIONS VS H(0)			D	QL	FLTEST	FLT/ALT
Definitely no fault									
271	32	N				0		(1 MAX)	
Probably a fault									
271	65	N	9.1			0	PR		PS 9
Definite fault (no alternatives)									
271	107	Y				3		1.217	16.8
Definite fault (alternatives not significant)									
271	98	Y	3.0	4.0		3		1.172	31.2
Non-definite decision (alternatives are significant)									
271	82	Y	9.1	8.1	2.0	3	PR	(.977)	PS 9,8

To save time and paper the program prints out detection decisions only in the region of interest - just before and just after the simulated fault. The second column contains the maximum log-likelihood ratio (MAXL, in

direction JPOS) over all nine reference directions. Whether or not it exceeds the threshold versus H_0 for direction JPOS is indicated by Y or N (YES or NO) in col. 3. If NO then JPOS is set to zero. The fourth section indicates the other failure directions (if any) for which the llr exceeds the corresponding threshold. To reduce the probability of uncertainty these llr's are compared with MAXL as in Section 6.5.4. These other H_0-significant directions are listed in descending order of llr magnitude from a vector in which '.0' is added to those directions which are not significant against MAXL and '.1' to those which are. Column 'D' is the decision JPOS, i.e. '0' = no fault,'3' = fault in direction 3. QL is a qualifier: if left blank then 'D' is a definite decision but if MAXL is not significant against all other H_0-significant directions (i.e. some other direction(s) followed by '.1' in col.4) then the decision under D is only 'probable', hence 'PR' in column QL. Column FLTEST gives the estimated magnitude of the fault in direction JPOS via Lemma 4.1 - in brackets if QL = PR. If JPOS = 0 then this column gives in brackets the direction having the maximum llr versus H_0. For a definite non-zero fault the final column FLT/ALT gives the angle in degrees between the current innovation and the reference vector for direction JPOS. For 'probable' faults this column contains the other 'possible' directions, i.e. those followed by a '.1' in col.4,in decreasing order of llr magnitude. The program also counts the total number of definite and probable decisions for each failure direction.

6.6 The RCP algorithm

A program named HYPOVEC was written to implement the RCP algorithm proposed in Section 4.9.4 and also as subsequently modified in Section 4.10.4. Several experiments were carried out using innovations generated by KALF02 from PLANT2 data and constant (ONA) gain KGAINX. Table 24 shows that the probabilities $P(H_i|k\text{-}1)$ were reset to their a priori values every W time steps, and gives the percentages of correct (H_0) and incorrect (H_i, i = 1,...9) decisions over 913 innovations.

From the table it is clear that the algorithm is totally unsuitable for the application due to the unacceptably high P_F. As an experiment the innovations from KALF02 were demeaned to see if this made any difference. For W = 2 and $P(H_0) = 0.91$ the probability of a false alarm was reduced only to 11.8%. This method of fault detection was pursued no further.

TABLE 24

A priori probabilities		reset every(W)	Decisions as percentage	
$P(H_0)$	$P(H_i)$,i=1,...9		H_0	H_i,i=1,...9
0.91	0.01	5	15.5	84.5
0.91	0.01	4	28.6	71.4
0.91	0.01	3	45.3	54.7
0.91	0.01	2	67.0	33.0
0.991	0.001	2	90.0	10.0
0.91	0.01	1	88.0	12.0
0.991	0.001	1	97.2	2.8
0.9955	0.0005	1	97.9	2.1

6.7 The χ^2 test

The LLR algorithm requires very much more computation than the χ^2 test and should reflect this with a marked improvement in performance. To check on this simulations were carried out using the modified χ^2 test of equation (4.61), with separate χ^2 random variables generated from each of the four components of the innovation vector.

In [44], [45] Willsky, Deyst and Crawford utilized a window length (N) of 3 and an alarm threshold (ε) of 10.5. From tables for the χ^2 distribution this corresponds to $P_F \sim 0.015$. These parameters were used in program CHISQUA, initially written to analyze innovations generated by KALF02 from PLANT2 data and constant (ONA) gain KGAINX.

Using as v_{ii}, i = 1,...4 the diagonal terms from VX (Section 6.4), the number of times $\ell_i(k)$ exceeded 10.5 is given in Table 25. For innovation component 4 this threshold was exceeded in 6% of cases, rather more than the expected 1.5%. Recall from Fig 21,

however, that component 4 had the worst approximation to a Gaussian distribution and that, with a window of three, a 'large' innovation affects the χ^2 r.v. for three time steps running. In order to de-sensitize the χ^2 test, as for LLR in Section 6.5.3, either the thresholds have to be increased or the variances can be increased to keep all four thresholds at 10.5. Selecting the latter method, the fictitious variances required to give no false alarms with the PLANT2 data are given in the last column of Table 25.

TABLE 25

i	v_{ii}	max $\ell_i(k)$	$\ell_i(k) > 10.5$	var.for no alarms
1	0.0035	18.06	7 (0.75%)	0.0065
2	0.0016	28.18	4 (0.44%)	0.0045
3	0.0032	19.90	13 (1.42%)	0.0065
4	0.0045	23.11	56 (6.13%)	0.01

Program CHISQUA was then tried with innovations from KALF07 (with PLANT7 data and ONA gain KGAINX7) and from KALF08 (PLANT8, KGAINX8). The values obtained for $\ell_i(k)$ were found to be larger than those from the PLANT2 data, particularly following the first setpoint change in each data set. This is primarily due to the fact that the innovation mean, although near zero, is never exactly so and changes with change in operating point because of instrument bias and system nonlinearity . As with the llr thresholds it was found necessary to increase the variances still further to prevent false alarms when monitoring innovations from PLANT7 and 8. Again using all the available data the parameters finally selected for the χ^2 test were as follows:

ε_i, i = 1,...4 = 10.5 N = 3

v_{ii}, i = 1,...4 = 0.0204, 0.0126, 0.0152, 0.0130

6.8 Fault simulation

Faults $\underline{y}_f(1)$ - $\underline{y}_f(4)$ and $\underline{u}_f(1)$ - $\underline{u}_f(3)$, defined in Section 4.3, have no effect on system operation and can therefore be simulated at will for any of the four fault types (a) - (d) in Fig 1. An 'ideal' step fault of +2°C on say TX110 between

PLANT7 data points 346 and 347 is simulated by adding 2.0 to every TX110 reading for $k \geq 347$ in the PLANT7 record before the data is processed by KALF07.

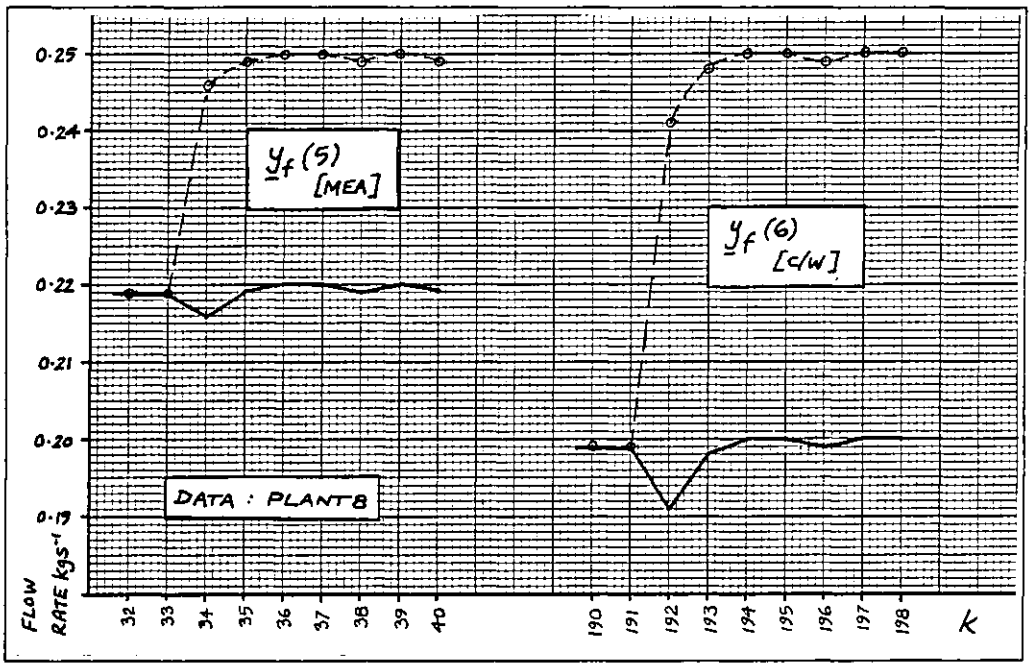

Fig.26 Effective flow signals following a step fault

Faults $y_f(5)$ and $\underline{y}_f(6)$ are flow faults and cause changes in setpoint. These are simulated by changing the setpoint in the opposite sense to the fault required (see 4.3.2) and then subtracting the setpoint change from the flow readings. This is illustrated by Fig 26 where the MEA flow setpoint is increased by 0.03 kgs^{-1} immediately following $k = 33$ thus simulating a step fault of -0.03 kgs^{-1} at $33 < k \leq 34$. If the setpoint change were caused by a step fault then the flow reading seen by the control system would be as shown by the solid lines in Fig 26. Equations (4.18) and (4.19) neglect the small 'kick' in the flow reading and assume that the affected temperatures reach their steady state values instantaneously. The analysis of Chapter 5 also assumes 'ideal' step faults whereas in reality these temperatures undergo a transient as described in Chapter 3.

The aim of the simulations was to compare the performances of three algorithms

(a) The χ^2 test
(b) LLR algorithm with ONA gain
(c) LLR algorithm with Set II gain

The steps required for every example were as follows. These are given for a fault on PLANT7 but the method is the same for any plant record. Detection decisions were printed out only in the region of the fault, but the total numbers of decisions were recorded by type.

(i) Edit KALFO7 to read in PLANT7 and then to modify the data to simulate the required fault as already described.
(ii) Run KALFO7 with gain KGAINX7 and store innovation file.
(iii) Set up CHISQUA with the parameters given at the end of Section 6.7 and run with the innovations from step (ii).
(iv) Set up LOGLRAT with FMATX7, VX and the thresholds in the 'ONA' columns of Table 23. Run with the innovations from step (ii).
(v) Re-run KALFO7 with the same fault but now with gain KGAINY7. Store innovation file.
(vi) Set up LOGLRAT with FMATY7, VY and the thresholds in the 'Set II' columns of Table 23. Re-run with the innovations from step (v).

6.9 Simulation examples

A comprehensive simulation programme was carried out on the data from PLANT7 and PLANT8. PLANT2 was not used for fault simulation because this would not have tested the algorithms away from the nominal plant operating point. Attention was concentrated on step faults with fifty faults simulated. To this were added nine jump faults, four 'break in rtd lead' faults and three ramps making a total of sixty-six examples. Some step faults were investigated for KGAINY only and KALFO7 and KALFO8 were run 129 times in all.

TABLE 26

i	Fault	Instrument	i	Fault	Instrument
1	$\underline{y}_f(1)$	TX110	6	$\underline{y}_f(6)$	FX124
2	$\underline{y}_f(2)$	TX177	7	$\underline{u}_f(4)$	TX173
3	$\underline{y}_f(3)$	TX174	8	$\underline{u}_f(5)$	TX175
4	$\underline{y}_f(4)$	TX172	9	$\underline{u}_f(6)$	TX176
5	$\underline{y}_f(5)$	FX101			

Step faults in directions 5 and 6 (Table 26) were limited to the four setpoint changes in PLANT7 and PLANT8. Faults in directions 1-4 and 7-9 were then investigated during a transient by injecting steps of +1° and +2° for each at data point 294 in PLANT7. Small faults (down to 0.25°) were investigated for one input (9) and one output (3) at PLANT7 data point 490 (steady state). A number of random step faults was obtained for PLANT8 by using NAG routine G05DAF to generate random data points between 5 and 336, random directions 1-9 (excluding 5 and 6) and random magnitude between 0.5 and 5.0. These were then signed alternately positive and negative and the first 'small' fault (magnitude < 1.5°) and the first 'large' fault (magnitude > 3.0°) were selected for each failure direction.

Jump faults were simulated for directions 1-4 and 7-9 using the random 'large' faults already used as step faults. Two experiments were tried with jump faults on different instruments at successive data points. The detection of breaks in rtd leads was investigated for one output (3) and all three inputs (7-9). Finally, ramps of +0.3 deg.C/min (i.e. +0.05 deg.C per data point) were tried for directions 1, 8 and 9 to determine the fault level at which each algorithm would correctly diagnose the fault.

Presentation of results

For step faults in each failure direction the first task is to compare the detection capabilities of the LLR algorithms with that of the χ^2 test. Selected results are presented in tabular form, where $\ell_i(k)$, $i = 1,\ldots 4$ are the χ^2 r.v's generated from

the four components of the innovation vector. For the χ^2 test:

$$'1' \Rightarrow \ell_i(k) > 10.5$$

$$'0' \Rightarrow \ell_i(k) \leq 10.5$$

while for the LLR variants the figure given is the failure direction 'j', j = 1,...9, as decided by each algorithm. If the direction given is 'probable' (see Section 6.5.5) then the number is shown primed, e.g. 5'. Each fault is described as, for example:

+1° fault at dp 294 (PLANT7 - 247 dp to eor)

This gives the fault magnitude and the first data point for which the instrument becomes faulty. The note in brackets gives the data set on which the fault was superimposed and the number of data points containing the fault that occur up to the end of the data set (eor = end of record). By adding up the non-zero decisions given under 'TOTALS' in each table it can be seen whether the fault had a continuous effect on the innovations right up to the end of the data set or whether the effect was short lived or intermittent. Totals 4(58)4'(3) signify that the algorithm recorded a definite "Direction 4" 58 times and a probable "4" 3 times. Total $\ell_1(5)$ signifies that component $\ell_1(k)$ was "1" 5 times. In each table the data point in the second column is the first to contain the fault.

The second task is to compare the estimation capabilities of the two LLR algorithms. These results, usually for larger faults, are given in graphical form. In order to be able to plot faults occurring at different times on the same axes, the first data point to contain the fault is labelled 'θ'. χ^2 test results for 'break in rtd lead' and ramp faults are presented graphically to facilitate comparison with the LLR algorithm responses.

6.9.1 Step faults

Direction 1: TX110 - Stripped MEA output from cooler

The χ^2 test gave some response to faults down to 1°, the smallest tried. For fault levels up to 2° only innovation

component 1 was affected but for levels above 3° both components 1 and 3 crossed the alarm threshold. For 1(a), a +1° fault at dp 294 (PLANT7 - 247 dp to eor):

TABLE 27a

k 1(a)	293	294			297	298 → 515	TOTALS +1°
ℓ_1(k)	0	1	1	1	0	0	ℓ_1(3) others (0)
LLR(ONA)	0	1'	0	0	0	0	1'(1)
LLR(SetII)	0	5	5	5	0	0	5 (3)

whereas for 1(b), a +2° fault at the same point:

TABLE 27b

k 1(b)	293	294				298	299 → 306	307				311	TOTALS +2°
LLR(ONA)	0	1	9'	9'	0	0	0	0	0	0	0	0	1(58) 1'(3) 9(2)
LLR(SetII)	0	1	1'	1'	1'	1	0	1'	0	1	1	1	1(208)1'(13)

Here ℓ_1(k) registered a '1' at 294 which continued almost uninterrupted to eor. LLR(Set II) clearly has a stronger response in Table 27b.

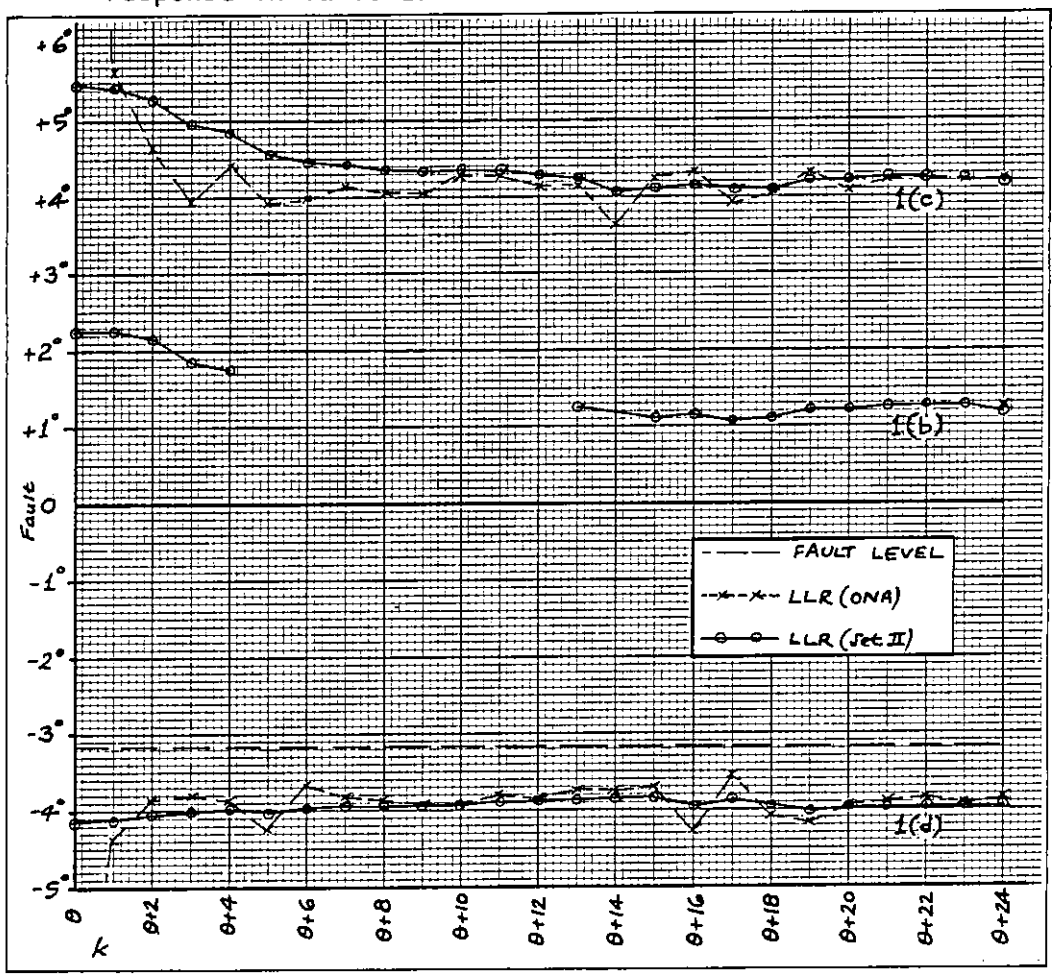

Fig.27 LLR response to failures in Direction 1 (TX110)

Compare the estimation accuracy for this +2° fault (1(b)) - Fig 27 - with those obtained for faults 1(c)+5° also at dp 294 (PLANT7) and 1(d)-3.17° at dp 238 (PLANT8). Clearly all the estimates are biased but the LLR (Set II) figures exhibit a lower estimation error variance.

Below 2°, LLR (Set II) has a stronger response than LLR (ONA) but tends to confuse the fault source with directions 5 and 9. Above 2° both LLR variants detect correctly but LLR (Set II) has a slight edge because of its 'smoother' estimates.

Direction 2: TX177 - cooling water output from cooler

At a 1° fault level the χ^2 test response was stronger than that for a similar fault in direction 1. For all faults tried up to +4.66° the response was almost always limited to $\ell_2(k)$ although $\ell_1(k)$ and $\ell_3(k)$ occasionally registered a '1'. Up to 2° the LLR response was unpredictable as can be seen by comparing the results for faults 2(a) -2° at dp 199 (PLANT8 - 148 dp to eor) and 2(b) +2° at dp 294 (PLANT7 - 247 dp to eor):

TABLE 28

k 2(a)	198	199						205					210	TOTALS -2°
LLR(ONA)	0	2	2'	6'	2'	2'	2'	2'	2'	2'	2'	6	6'	2(3)2'(90)6(1)6'(54)
LLR(SetII)	0	6'	6'	6'	6'	6'	2'	2'	2'	2'	2'	6'	6'	2(1)2'(91) 6'(56)

TABLE 29

k 2(b)	293	294						300					305	TOTALS +2°
LLR(ONA)	0	2	2	2	2	2	2	2	2	2	2	2	2	2(240)2'(7)
LLR(SetII)	0	2	2	2	2	2	2	2	2	2	2	2	2	2(247)

A -1.49° fault behaved similarly to Table 28 while fault 2(c) +1° at dp 294 (PLANT7) was diagnosed quite well at least by LLR (Set II). Fig 28 shows the estimates obtained from faults 2(b), 2(c) and fault 2(d) +4.66° at dp 98 (PLANT8).

Below 2°, LLR (Set II) is sometimes better than LLR(ONA) but both are likely to confuse the fault source with direction 6. Above 2° both are reliable with LLR (Set II)

again providing smoother estimates. The estimates from all Direction 2 examples were found to be almost unbiased.

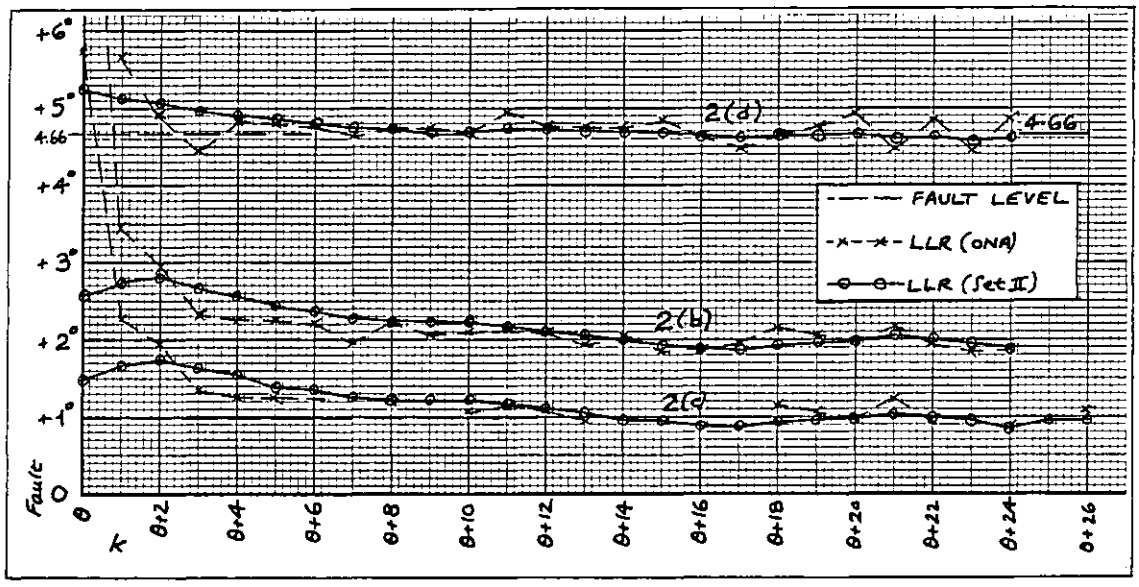

Fig.28 LLR response to failures in Direction 2 (TX177)

Direction 3: TX174 - Stripped MEA between heat exchanger and cooler

Very small faults down to +0.25° were tried in Direction 3 but the χ^2 test still detected these, albeit with a slight delay. The effects of faults in this direction were confined almost exclusively to $\ell_3(k)$ with very occasional 1's on $\ell_1(k)$. LLR (Set II) managed to pick up fault 3(a) +0.25° at dp 490 (PLANT7 - 51 dp to eor) and a +0.5° fault at the same point, but missed a -0.75° fault (elsewhere) completely. In the range 1°-2° LLR (Set II) was much better than LLR (ONA); Table 31 shows 3(b), a +1° fault also at dp 490 (PLANT7):

TABLE 30

k 3(a,b)	489	490					495						501	TOTALS +0.25°,+1°
$\ell_3(k)$	0	0	0	0	0	1	1	1	0	1	0	0	1	$\ell_3(5)$ others (0)
LLR(ONA)	0	3	0	0	0	0	0	0	0	0	0	0	0	3(1)
LLR(SetII)	0	3'	3'	3	3	3'	3'	3	3	3	0	0	0	3(8) 3'(6)

TABLE 31

LLR(ONA)	0	3	9'	0	0	3'	0	3'	0	3'	0	0	0	11'39(lea.)3'(7)9'(2)
LLR(SetII)	0	3	3	3	3	3	3	3	3	3	3	3	3	3(30)3'(21)

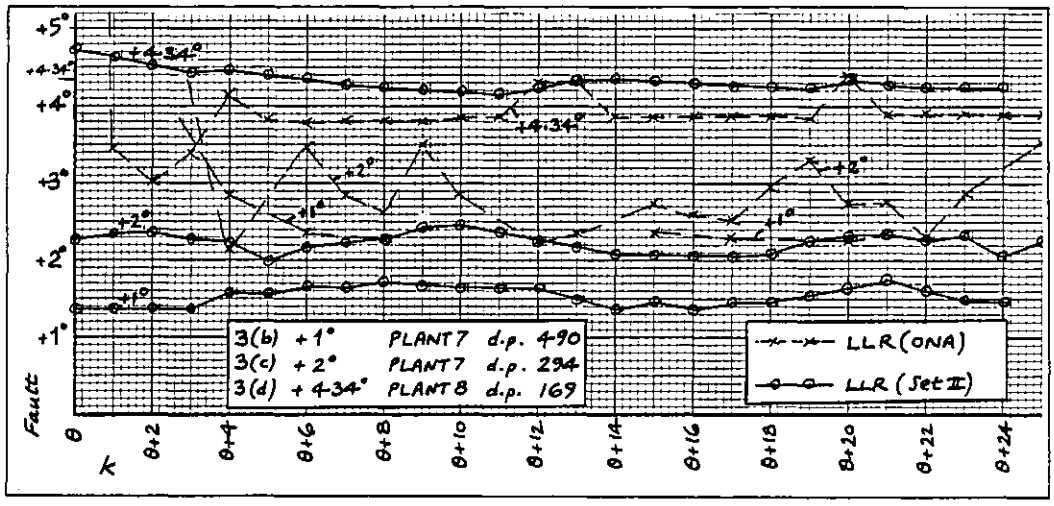

Fig.29 LLR response to failures in Direction 3 (TX174)

Fig 29 shows that unlike Directions 1 and 2 the mean value of the estimate is not the same for the two LLR variants. While LLR (ONA) becomes as reliable as LLR (Set II) for faults over 2° the estimation accuracy of the latter is superior for all the Direction 3 examples.

Direction 4: TX172 - Spent MEA output from heat exchanger

Direction 4 faults were reliably detected by the χ^2 test down to +0.96°, the response always limited to $\ell_4(k)$ only. Neither LLR algorithm performed very well: LLR (ONA) responded very weakly to all faults up to +3.97° while below 2° LLR (Set II) failed to detect. At 2° and above the LLR (Set II) response was stronger but there was a marked tendency to confuse the fault source with Direction 7. Tables 32 and 33 show faults 4(a) +2° at dp 294 (PLANT7 - 247 dp to eor) and 4(b) +3.97° at dp 40 (PLANT8 - 307 dp to eor).

TABLE 32

k 4(a)	293	294							301	TOTALS +2°
$\ell_4(k)$	0	1	1	1	0	0	0	0	0	$\ell_4(35)$ others (0)
LLR(ONA)	0	4	0	0	0	0	0	0	0	4(1)
LLR(SetII)	0	4'	7'	7'	7'	7'	7'	0	0	4'(1)5(3)5'(7)7(125)7'(67)

TABLE 33

k 4(b)	39	40							47	TOTALS +3.97°
LLR(ONA)	0	4	0	0	0	0	0	0	0	4(1)4'(7)7(1)7'(1)
LLR(SetII)	0	4	4	4	4'	4'	4'	4'	4'	4(3)4'(263)7'(41)

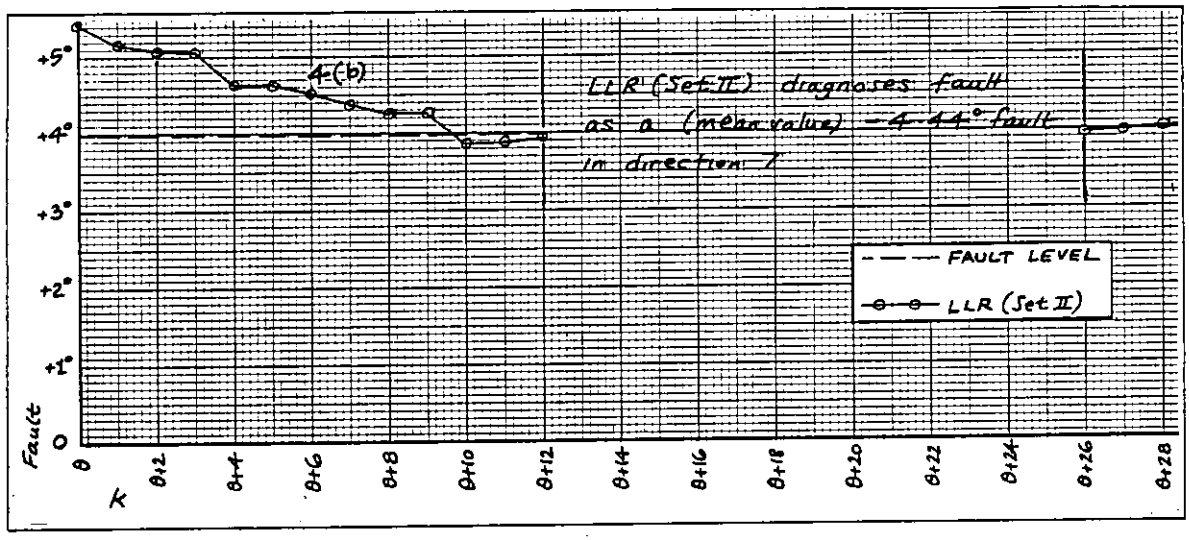

Fig.30 LLR response to a failure in Direction 4 (TX172)

LLR(Set II) estimates are illustrated in Fig 30 for fault 4(b).

Direction 5: FX101 - MEA flow rate

MEA flow measurement faults were characterized by a strong χ^2 test response on components $\ell_1(k)$ and $\ell_2(k)$. LLR (Set II) was much more positive than LLR (ONA) in detecting these faults particularly the -0.03 kgs^{-1} fault on PLANT8. Recalling that a +X setpoint change is used to simulate a step fault of -X, Tables 34 and 35 and Fig 31 illustrate faults 5(a) -0.03 kgs^{-1} at dp 34 (PLANT8 - 307 dp to eor) and 5(b) -0.05 kgs^{-1} at dp 290 (PLANT7 - 251 dp to eor).

TABLE 34

k 5(a)	33	34		36		38				42	TOTALS -0.03 kgs^{-1}
$\ell_1(k)$	0	0	0	1	1	1	1	1	1	1	$\ell_1(305)$ $\ell_3(3)$
$\ell_2(k)$	0	0	0	1	1	1	1	1	1	1	$\ell_2(70)$ $\ell_4(1)$
LLR(ONA)	0	0	0	5	0	5	5'	9'	5	5'	5(33) 5'(9) 9'(13)
LLR(SetII)	0	0	0	0	0	5	5	5	5	5'	5(163) 5'(146)

TABLE 35

k 5(b)	289	290		292		294				298	TOTALS -0.05 kgs^{-1}
LLR(ONA)	0	0	8'	8	5	5	5	5'	9'	5'	5(8)5'(232)88'(1ea.)9'(8)
LLR(SetII)	0	0	0	5	5	5	5	5	5	5	5(249)

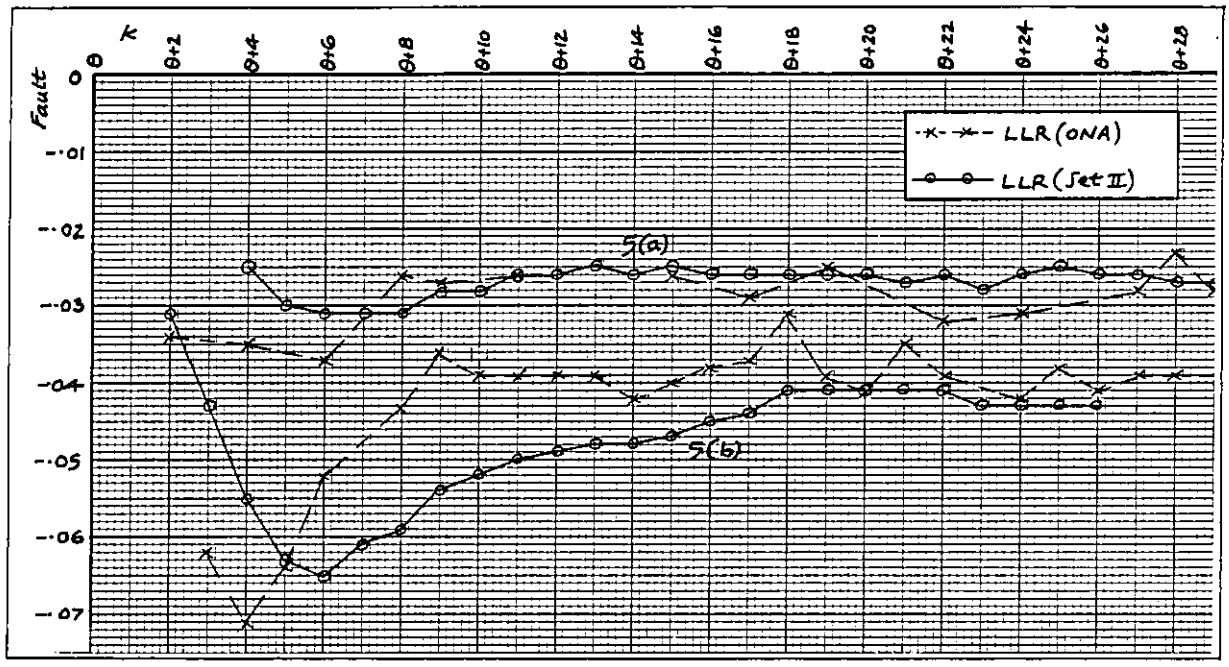

Fig.31 LLR response to failures in Direction 5 (FX101)

Note the delay in detection and the transients in the estimation due to the use of steady state temperature changes.

Direction 6: FX124 - Cooling water flow rate

All components except for $\ell_4(k)$ were strongly affected by cooling water flow rate measurement faults. The two LLR variants behaved similarly but LLR (Set II) was more likely to confuse the fault source with Direction 9. Tables 36 and 37 and Fig 32 illustrate faults 6(a) -0.05 kgs^{-1} at dp 515 (PLANT7 - 26 dp to eor) and 6(b) -0.05 kgs^{-1} at dp 192 (PLANT8 - 155 dp to eor).

TABLE 36

k 6(a)	514	515	516								524	TOTALS -0.05kgs^{-1}
$\ell_1(k)$ $\ell_2(k)$	0	0	1	1	1	1	1	1	1	1	1	$\ell_1(25)$ $\ell_2(25)$
$\ell_3(k)$	0	0	0	0	1	1	1	1	1	1	1	$\ell_3(23)$ $\ell_4(0)$
LLR(ONA)	0	0	6	6	6	6	6'	6	6	6	6	6(21)6'(4)
LLR(SetII)	0	0	9'	9'	9	9'	9'	9'	6'	6	6	6(18)6'9(1ea.)9'(5)

TABLE 37

k 6(b)	191	192	193								201	TOTALS -0.05kgs^{-1}
LLR(ONA	0	0	6	6	6	6	6	6	6	6	6	6(154)
LLR(SetII)	0	0	6'	6'	6	6	6	6	6	6	6	6(152)6'(2)

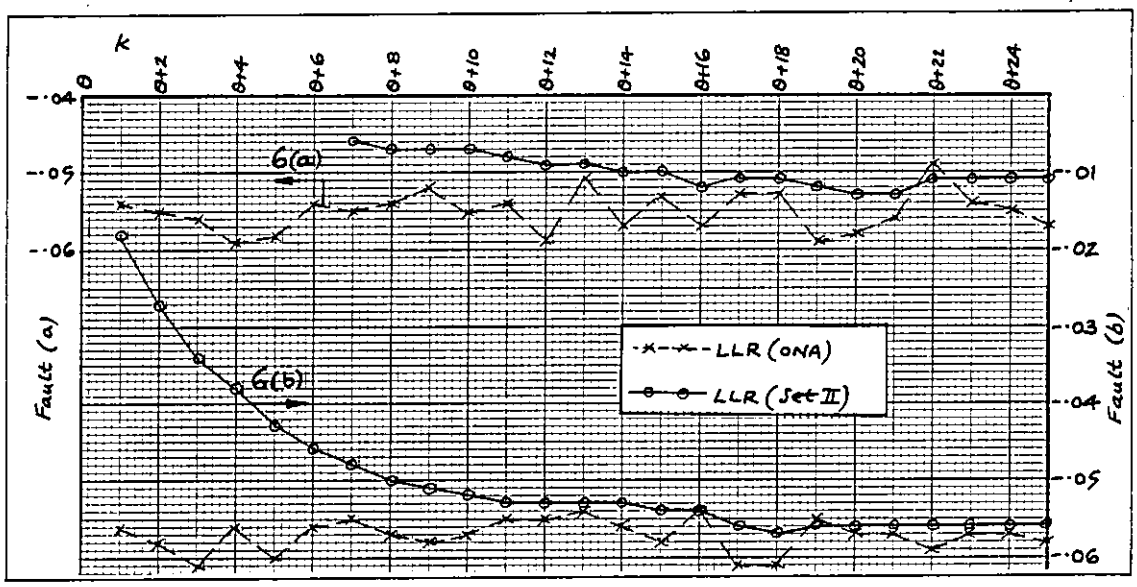

Fig.32 LLR response to failures in Direction 6 (FX124)

Note again the delay in detection and the marked transients on the LLR (Set II) results. The 2 data point delay in $\ell_3(k)$ changing to '1' occurred in both examples and may be a useful characteristic to aid fault isolation by means of the χ^2 test. After the initial transients, LLR (Set II) produces a lower variance estimate than LLR (ONA) in both Direction 5 and Direction 6.

Direction 7: TX173 - Stripped MEA input to heat exchanger

The χ^2 test missed a +0.8° fault but just picked up a step of 1°. Fault levels over 2° were detected although not strongly, the effect usually being confined to $\ell_4(k)$ as for Direction 4 faults. LLR (ONA) failed to detect any faults at all while a fault of -3.52° was the only one detected at all satisfactorily by LLR (Set II). Tables 38 and 39 include faults 7(a) +2° at dp 294 (PLANT7 - 247 dp to eor) and 7(b) -3.52° at dp 298 (PLANT8 - 49 dp to eor). Fault 7(b) is illustrated by Fig 33.

The LLR (Set II) delay to detection is about 1½ minutes for each of these examples and Fig 33 shows that the estimation bias decays slowly.

TABLE 38

k 7(a)	293	294						300			303	304	TOTALS +2°
$\ell_4(k)$	0	0	0	0	0	0	0	1	1	1	1	1	$\ell_1(2)$ $\ell_4(25)$ others(0)
LLR(ONA)	0	0	0	0	0	0	0	0	0	0	0	0	no failures detected
LLR(SetII)	0	0	0	0	0	0	0'	0'	0'	0'	4'	4'	4'(232)

TABLE 39

k 7(b)	297	298									307	308	TOTALS -3.52°
LLR(ONA)	0	0	0	0	0	0	0	0	0	0	0	0	no failures detected
LLR(SetII)	0	0	0	0	0	0	0	0	0	0	7	7	7(9) 7'(31)

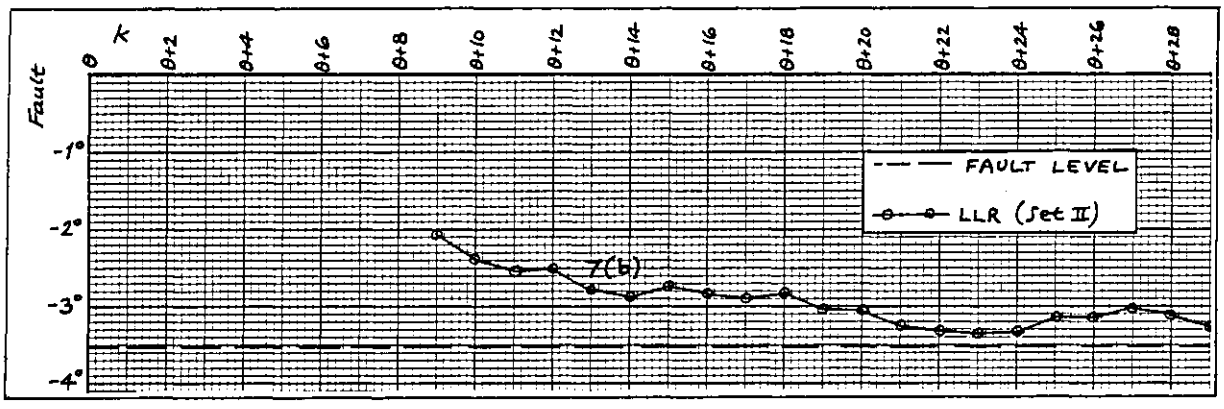

Fig.33 LLR response to a failure in Direction 7 (TX173)

Direction 8: TX175 - Spent MEA input to heat exchanger

Faults between 1 and 2° were picked up by the χ^2 test on $\ell_1(k)$ only. At -3.57° however the effect was restricted to $\ell_3(k)$ and a +5° fault influenced all components except for $\ell_4(k)$. Both LLR variants were incapable of detecting faults up to 2° but were able to cope with faults 8(a) -3.57° at dp 150 (PLANT7 - 247 dp to eor) and 8(b) +5° at dp 294 (PLANT7 - 247 dp to eor). These faults are illustrated by Tables 40 and 41 and by Fig 34.

TABLE 40

k 8(a)	149	150			153	154						160	TOTALS -3.57°
LLR(ONA)	0	0	0	0	8	8	8	8	8'	8			3'(45)8(55)8'(94)
LLR(SetII)	0	0	0	0	0	8	8'	8'	8	8			8(148) 8'(45)

TABLE 41

k 8(b)	293	294			297		299					304	TOTALS +5°
LLR(ONA)	0	0	0	0'	8	8	8	0	0	8	0	0	8(194)
LLR(SetII)	0	0	0	0	0	0	8	8	8	8	8	8	8(242)

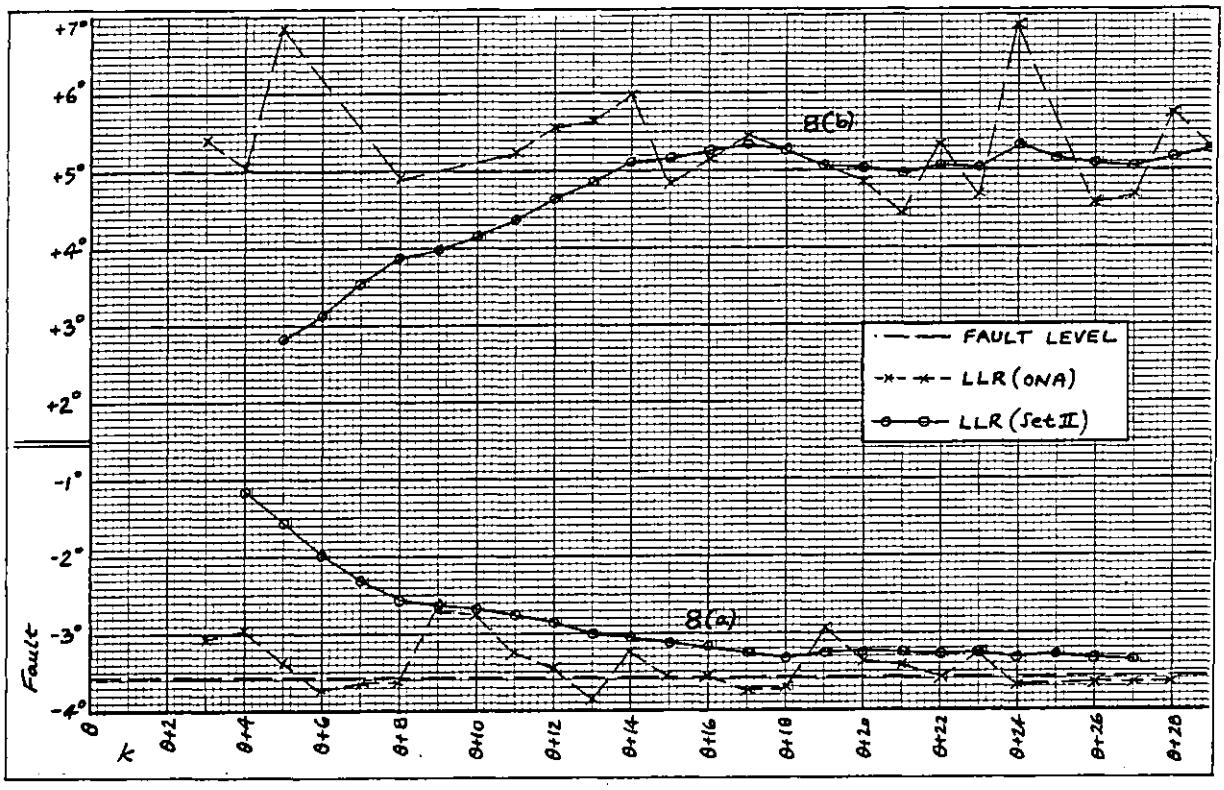

Fig.34 LLR response to failures in Direction 8 (TX175)

Note again the delay to detection (c30-45s) and the slowly decaying bias on the LLR (Set II) estimate. Once settled however the latter estimate exhibits a far lower error variance.

Direction 9: TX176 - Cooling water input to cooler

The χ^2 test response to a Direction 9 fault was variable but usually characterized by a strong response on $\ell_1(k)$ and a weaker response on $\ell_3(k)$. This test picked up faults of +0.25°, +0.5° and +1.0° but missed two faults at -1.38° and -1.6° which were also missed or cross-detected by the LLR algorithms. At +3.72° all components except for $\ell_4(k)$ were affected. Neither LLR variant was very convincing for faults below 2° as is shown by faults 9(a) +0.5° at dp 490 (PLANT7 - 51 dp to eor) and 9(b) +1.0° (at the same point) in Tables 42 and 43.

TABLE 42

k 9(a)	489	490				494							501	TOTALS +0.5°
LLR(ONA)	0	0	0'	0	0	3'	0	0	0	0	0	0	0	1(1) 3'(1)
LLR(SetII)	0	0	0	0	0	9'	9'	9'	9'	9'	9'	9	0'	1'(9) 9(2) 9'(16)

TABLE 43

k 9(b)	489	490				494							501	TOTALS +1°
$\ell_1(k)$	0	0	1	1	1	1	1	1	1	1	1	1	1	$\ell_1(47)\ell_2(0)$
$\ell_3(k)$	0	0	0	0	0	1	1	1	0	1	0	0	1	$\ell_3(9)\ \ell_4(0)$
LLR(ONA)	0	0	9'	0	0	9'	9'	0'	0	9'	0'	0	0'	1(5)1'(5)5(1)9'(9)
LLR(SetII)	0	0	9'	9'	9'	9'	9'	9'	9'	9'	9'	9'	9'	1'(20)9'(27)

Fig 35 illustrates faults 9(c) +2° at 290 (PLANT7 - 251 dp to eor and coincident with cooling water flow rate step change) and 9(d) +3.72° at dp 329 (PLANT8 - 18 dp to eor).

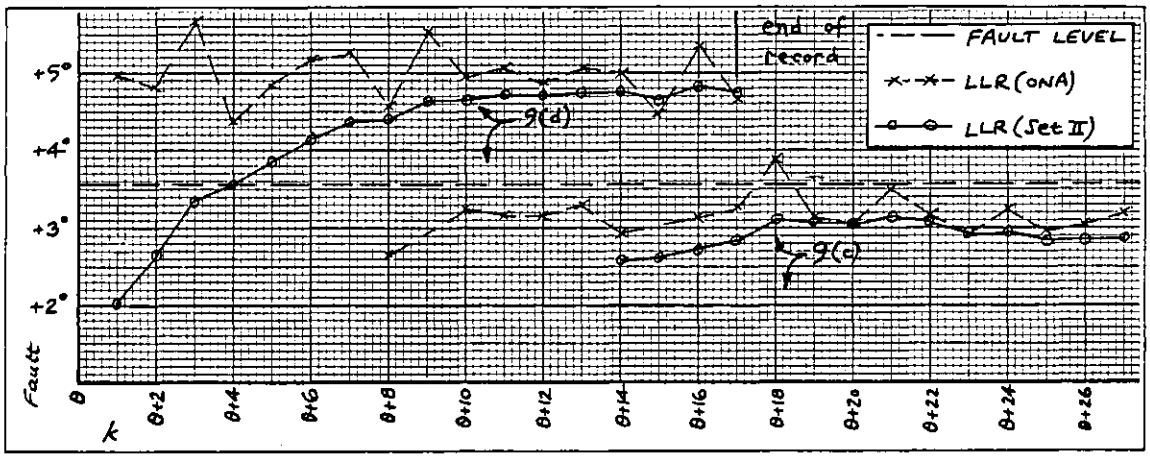

Fig.35 LLR response to failures in Direction 9 (TX176)

The pattern is very similar to those of Figs 33 and 34.

6.9.2 Jump faults

Table 44 gives the results obtained for jump faults in each direction except for 5 and 6 (Flow rate faults). The faults are random and their effect on each algorithm is shown over three data points. Jumps in directions 7 and 8 were missed by all methods.

The LLR (ONA) response is characterized by a large fault declared in the same sense as the actual jump followed by a slightly smaller one in the opposite sense. LLR (Set II) produces for Directions 1-4 a much more accurate estimate at the affected data point only.

With LLR (Set II) it would appear that an output jump fault significantly affects only a single innovation whereas for LLR (ONA) at least two are affected. To

TABLE 44

Fault			χ^2 - test				LLR(ONA)		LLR(Set II)	
D	Mag	d.p.	$\ell_1(k)$	$\ell_2(k)$	$\ell_3(k)$	$\ell_4(k)$	Dec	Est	Dec	Est
1	-3.17°	238	1	0	0	0	1	-13.48	1	-4.14
		239	1	0	1	0	1	8.43	0	-
		240	1	0	1	0	0	-	0	-
2	+4.66°	98	0	1	0	0	2	22.84	2	5.25
		99	0	1	0	0	2	-16.81	0	-
		100	0	1	1	0	0	-	0	-
3	-4.34°	169	0	0	1	0	3	-22.99	3	-4.76
		170	0	0	1	0	3	19.56	0	-
		171	0	0	1	0	0	-	0	-
4	+3.97°	40	0	0	0	1	4	42.71	4	5.40
		41	0	0	0	1	4	-38.67	0	-
		42	0	0	0	1	0	-	0	-
7	-3.52°	299	0	0	0	0	0	-	0	-
		300	0	0	0	0	0	-	0	-
		301	0	0	0	0	0	-	0	-
8	-3.57°	151	0	0	0	0	0	-	0	-
		152	0	0	0	0	0	-	0	-
		153	0	0	0	0	0	-	0	-
9	+3.72°	330	1	1	0	0	9'	4.99	9	2.02
		331	1	1	0	0	0	-	9	1.73
		332	1	1	0	0	0	-	9	1.73

For directions 1-4 the three data points are θ (the point containing the fault), $\theta + 1$ and $\theta + 2$. For directions 6-9 the points are $\theta + 1$, $\theta + 2$ and $\theta + 3$ as an input jump at θ has no effect on $\Upsilon(\theta)$. For the LLR variants the algorithm decisions and estimates are given in columns 8-11. All faults were superimposed on the PLANT8 data record.

examine this further two multiple jump experiments were performed again on PLANT8 data. The results are given in Table 45.

Expt 1: 5° jump in Direction 1 at dp 98, 5° in 2 at dp 99,... 5° in 9 at dp 104

Expt 2: 5° jump in Direction 9 at dp 98, 5° in 8 at dp 99,... 5° in 1 at dp 104

While neither variant can cope with the input jumps (7-9), LLR (Set II) is shown to be superior to LLR (ONA) with regard both to discrimination between output jumps and to the estimation of the magnitudes thereof.

TABLE 45

	EXPT 1					EXPT 2				
dp	D	LLR(ONA)		LLR(SetII)		D	LLR(ONA)		LLR(SetII)	
		Dec	Est	Dec	Est		Dec	Est	Dec	Est
98	1	1	19.84	1	4.88	9	0	-	0	-
99	2	2	24.80	2	5.62	8	5'	0.05	0'	-
100	3	6	- 0.28	3	5.56	7	0	-	0'	-
101	4	4	54.53	4	7.30	4	4	52.79	4	7.03
102	7	4	-48.45	0	-	3	3	25.78	3	4.99
103	8	0	-	0	-	2	2	26.35	2	5.20
104	9	0	-	0	-	1	2	-19.61	1	4.37
105	0	5'	0.06	5'	0.02	0	1	-14.95	0	-
106	0	0	-	5	0.018	0	1'	- 1.10	0	-

6.9.3 'Break in rtd lead' faults

This type of fault was simulated for one output (2) and for all three inputs (7-9). If an rtd lead breaks, the infinite resistance is seen by the measurement loop as a constant temperature at the top end of the range: 120°C for Direction 7 and 50°C for Directions 2, 8 and 9. The fault looks almost exactly the same as a step fault and whether or not it will be detected depends on how close the temperature was to the top of the range at the time of the break. All simulations were on PLANT8 data, details as given in Table 46.

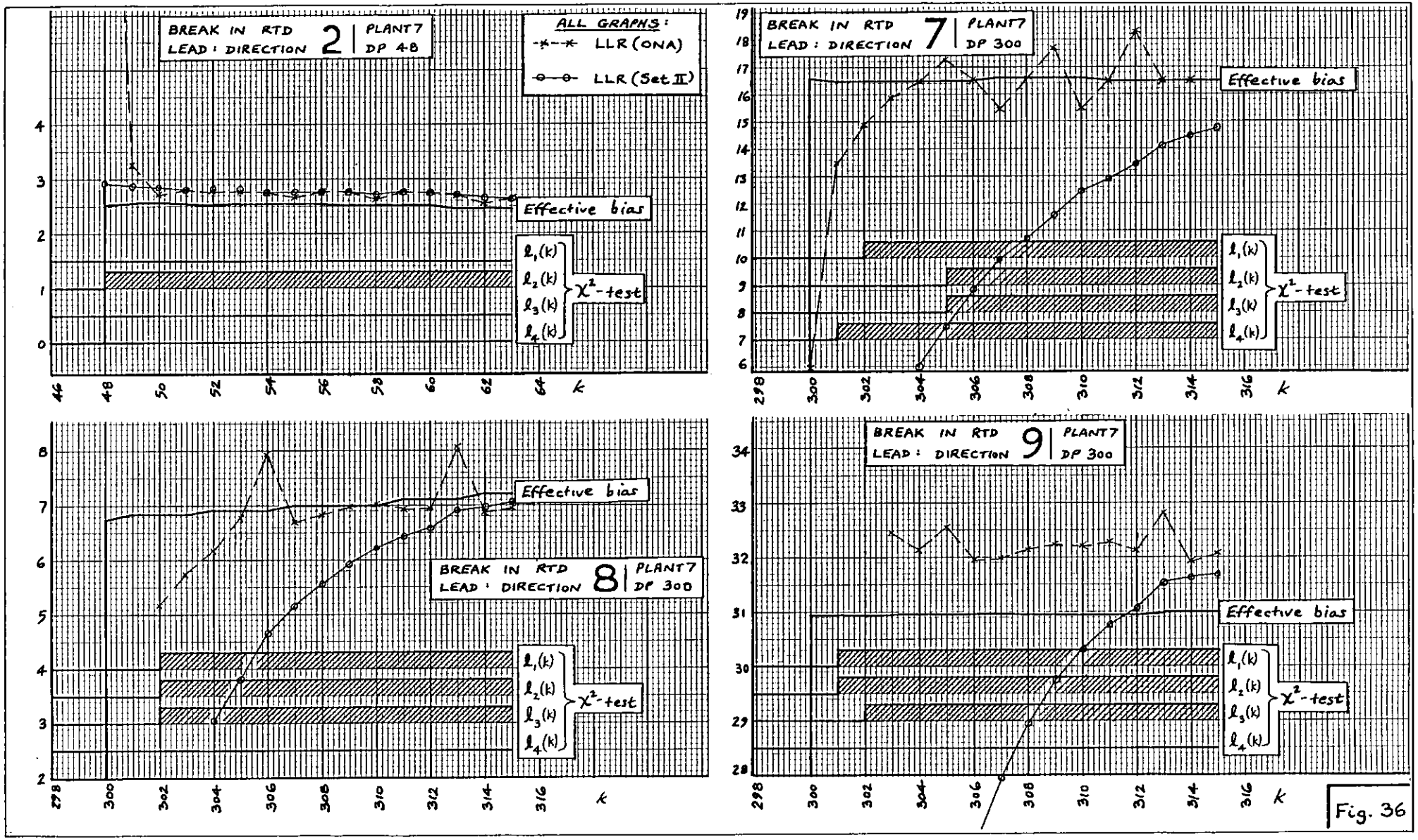
BREAK IN RTD LEAD : DIRECTION 2 | PLANT 7 DP 48
ALL GRAPHS :
LLR (ONA)
LLR (Set II)
Effective bias
$\ell_1(k)$
$\ell_2(k)$
$\ell_3(k)$
$\ell_4(k)$
χ^2-test
k
BREAK IN RTD LEAD : DIRECTION 7 | PLANT 7 DP 300
BREAK IN RTD LEAD : DIRECTION 8 | PLANT 7 DP 300
BREAK IN RTD LEAD : DIRECTION 9 | PLANT 7 DP 300

Fig. 36

TABLE 46

D	RTD	Break at dp	Process var at break °C	Range °C	Effective Step °C
2	TX177	48	47.48	50.0	+ 2.52
7	TX173	300	103.4	120.0	+16.6
8	TX175	300	43.28	50.0	+ 6.72
9	TX176	300	19.06	50.0	+30.94

These examples are illustrated in Fig 35. As far as the χ^2 test is concerned only the breaks in Directions 2 and 8 follow the pattern obtained from the step fault examples. The response to a break in Direction 7 is the only example in which all four χ^2 components were affected, and previous examples in Direction 9 affected $\ell_1(k)$ and $\ell_3(k)$ only.

The LLR algorithms had little difficulty in isolating the faults although both were hesitant about the break in rtd TX173. LLR (ONA) recorded a definite '7' at dp 301 but thereafter 83% of decisions were 7-probable. LLR (Set II) declared 4-probable twice at dp 302 and 303, followed by 7-probable at 304 and 305 before reaching a firm decision in favour of Direction 7. Fig 35 shows the usual slow decay in the estimation bias exhibited by LLR (Set II) for input faults.

6.9.4 Ramp faults

Ramps of +0.05°C/dp (0.3°C/min) were tried for output TX110 (D1) and inputs TX175 and TX176 (D8,9). Each ramp was superimposed on PLANT7 data starting from zero at dp 299. This was to make use of the longest possible steady state data set free from setpoint changes (the next was a c/w flow change at dp 515) that was also away from the nominal operating/linearization point.

Table 47 compares the response expected from the step fault examples with that actually obtained from the ramp fault examples which are illustrated in Figs 36, 37 and 38. Note that the χ^2 test responds similarly to all

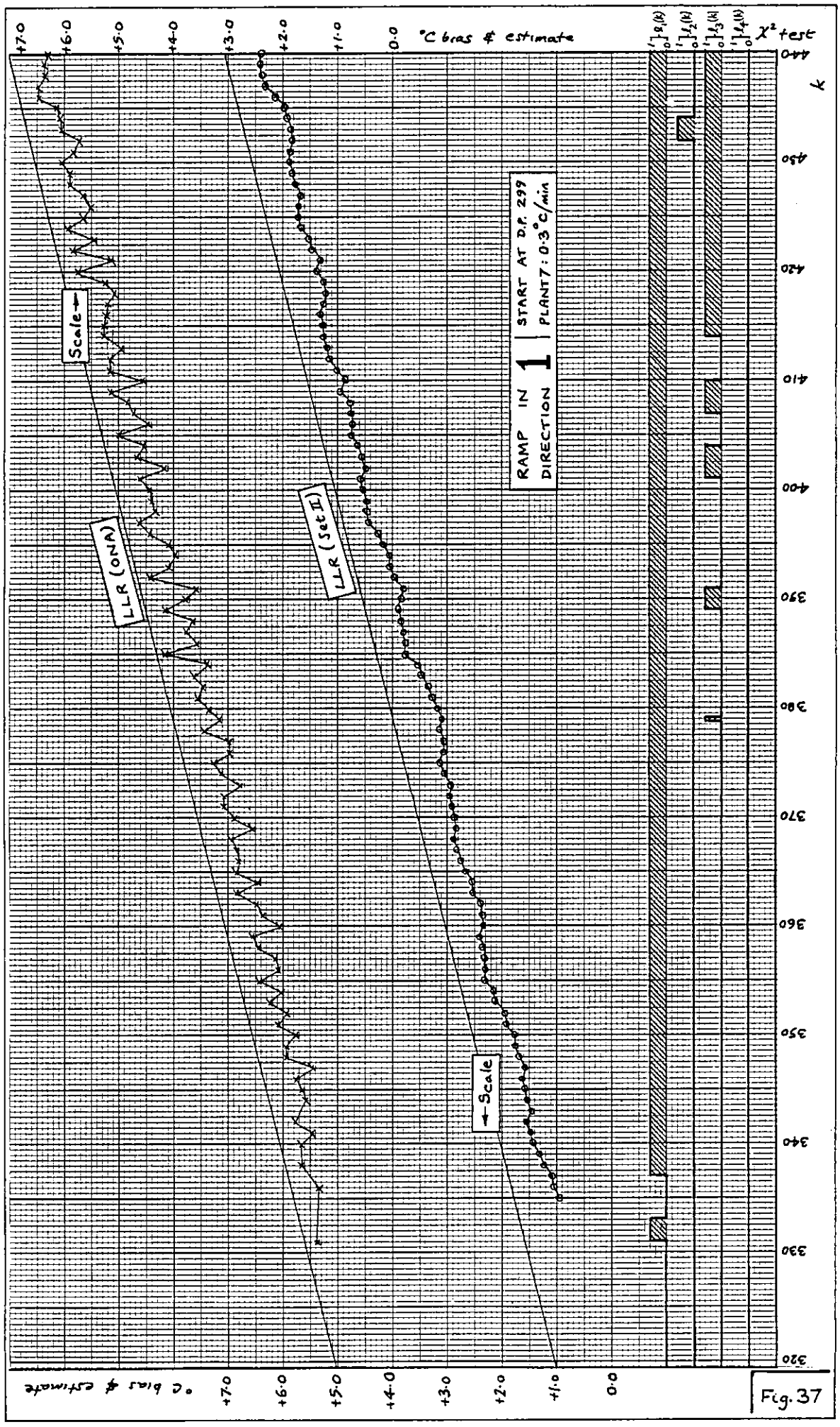
°C bias & estimate
χ² test
k
RAMP IN DIRECTION 1
START AT D.P. 299
PLANT 7: 0·3°C/min
LLR (ONA)
LLR (Set II)
Scale
Scale
°C bias & estimate

Fig. 37

°C bias & estimate
+7·0
+6·0
+5·0
+4·0
+3·0
+2·0
+1·0
0·0
Scale→
LLR (ONA)
Scale→
LLR (Set II)
←Scale
RAMP IN DIRECTION 8
START AT D.P. 299
PLANT 7: 0·3°C/min
$\ell_1(k)$ also '1' at d.p. 308 & 9
$\ell_1(k)$
$\ell_2(k)$
$\ell_3(k)$
$\ell_4(k)$
χ^2-test
320
330
340
350
360
370
380
390
400
410
420
430
440
k

Fig. 38

°C bias of estimate
+7·0
+6·0
+5·0
+4·0
+3·0
+2·0
+1·0
0·0
Gaps * 5'
All x 9'
LLR (ONA)
Scale →
← 9' | 9 →
LLR (Set II)
← Scale
RAMP IN DIRECTION 9
START AT D.P. 279
PLANT T: 0·3°C/min
+7·0
+6·0
+5·0
+4·0
+3·0
+2·0
+1·0
0·0
°C bias of estimate
1
0
$\theta_1(k)$
$\theta_2(k)$
$\theta_3(k)$
$\theta_4(k)$
300
310
320
330
340
350
360
370
380
390
400
410
420
k
χ²-test

Fig. 29

three ramps, i.e. $\ell_1(k)$ followed by $\ell_3(k)$ then $\ell_2(k)$. Variable $\ell_4(k)$ remains unaffected.

TABLE 47

D	χ^2-test		LLR(ONA)		LLR(Set II)	
	Expected	Actual	Expected	Actual	Expected	Actual
1	≤1°C	First 1.6° Cont. 1.9°	<2° weak >2° good	Reliable ≥1.5÷2°	<2°x5'9' >2° good	Reliable ≥1.8°
8	≤1°C	First 0.4° Cont. 0.8°	<2° miss >2° good	Reliable ≥3.5-4°	<2° miss >2° good	Reliable ≥2.9°
9	≤0.25°C possible	First 0.4° Cont. 0.8°	<2° poor >2° good	Reliable ≥1-1.5°	<2° poor >2° good	Reliable ≥0.9°

The table shows the 'ramp' results to be fairly consistent with the 'step' results except for the LLR algorithms in Direction 8. The χ^2 test is consistently the first to detect the fault and LLR (Set II) is as good if not better than LLR (ONA) in each case.

6.9.5 Summary of results

On the basis of the simple example of Section 4.10 it was originally envisaged that the χ^2 test would be able to separate input and output faults and to isolate the actual measurement loop in the case of an output fault only. Each fault direction 'i', i = 1,...4 was to affect $\ell_i(k)$ only whereas input faults would affect 'more than one' of the $\ell_i(k)$'s. The structure of matrices FMATX and FMATY2 (Section 6.3.2) is sufficiently close to the equivalent matrix for the simple example to promote expectation of a degree of success in practice.

The examples show the technique to have been reasonably successful for faults in Directions 2, 3 and 4 but small faults in Direction 7 also tended to affect $\ell_4(k)$ only, rendering indistinguishable faults in Directions 4 and 7. Faults in Directions 6, 8 and 9 and larger faults in Direction 1 all tended to affect $\ell_1(k)$, $\ell_2(k)$ and $\ell_3(k)$.

Flow faults were distinguishable only by virtue of the fact that unlike cooling water flow faults (D6), MEA flow faults (D5) affected $\ell_1(k)$ and $\ell_2(k)$ only.

The χ^2 test never detected any fault later than the LLR algorithms and was often earlier. Its isolation capabilities are clearly limited but it has some value as a detection only technique.

With the LLR algorithms it is important to retain a sense of proportion with regard to fault magnitude. Both variants were capable of excellent isolation for step faults over $2^\bullet$ for Directions 1-4 and 9, and of approximately $3.5^\bullet$ for Directions 7 and 8. In real terms these faults are very small and apart from chemical reactions requiring critical temperatures, could probably be tolerated by a good many process plants.

Both variants were happier with output faults than input faults whose effects are more distributed. LLR (Set II) was noticeably better than LLR (ONA) for faults in Directions 2, 3, 5 and 7 but had a slightly higher tendency to cross-detect on smaller faults. The overall impression gained was that where LLR (ONA) tended to dither, LLR (Set II) was much more decisive as shown,for example, by Tables 31 and 35. A second advantage of LLR (Set II) was in the reduction in estimation error variance. While the innovation bias precludes unbiased estimates the error variance is seen to be reduced in every case particularly for faults in Directions 3 (Fig 29), 5 & 6 (Figs 31 and 32) and 8 & 9 (Figs 34 and 35).

Although classed as 'multiple output faults', flow faults are really input faults and share with Directions 7-9 a slow decay in estimation bias with the LLR (Set II) algorithm. This slight disadvantage with latter is outweighed by the much smoother estimates once the transient has died away. Table 44 shows LLR (Set II) to be vastly superior to LLR (ONA) in the estimation of jump faults

although neither can cope with a jump in Directions 7 or 8.

6.10 Summary of Chapter

In this chapter the modelling work of Chapters 2-4 and the theoretical work of Chapter 5 were brought together to test the ideas by simulation with real plant data. Fault reference vectors were calculated and incorporated into two designs for log-likelihood ratio based algorithms, the second employing a suboptimal Kalman gain which it was hoped would lead to improved performance. While attempting to obtain a suitable design for a recursive conditional probability algorithm it was found that this approach was far too unstable for use with real data.

Alarm thresholds were obtained empirically for use with the LLR and χ^2 algorithms and a comprehensive simulation programme carried out. The examples showed that the χ^2 test, while useful for detection purposes, was not particularly good at fault isolation. The LLR algorithms were very much better and both variants were capable of quite good fault isolation and estimation. The algorithm employing a suboptimal gain was shown to be a substantial improvement in many cases.

CHAPTER 7

CONCLUSION

7.0 Introduction

The purpose of this concluding chapter is fourfold. Firstly the LLR algorithms are subjected to computer analysis in order to explain their behaviour in selected examples from the simulations of Chapter 6. This is followed by the conclusions that can be drawn from the project and a look at the extent to which the declared aims have been achieved. The third section steps back from this particular application to examine the LLR algorithm in the perspective of fault detection algorithms in general and the chapter ends with suggestions for further work.

7.1 Computer analysis

This section includes step responses, estimation and cross-detection.

7.1.1 Step responses

The theoretical response of an LLR algorithm to a step fault of unit magnitude in direction 'i' is given by evaluating $E[\rho_i]$ over the region of interest. Using the notation of Section 5.9, the post fault $E[\Upsilon] = f_i$ so that

$$E[\rho_i] = \frac{f_i^T d_i}{d_i^T d_i} \quad \text{by Lemma 4.1} \qquad \ldots \quad (7.1)$$

$B_y(\Upsilon;\theta+N)$ and $B_u(\Upsilon;\theta+N)$ can be calculated by computer from Theorems 5.1 and 5.3 for the two gains KGAINX and KGAINY to obtain f_i vectors for LLR (ONA) and LLR (Set II) respectively.

The above approach generates f_i vectors resulting from a true step fault applied at time θ. For Directions 5 and 6 however, Fig 26 shows that the error in the flow rate measurement is apparent for a few seconds only. While the fault itself can be considered a true step at θ, the algorithms actually detect it via the apparent biases

induced in the output temperature measurements. These biases are zero at θ and undergo transients similar to those shown in Figs 12, 15 and 17. For a step fault in Direction 5 (MEA) the theoretical responses of TX174 and TX172 are obtained from equations (3.58) and (3.59) respectively while the responses of TX110 and TX177 follow as in Section 3.5.4. A cooling water flow rate fault (D6) affects TX110 and TX177 only, these approximating to simple exponentials as covered in Section 3.5.3.

By assuming that a flow fault occurs immediately prior to sample θ and neglecting the flow rate transient shown in Fig 26, flow rate f_i vectors can be obtained as follows. Each affected temperature measurement is represented by a series of small step changes at successive sampling instants (cf curve (3) in Fig 13). For Direction 'i' the cumulative effect on the innovations is calculated for these small steps using the f_i's already calculated. These effects are summated for i = 1,...4 to obtain the effective f_i's for D5 and 6 for each LLR variant.

Figs 40 and 41 show the theoretical responses to step faults of +1°C in each Direction except for 5 and 6 which are for faults of $-1 kgs^{-1}$. The initial setpoint (PLANT7 or 8) at which the f_i vectors were calculated is given in each case. The curves serve to explain a number of the Chapter 6 simulation results: the LLR (ONA) response to a fault in Direction 3 is seen clearly in the curve for +4.34° in Fig 29 while Figs 31 and 32 show the expected responses to flow rate faults. In every case LLR (Set II) is seen to take rather longer than LLR (ONA) to reach a steady unbiased estimate.

For Directions 1-4, LLR (ONA) dramatically overestimates the fault magnitude at sample θ, the first exhibiting the fault, but the estimate drops sharply at $k = \theta + 1$. The LLR (Set II) response for these Directions is nearer the ideal, which explains the difference in response to a

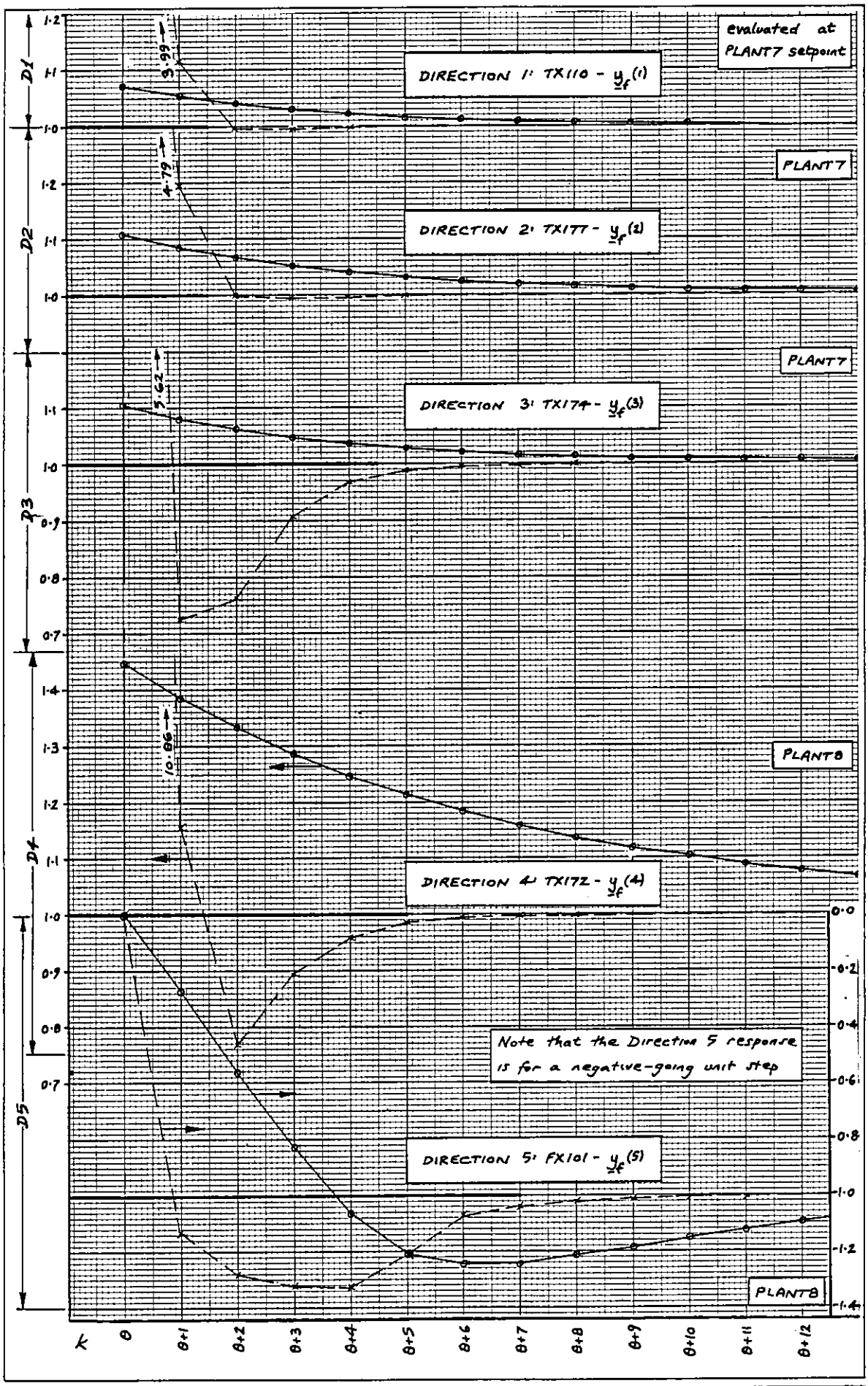

Fig.40 LLR unit step responses for failure directions 1 - 5

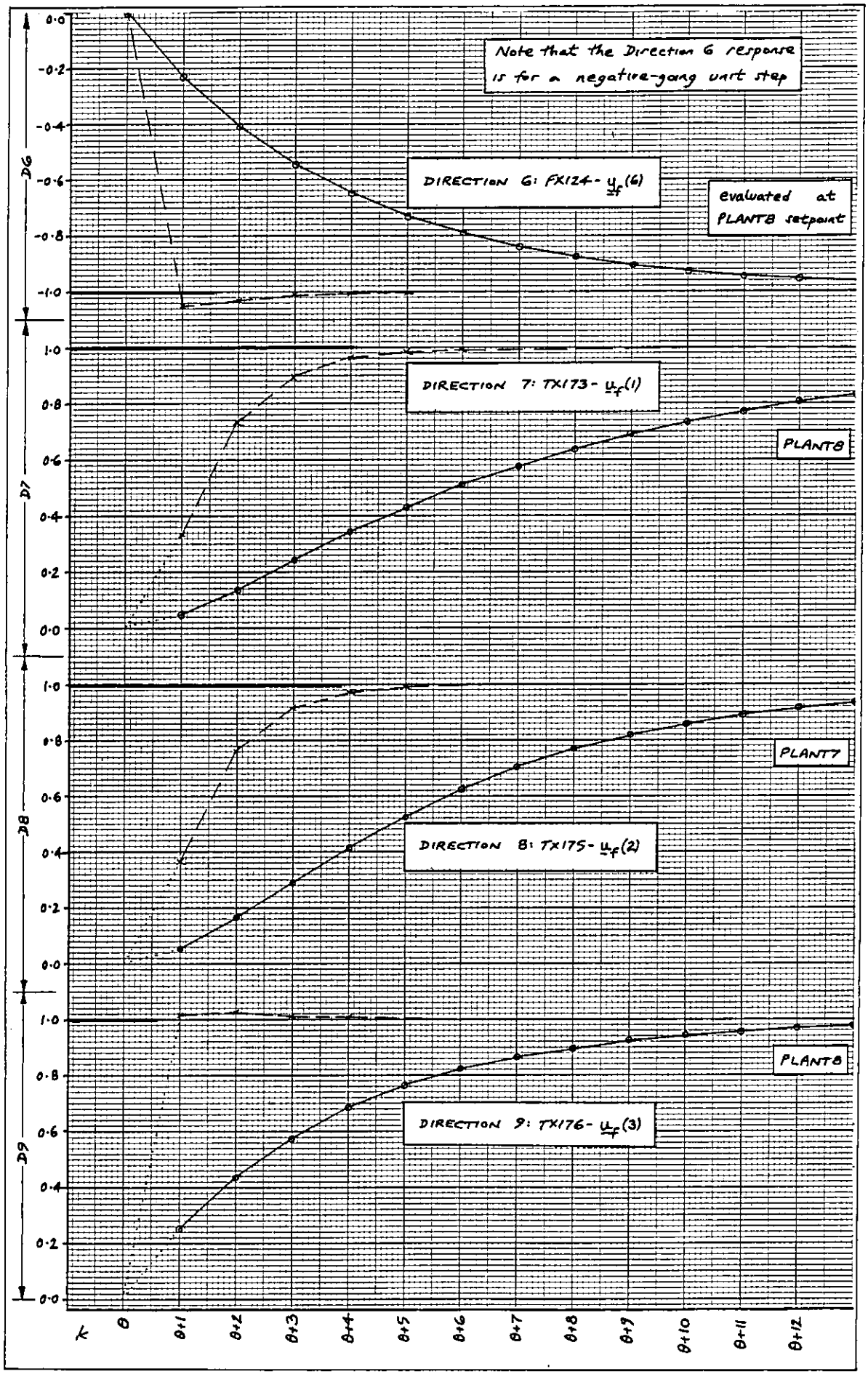

Fig.41 LLR unit step responses for failure directions 6 - 9

jump fault which is effectively two step faults in opposite senses applied at successive sampling instants.

7.1.2 Delay to detection

Some of the step responses have the appearance of a step input passed through a first or second order delay. The former are straightforward and the latter can be approximated by simple exponentials if these are timed to start at some point after fault time θ. Examples are given in Table 48 where τ is the time constant.

TABLE 48

D	LLR(ONA)		LLR(SetII)	
	τ s	start(secs)	τ s	start(secs)
6			40	θ
7	8	θ + 10	72	θ + 10
8	10	θ + 6	40	θ + 20
9			35	θ

These approximations could be useful in attempting to estimate the actual fault time θ from estimates which clearly form part of an exponential curve (see Figs 33, 34) but where a delay to detection has occurred. Conversely the sequence of expected post-fault innovations f_i could be used with equation (4.65) and Lemma 4.1 to estimate for a step fault of given magnitude the point at which the llr statistic would exceed the threshold n_i.

7.1.3 Estimation error variance

Quality of estimation is characterized by two parameters: bias and error variance. In Section 5.9 it was shown that Lemma 4.1 guarantees an asymptotically unbiased estimate from unbiased innovations and that the error variance can be obtained via equation (5.66).

Substitution into (5.66) of covariance matrices VX and VY (Section 6.4) together with the reference vectors d_i for the two LLR variants indicates that the error variance

will always be higher for LLR (Set II) than for LLR (ONA). For Direction 1, LLR (ONA) produces a theoretical error variance of 0.0026 compared with 0.0085 for LLR (Set II), while for Direction 9 the figures are 0.0034 and 0.0129 respectively. These variances correspond to standard deviations of the order of 0.1°C, quite small on an estimate of one degree or more.

This level of error variance would hardly show up on a graph drawn to the scale of Figs 27 to 35 but the simulation results depart from the theory on three counts. Firstly the innovations do not have zero mean which gives rise to bias in the estimates. Secondly both LLR variants show a higher error variance than anticipated and thirdly the LLR (ONA) estimates tend to exhibit a much higher error variance than those generated by LLR (Set II).

These points can be examined more closely with the aid of Fig 42 which illustrates step fault 1(d), Section 6.9.1, which is a -3.17°C fault on TX110 (Direction 1) superimposed on data set PLANT8 at d.p.238. This example is also shown in Fig 27.

Fig 42 shows temperature TX110 drifting slowly downwards following the cooling water step change at d.p.192 (Section 6.1.1). This is on a large scale to emphasize changes of 0.1 - 0.2°C and the slight disturbance around d.p.255. From the top the traces are the four innovation components generated by a filter utilizing KGAINX (i.e. for LLR (ONA)), TX110 itself, the LLR (ONA) and LLR (Set II) estimates and the innovations corresponding to KGAINY (for LLR (Set II)). Under no-fault conditions, LLR (Set II) exhibits the greater innovation bias because this algorithm magnifies the steady state effect of instrument bias on the innovations. The estimates prior to d.p.238 (shown pecked) indicate the ρ values obtained by processing the no-fault innovations via Lemma 4.1. These estimates are suppressed by the llr threshold comparison which declares 'H_0 true' during this period. After d.p.238 each

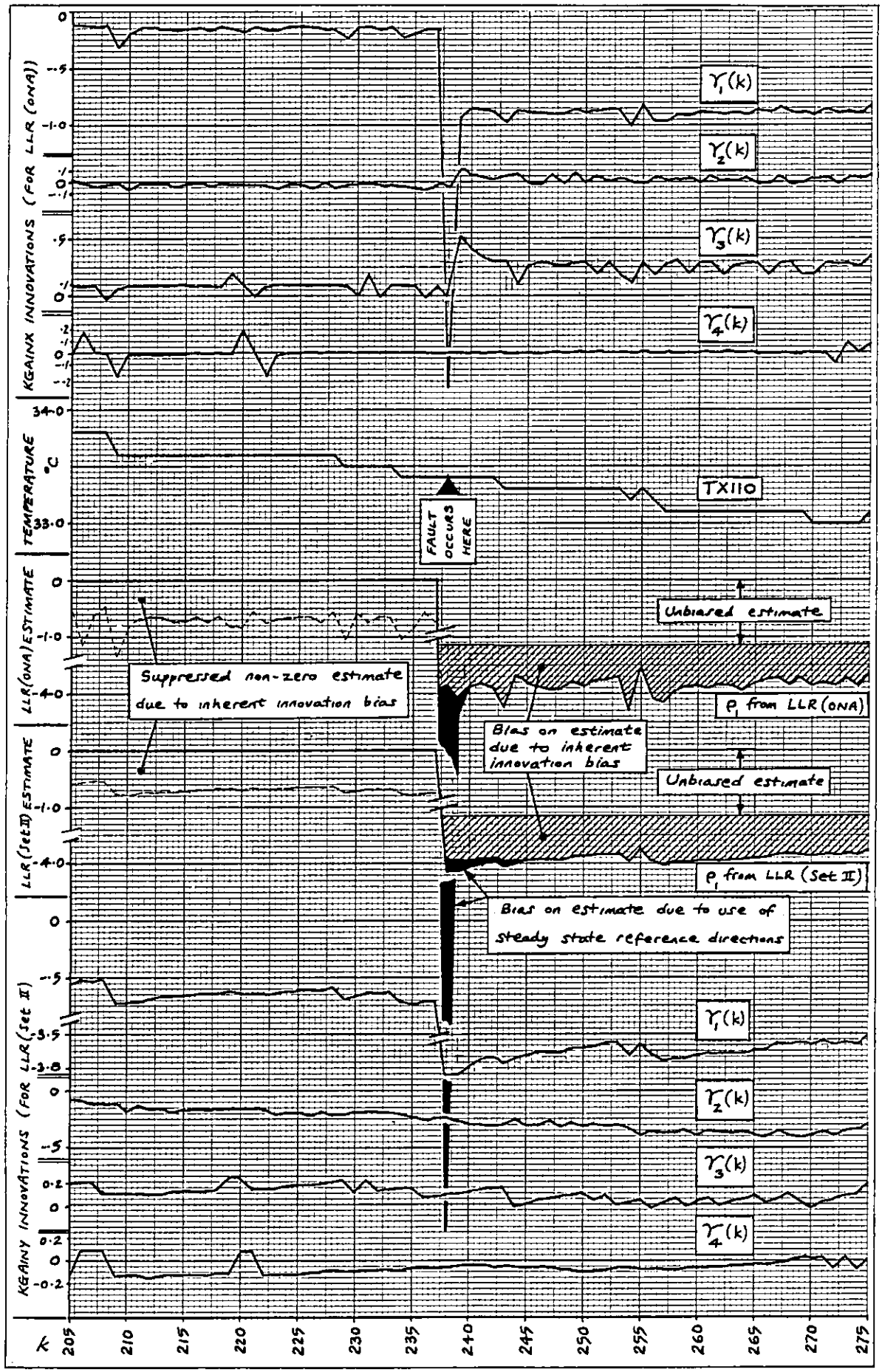

Fig.42 Analysis of Example 1(d), a -3.17°C step fault in Direction 1 (TX110) at d.p. 238 (PLANT8)

estimate is broken down into three components: the clear area corresponding to an unbiased estimate of the -3.17° fault itself, the shaded area caused by innovation bias and the solid area due to reference vector transients.

The key to error variance is sensitivity to the innovations. Because of the crude modelling and the fact that TX110 only measures to one place of decimals, small changes in TX110 are seen as negative-going step faults and are clearly picked up by KGAINX innovation components γ_1 and γ_3 and by KGAINY innovation component γ_1. The LLR (ONA) estimate relies primarily on γ_1 but to some extent on γ_2 and γ_3 as can be seen by lining up the disturbances in the appropriate traces. The LLR (Set II) estimate relies almost exclusively on γ_1 and follows it variations faithfully.

The theoretical comparison of error variance for the two algorithms fails because it does not take into account unmodelled disturbances: VX and VY were after all estimated from the comparatively smooth steady state data of run PLANT2. The downfall of LLR (ONA) comes with the dramatic overshoot of the estimate on each sample that contains a new fault: the algorithm magnifies every unmodelled disturbance in at least two of the four innovation components.

7.1.4 Cross-detection

In Section 5.8.5 it was shown by counterexample that maximum llr and minimum angle were not necessarily equivalent criteria for fault isolation decisions. Despite this it was still felt, at least before any simulation work had been carried out, that study of the variation in angle between f_i and d_i before reaching steady state could be a useful guide to algorithm performance as hinted in Section 5.6. A computer program was written to calculate the angle between the theoretical post-fault innovation bias f_i and the reference vector d_i, to which it tends, for

each failure direction 'i'. This showed that while LLR (Set II) reference vectors rotated no more than 5° in r-space before coming to rest in Direction d_i, LLR (ONA) vectors tended to swing four or five times as much over the first few time steps.

For a definite fault in Direction 'i', program LOGLRAT (Section 6.5.5) printed out the angle between the current innovation vector and reference vector d_i. Large faults tended to produce small angles, less than 10°, but with smaller faults a definite decision could surprisingly still be made with the innovation vector up to 60° away from the reference vector.

This result did not bode well for the success of the transient analysis. A fault in Direction 'A' might be detected correctly in one example only to be cross-detected as Direction 'B' in a second and Direction 'C' in a third. If a fault in Direction 'A' was cross-detected as Direction 'B' there was no guarantee that a fault in Direction 'B' would be confused with Direction 'A' as might have been expected. None of the transient cross-detections experienced was in fact sufficiently consistent to be satisfactorily explained by transient analysis of the f_i/d_i angle.

It was shown in Section 5.8.1 that P_U, the probability of uncertainty in making a fault isolation decision, could be reduced at the expense of increasing P_X, the probability of cross-detection. From the simulations certain examples such as 4(a)/LLR (Set II) were classic cases of cross-detection: here a fault in Direction 4 was confused with Direction 7. In every case such as this, the llr for the correct fault source was also significant against H_0 but was not sufficiently large when compared with H_j, the declared fault direction, to make the algorithm declare the fault as j-probable instead of j-definite. The number of occurrences of this type was far outweighed by the number of examples in which the Section 5.8.1 modification enabled the correct decision to be reached.

For almost every fault over 1° there were at least two, and sometimes four or five H_0-significant directions. Without the modification both LLR algorithms would have declared almost every fault as 'probable'.

7.1.5 Performance statistics

The large number of simulation examples carried out enables the two LLR algorithms to be compared on a statistical basis. Table 49 shows that the two variants are comparable with regard to the number of miss alarms and that each is more likely to miss an input fault than an output fault.

TABLE 49 - MISS ALARMS

D	1	2	3	4	5	6	7	8	9	TOT
ONA							4	3	2	9
SetII	1			1			1	3	1	7

For each example the data points between θ and the end-of-record can be divided into three categories: correct decision, cross-detection and miss. These are totalled for all examples and the results given in Tables 50-53. The first two tables give respectively the percentage of 0's declared after a fault and the percentage of correct decisions. Each is based on nearly 8000 post-fault data points with definite and probable decisions not differentiated.

TABLE 50 - PERCENTAGE '0' DECISIONS

D	1	2	3	4	5	6	7	8	9	o/a
ONA	57.2	7.4	30.0	98.8	45.7	1.1	100.0	65.6	46.6	53.9
SetII	43.7	0	0.1	53.0	1.1	1.1	54.8	61.4	33.3	32.3

TABLE 51 - PERCENTAGE CORRECT DECISIONS

D	1	2	3	4	5	6	7	8	9	o/a
ONA	41.0	73.7	63.1	1.0	50.0	98.9	0.0	30.4	45.5	40.3
SetII	55.6	83.5	99.5	24.5	98.9	95.6	6.4	38.6	58.6	57.6

In both respects LLR (Set II) shows a distinct improvement over LLR (ONA) with the single exception of Direction 6.

It is interesting to note how the non-zero decisions are distributed between correct decisions and cross-detections. Tables 52 and 53 give the percentages of non-zero decisions for Directions 1-9 following a fault in the direction given in column 1. Despite the failure of the transient analysis of the f_i/d_i angle in explaining

TABLE 52 - DISTRIBUTION OF NON-ZERO DECISIONS FOR LLR(ONA)

D	1	2	3	4	5	6	7	8	9
1	95.8				0.8				3.4
2	4.6	79.7				15.7			
3	1.4		90.1					0.4	8.1
4				84.6			15.4		
5					92.1		0.3	0.7	6.9
6						100			
7							0		
8			11.6					88.4	
9	9.4		0.3		5.1				85.2

TABLE 53 - DISTRIBUTION OF NON-ZERO DECISIONS FOR LLR(SetII)

D	1	2	3	4	5	6	7	8	9
1	98.8				1.2				
2	0.4	83.5				16.1			
3			99.6					0.4	
4				52.1	2.5		45.4		
5					100				
6						96.6			3.4
7			0.4	85.6			14.0		
8								100	
9	11.9					0.4			87.7

transient cross-detection, the steady state angles between reference vectors do have a bearing on the overall numbers of cross-detection decisions. Referring back to the angle tables of Section 6.3.3 the smallest angles were between Directions (5,9), (6,9), (2,6) and especially (4,7). Use of KGAINY improved only the first of these and it can be seen from Tables 52 and 53 that the percentages of

incorrect decisions between the Directions in each of these pairs increases with decreasing angle. There is a definite correlation between large numbers of cross-detections and small angles between reference directions, the best example being the confusion between Directions 4 and 7. Calculation of these angles is therefore justified and, as a rule of thumb, reference directions less than about 35° apart in r-space may give rise to cross-detection problems for this particular application.

7.2 Conclusions

In evaluating this thesis as a contribution to the field of fault detection, consideration should be given to the form the thesis might have taken had the work been approached from a purely theoretical viewpoint. The ideas formulated at the end of Chapter 4 could perhaps have been developed more formally than was done in Chapter 5, but the project would almost certainly have ended with computer simulation of a simple example. Supposing that the plant in Section 'A' of Fig A1.1 were chosen for this example, is it possible that the model chosen for simulation purposes would have resembled that developed in Chapters 2-4 of this thesis? Not only is this most unlikely, but also the 'ideal' nature of computer generated Gaussian noise, the unbiased measurements and the lack of linearization errors would almost certainly have led to a set of consistent and extremely promising results.

As shown by Jo and Bankoff [21], simulation studies of Kalman filtering may easily lead to overoptimistic conclusions. Willsky [27] points out that most fault detection work has been at a theoretical level with much work remaining in the development of implementable systems. This project is the antithesis of the purely theoretical approach, starting with the practical problem of designing an implementable fault detection system for Section 'A' of the plant illustrated in Fig A1.1 and testing it with real rather than simulated data.

The computational effort required to run a Kalman filter rises dramatically with increasing numbers of states and with the

accent on designing an implementable system the first requisite was to build a model with as few states as possible. The original intention was to employ a simple model based on the work of Palmquist [66] but it soon became apparent that this approach was inadequate for use with real data. It was not envisaged at the outset that so much effort would be required to develop a suitable model but the end result is a thesis falling neatly into two halves: Chapters 2 and 3 on modelling, Chapters 5 and 6 on fault detection with Chapter 4 as a bridge between the two.

It cannot be overemphasized that the first half of this thesis is not intended to be an attempt either to produce a very accurate model or to consider and model all physical aspects of the system. In either case many more parameters would be required and many other effects taken into account. It is, however, worth reiterating the observation from [19] that 'In engineering applications, the value of a model is not usually judged by its mathematical rigour or the elegance of the derivation but rather how well it fulfills a specific need in comparison with other alternatives.'

A poor model requires less effort to produce but the cost is measured in terms of loss of isolation capability and sensitivity. Suppose the system operation is stable at the nominal linearization point, i.e. the point at which the model matrices Φ and G have been evaluated. If there is a change in setpoint then there is a transient phase, lasting some four minutes, followed by a period of quasi-steady state operation, in reality a slow drift to a new stable operating point. Model predictions of the trajectories during the transient and the new level at which each variable stabilizes are governed by both Φ and G. Inaccuracy in either matrix leads to discrepancies between the modelled and actual trajectories, biased innovations and increase in log-likelihood ratio during the transient. This in turn means that the llr threshold above which a fault is declared must be set higher to avoid false alarms during the transient, thus reducing sensitivity. Note that many of the maximum llr's identified in Section 6.5.3 occurred during transients.

It is implied throughout that when the algorithm is first set up, the filter is based on a model whose matrices are evaluated at the stable operating point at which the plant is operating at that time. Recall that due to nonlinearity the partial derivatives required to evaluate Φ and G are dependent on the operating point. While the plant remains at this initial operating point, any instrument bias already present has no effect because it is effectively subtracted out by the linearization procedure. Note that none of the Chapter 6 examples were of faults occurring before the first setpoint change on either PLANT7 or PLANT8. This would have been almost as potentially unreliable a guide to performance as the use of computer simulated data. If there is any inherent instrument bias then the operating point about which the system is linearized is not the true operating point, giving rise to errors in the partial derivatives and model inaccuracy. Linearization error cannot be removed without resorting to some form of nonlinear filtering: as soon as a change in setpoint occurs the linearization error and the modelling errors give rise to an innovation bias which may drive the log-likelihood ratios higher than those experienced during transients. This results in even higher thresholds and further loss of sensitivity.

Isolation is effected by comparison of the orientation in r-space of the post-fault innovation vector with that of a reference vector. If innovation bias already exists then the resultant post-fault innovation will deviate from the reference direction by an amount dependent on the magnitude and direction of the existing bias and may result in uncertainty or cross-detection. The time spent in developing a 'reasonably' accurate steady state model is therefore seen to be necessary. Clearly it is also important to ensure that measurement loops introduce little or no bias at the commencement of filtering.

The optimal Kalman filter requires the specification of an a priori error covariance $P(0|0)$ which is usually chosen fairly conservatively. This results in a Kalman gain whose elements decrease in magnitude over the first few time steps so that the gain lends more weight to the first few innovations to correct any error in the a priori state estimate $\hat{x}(0|0)$. Constant gain

filters dispense with this refinement but this does not matter in the present application where, by linearizing at the initial stable operating point, all states are assumed to be initially zero. Chapter 5 goes to some lengths to 'throw off the shackles' of having either to design a filter to conform to some physically realisable system or to try to obtain reliable state estimates. Once these constraints are discarded the system can be designed purely for fault detection purposes.

Fault detection is essentially a decoupling problem. The first filter, designed around the 'original noise assumptions' and used for LLR (ONA), can be considered close enough to optimal to assume that it at least gives a guide to the way an optimal filter would behave. With this filter the effect of any fault is distributed over the four innovation vector components. Isolation is enhanced if faults can be decoupled, i.e. if two faults can be constrained to affect non-overlapping sets of innovation components then the reference vectors for these faults will be orthogonal. Clearly nine faults cannot be totally decoupled using only four innovation components but KGAINY, derived from the Set II noise assumptions, succeeded in decoupling the effects of output faults $\underline{y}_f(1)$ - (4). Having paved the way to unrestricted manipulation of the Kalman gain for fault detection purposes, no method was found to take full advantage of this. KGAINY is still based on physically realisable noise covariance matrices but is at least a step in the right direction.

The question of divergence has been discussed but it cannot be categorically stated that there exists no Kalman gain that would eventually cause divergence with this system despite giving rise to a stable filter transition matrix Ψ. Another weakness of the LLR algorithms is the setting of alarm thresholds. It was in an attempt to avoid having to specify these that the unsuccessful RCP algorithm was proposed. Having shown in Section 5.8.3 that it is extremely difficult to set thresholds to give desired values for P_M, P_F etc, it is envisaged that suitable thresholds could only be obtained in practice by monitoring over a period of time the log-likelihood ratios generated for each failure direction under normal operation. It is probable that the thresholds would be pushed higher than those given in Table 23

and that the algorithms would become less sensitive as a result.

The algorithm design does not appear to be particularly well suited to the detection of input faults except for flow faults which are treated and detected as if they were output faults. Input faults have very little effect on the innovations when using KGAINX (Table 17), while LLR (Set II), which uses KGAINY, exhibits an overdamped response to an input step, again causing problems.

In conclusion, this project has shown that the selected portion of the CO_2/N_2 separation plant can be modelled using six states only and with sufficient accuracy to permit its use with a log-likelihood ratio technique for fault detection. Two LLR algorithms were designed and tested with real plant data in comparison with a simple χ^2 method. Although the latter showed some promise as a detector, the LLR algorithms provided in addition fairly reliable fault isolation and estimation. While no one design was suitable for all types of fault the suboptimal LLR (Set II) was found to perform consistently better than the approximately optimal LLR (ONA).

The main limitations of the technique are that it can be used only for instrumentation faults, it cannot handle multiple faults and it is restricted to time-invariant systems.

7.3 The LLR algorithm in perspective

Although Willsky's survey paper [27] divides fault detection methods into a number of basic types, many algorithms use similar ideas and could be placed in more than one category. The LLR algorithms presented in this thesis have much in common with other fault detection techniques employing Kalman filters and this section serves to highlight the differences and similarities.

Modification of a filter to enhance its fault detection capabilities almost inevitably leads to degradation of the state estimates. If a system required estimates for control purposes it would be necessary to use a separate optimal filter to provide these in addition to the suboptimal filter used with an algorithm

such as LLR (Set II).

The only filtering described by Willsky as being tailored specifically to fault detection at the expense of reliable state estimation is that of Beard and Jones (see Willsky [27], Beard [31]). From their work on continuous-time deterministic systems comes the idea of monitoring the innovation direction to identify the fault or at least to narrow it down to a small number of possibilities.

The unsuccessful RCP algorithm (Section 4.9.4) was derived from Bayes' theorem,but the idea of using the theorem in this way was culled from the multiple hypothesis technique of Buxbaum and Haddad [43] (see also Willsky, Deyst and Crawford [44], [45]). These last two references include work on the χ^2 test which was used in this project for comparison. This method is the simplest of the schemes falling into Willsky's "innovation based detection systems", a category which includes the LLR algorithms presented in this thesis and the GLR techniques to which they are related. The (log-) likelihood ratio is defined in Van Trees [54] as a means of attributing a sequence of observations to one of a pair of distributions whose parameters are based on hypotheses H_1 and H_0. If the parameters cannot be estimated until the correct hypothesis is known then the generalized likelihood ratio (GLR) must be used. The 'LLR' algorithms do require estimation of the fault magnitude (i.e. by assuming H_i true, $i \neq 0$) before the log-likelihood ratio can be calculated. Although this technically qualifies them as 'GLR' algorithms the name 'GLR' has deliberately not been used to avoid confusion with the GLR algorithms described by Willsky [27] and by Willsky and Jones [55], [56]. These algorithms were discussed in the introductory chapter and so it is only necessary to give here a comparison of the salient points of GLR and LLR (Set II). Table 54 is based on input and output measurement faults only; the word 'filter' refers to the part of the algorithm which generates the innovations and 'detector' to the part which monitors the innovations for fault detection purposes.

While LLR (Set II) borrows some ideas, particularly from CGLR, it is clearly a distinct algorithm and, for a system which does not

TABLE 54

	GLR	LLR(Set II)
1. Type of filter	Optimal Kalman	Suboptimal Kalman
2. Fault isolation and estimation	Yes	Yes subject to (3)
3. Constraints on type of fault for which algorithm can be used	Full GLR:unconstrained	Fault lies in direction d_i,i=1,...q
	CGLR: fault lies in direction d_i,i=1,...q	
	SGLR: fault exactly specified	
4. Looks at full transient effect of fault on innovations	Full GLR: yes. Simplified version looks at transient inside moving window of innovations	No: only at a single innovation and at the steady state effect of the fault
5. A single detector can be used to look for faults in both input and output measurements	No: would require separate detectors with 'u' and 'y' failure signature matrices	Yes: the 'u' and 'y' failure signatures are effectively combined into FMAT
6. A single detector can be used for either step or jump faults on a given type of measurement	No: would require separate 'step' and 'jump' failure signature matrices	Yes: single innovation monitoring ignores differing transient effects of step and jump faults
7. Innovation storage requirements	Full GLR stores all innovations since start of filtering. Simplified version stores all innovations from start of window to present	No storage required
8. Comparisons with likelihood ratio threshold at time k	One	One for each of the 'q' hypothesized failure directions
9. Estimation of the time of occurrence of the fault	MLE requiring linear combination of all stored innovations	Not estimated as such: fault assumed to occur when alarm threshold crossed by any $\ell n\Lambda(\gamma)$
10. Estimation of the fault magnitude	MLE which is an explicit function of time estimate $\hat{\theta}$	Least squares estimate from single innovation (equivalent to MLE)
11. Provides optimal estimate of x under no-fault conditions	Yes	No: would require optimal filter running in parallel
12. Adaptive state estimation	Yes: extension to algorithm available	Not at present, but detector output could be used to update parallel optimal filter (see Sec.7.4)

require state estimates, offers several advantages. LLR involves less computational effort than GLR, requires no storage of innovations and can detect, isolate and estimate both step and jump faults on both outputs and to some extent inputs without the need for additional detectors.

The first half of this project was developed along similar lines to the contribution of Bellingham and Lees [50],although the modelling is somewhat cruder than theirs and includes six states and four observations against two of each in [50]. Selection of a part of the pilot plant has the advantage that the LLR algorithms were tested on something approaching an industrial plant rather than an isolated laboratory rig and the inclusion of input measurement faults is an unusual feature in any published work on fault detection. The path followed in this thesis diverges from that of Bellingham and Lees following the failure of the Mehra/ Godbole algorithm [10], [11] due to low plant noise levels: they added artificial measurement noise in an attempt to develop an optimal filter. Neither LLR variant makes any attempt to measure or compensate for bias, while Bellingham and Lees used Friedland's technique [15] to reduce innovation bias and to provide another fault indication, the bias estimate.

Another important difference in the testing of algorithms is that in [50] the plant was always run at the setpoint at which the model was derived, something specifically avoided in this project. Bellingham and Lees suggest that no-fault innovation means and/or bias values could be stored at selected setpoints for retrieval when necessary. This may well be possible on a small isolated rig,but experience on the pilot plant suggests that where heat transfer is involved results are not sufficiently repeatable to make this a practical proposition. In this situation it may be better to use a robust algorithm which will work over a range of setpoints in the presence of small but variable bias.

7.4 Suggestions for further work

While the thesis is fairly evenly divided between plant modelling and fault detection, most of the areas where extension is possible fall into the second category: there is little that can be done

to improve the work covered by Chapters 2 and 3 without making the model more complex by the introduction of more parameters.

The numerical methods of Chapter 2 leave something to be desired and work could be done on calculating and perhaps improving the accuracy of parameter estimation. The validity of the assumption that the liquid temperatures are independent of the actual ambient temperature could also be investigated more thoroughly, although this is not easy to arrange in practice. A useful addition would be determination of the range of flow rates either side of setpoint over which the linearization holds good.

The logical next step in modelling is the extension of the section of plant covered by the detection system to include Section 'B' of Fig.A1.1, i.e. the level control loop at the base of the absorber. In isolation Section 'B' resembles the laboratory rig of Bellingham and Lees [50] but differs in that advantage can be taken of the interaction between this loop and Section 'A' of the plant (Fig.A1.1). Run PLANT8 included a level setpoint change (Table 15) and the resulting changes in temperature are shown in Fig.43. FX101, the flow rate of stripped MEA into the absorber, is unaffected by a level setpoint change; to make level LX111 rise some liquid is held back by partial closure for a few seconds of valve CV111 which is reflected by a dip in the recorded spent MEA flow rate FX125. In this case it will not be possible for modelling purposes to substitute a delayed version of FX101 for the noisy FX125 measurement because FX101 remains at setpoint. The approach that suggests itself is to derive an idealized FX125 from the LX111 measurement itself. Level faults could be treated and detected as output temperature faults in much the same way as for FX101 and FX124, except that here the effect on the temperatures is only temporary as shown by Fig.43.

It may well not be possible to manipulate the Kalman gain for complete control over the orientation of the fault reference vectors in r-space, except perhaps in certain special cases such as full state measurement (cf. the example given by Willsky in [27] from the work of Beard and Jones). The ideal is to gain sufficient control over the reference vectors to be able to separate out those between which fault isolation is considered

Fig.43 Effect on the plant temperatures of a setpoint change in absorber MEA level (LX111) Data: PLANT8

the most important, if necessary 'bunching up' the remainder. There is no reason why several filters employing constant gains with different isolation properties could not be run in parallel. This is not as computationally expensive as it sounds, because the use of a constant gain eliminates filter steps (3), (4) and (8) in Section 4.4 and saves a matrix inversion at step (5).

The tradeoff between sensitivity and cross-detection could be further investigated: it may pay to set certain alarm thresholds higher to avoid declaring a fault unless it is large enough to ensure correct isolation. The method of comparing log-likelihood ratios when more than one H_i, $i \neq 0$ is significant against H_0 could also be reviewed. The intuitive approach in Section 6.5.4 was to declare a definite fault in direction 'j' only if the llr for H_j was in excess of that for H_i by at least as much as it was in excess of the H_j:H_0 threshold.

Perhaps new thresholds should be set for llr tests on each pair of H_0-significant hypotheses when this situation arises. Another possibility to improve sensitivity is to suppress the larger log-likelihood ratios that occur during transients following setpoint changes,thus allowing lower thresholds to be used during periods of steady operation. This approach has a precedent in vibration monitoring systems often used in industry to protect large rotating machines. A higher threshold is used for a specified time during start-up to avoid spurious alarm or trip out.

Both estimation accuracy and isolation capability are reduced by the presence of bias in the innovations. While in practice measurement loop bias should be kept at a minimum by a comprehensive maintenance programme and regular instrument recalibration, the LLR algorithm would be improved by greater robustness in the presence of such bias. This can only be done at the expense of increased computational effort and might be tackled either by augmenting the state vector or by re-linearizing about the new operating point after a change in setpoint. To judge the efficiency of the LLR algorithm in terms of performance against computation time and storage, it would be instructive to

compare its performance with the CGLR algorithm both in its full and simplified forms. Note that the computational requirements of LLR could be reduced by employing a simpler technique, such as the χ^2 test, to give an alarm on the occurrence of a fault and to trigger off the llr-based detector.

Subjects closely allied to fault detection are compensation and system re-organization. Ideally, having identified and estimated the fault, the detector should then be able to reset itself so that it can look for subsequent faults. In the case of the LLR algorithm, a new fault estimate is generated from every innovation. The technique would require some modification to enable the steady state effect of the fault to be subtracted out of the innovations to bring the mean back to (near) zero.

Mention was made in Section 7.3 of the provision of optimal state estimates and the fact that with LLR (Set II) an optimal filter would have to be run in parallel if estimates were required for control purposes. The parallel filter would be entirely separate and could be based on a higher order model of the plant, perhaps with the inclusion of some of the filter 'adjustments' which abound in the literature. In this case it would be interesting to see whether the use of a GLR or LLR detector in conjunction with the optimal filter was more efficient than the combined use of an optimal filter for state estimation and a parallel lower order suboptimal filter coupled to an LLR detector. In either case the detector output could be used to compensate for the effects of the fault on the optimal filter state estimates, a method for achieving this being given by Willsky and Jones [55].

System re-organization may be possible in some instances if certain instruments become unreliable. In the case of the pilot plant, measurement of the flow rate of cooling water to the cooler (FX124) is a good example. This flow rate is normally controlled by the loop CV110/FX124, but if FX124 were to fail the loop could be reconfigured by modifying the existing LLR algorithm to maintain at a setpoint the stripped MEA outlet temperature, TX110. On some plants it may be possible to use a state estimate as a substitute measurement. This could not

however be done on the subsequent failure of TX110 even though it is a system state (x_1) because, as shown in Section 4.5, this would result in the system becoming unobservable.

APPENDIX I

A BRIEF DESCRIPTION OF THE PLANT

A1.0 Introduction

Chemical solvent processes for gas sweetening involve the use of either alkanolamines or of alkaline salt solutions. In Ammonia synthesis-gas purification, for example, removal of Carbon Dioxide is required. Hydrogen Sulphide being absent, [85] proposes as a suitable choice of solvent an aqueous solution of monoethanolamine (MEA). First developed in the 1920's, processes utilizing MEA are widely used in industry on account of the relatively low plant investment required, low solvent costs and ease of reclamation [86]. Serious corrosion problems at high MEA concentrations, as discussed in [87], have been largely overcome by the addition of the corrosion inhibitor "Amine Guard", developed by Union Carbide [88], [89].

A1.1 Plant Operation

The pilot plant removes Carbon Dioxide from a Nitrogen stream by counter-current absorption in a 10% aqueous solution of monoethanolamine, $HO.CH_2.CH_2.NH_2$.

As shown diagrammatically in Fig. A1.1, the gas mixture, containing up to 10% CO_2, is introduced near the base of an absorption column packed with ceramic 'pall rings' and operating at about 250 kNm^{-2}. MEA, at about 35^0C, percolates down through the packing to a pool at the base, removing the Carbon Dioxide by chemisorption so that almost pure Nitrogen issues from the top where it is passed to a cyclone for removal of spray.

The Carbon Dioxide dissolved in the 'spent' MEA is released by reduction of pressure and boiling in a stripper column containing twenty sieve plates. The MEA passes through a counter flow heat exchanger to enter the column a few plates from the top via a flash valve. Steam and vapour from the reboiler system constantly bubble through the plates liberating much of the dissolved gas from the solvent. Now containing about half as much Carbon Dioxide as before, 'stripped' MEA at over 100^0C is pumped from

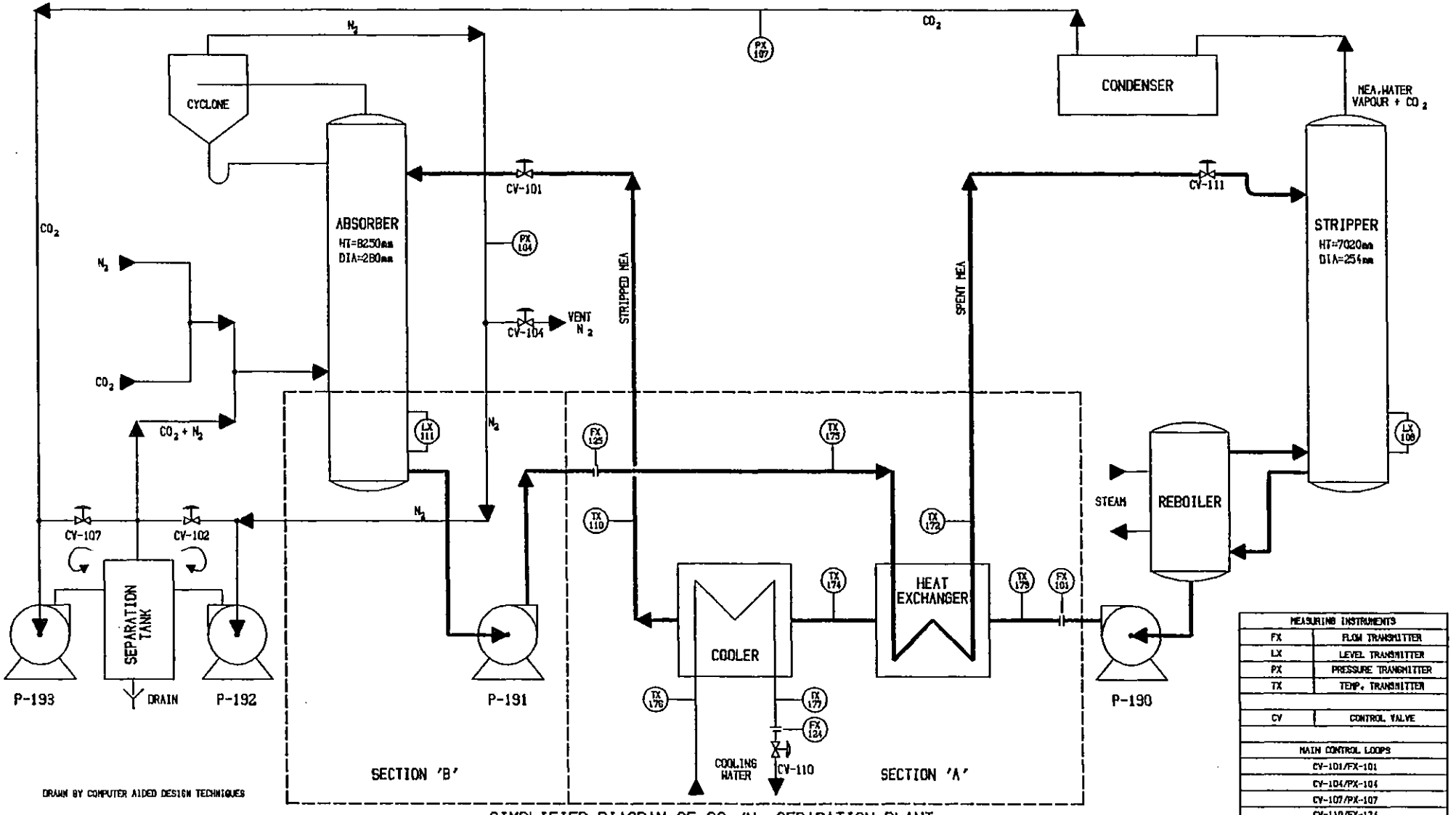

FIG A1.1 SIMPLIFIED DIAGRAM OF CO_2/N_2 SEPARATION PLANT
DEPT. OF CHEMICAL ENGINEERING IMPERIAL COLLEGE LONDON

the bottom of the reboiler. The liquid must be cooled before re-use, this being done in two stages by first using it to preheat the incoming spent MEA and then by passing it through a cooler on its way back to the absorber.

This particular plant can be run in the 'closed loop' configuration shown in Fig. A1.1, in which case both gases are recycled. The seal water required by positive displacement type compressors P-192 and P-193 is pumped out with the gases and is drained off by a separation tank.

Pressure in the absorber, PX104, is maintained at setpoint by allowing a small amount of Nitrogen to bleed to atmosphere via CV104, also limiting the build-up of impurities. The stripper pressure, PX107, is regulated by control valve CV107 which acts as a variable 'short circuit' across compressor P-193. Valve CV102, performing a similar function on compressor P-192, is usually left set at 50% open.

An interesting control problem arises in maintaining a steady flow of MEA around the figure-of-eight path indicated by heavy lines in Fig. A1.1. It is important that the level of the pool at the base of the absorber is kept within limits: too high and the MEA will run back down the gas inlet pipe; too low and the pressure at the inlet of compressor P-191 may fall below the required net positive suction head resulting in cavitation.

There is considerable liquid hold up in the absorber due to the packing, which introduces a flow-dependent transport delay measurable in tens of seconds. This prohibits the regulation of level by manipulation of flow FX101 into the absorber due to the delayed effect of any control action. Absorber level LX111 must therefore be controlled by using CV111 to regulate the amount of spent MEA pumped out of the absorber.

Having thus constrained liquid transfer from absorber to stripper, attention can be focussed on the return of stripped MEA from stripper to absorber. In maintaining the absorber level at setpoint, the spent MEA flow rate FX125 fluctuates slightly resulting in a varying rate of liquid build-up at the stripper

base. If CV101 is used to control the stripper level, this varying MEA input will be reflected in larger variations in the spent MEA flow rate out of the stripper. The effect will propagate around the system resulting in instability.

In practice CV101 is incorporated into a second control loop to regulate stripped MEA flow rate FX101, using the reservoir of MEA in the reboiler and stripper as a buffer and allowing its level to fluctuate slightly.

A1.2 Instrumentation

It should be noted that Fig A1.1 does not show all control loops and includes only the instrumentation of interest for this particular project. The plant in fact carries a variety of conventional instruments typical of the process industry, allowing a wide range of experiments to be carried out.

The Fisher control valves are of the equal percentage type with 1, 2 or 3 flutes and all flow rates required for this project are measured by means of orifice plates. The latter are used in conjunction with pressure to current convertors as are the differential pressure cells used for level measurement. Temperatures are measured by platinum resistance thermometers from which voltage signals are obtained by bridge circuits.

The accuracy of an orifice plate drops off slightly with wear, but a loop accuracy of around ±2% might be expected, compared with about ±1% for a level measurement loop.

A1.3 Computer System

The system, described in greater detail in [90], is built around a Honeywell DDP 516 computer with 32K of core and a 1M fixed head disk back-up. Peripherals include an operator's console, an ASR teletype for program manipulation and a VDU, while a second teletype and a high speed paper tape punch are provided for data logging.

A1.3.1 Computer Control of Plant

To create simple control loops based on a discrete time 3-term (PID) algorithm, a process variable is assigned to each control valve using the operator's console from which proportional gain, integral time and, if required, derivative time can also be specified. The console is also used to enter the loop setpoint. For loops with a short response time a setpoint alteration can be used to obtain a good approximation to a step change in a regulated variable.

Electrical signals from the plant reach the computer via a real time interface which sequentially scans the inputs. For critical variables, such as absorber level or pressure, the scanning interval is set to half a second, while a temperature not used in a control loop may only be scanned every 32 seconds.

For each loop the computer uses the velocity form of the PID algorithm (see Smith [91]) to arrive at a control signal. This is transmitted via a standard 4-20 mA loop to a current/pneumatic pressure convertor which drives the valve.

A1.3.2 Recording of Process Variables

Process variables can be recorded on paper or paper tape by the use of a logging routine. For monitoring purposes, instrument readings can be printed out every few minutes by the ASR teletype, but for recording of transients requiring sampling intervals of a few seconds this is clearly impracticable. The high speed punch allows data to be recorded on tape at a much higher rate and in a form suitable for direct loading onto another computer for subsequent off-line data analysis.

This facility was used in conjunction with this project to create permanent data files on the college computer system from real plant runs recorded on tape. The performance of various fault detection algorithms could

then be compared under absolutely identical plant conditions.

A1.3.3 Operation in the steady state

Steady state operation is reached an hour or so after start up of the plant. If liquid temperatures such as TX110, TX174, TX175 and TX177 are printed out every few minutes on the ASR, this helps to determine the point at which the plant has settled down sufficiently for experimental work to begin.

Typical setpoints for process variables are:

Stripped MEA flow rate	CV101/FX101	0.15-0.35 kgs^{-1}
Absorber pressure	CV104/PX104	250 kNm^{-2}
Stripper pressure	CV107/PX107	105 kNm^{-2}
Cooler c/w	CV110/FX124	0.1-0.3 kgs^{-1}
Absorber MEA level	CV111/LX111	0.2-0.3 m

Derivative terms are not normally used with these loops but typical values of the proportional and integral terms, κ_P and κ_I, for the PID algorithm are given below. It should be noted that each value includes a normalization factor for the controlled variable based on the range of the measuring instrument. The terms do not therefore correspond directly to those of Section 6.9 in Smith and are quoted primarily for the benefit of future researchers at Imperial College.

Controlled variable	κ_P	κ_I
FX101	0.5	0.2
PX104	20.0	2.0
PX107	5.0	0.2
FX124	1.0	0.2
LX111	30.0	0.9

These settings were used as standard for all experimental work covered by this thesis.

APPENDIX II

MEAN TEMPERATURE CALCULATION FOR A COUNTER-FLOW HEAT EXCHANGER

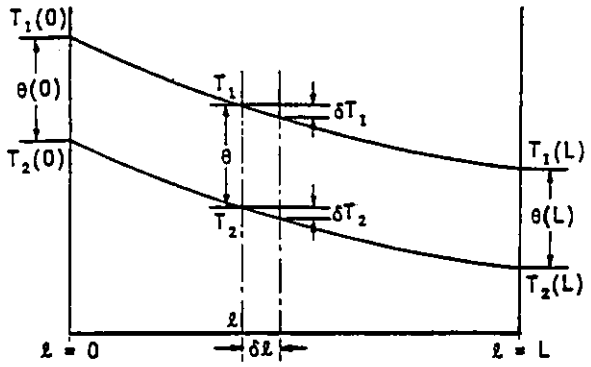

$T_1(\ell)$ = hot fluid temperature at 'ℓ'
$T_2(\ell)$ = cold fluid temperature at 'ℓ'
$\theta(\ell) = T_1(\ell) - T_2(\ell)$
T_{1m} = mean temperature hot fluid
T_{2m} = mean temperature cold fluid
θ_m = mean temperature difference

Fig.A2.1 Temperature profiles for counter flow heat exchanger

Assuming no losses to the air, the total heat transfer, Q_h, between the two fluids is governed by the mean temperature difference, θ_m, between them. Clearly $\theta_m = T_{1m} - T_{2m}$, the difference between the mean temperatures of the fluids themselves.

The total heat transfer, Q_h, can be written in three ways:

$$Q_h = K_{12}\theta_m \qquad \ldots (A2.1)$$

$$Q_h = F_1 C_{p1} \{T_1(0) - T_1(L)\} \qquad \ldots (A2.2)$$

$$Q_h = F_2 C_{p2} \{T_2(0) - T_2(L)\} \qquad \ldots (A2.3)$$

where K_{12} is the heat transfer coefficient between the fluids.

(A2.1) and (A2.2) can be combined to give

$$\left[\frac{1}{F_1 C_{p1}} - \frac{1}{F_2 C_{p2}}\right] = \frac{T_1(0)-T_2(0)-\{T_1(L)-T_2(L)\}}{Q_h} \qquad \ldots (A2.4a)$$

$$= \frac{\theta(0)-\theta(L)}{Q_h} \qquad \ldots (A2.4b)$$

Now define $\theta(\ell) = T_1(\ell) - T_2(\ell)$ and consider the heat transfer across a small element of the exchanger, length $\delta\ell$. With reference to Fig. A2.1, δT_1, δT_2 and F_2 are all in the negative sense giving rise to three equations for heat transfer δQ_h:

$$\delta Q_h = K_{12}\theta(\ell)\frac{\delta\ell}{L} \qquad \ldots \quad (A2.5)$$

$$\delta Q_h = -F_1 C_{p1} \delta T_1 \qquad \ldots \quad (A2.6)$$

$$\delta Q_h = F_2 C_{p2} \delta T_2 \qquad \ldots \quad (A2.7)$$

$$\therefore \quad \delta\theta = \delta T_1 - \delta T_2 = -\delta Q_h \left[\frac{1}{F_1 C_{p1}} - \frac{1}{F_2 C_{p2}} \right] \qquad \ldots \quad (A2.8)$$

Substituting from (A2.4b) for the term in square brackets

$$\delta\theta = -\frac{\delta Q_h}{Q_h} \{\theta(0) - \theta(L)\} \qquad \ldots \quad (A2.9)$$

and from (A2.5) for δQ_h

$$\delta\theta = -\frac{K_{12} \{\theta(0) - \theta(L)\} \theta(\ell)}{Q_h} \cdot \frac{\delta\ell}{L} \qquad \ldots \quad (A2.10)$$

Integrating over the length of the exchanger and re-arranging

$$Q_h = K_{12} \frac{\{\theta(L) - \theta(0)\}}{\ell n \left[\frac{\theta(L)}{\theta(0)}\right]} \qquad \ldots \quad (A2.11)$$

But $Q_h = K_{12}\theta_m$ (A2.1)

$$\therefore \quad \theta_m = \frac{\theta(L) - \theta(0)}{\ell n \left[\frac{\theta(L)}{\theta(0)}\right]} \qquad \ldots \quad (A2.12)$$

This is a standard result and may be found in Simonson [92]

Equation (A2.11) allows substitution for Q_h in (A2.10) leading to an expression for the distribution of $\theta(\ell)$ with distance 'ℓ' along the exchanger:

$$\delta\theta = \theta(\ell)\,\frac{\delta\ell}{L}\,\ell n\left[\frac{\theta(L)}{\theta(0)}\right] \qquad \ldots (A2.13)$$

$$\int_0^{\ell}\frac{d\theta}{\theta(\ell)} = \frac{1}{L}\,\ell n\left[\frac{\theta(L)}{\theta(0)}\right]\int_0^{\ell} d\ell \qquad \ldots (A2.14)$$

$$\ell n\left[\frac{\theta(\ell)}{\theta(0)}\right] = \frac{\ell}{L}\,\ell n\left[\frac{\theta(L)}{\theta(0)}\right] \qquad \ldots (A2.15)$$

$$\left[\frac{\theta(\ell)}{\theta(0)}\right] = \left[\frac{\theta(L)}{\theta(0)}\right]^{\frac{\ell}{L}} \qquad \ldots (A2.16)$$

and re-arranging

$$\theta(\ell) = \theta(0)\left[\frac{\theta(L)}{\theta(0)}\right]^{\frac{\ell}{L}} \qquad \ldots (A2.17)$$

This result can now be used to derive the temperature distributions and hence the mean temperatures of fluids 1 and 2.

Combining (A2.5) and (A2.6)

$$\delta T_1 = -\frac{K_{12}\theta(\ell)}{F_1 C_{p1}}\cdot\frac{\delta\ell}{L} \qquad \ldots (A2.18)$$

and substituting for $\theta(\ell)$ from (A2.17)

$$\delta T_1 = \frac{K_{12}\theta(0)}{F_1 C_{p1} L}\left[\frac{\theta(L)}{\theta(0)}\right]^{\frac{\ell}{L}}\delta\ell \qquad \ldots (A2.19)$$

Integrating

$$T_1(\ell) - T_1(0) = -\frac{K_{12}\theta(0)}{F_1 C_{p1} L} \int_0^{\ell} \left[\frac{\theta(L)}{\theta(0)}\right]^{\frac{\ell}{L}} d\ell \qquad \ldots (A2.20)$$

$$T_1(\ell) = T_1(0) + \frac{K_{12}\theta(0)}{F_1 C_{p1} \ell n\left[\frac{\theta(L)}{\theta(0)}\right]} \left\{1 - \left[\frac{\theta(L)}{\theta(0)}\right]^{\frac{\ell}{L}}\right\} \qquad \ldots (A2.21)$$

The mean value of $T_1(\ell)$ is found by a second integration:

$$T_{1m} = T_1(0) + \frac{K_{12}}{LF_1 C_{p1} \ell n\left[\frac{\theta(L)}{\theta(0)}\right]} \int_0^{L} \left\{1 - \left[\frac{\theta(L)}{\theta(0)}\right]^{\frac{\ell}{L}}\right\} d\ell \qquad \ldots (A2.22)$$

and by using (A2.12)

$$= T_1(0) + \frac{K_{12}}{F_1 C_{p1} \ell n\left[\frac{\theta(L)}{\theta(0)}\right]} \{\theta(0) - \theta_m\} \qquad \ldots (A2.23)$$

(A2.1) and (A2.2) combine to give

$$\frac{K_{12}}{F_1 C_{p1}} = \frac{T_1(0) - T_1(L)}{\theta_m} \qquad \ldots (A2.24)$$

and by substitution into (A2.23) and simplification using (A2.12)

$$T_{1m} = T_1(0) + \frac{T_1(0) - T_1(L)}{\theta(L) - \theta(0)} \{\theta(0) - \theta_m\} \qquad \ldots (A2.25)$$

Hence $T_{1m} = \dfrac{T_1(0)\theta(L) - T_1(L)\theta(0) - \theta_m \{T_1(0) - T_1(L)\}}{\theta(L) - \theta(0)}$ ... (A2.26)

By definition $T_{2m} = T_{1m} - \theta_m$

$$\therefore \quad T_{2m} = \frac{T_1(0)\theta(L) - T_1(L)\theta(0) - \theta_m \{T_2(0) - T_2(L)\}}{\theta(L) - \theta(0)} \qquad \ldots \quad (A2.27)$$

APPENDIX III

STEADY STATE MEAN LIQUID TEMPERATURES FOR THE THREE-FLUID HEAT EXCHANGER MODEL

Expression (2.28), here renumbered (A3.1), gives the temperature distributions of the liquids within the three fluid heat exchanger model. From this equation an expression for the steady state mean liquid temperatures can be derived.

The temperature distributions are given by:

$$\begin{bmatrix} T_1(\ell) \\ T_2(\ell) \end{bmatrix} = e^{B\frac{\ell}{L}} \begin{bmatrix} T_1(0) - T_3 \\ T_2(0) - T_3 \end{bmatrix} + \begin{bmatrix} T_3 \\ T_3 \end{bmatrix} \quad \ldots \quad (A3.1)$$

A3.1 Mean liquid temperatures

From (A3.1)

$$\begin{bmatrix} T_{1m} \\ T_{2m} \end{bmatrix} = \left[\frac{1}{L} \int_0^L e^{B\frac{\ell}{L}} \, d\ell \right] \begin{bmatrix} T_1(0) - T_3 \\ T_2(0) - T_3 \end{bmatrix} + \begin{bmatrix} T_3 \\ T_3 \end{bmatrix} \quad \ldots \quad (A3.2)$$

which leads, for nonsingular B, to

$$\begin{bmatrix} T_{1m} \\ T_{2m} \end{bmatrix} = B^{-1}[e^B - I] \begin{bmatrix} T_1(0) - T_3 \\ T_2(0) - T_3 \end{bmatrix} + \begin{bmatrix} T_3 \\ T_3 \end{bmatrix} \quad \ldots \quad (A3.3)$$

But by writing $\ell = L$ in (A3.1)

$$e^B \begin{bmatrix} T_1(0) - T_3 \\ T_2(0) - T_3 \end{bmatrix} + \begin{bmatrix} T_3 \\ T_3 \end{bmatrix} = \begin{bmatrix} T_1(L) \\ T_2(L) \end{bmatrix} \quad \ldots \quad (A3.4)$$

and substituting in (A3.3)

$$\begin{bmatrix} T_{1m} \\ T_{2m} \end{bmatrix} = B^{-1} \begin{bmatrix} T_1(L) - T_1(0) \\ T_2(L) - T_2(0) \end{bmatrix} + \begin{bmatrix} T_3 \\ T_3 \end{bmatrix} \quad \ldots \quad (A3.5)$$

Writing $T_i(L) - T_i(0) = \Delta_i, \quad i = 1,2$

$$[\Delta_1 \quad \Delta_2]^T = \underline{\Delta}$$

$$[T_{1m} \quad T_{2m}]^T = \underline{T}_m$$

and $$[T_3 \quad T_3]^T = \underline{T}_3$$

We have the result

$$\underline{T}_m = B^{-1}\underline{\Delta} + \underline{T}_3 \qquad \ldots \quad (A3.6)$$

The mean temperature excess over effective ambient temperature T_3 is therefore simply given by

$$\underline{T}_{mxs} = B^{-1}\underline{\Delta} \qquad \ldots \quad (A3.7)$$

where $$\underline{T}_{mxs} = \left[T_{1m} - T_3 \quad T_{2m} - T_3\right]^T$$

and the mean temperature difference between liquids, $\theta_m = T_{1m} - T_{2m}$ by

$$\theta_m = [1 \quad -1]B^{-1}\underline{\Delta} \qquad \ldots \quad (A3.8)$$

APPENDIX IV

ANALYSIS OF TRANSIENTS USING THE THREE-FLUID MODEL

The method employed for this analysis is essentially that of Section 3.6.6 "Frequency response of a heat exchanger" in Seinfeld & Lapidus [8].

Re-arranging instantaneous heat balance equations (3.3) and (3.4), we obtain

$$F_1(t)C_{p1}L\left\{\frac{\partial T_1(\ell,t)}{\partial \ell}\right\} + (K_{12} + K_{13})T_1(\ell,t)$$

$$- K_{12}T_2(\ell,t) - K_{13}T_3(t) + m_1C_{p1}\left\{\frac{\partial T_1(\ell,t)}{\partial t}\right\} = 0 \quad \ldots \quad (A4.1)$$

$$F_2(t)C_{p2}L\left\{\frac{\partial T_2(\ell,t)}{\partial \ell}\right\} + K_{12}T_1(\ell,t)$$

$$+(K_{12}+K_{23})T_2(\ell,t) + K_{23}T_3(t) - m_2C_{p2}\left\{\frac{\partial T_2(\ell,t)}{\partial t}\right\} = 0 \quad \ldots \quad (A4.2)$$

Note that if the time derivatives are set to zero, these equations reduce to steady state equations (2.23) and (2.24).

Suppose that each variable is now perturbed by a small amount (lower case letter) from its steady state value (upper case letter) such that

$$T_j(\ell,t) = T_j(\ell) + t_j(\ell,t) \qquad j = 1,2 \qquad \ldots \quad (A4.3a)$$

$$F_j(t) = F_j + f_j(t) \qquad j = 1,2 \qquad \ldots \quad (A4.3b)$$

$$T_3(t) = T_3 + t_3(t) \qquad \ldots \quad (A4.3c)$$

Substituting from equations (A4.3) into (A4.1) and (A4.2) and subtracting steady state equations (2.23) and (2.24):

$$\{F_1+ f_1(t)\}C_{p1}L\left\{\frac{dT_1(\ell)}{d\ell} + \frac{\partial t_1(\ell,t)}{\partial \ell}\right\} - F_1C_{p1}L\frac{dT_1}{d\ell} + (K_{12}+K_{13})t_1(\ell,t)$$

$$- K_{12}t_2(\ell,t) - K_{13}t_3(t) + m_1C_{p1}\left\{\frac{\partial t_1(\ell,t)}{\partial t}\right\} = 0 \quad \ldots (A4.4)$$

$$\{F_2+ f_2(t)\}C_{p2}L\left\{\frac{dT_2(\ell)}{d\ell} + \frac{\partial t_2(\ell,t)}{\partial \ell}\right\} - F_2C_{p2}L\frac{dT_2}{d\ell} + K_{12}t_1(\ell,t)$$

$$- (K_{12}+K_{23})\, t_2(\ell,t) + K_{23}t_3(t) - m_2C_{p2}\left\{\frac{\partial t_2(\ell,t)}{\partial t}\right\} = 0 \quad \ldots (A4.5)$$

Dividing through by LF_jC_{pj}, $j = 1,2$ and neglecting terms

$f_j(t)\left\{\frac{\partial tj(\ell,t)}{\partial \ell}\right\}$, $j = 1,2$ for small perturbations in F_j, $j = 1,2$

$$\left\{\frac{\partial t_1(\ell,t)}{\partial \ell}\right\} + \left\{\frac{dT_1(\ell)}{d\ell}\right\}\frac{f_1(t)}{F_1} + \frac{1}{L}\frac{(K_{12}+K_{13})}{F_1C_{p1}}t_1(\ell,t) - \frac{1}{L}\frac{K_{12}}{F_1C_{p1}}t_2(\ell,t)$$

$$- \frac{1}{L}\frac{K_{13}}{F_1C_{p1}}\, t_3(t) + \frac{m_1}{LF_1}\left\{\frac{\partial t_1(\ell,t)}{\partial t}\right\} = 0 \quad \ldots (A4.6)$$

$$\left\{\frac{\partial t_2(\ell,t)}{\partial \ell}\right\} + \left\{\frac{dT_2(\ell)}{d\ell}\right\}\frac{f_2(t)}{F_2} + \frac{1}{L}\frac{K_{12}}{F_2C_{p2}}\, t_1(\ell,t) - \frac{1}{L}\frac{(K_{12}+K_{23})}{F_2C_{p2}}t_2(\ell,t)$$

$$+ \frac{1}{L}\frac{K_{23}}{F_2C_{p2}}\, t_3(t) - \frac{m_2}{LF_2}\left\{\frac{\partial t_2(\ell,t)}{\partial t}\right\} = 0 \quad \ldots (A4.7)$$

In order to obtain equations in terms of perturbation variable derivatives only, $dT_j(\ell)/d\ell$, $j = 1,2$ can be eliminated by differentiating equation (2.28) with respect to 'ℓ'

$$\text{i.e.} \quad \begin{bmatrix}\dot{T}_1(\ell)\\ \dot{T}_2(\ell)\end{bmatrix} = \frac{1}{L}Be^{B\frac{\ell}{L}}\begin{bmatrix}T_1(0) - T_3\\ T_2(0) - T_3\end{bmatrix} \quad \ldots (A4.8)$$

Substituting from (A4.8) into (A4.6/7) and recalling the definition of matrix B from equation (2.25), we obtain in matrix-vector form:

$$\begin{bmatrix} \frac{\partial t_1(\ell,t)}{\partial \ell} \\ \frac{\partial t_2(\ell,t)}{\partial \ell} \end{bmatrix} + \begin{bmatrix} \frac{f_1(t)}{F_1} & \\ & \frac{f_2(t)}{F_2} \end{bmatrix} \frac{1}{L} Be^{B\frac{\ell}{L}} \begin{bmatrix} T_1(0) - T_3 \\ T_2(0) - T_3 \end{bmatrix} - \frac{1}{L} B \begin{bmatrix} t_1(\ell,t) \\ t_2(\ell,t) \end{bmatrix}$$

$$+ \frac{1}{L} \begin{bmatrix} -\frac{K_{13}}{F_1 C_{p1}} \\ \frac{K_{23}}{F_2 C_{p2}} \end{bmatrix} t_3(t) + \frac{1}{L} \begin{bmatrix} \frac{m_1}{F_1} & \\ & -\frac{m_2}{F_2} \end{bmatrix} \begin{bmatrix} \frac{\partial t_1(\ell,t)}{\partial t} \\ \frac{\partial t_2(\ell,t)}{\partial t} \end{bmatrix} = \underline{0} \quad \ldots \text{(A4.9)}$$

Defining the Laplace Transform with respect to time such that

$$\mathcal{L}\{y(\ell,t)\} \rightarrow \bar{y}(\ell,s)$$

$$\mathcal{L}\left\{\frac{\partial y(\ell,t)}{\partial t}\right\} \rightarrow s\bar{y}(\ell,s) - y(\ell,0)$$

we transform equation (A4.9) to give

$$\begin{bmatrix} \frac{d\bar{t}_1(\ell,s)}{d\ell} \\ \frac{d\bar{t}_2(\ell,s)}{d\ell} \end{bmatrix} + \begin{bmatrix} \frac{\bar{f}_1(s)}{F_1} & \\ & \frac{\bar{f}_2(s)}{F_2} \end{bmatrix} \frac{1}{L} Be^{B\frac{\ell}{L}} \begin{bmatrix} T_1(0) - T_3 \\ T_2(0) - T_3 \end{bmatrix} - \frac{1}{L} B \begin{bmatrix} \bar{t}_1(\ell,s) \\ \bar{t}_2(\ell,s) \end{bmatrix}$$

$$+ \frac{1}{L} \begin{bmatrix} -\frac{K_{13}}{F_1 C_{p1}} \\ \frac{K_{23}}{F_2 C_{p2}} \end{bmatrix} \bar{t}_3(s) + \frac{1}{L} \begin{bmatrix} \frac{m_1}{F_1} & \\ & -\frac{m_2}{F_2} \end{bmatrix} \begin{bmatrix} s\bar{t}_1(\ell,s) - t_1(\ell,0) \\ s\bar{t}_2(\ell,s) - t_2(\ell,0) \end{bmatrix} = \underline{0} \ldots \text{(A4.10)}$$

Using the following substitutions

$$T = \begin{bmatrix} -\frac{m_1}{F_1} & \\ & \frac{m_2}{F_2} \end{bmatrix} \qquad W(s) = \begin{bmatrix} \frac{\bar{f}_1(s)}{F_1} & \\ & \frac{\bar{f}_2(s)}{F_2} \end{bmatrix} \frac{1}{L} B$$

$$\underline{k}(s) = -\frac{1}{L} \begin{bmatrix} -\frac{K_{13}}{F_1 C_{p1}} \\ \\ \frac{K_{23}}{F_2 C_{p2}} \end{bmatrix} \quad \text{and} \quad \underline{\theta} = \begin{bmatrix} T_1(0) - T_3 \\ T_2(0) - T_3 \end{bmatrix}$$

and taking the simplest case in which the system is in the steady state before any perturbation occurs so that

$$t_1(\ell,0) = t_2(\ell,0) = 0 \qquad \ldots (A4.11)$$

equation (4.10) reduces to

$$\begin{bmatrix} \frac{d\bar{t}_1(\ell,s)}{d\ell} \\ \\ \frac{d\bar{t}_2(\ell,s)}{d\ell} \end{bmatrix} = \frac{1}{L}(sT+B) \begin{bmatrix} \bar{t}_1(\ell,s) \\ \\ \bar{t}_2(\ell,s) \end{bmatrix} - W(s) e^{B\frac{\ell}{L}} \underline{\theta} + \underline{k}(s)\bar{t}_3(s) \qquad \ldots (A4.12)$$

By defining $\underline{\bar{t}}(\ell,s) = [\bar{t}_1(\ell,s)\ \bar{t}_2(\ell,s)]^T$ this can also be written

$$\dot{\underline{t}}\,(\ell,s) = \frac{1}{L}(sT + B)\,\underline{\bar{t}}\,(\ell,s) - W(s) e^{B\frac{\ell}{L}} \underline{\theta} + \underline{k}(s)\bar{t}_3(s) \qquad \ldots (A4.13)$$

where $\dot{t}$ denotes the derivative with respect to length 'ℓ'.

Equation (A4.13) has the solution

$$\underline{\bar{t}}(\ell,s) = e^{(sT + B)\frac{\ell}{L}}\left\{\underline{\bar{t}}(0,s) - L(sT + B)^{-1}\underline{k}(s)t_3(s)\right\}$$

$$- L(sT + B)^{-1}\,\underline{k}(s)t_3(s)$$

$$- e^{(sT + B)\frac{\ell}{L}}\,[\lambda_1 Z_2 - \lambda_2 Z_1]\,W(s)\underline{\theta}$$

$$- \lambda_2 Z_1 W(s)\underline{\theta}.e^{\lambda_1 \ell} + \lambda_1 Z_2 W(s)\underline{\theta}.e^{\lambda_2 \ell}$$

$$- e^{(sT + B)\frac{\ell}{L}}\,[Z_1 - Z_2]\,W(s)\frac{B}{L}\,\underline{\theta}$$

$$+ Z_1 W(s)\frac{B}{L}\,\underline{\theta}.e^{\lambda_1 \ell} - Z_2 W(s)\frac{B}{L}\,\underline{\theta}.e^{\lambda_2 \ell} \qquad \ldots \quad (A4.14)$$

where λ_1 and λ_2 are the eigenvalues of matrix B/L and

$$Z_1 = \frac{1}{\lambda_2 - \lambda_1}\left[\lambda_1 I_2 - (sT + B)\frac{1}{L}\right]^{-1}$$

$$Z_2 = \frac{1}{\lambda_2 - \lambda_1}\left[\lambda_2 I_2 - (sT + B)\frac{1}{L}\right]^{-1}$$

APPENDIX V

PROOF OF EQUIVALENCE OF TWO TESTS FOR (UNIFORM) COMPLETE OBSERVABILITY

Consider the n-dimensional constant coefficient deterministic system

$$x(k+1) = \Phi x(k) + Gu(k) \quad \ldots \quad (A5.1)$$

$$y(k) = Hx(k) \quad \ldots \quad (A5.2)$$

Kalman [76] introduced a test whereby (uniform) complete observability for the system (A5.1, A5.2) is guaranteed if the matrix Γ_o has full rank where

$$\Gamma_o = \begin{bmatrix} H \\ H\Phi \\ H\Phi^2 \\ \vdots \\ H\Phi^{n-1} \end{bmatrix} \quad \ldots \quad (A5.3)$$

A second test proposed by Rosenbrock [77] requires that matrix R_o has full rank for all s_i, where

$$R_o = \begin{bmatrix} s_i I_n - \Phi \\ H \end{bmatrix} \quad \ldots \quad (A5.4)$$

Clearly $(s_i I_n - \Phi)\underline{\kappa}_i = \underline{0}$ for all eigenvalue/eigenvector pairs $(s_i, \underline{\kappa}_i)$ of matrix Φ. Those values of s_i for which $\underline{\kappa}_i \in N(H)$ so that rank $(R_o) < n$ are the unobservable modes of system (H,Φ).

Equivalence is demonstrated by showing

(a) that rank $(R_o) < n \Rightarrow$ rank $(\Gamma_o) < n$

(b) that rank $(\Gamma_o) < n \Rightarrow \exists$ a value of s_i for which rank $(R_o) < n$

Part (a) is trivial:

If R_0 does not have full rank then $\exists$ a non-zero vector $\underline{\kappa}$, an eigenvector of Φ associated with eigenvalue λ, such that

$$\begin{bmatrix} \lambda I - \Phi \\ H \end{bmatrix} \underline{\kappa} = \underline{0}$$

Now consider $\Gamma_0\underline{\kappa}$: $\Phi^j\underline{\kappa} = \lambda^j\underline{\kappa}$ and so

$$\Gamma_0\underline{\kappa} = \begin{bmatrix} H \\ H\Phi \\ H\Phi^2 \\ \vdots \\ H\Phi^{n-1} \end{bmatrix} \underline{\kappa} = \begin{bmatrix} H\underline{\kappa} \\ \lambda H\underline{\kappa} \\ \lambda^2 H\underline{\kappa} \\ \vdots \\ \lambda^{n-1} H\underline{\kappa} \end{bmatrix}$$

but $H\underline{\kappa} = \underline{0} \quad \Rightarrow \quad \Gamma_0\underline{\kappa} = \underline{0}$

$\underline{\kappa}$ is non-zero and so Γ_0 does not have full rank. ∎

Part (b) is less straightforward and is an original contribution:

The aim is to show that if Γ_0 does not have full rank then at least one eigenvalue of Φ has an associated eigenvector lying in $\mathcal{N}(H)$.

If rank $(\Gamma_0) < n$, $\exists$ a non-zero vector $\underline{v}$ s.t. $\Gamma_0\underline{v} = \underline{0}$
$\Rightarrow$ the 'n' n-vectors $\underline{v}$, $\Phi\underline{v}$, $\Phi^2\underline{v}$ ... $\Phi^{n-1}\underline{v} \in \mathcal{N}(H)$.

Now $\mathcal{N}(H)$ has dimension $q(\leq n-1)$. Note that if $q = n$ then the problem is trivial; if $q = 0$ then both Γ_0 and R_0 have full rank.

Let $\mathcal{N}(H)$ be spanned by the 'q' linearly independent n-vectors $\underline{\omega}_1$ ... $\underline{\omega}_q$. The vectors $\underline{v}$, $\Phi^i\underline{v}$, $i = 1,\ldots n-1$ can be written as linear combinations of the $\underline{\omega}_i$'s as follows:

$$\underline{v} = \xi_{11}\underline{\omega}_1 + \xi_{12}\underline{\omega}_2 \quad \ldots \quad + \xi_{1q}\underline{\omega}_q \qquad \ldots \quad (A5.5) \quad (i)$$

$$\Phi\underline{v} = \xi_{21}\underline{\omega}_1 + \xi_{22}\underline{\omega}_2 \quad \ldots \quad + \xi_{2q}\underline{\omega}_q \qquad \ldots \qquad (ii)$$

$$\Phi^2\underline{v} = \xi_{31}\underline{\omega}_1 + \xi_{32}\underline{\omega}_2 \quad \ldots \quad + \xi_{3q}\underline{\omega}_q \qquad \ldots \qquad (iii)$$

$$\vdots \qquad \vdots \qquad \vdots \qquad \vdots$$

$$\Phi^{n-1}\underline{v} = \xi_{n1}\underline{\omega}_1 + \xi_{n2}\underline{\omega}_2 \quad \ldots \quad + \xi_{nq}\underline{\omega}_q \qquad \ldots \qquad (n)$$

where coefficients ξ_{ij} are scalars.

Premultiply the r.h.s. of equation (i) by Φ and equate to the r.h.s. of equation (ii). Similarly premultiply the r.h.s. of (ii) and equate to the r.h.s. of (iii). Continuing the process yields the n-1 equations: (A5.6) (i) ... (n-1).

$$\xi_{11}\underline{\sigma}_1 + \xi_{12}\underline{\sigma}_2 + \ldots + \xi_{1q}\underline{\sigma}_q = \xi_{21}\underline{\omega}_1 + \xi_{22}\underline{\omega}_2 + \ldots \xi_{2q}\underline{\omega}_q \quad \ldots \quad (A5.6)\ (i)$$

$$\vdots \qquad \vdots \qquad \vdots \qquad \vdots \qquad \vdots \qquad \vdots$$

$$\xi_{n-1,1}\underline{\sigma}_1 + \xi_{n-1,2}\underline{\sigma}_2 + \ldots + \xi_{n-1,3}\underline{\sigma}_q = \xi_{n1}\underline{\omega}_1 + \xi_{n2}\underline{\omega}_2 + \ldots \xi_{nq}\underline{\omega}_q \quad \ldots \quad (n-1)$$

where $\Phi\underline{\omega}_i = \underline{\sigma}_i, \quad i = 1,\ldots q.$

These n-1 equations are consistent and can be solved for the (maximum) n-1 'unknowns' $\underline{\sigma}_i$. Each $\underline{\sigma}_i$ can then be expressed as a linear combination of the $\underline{\omega}_i$'s, i.e:

$$\underline{\sigma}_i = L_i\{\underline{\omega}_1 \ldots\ldots \underline{\omega}_q\}, \quad i = 1,\ldots q \qquad \ldots \quad (A5.7)$$

We now attempt to construct an eigenvector of Φ using a linear combination of $\underline{\omega}_i$'s, thus ensuring it lies in $N(H)$. Assume $\exists$ an eigenvector $\underline{\kappa}$ s.t.

$$\underline{\kappa} = \pi_1\underline{\omega}_1 + \pi_2\underline{\omega}_2 + \quad \ldots \quad + \pi_q\underline{\omega}_q \qquad \ldots \quad (A5.8)$$

We need to show that at least one solution exists for scalar coefficients $\pi_1 \ldots\ldots \pi_q$ such that $\underline{\kappa}$ is an eigenvector.

Premultiplying by Φ we obtain

$$\Phi\underline{\kappa} = \pi_1\Phi\underline{\omega}_1 + \pi_2\Phi\underline{\omega}_2 + \ldots + \pi_q\Phi\underline{\omega}_q \quad \ldots \text{(A5.9)}$$

$$= \pi_1\underline{\sigma}_1 + \pi_2\underline{\sigma}_2 + \ldots + \pi_q\underline{\sigma}_q \quad \ldots \text{(A5.10)}$$

Now $\underline{\sigma}_1 \ \ldots \ \underline{\sigma}_q$ are known in terms of $\underline{\omega}_1 \ \ldots \ \underline{\omega}_q$ and so we can write

$$\Phi\underline{\kappa} = \pi_1 L_1\{\underline{\omega}_1 \ldots \underline{\omega}_q\} + \pi_2 L_2\{\underline{\omega}_1 \ldots \underline{\omega}_q\} + \ldots + \pi_q L_q\{\underline{\omega}_1 \ldots \underline{\omega}_q\} \quad \ldots \text{(A5.11)}$$

Re-arranging, and using $G_i\{\pi_1 \ \ldots \ \pi_q\}$ to represent a linear function of scalars π_i

$$\Phi\underline{\kappa} = G_1\{\pi_1 \ldots \pi_q\}\underline{\omega}_1 + G_2\{\pi_1 \ldots \pi_q\}\underline{\omega}_2 + \ldots + G_q\{\pi_1 \ \ldots \ \pi_q\}\underline{\omega}_q \quad \ldots \text{(A5.12)}$$

If $\underline{\kappa}$ is to be an eigenvalue of Φ then it must obey the relation $\Phi\underline{\kappa} = \lambda\underline{\kappa}$.

$$\text{Now} \quad \lambda\underline{\kappa} = \lambda(\pi_1\underline{\omega}_1 + \pi_2\underline{\omega}_2 + \ldots + \pi_q\underline{\omega}_q) \quad \ldots \text{(A5.13)}$$

and by equating coefficients of $\underline{\omega}_i$, $i = 1,\ldots q$ between (A5.12) and (A5.13) we obtain:

$$\begin{aligned} G_1\{\pi_1 \ \ldots \ \pi_q\} &= \lambda\pi_1 \\ G_2\{\pi_1 \ \ldots \ \pi_q\} &= \lambda\pi_2 \qquad \ldots \text{(A5.14)} \\ &\vdots \\ G_q\{\pi_1 \ \ldots \ \pi_q\} &= \lambda\pi_q \end{aligned}$$

(A5.14) can be written in matrix form where W is a q x q matrix

$$W \begin{bmatrix} \pi_1 \\ \pi_2 \\ \vdots \\ \pi_q \end{bmatrix} = \lambda \begin{bmatrix} \pi_1 \\ \pi_2 \\ \vdots \\ \pi_q \end{bmatrix} \quad \ldots \text{(A5.15)}$$

Now W must have at least one eigenvalue and hence at least one eigenvector. There is thus at least one solution for $\pi_1 \ldots \pi_q$ in equation (A5.8), such that $\underline{\kappa}$ is an eigenvector of Φ. Hence there is at least one eigenvector of $\Phi \in N(H)$.

If rank $(\Gamma_0) < n$ then $N(H)$ contains at least one eigenvector of Φ

$\Rightarrow$ rank $(R_0) < n$ for at least one value of s_i. ∎

Part (b) of the proof can be followed more easily with the aid of a simple example. Equation numbers AX are repeated as A'X.

Suppose $\Phi = \begin{bmatrix} 1 & 2 & 0 \\ 0 & 1 & 0 \\ 0 & 0 & 2 \end{bmatrix}$ and $H = \begin{bmatrix} 0 & 1 & 0 \end{bmatrix}$

Then $\Gamma_0 = \begin{bmatrix} 0 & 1 & 0 \\ 0 & 1 & 0 \\ 0 & 1 & 0 \end{bmatrix}$ which clearly does not have full rank.

We must show that this implies that $\exists$ an eigenvector of $\Phi \in N(H)$.

Rank $(\Gamma_0) < n \Rightarrow \exists$ a non-zero $\underline{v}$ that satisfies $\Gamma_0 \underline{v} = \underline{0}$, for instance:

$$\underline{v} = [3 \quad 0 \quad 5]^T$$

Dim $N(H) = q = 2$. Select any two linearly independent vectors $\underline{\omega}_1$ and $\underline{\omega}_2$ that span $N(H)$, such as

$$\underline{\omega}_1 = [1 \quad 0 \quad 2]^T \text{ and } \underline{\omega}_2 = [2 \quad 0 \quad 3]^T$$

Since $\Gamma_0 \underline{v} = \underline{0}$, $\underline{v}$, $\Phi \underline{v} \ldots \Phi^{n-1} \underline{v}$ are all in $N(H)$ and can thus be represented as linear combinations of $\underline{\omega}_1$ and $\underline{\omega}_2$.

Thus $\underline{v} = \underline{\omega}_1 + \underline{\omega}_2$ ... (A'5.5) (i)

$$\Phi \underline{v} = \begin{bmatrix} 3 \\ 0 \\ 10 \end{bmatrix} = 11\underline{\omega}_1 - 4\underline{\omega}_2 \quad \ldots \quad \text{(ii)}$$

$$\Phi^2 \underline{v} = \begin{bmatrix} 3 \\ 0 \\ 20 \end{bmatrix} = 31\underline{\omega}_1 - 14\underline{\omega}_2 \quad \ldots \quad \text{(iii)}$$

Premultiplying the r.h.s. of (i) and (ii) by Φ, equating to the r.h.s. of (ii) and (iii) respectively and writing $\Phi\underline{\omega}_1 = \underline{\sigma}_1$ and $\Phi\underline{\omega}_2 = \underline{\sigma}_2$

$$\underline{\sigma}_1 + \underline{\sigma}_2 = 11\underline{\omega}_1 - 4\underline{\omega}_2 \quad \ldots \text{ (A'5.6) (i)}$$

$$11\underline{\sigma}_1 - 4\underline{\sigma}_2 = 31\underline{\omega}_1 - 14\underline{\omega}_2 \quad \ldots \text{ (ii)}$$

Solution

$$\underline{\sigma}_1 = L_1\{\underline{\omega}_1, \underline{\omega}_2\} = 5\underline{\omega}_1 - 2\underline{\omega}_2 \quad \ldots \text{ (A'5.7) (i)}$$

$$\underline{\sigma}_2 = L_2\{\underline{\omega}_1, \underline{\omega}_2\} = 6\underline{\omega}_1 - 2\underline{\omega}_2 \quad \ldots \text{ (ii)}$$

We now attempt to construct $\underline{\kappa}$, an eigenvalue of Φ, from a linear combination of $\underline{\omega}_i$'s. Such a $\underline{\kappa}$, if it can be shown to exist, would lie in $N(H)$ since the $\underline{\omega}_i$'s span $N(H)$.

$$\underline{\kappa} = \pi_1\underline{\omega}_1 + \pi_2\underline{\omega}_2 \quad \ldots \text{ (A'5.8)}$$

We must find at least one solution for π_1, π_2 such that $\Phi\underline{\kappa} = \lambda\underline{\kappa}$

$$\Phi\underline{\kappa} = \pi_1\underline{\sigma}_1 + \pi_2\underline{\sigma}_2 \quad \ldots \text{ (A'5.10)}$$

$$= \pi_1(5\underline{\omega}_1 - 2\underline{\omega}_2) + \pi_2(6\underline{\omega}_1 - 2\underline{\omega}_2) \quad \ldots \text{ (A'5.11)}$$

and re-arranging

$$\Phi\underline{\kappa} = G_1\{\pi_1, \pi_2\}\underline{\omega}_1 + G_2\{\pi_1, \pi_2\}\underline{\omega}_2 \quad \ldots \text{ (A'5.12)}$$

$$= (5\pi_1 + 6\pi_2)\underline{\omega}_1 + (-2\pi_1 - 2\pi_2)\underline{\omega}_2$$

Since we want $\underline{\kappa}$ to be an eigenvector it must satisfy

$$\Phi\underline{\kappa} = \lambda\underline{\kappa} = \lambda\pi_1\underline{\omega}_1 + \lambda\pi_2\underline{\omega}_2 \quad \ldots \text{ (A'5.13)}$$

and equating coefficients of $\underline{\omega}_1$ we obtain (A'5.15) and (A'5.16)

$$\begin{aligned} 5\pi_1 + 6\pi_2 &= \lambda\pi_1 \\ -2\pi_1 - 2\pi_2 &= \lambda\pi_2 \end{aligned} \qquad \text{i.e. } W = \begin{bmatrix} 5 & 6 \\ -2 & -2 \end{bmatrix}$$

which has distinct eigenvalues 1 and 2

For $\lambda = 1$ $\begin{bmatrix} \pi_1 \\ \pi_2 \end{bmatrix} = \begin{bmatrix} -3 \\ 2 \end{bmatrix}$ $\lambda = 2$ $\begin{bmatrix} \pi_1 \\ \pi_2 \end{bmatrix} = \begin{bmatrix} 2 \\ -1 \end{bmatrix}$

In this case there are two eigenvectors of $\Phi \in N(H)$

$$\underline{\kappa}_1 = -3\underline{\omega}_1 + 2\underline{\omega}_2 = \begin{bmatrix} 1 \\ 0 \\ 0 \end{bmatrix} \quad \text{and} \quad \underline{\kappa}_2 = 2\underline{\omega}_1 - \underline{\omega}_2 = \begin{bmatrix} 0 \\ 0 \\ 1 \end{bmatrix}$$

APPENDIX VI

ESTIMATION ERROR AND INNOVATION COVARIANCES FOR A SUBOPTIMAL FILTER

If the optimal steady state innovation covariance is known then the degradation P_s in the estimation error covariance matrix can be calculated directly for any Kalman gain K.

Assuming that the filter has reached a steady state and that we are using a constant suboptimal gain K_a, we use the following notation for Lemma A6.1 and Theorem A6.1.

$P(k\|k) = P(k-1\|k-1) = P$	Subscript 'a' denotes 'actual'
$P(k\|k-1) = P^+$	Subscript 's' denotes 'degradation'
$V(k) = V$	No subscript indicates 'optimal'

Lemma A6.1

From (5.4) $K = P^+H^TV^{-1}$

$\Rightarrow \quad KV = P^+H^T$

but from (5.3) $V = HP^+H^T + R$ ... (A6.1)

$\Rightarrow \quad K[HP^+H^T + R] = P^+H^T$

transposing $[HP^+H^T + R]K^T = HP^+$

or $[HP^+H + R]K^T - HP^+ = 0$ ... (A6.2)

■

Theorem A6.1 Calculation of P_s

This theorem is an original extension of the work of Friedland [14] who derived a similar result for the continuous-time case.

Consider the time invariant system

$$x(k+1) = \Phi x(k) + w(k) \quad \ldots \quad (A6.3)$$

$$y(k) = Hx(k) + v(k) \quad \ldots \quad (A6.4)$$

This is a similar system to (4.23, 4.24) except that it is driven by white noise only. The input 'u' makes no difference to the result and there is no loss of generality by omitting it.

Now write $K_a = K + \Delta$, i.e. Δ is the difference between actual and optimal gains

$$P_a = P + P_s$$
$$V_a = V + V_s$$

From Jazwinski [5]

$$P_a^+ = P^+ + P_s^+ = \Phi P_a \Phi^T + Q$$

but $$P^+ = \Phi P \Phi^T + Q$$

and subtracting: $$P_s^+ = \Phi P_s \Phi^T \qquad \ldots \quad (A6.5)$$

Also from [5]

$$\begin{aligned} P_a = P + P_s &= [I-K_aH]\{P^+ + P_s^+\}[I-K_aH]^T + K_aRK_a^T \\ &= [I-K_aH]P_s^+[I-K_aH]^T \\ &\quad + [I-KH]P^+[I-KH]^T + KRK^T \\ &\quad - \Delta HP^+[I-KH]^T + \Delta RK^T \\ &\quad - [I-KH]P^+[\Delta H]^T + KR\Delta^T \\ &\quad + \Delta HP^+[\Delta H]^T + \Delta R\Delta^T \qquad \ldots \quad (A6.6) \end{aligned}$$

but $$P = [I-KH]P^+[I-KH]^T + KRK^T$$

and subtracting:

$$\begin{aligned} P_s = {} & [I-K_aH]P_s^+[I-K_aH]^T \\ & - \Delta HP^+[I-KH]^T + \Delta RK^T \\ & -[I-KH]P^+[\Delta H]^T + KR\Delta^T \\ & + \Delta HP^+[\Delta H]^T + \Delta R\Delta^T \qquad \ldots \quad (A6.7) \end{aligned}$$

The terms in the second row combine to give

$$\Delta\{[HP^+H^T + R]K^T - HP^+\} = 0 \text{ by Lemma A6.1}$$

The terms in the third row of (A6.7) add to the transpose of this and cancel out also. This leaves

$$P_s = [I-K_aH]P_s^+[I-K_aH]^T + \Delta[HP^+H^T + R]\Delta^T \qquad \ldots \quad (A6.8)$$

and from (A6.1) and (A6.8)

$$P_s = [I-K_aH]P_s^{+}[I-K_aH]^T + \Delta V\Delta^T \qquad \ldots \quad (6.9)$$

■

Corollary Calculation of V_s

$$V_a = HP_aH^T + R$$

i.e. $$V + V_s = H[P + P_s]H^T + R$$

but $$V = HPH^T + R \quad \text{from (A6.1)}$$

and subtracting $$V_s = HP_sH^T \qquad \ldots \quad (A6.10)$$

■

For the scalar system of Section 5.4, K = 0.837 and v = 1.227

Taking $K_a = 2.0$, $\Delta = 1.163$ and from (A6.5) and (A6.9), $p_s = 1.976$

Hence, from (A6.10), $v_s = 0.316$ so that $v_a = 1.227 + 0.316 = 1.543$ which agrees closely with the value obtained by computer simulation (Fig 24 - Chapter 5).

APPENDIX VII

TRANSFORMED VARIABLES FOR THE DETERMINATION OF FALSE AND MISS ALARM PROBABILITIES FOR COMPLETELY SPECIFIED FAULTS

This appendix, which is original work, should be read in conjunction with Fig 25(b). Consider the problem of testing a single innovation $\Upsilon = [\Upsilon_1, \Upsilon_2, \ldots \Upsilon_r]^T$ via expression (4.65) to decide between $H_0(E[\Upsilon] = \underline{0})$ and $H_1(E[\Upsilon] = \underline{m})$. At the llr threshold we have, from (4.65)

$$\Upsilon^T V^{-1} \Upsilon - (\Upsilon - \underline{m})^T V^{-1} (\Upsilon - \underline{m}) = \eta \qquad \ldots \quad (A7.1)$$

$$\Rightarrow \quad \Upsilon^T V^{-1} \underline{m} = \tfrac{1}{2}(\underline{m}^T V^{-1} \underline{m} + \eta) \qquad \ldots \quad (A7.2)$$

This contour of constant llr is an (r-1) dimensional hyperplane orthogonal to $V^{-1}\underline{m}$. Let A be the orthogonal matrix which rotates $V^{-1}\underline{m}$ so that it lies in the $+\Upsilon_1$ direction. We define

$$\underline{\tilde{m}} = A\underline{m} \quad \text{and} \quad \tilde{\Upsilon} = A\Upsilon$$

hence $\tilde{V} = E[\Upsilon\Upsilon^T] = AVA^T$

and $\tilde{V}^{-1} = AV^{-1}A^T$ by the orthogonality of A

The regions on either side of the contour now depend only on the marginal density $f_{\tilde{\Upsilon}_1}(\tilde{\Upsilon}_1)$ obtained by integrating out the remaining (r-1) r.v.'s (Papoulis [93]). We have

$$f_{\tilde{\Upsilon}_1}(\tilde{\Upsilon}_1) = \frac{1}{(2\pi)^{1/2}\tilde{\sigma}_1} . e^{-(\tilde{\Upsilon}_1 - \tilde{m}_1)^2 / 2\tilde{\sigma}_1^2} \qquad \ldots \quad (A7.3)$$

where $\tilde{\sigma}_1 = (\tilde{V}_{11})^{1/2}$ and $\tilde{m}_1$ is the first component of $\underline{\tilde{m}}$

Normalizing $V^{-1}\underline{m}$ we have, by definition

$$A\frac{V^{-1}\underline{m}}{|V^{-1}\underline{m}|} = \begin{bmatrix}1\\0\end{bmatrix} \rightarrow A^T\begin{bmatrix}1\\0\end{bmatrix} = \frac{V^{-1}\underline{m}}{|V^{-1}\underline{m}|} \quad \ldots \quad (A7.4)$$

Thus

$$\tilde{V}_{11} = \begin{bmatrix}1 & 0\end{bmatrix}AVA^T\begin{bmatrix}1\\0\end{bmatrix} = \frac{(V^{-1}\underline{m})^T V(V^{-1}\underline{m})}{|V^{-1}\underline{m}|^2} = \frac{\underline{m}^T V^{-1}\underline{m}^T}{|V^{-1}\underline{m}|^2} \quad \ldots \quad (A7.5)$$

In terms of transformed variables, (A7.2) becomes

$$\tilde{\gamma}^T\tilde{V}^{-1}\tilde{\underline{m}} = \tfrac{1}{2}(\tilde{m}^T\tilde{V}^{-1}\tilde{\underline{m}} + \eta) \quad \ldots \quad (A7.6)$$

$\bar{\gamma}_1$, the value of $\tilde{\gamma}_1$ at which the transformed constant LLR contour crosses the γ_1 axis, is obtained by setting $\tilde{\gamma}_2$ equal to zero in (A7.6).

$$\begin{bmatrix}\bar{\gamma}_1 & 0\end{bmatrix}\tilde{V}^{-1}\tilde{\underline{m}} = \tfrac{1}{2}(\tilde{m}^T\tilde{V}^{-1}\tilde{\underline{m}} + \eta) \quad \ldots \quad (A7.7)$$

$$\rightarrow \bar{\gamma}_1\begin{bmatrix}1 & 0\end{bmatrix}A\,V^{-1}\underline{m} = \tfrac{1}{2}(\underline{m}^T V^{-1}\underline{m} + \eta) \quad \ldots \quad (A7.8)$$

Hence, from (A7.4)

$$\bar{\gamma}_1 = \frac{\tfrac{1}{2}(\underline{m}^T V^{-1}\underline{m} + \eta)}{|V^{-1}\underline{m}|} \quad \ldots \quad (A7.9)$$

We require also $\tilde{m}_1 = \begin{bmatrix}1 & 0\end{bmatrix}A\underline{m}$ ... (A7.10)

and, again from (A7.4)

$$\tilde{m}_1 = \frac{\underline{m}^T V^{-1}\underline{m}}{|V^{-1}\underline{m}|} \quad \ldots \quad (A7.11)$$

REFERENCES

[1] MARSHALL, E. and SHEPHERD, A. Strategies adopted by operators when diagnosing plant failures from a simulated control panel. Symposium on Human Operators and Simulation, Loughborough, Leics. 29-31 March (1977)

[2] HARLAND, P. and FRYER, J. The ICI lament: where have all our tiffies gone ? The Sunday Times Business News, 18 June (1978)

[3] KALMAN, R.E. A new approach to linear filtering and prediction problems. ASME J.Basic Eng. pp 35-45 March (1960)

[4] KALMAN, R.E. and BUCY, R.S. New results in linear filtering and prediction theory. ASME J.Basic Eng. pp 95-108 March (1961)

[5] JAZWINSKI, A.H. Stochastic processes and filtering theory. Academic Press (1970)

[6] SAGE, A.P. and MELSA, J.L. Estimation theory with applications to communications and control. McGraw-Hill, New York (1971)

[7] KWAKERNAAK, H. and SIVAN, R. Linear optimal control systems. Wiley (1972)

[8] SEINFELD, J.H. and LAPIDUS, L. Mathematical methods in Chemical Engineering, Vol 3: Process modelling, estimation and identification. Prentice-Hall (1974)

[9] BELLINGHAM, B. and LEES, F.P. Practical state and bias estimation of process systems with initial information uncertainty. Int.J.Systems Sci., 8 (7) pp 813-840 (1977)

[10] MEHRA, R.K. On the identification of variances and adaptive Kalman filtering. IEEE Trans.Aut.Control, AC-15 (2) pp 175-184 (1970)

[11] GODBOLE, S.S. Kalman filtering with no a priori information about noise - white noise case: identification of covariances. IEEE Trans.Aut.Control, AC-19 pp 561-563 Oct (1974)

[12] MARTIN, W.C. and STUBBERUD, A.R. The innovations process with applications to identifications. Control and Dynamical Systems (1976)

[13] HEFFES, H. The effect of erroneous models on the Kalman filter response. IEEE Trans.Aut.Control, AC-11 pp 541-3 (1966)

[14] FRIEDLAND, B. On the effect of incorrect gain in the Kalman filter. IEEE Trans.Aut.Control, AC-12 p 610 (1967)

[15] FRIEDLAND, B. Treatment of bias in recursive filtering. IEEE Trans.Aut.Control, AC-14 (4) pp 359-367 Aug (1969)

[16] COGGAN, G.C. and NOTON, A.R.M. Discrete-time sequential state and parameter estimation in Chemical Engineering. Trans.Instn.Chem.Engrs., 48 p 255 (1970)

[17] GOLDMANN, S.F. and SARGENT, R.W.H. Applications of linear estimation theory to chemical processes: a feasibility study. Chem.Eng.Sci., 26 pp 1535-1553 (1971)

[18] JOFFE, B.L. and SARGENT, R.W.H. The design of an on-line control scheme for a tubular catalytic reactor. Trans.Instn.Chem.Engrs., 50 pp 270-282 (1972)

[19] NEWELL, R.B. and FISHER, D.G. Model development, reduction and experimental evaluation for an evaporator. Ind.Eng.Chem.Process Des.Develop., 11 (2) pp 213-221 (1972)

[20] HAMILTON, J.C., SEBORG, D.E. and FISHER, D.G. An experimental evaluation of Kalman filtering. AIChE Journal, 19 (5) pp 901-9 (1973)

[21] JO, J.H. and BANKOFF, S.G. Digital monitoring and estimation of polymerization reactors. AIChE Journal, 22 (2) pp 361-9 (1976)

[22] LITCHFIELD, R.J., CAMPBELL, K.S. and LOCKE, A. The application of several Kalman filters to the control of a real chemical reactor. Trans.I.Chem.E., 51 pp 113-120 (1979)

[23] WELLS, C.H. and WISMER, D.A. in Advances in Control Systems; Theory and Applications. Ed. C.T. Leondes. Academic Press, New York (1971)

[24] ANYAKORA, S.N., ENGEL, G.F.M. and LEES, F.P. Some data on the reliability of instruments in the chemical plant environment. The Chemical Engineer pp 396-402 Nov (1971)

[25] LEES, F.P. Some data on failure modes of instruments in the chemical plant environment. The Chemical Engineer pp 418-20 Sept (1973)

[26] HIMMELBLAU, D.M. Fault detection and diagnosis in chemical and petrochemical processes. Elsevier Scientific Publishing Co. Amsterdam, Oxford, New York (1978)

[27] WILLSKY, A.S. A survey of design methods for failure detection in dynamic systems. Automatica, 12 pp 601-11 (1976)

[28] FAGIN, S.L. Recursive linear regression theory, optimal filter theory and error analyses of optimal systems. IEEE Int.Conv.Record pp 216-240 March (1964)

[29] TARN, T.J. and ZABORSKY, J. A practical nondiverging filter. AIAA Jl., 8 pp 1127-1133 (1970)

[30] JAZWINSKI, A.H. Limited memory optimal filtering. IEEE Trans.Aut.Control, AC-13 pp 558-563 (1968)

[31] BEARD, R.V. Failure accommodation in linear systems through self-reorganization. Rept.NASA-CR-118314, MIT Feb (1971)

[32] LABARRERE, M., GIMONET, B. and BUCHARLES, A. An estimation technique applied to failure detection. Proc.7th IFAC Triennial World Congress, Helsinki, 12-16 June(1978)

[33] CLARK, R.N., FOSTH, D.C. and WALTON V.M. Detecting instrument malfunction in control systems. IEEE Trans.Aerospace Elec.Sys., AES-11 (4) pp 465-473 (1975)

[34] MONTGOMERY, R.C. and CAGLAYAN, A.K. A self reorganizing digital flight control system for aircraft. AIAA 12th Aerospace Sciences Meeting, Washington DC. 30 Jan-1 Feb AIAA paper 74-21 (1974)

[35] MONTGOMERY, R.C. and PRICE, D.B. Management of analytical redundancy in digital flight control systems for aircraft. AIAA Mechanics and Control of Flight Conference, Anaheim CA 5-9 Aug AIAA paper 74-887 (1974)

[36] ATHANS, M., DUNN, K.P., GREENE, C.S., LEE, W.H., SANDELL, N.R., SEGALL, I. and WILLSKY, A.S. The stochastic control of the F-8C aircraft using the multiple model adaptive control (MMAC) method. Proc.1975 IEEE Conf.on Decision and Control, Houston Dec (1975)

[37] ATHANS, M. and CHANG, C.B. Adaptive estimation and parameter identification using 'multiple model estimation algorithm' MIT Lincoln Lab.Tech.Note 1976-28, 23 June (1976)

[38] DIGERNES, T. Real-time failure detection and identification applied to supervision of oil transport in pipelines Modeling, Identification and Control, 1 (1) pp 39-49 (1980)

[39] WALD, A. Sequential analysis. Wiley, New York (1947)

[40] HANCOCK, J.C. and WINTZ, P.A. Signal detection theory. McGraw-Hill, New York (1966)

[41] NEWBOLD, P.M. and HO, Y.C. Detection of changes in the characteristics of a Gauss-Markov process IEEE Trans.Aerospace Elec.Sys., AES-4 (5) pp 707-718 Sept (1968)

[42] CHIEN, T.T. and ADAMS, M.B. A sequential failure detection technique and its application IEEE Trans.Aut.Control, AC-21 pp 750-757 Oct (1976)

[43] BUXBAUM, P.J. and HADDAD, R.A. Recursive optimal estimation for a class of nongaussian processes Proc.Symp.on Computer Processing in Communications, Polytech Inst.of Brooklyn 8-10 April (1969)

[44] WILLSKY, A.S., DEYST, J.J. and CRAWFORD, B.S. Adaptive filtering and self-test methods for failure detection and compensation. Proc.of the 1974 JACC, Austin Texas 19-21 June (1974)

[45] WILLSKY, A.S., DEYST, J.J. and CRAWFORD, B.S. Two self-test methods applied to an inertial system problem J.Spacecr.Rockets, 12 (7) pp 434-437 July (1975)

[46] CHIEN, T.T. An adaptive technique for a redundant-sensor navigation system. Rept. T-560, Draper Labs.Cambridge MA Feb (1972)

[47] KAILATH, T. An innovations approach to least-squares estimation, Part I IEEE Trans.Aut.Control, AC-13 pp 646-655 (1968)

[48] MEHRA, R.K. and PESCHON, J. An innovations approach to fault detection and diagnosis in dynamic systems Automatica, 7 pp 637-640 (1971)

[49] BELLINGHAM, B. and LEES, F.P. The detection of malfunction using a process control computer: a simple filtering technique for flow control loops Trans.I.Chem.E., 55 pp 1-16 (1977)

[50] BELLINGHAM, B. and LEES, F.P. The detection of malfunction using a process control computer: a Kalman filtering technique for general control loops Trans.I.Chem.E, 55 pp 253-265 (1977)

[51] ROONEY, T.B., MEHRA, R.K., KRAMERICH, G.L. and EVANS, L.B. Estimating plant flows and inventories using material balance relations Proc.7th IFAC Triennial World Congress, Helsinki, 12-16 June (1978)

[52] NEWMAN, R.S. and PERKINS, J.D. Some tests of a method for fault detection on chemical plants.The Inst.of Chem.Eng.(N.W. branch) Symp.on the profitable use of statistics in Chemical Engineering, Manchester 26 Sept. (1979)

[53] NEWMAN, R.S. Robustness of Kalman filter based fault detection methods. PhD thesis, Dept. of Chemical Engineering and Chemical Technology, Imperial College, London (1982)

[54] VAN TREES, H.L. Detection, Estimation and Modulation Theory, Part I: Detection, Estimation and Modulation Theory, Wiley (1971)

[55] WILLSKY, A.S. and JONES, H.L. A generalized likelihood ratio approach to state estimation in linear systems subject to abrupt changes Proc.of 1974 IEEE Conf.on Decision and Control, Phoenix Arizona Nov (1974)

[56] WILLSKY, A.S. and JONES, H.L. A generalized likelihood ratio approach to the detection and estimation of jumps in linear systems. IEEE Trans.Aut.Control, AC-21 pp 108-112 Feb (1976)

[57] LIU, J.S.H. and JONES, H.L. Linear manifold constrained GLR IEEE Trans.Aut.Control, AC-22 pp 988-989 Dec (1977)

[58] LIU, J.S.H. Detection, isolation and identification techniques for noisy degradation in linear discrete-time systems. Proc.1977 IEEE Conf.on Decision and Control, Part I. New Orleans 7-9 Dec (1977)

[59] SORENSON, H.W. 'Kalman filtering techniques' in Advances in Control Systems, ed. C.T.Leondes. Vol 3 (1966)

[60] CHANG, C.B. and DUNN, K.P. A recursive generalized likelihood ratio test algorithm for detecting sudden ghanges in linear discrete systems Proc.17th IEEE Conf.on Decision and Control San Diego CA Jan (1977)

[61] CHANG, C.B. and DUNN, K.P. On GLR detection and estimation of unexpected inputs in linear discrete systems IEEE Trans.Aut.Control, AC-24 (3) June (1979)

[62] POULIEZOS. A. Fault monitoring schemes for linear stochastic systems. PhD thesis, Dept. of Electrical Engineering and Electronics, Brunel University, Uxbridge, Middx. (1980)

[63] USHER, J.D. Evaluating plate heat exchangers Chemical Engineering 23 Feb (1970)

[64] LAWRY, F.J. Plate-type heat exchangers Chemical Engineering 29 June (1959)

[65] BUONOPANE, R.A., TROUPE, R.A. and MORGAN, J.C. Heat transfer design method for plate heat exchangers. Chem.Eng.Progress, 59 (7) July (1963)

[66] PALMQUIST, U. Some aspects of model reduction for a chemical plant. DIC thesis, Dept. of Chemical Engineering and Chemical Technology, Imperial College, London July (1978)

[67] ALBRECHT, J.J. Modelling, identification and multivariable control of an absorption-desorption system. PhD thesis, Dept. of Chemical Engineering and Chemical Technology, Imperial College, London (1977)

[68] ROBERTS, M.P. The development and implementation of nonlinear control and filtering algorithms on an absorption/stripping pilot plant. PhD thesis, Dept. of Chemical Engineering and Chemical Tecnology, Imperial College, London (1978)

[69] LUENBERGER, D.G. Introduction to linear and nonlinear programming. Addison-Wesley, Reading, Mass. (1973)

[70] KERSCHENBAUM, L.S. Dept.of Chemical Engineering and Chemical Technology, Imperial College, London. Private communication.

[71] CHEN, C.T. Introduction to linear system theory. Holt Rheinhart and Winston Inc. (1970)

[72] STEPHENSON, G. An introduction to matrices, sets and groups for science students. Longmans, Green & Co. Ltd. (1965)

[73] NEWELL, R.B. and FISHER, D.G. Experimental evaluation of optimal, multivariable regulatory controllers with model following capabilities. Automatica, 8 pp 247-262 (1972)

[74] MARSHALL, S.A. An approximate method for reducing the order of a linear system. Control Dec (1966)

[75] AOKI, M. Optimization of stochastic systems. Academic Press New York (1967)

[76] KALMAN, R.E. Contributions to the theory of optimal control Proc.of the conf.on ordinary differential equations, Mexico City, 1959; Bol.Soc.Mat.Mex. (1961)

[77] ROSENBROCK, H.H. State space and multivariable theory. Nelson (1970)

[78] LINDGREN, B.W. Statistical theory. 2Ed.The Macmillan Company (1968)

[79] WELLINGS, P.H. Dept.of Electrical Engineering, Imperial College, London. Private communication.

[80] WHITE, J., YEATS, A. and SKIPWORTH, G. Tables for statisticians. 3Ed. Stanley Thornes (Publishers) (1979)

[81] WETHERILL, G.B. Elementary statistical methods. Chapman Hall 2Ed. (1979)

[82] ALDER, H.L. and ROESSLER, E.B. Introduction to probability and statistics. W.H. Freeman & Co. 6Ed. (1977)

[83] KERR, T.H. A two ellipsoid overlap test for real time failure detection and isolation by confidence regions. Pittsburgh Conf. on Modelling and Simulation, 24-26 April (1974)

[84] FITZGERALD, R.J. Error divergence in optimal filtering problems. 2nd IFAC Symp. Automatic Control Space, Vienna, Austria (1967)

[85] TENNYSON R.N. and SCHAAF R.P. Guidelines can help choose proper process for gas treating plants Oil and gas journal 10 Jan (1977)

[86] GOAR, B.G. Today's gas treating processes - 1 Oil and gas journal 12 July (1971)

[87] BAKER, G.H. Corrosion-free gas sweetening. Hydrocarbon Processing Aug (1975)

[88] HAWKES, E.N. and MAGO, B.F. Stop MEA CO_2 unit corrosion. Hydrocarbon Processing Aug (1971)

[89] BUTWELL, K.F., HAWKES, E.N. and MAGO, B.F. Corrosion control in CO_2 removal systems. Chem.Eng.Progress Feb (1973)

[90] CHEMICAL ENGINEERING LABORATORY: PILOT PLANTS AND DIGITAL COMPUTER. Notes from the Dept. of Chemical Engineering and Chemical Technology, Imperial College, London.

[91] SMITH, C.L. Digital computer process control. Intext series in Chemical Engineering (1972)

[92] SIMONSON, J.R. An introduction to engineering heat transfer. McGraw-Hill (1967)

[93] PAPOULIS, A. Probability, random variables and stochastic processes. McGraw-Hill (1965)